NON-COVALENT INTERACTIONS IN β-HAIRPIN PEPTIDES AND SMALL MOLECULE MODEL SYSTEMS.

Robert Murray Hughes IV

A dissertation submitted to the faculty of the University of North Carolina at Chapel Hill in partial fulfillment of the requirements for the degree of Doctor of Philosophy in the Department of Chemistry.

Chapel Hill
2007

Approved by

Advisor: Professor Marcey Waters

Reader: Professor Maurice Brookhart

Reader: Professor Jeff Johnson

ABSTRACT

ROBERT MURRAY HUGHES IV: Non-Covalent Interactions In β-Hairpin Peptides And Small Molecule Model Systems
(Under the direction of Marcey L. Waters)

Post-translational modifications of proteins are a key component of cell signaling. In particular, post-translational modifications of histone tails are known to modulate transcription of DNA. These modifications function via a number of different non-covalent interactions with both DNA and various nuclear proteins. Some relevant modifications include methylation or acylation of lysine and the methylation of arginine and are thought to trigger binding with aromatic rings (Trp, DNA bases) through cation-π and amide-π interactions. In order to characterize these biologically relevant interactions, they have been studied within the context of β-hairpin peptide model systems, which enable the description and quantification of specific sidechain-sidechain interactions. In our system, the interaction between Trp and trimethylated Lys is shown to be worth 1.0 kcal/mol, a stabilization of about 0.7 kcal/mol over the nonmethylated Lys-Trp interaction. The methylated interaction occurs with an enhanced entropic driving force over the unmethylated interaction. Methylation of Arg is also shown to enhance its interaction with Trp, by about 0.5 kcal/mol. Additionally, the acyl Lys-Trp interaction is found to be equivalent in magnitude to the nonmethylated Lys-Trp interaction (0.3 kcal/mol). Acylation of lysine in our model system is shown to induce a switch from a cation-π to an amide-π interaction. Investigations into neutral analogues of trimethylated

Lys reveals the critical nature of the cation-π interaction to the interaction of histone tails with chromodomain proteins. This is confirmed both in our β-hairpin model system and with binding studies with the HP1 chromodomain.

Additional investigations in this thesis include mutational studies of a β-hairpin receptor for ATP and the study of a cation-π interaction within a small molecule model system. Through experimental and computational studies, the β-hairpin receptor for ATP is shown to form a well-defined binding pocket with a number of important electrostatic contacts. The cation-π interaction in the small molecule model system is found to prevail in both aqueous and organic solvent, despite the possible presence of competing non-covalent interactions. X-ray and computational evidence suggests the possible presence of an oxy-arene interaction in organic solvent, but the interpretation of conformational differences from NMR data is ambiguous.

ACKNOWLEDGEMENTS

I would like to thank Professor Marcey Waters for her outstanding mentorship, support, and creativity.

I would like to thank my committee: Maurice Brookhart, Mike Gagne, Jeff Johnson, and Lee Pedersen for their guidance and insight.

I would also like to thank Marc ter Horst, Dave Harris, and Greg Young for lending a great deal of help with the NMR spectrometers.

Finally, I would like to thank my wife, Betsy, for her unfailing support of my professional studenthood. Without her help and patience, the completion of this dissertation would not have been possible.

TABLE OF CONTENTS

LIST OF TABLES

Table Page

LIST OF FIGURES

Figure Page

LIST OF SCHEMES

Scheme Page

ABBREVIATIONS

A	Alanine
ACN	Acetonitrile
Arg	Arginine
Asn	Asparagine
Asp	Aspartic Acid
Boc	t-Butoxycarbonyl
C	Cysteine
CD	Circular Dichroism
Cit	Citrulline
Cys	Cysteine
D	Aspartic Acid
Dab	Diaminobutyric Acid
DCM	Dichloromethane
DIPEA	Diisopropylethyl amine
DMF	Dimethylformamide
DSS	3-(Trimethylsilyl)-1-propanesulfonic acid sodium salt
E	Glutamic Acid
F	Phenylalanine
Fmoc	N-9-Fluorenylmethyloxycarbonyl
G	Glycine
Gln	Glutamine
Glu	Glutamic Acid

Gly	Glycine
H	Histidine
HBTU	2-(1H-Benzotriazole-1-yl)-1,1,3,3-tetramethyluronium hexafluorophosphate
His	Histidine
HOBT	N-hydroxybenzotriazole H_2O
HPLC	High Pressure Liquid Chromatography
I	Isoleucine
Ile	Isoleucine
K	Lysine
L	Leucine
Leu	Leucine
Lys	Lysine
M	Methionine
Met	Methionine
N	Asparagine
Nle	Norleucine
NMR	Nuclear Magnetic Resonance
O	Ornithine
Orn	Ornithine
P	Proline
Pbf	2, 2, 4, 6, 7-Pentamethyl-dihydrobenzofurane-5-sulfonyl
PEG	Polyethylene glycol
Phe	Phenylalanine

Pro	Proline
Q	Glutamine
R	Arginine
S	Serine
Ser	Serine
T	Threonine
tBu	t-Butyl
TFA	Trifluoroacetic acid
Thr	Threonine
TIPS	Triisopropyl silane
Trp	Tryptophan
Trt	Trityl
Tyr	Tyrosine
V	Valine
Val	Valine
W	Tryptophan
Y	Tyrosine

CHAPTER I

INTRODUCTION

i. Significance. Non-covalent interactions involving aromatic groups within proteins (π-π, cation-π, amide-π) are known to contribute to a wide array of biologically significant phenomena, including protein folding, protein-protein interactions, ligand binding, and protein-DNA interactions. The proposed importance of these interactions, relative to hydrophobic and hydrogen bonding interactions, is that they can retain both strength and specificity in solvent exposed environments, making them critical to numerous protein-mediated cell signaling pathways. Our goal is to quantify the magnitude and dynamics of these aromatic interactions using peptide models for protein structure in aqueous solution. By characterizing these interactions within an isolated model system, we are able to understand how they may individually contribute to overall protein structure and function. Through this work, we are able to see that indeed, non-covalent interactions with aromatic groups are critical to various aspects of protein folding, cellular signaling, and gene transcription.

ii. β-Hairpin peptides as model systems. Short peptides (<20 residues) that fold autonomously into monomeric, antiparallel β-sheet structures in aqueous solution have been known since the early 1990's.[1] Investigation of these types of structures was

[1] Gellman, S. H. *Curr. Opin. Struct. Biol.* **1998**, *2*, 717-725.

motivated by the prevalence of β-sheet motifs in protein structure, and the more poorly understood (relative to α-helices) factors contributing to their formation and stability. Since the discovery of these initial peptide sequences, much work has focused on elucidating the various contributions of β-turn and loop sequences, sidechain-sidechain interactions, and individual amino acid β-sheet propensities to the stability of the hairpin fold.[1,2,3] Additionally, as the field has matured, many attempts have been made to incorporate functionality into β-hairpins and β-sheet mimics, many of which mimic the behaviour of β-sheet motifs found in protein structures. Some of these discoveries include anti-microbial peptides, the design of receptors for nucleotides and other biologically relevant molecules, the design of model systems for β-sheet dependent disease states (i.e., Alzheimer's Disease), the incorporation of designed β-hairpin sequences into globular proteins, and their use in materials/nanotechnology applications.[3,4]

Still, even with the explosion of the field, one of the most valuable applications of β-sheet model systems, such as β-hairpin peptides, remains as a framework for studying the non-covalent interactions that guide protein folding, molecular recognition, and biomolecular interactions. These interactions range from such common motifs as

[2] Ramierz-Alvarado, M.; Kortemme, T.; Blanco, F. J.; Serrano, L. *Bioorg. Med. Chem.* **1999**, *7*, 93-103.

[3] Stotz, C. E.; Topp, E. M. *J. Pharm. Sci.* **2004**, *93*, 2881-2894.

[4] Hughes, R. M.; Waters, M. L. *Curr. Op. Struct. Biol.* **2006**, *16*, 514-524.

hydrogen bonding and salt-bridges[5] to more subtle interactions, such as π-π stacking, cation-π and amide-π interactions, to name a few.[6] As these interactions are often required to function in water-exposed environments *in vivo*,[7] the β-hairpin model system provides an ideal framework for their investigation and quantification in aqueous solution.

Some of the advantages of using β-hairpins as model systems for biologically relevant phenomena include their well-dispersed proton NMR spectra, which lends them analysis by conventional 1D and 2D NMR techniques, their two-state folding,[8] which gives them an important common ground with globular proteins and allows the quantification of free energies, and the presence of isolatable sidechain-sidechain interactions in both the diagonal and cross-strand positions. Furthermore, β-hairpins are readily synthesized through solid-phase peptide synthesis and amenable to study in aqueous solution.

iii. Some details regarding the structural analysis of β-Hairpin Peptides. It is important, at the outset, to briefly mention some of the methods of analysis used to investigate β-hairpin structure (additional details are provided in the Experimental Section at the end of each chapter). Of particular note is the turn sequence that nucleates

---

[5] a) Searle, M. S.; Griffiths-Jones, S. R.; Skinner-Smith, H., *J. Am. Chem. Soc.* **1999,** 121, (50), 11615-11620. b) Sharman, G. J.; Searle, M. S., *J. Am. Chem. Soc.* **1998,** 120, (21), 5291-5300.

[6] (a) Hughes, R. M.; Waters, M. L., *J. Am. Chem. Soc.* **2005,** *127*, 6518 - 6519. (b) Hughes, R. M.; Waters, M. L., *J. Am. Chem. Soc.* **2006**, *128*, 12735 - 12742. (c) Tatko, C. D.; Waters, M. L., *Prot. Sci.* **2003,** 12, 2443 - 2452. (d) Tatko, C. D.; Waters, M. L., *J. Am. Chem. Soc.* **2004,** 126, 2028 - 2034.

[7] Gallivan, J. P.; Dougherty, D. A. *Proc. Nat. Acad. Sci. USA* **1999**, *96*, 9459 – 9464.

[8] Streicher, W. W.; Makhatadze, G. I. *J. Am. Chem. Soc.* **2006**, *128*, 30–31.

a β-hairpin turn structure. In structurally biology, strands in β-sheets are often linked by loops and bulges of various length and amino acid composition. Turn sequences containing two amino acids are also present in protein structures, generally assuming Type I and Type II conformations (turn types based on the ϕ and ψ angles present in the turn), imbuing a left-handed twist to the β-turn, which opposes the right-handed twist of the strands (Figure 1.1). In the systems employed in this thesis, the turn types are Type I' (with inverse ϕ and ψ angles from the Type I turn sequence), thereby giving a right-handed twist to the hairpin sequence and resulting in a stable, isolated β-sheet.[1]

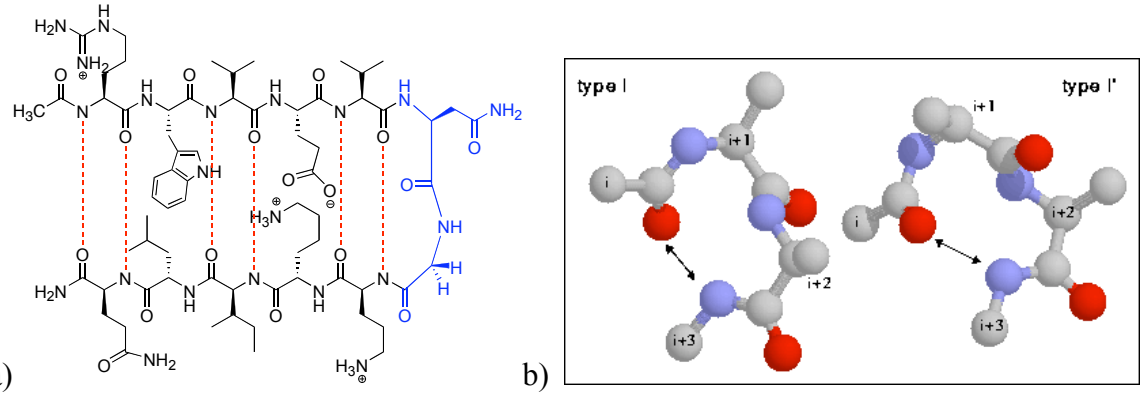

Figure 1.1. (a) Diagram of β-hairpin peptide. Hydrogen bonds shown in red. Turn residues shown in blue. (b) Type I and I' turns (source: http://e106.life.nctu.edu.tw/~hwhuang/dssp/type1turn.gif).

A number of methods are used to both confirm β-hairpin structure and quantify β-hairpin stability. To confirm structure, the chemical shifts of the H_α residues are measured and compared to random coil values. Relative chemical shifts of greater than 0.1 ppm are indicative of β-hairpin structure (Figure 1.2a). Additionally, the Type I' turn sequence is composed of the sequence Asn-Gly. The Gly sidechain protons are diastereotopic and their chemical shifts differ significantly in the β-hairpin conformation. The more rigid, or better folded, the hairpin, the greater the splitting is between the two

protons (Figure 1.2b). This difference, when compared to the splitting of the Gly protons in a cyclic β-hairpin (our approximation of the fully folded stated) has been shown to be an accurate indicator of the degree of β-hairpin structure.[9] Finally, the expected antiparallel hydrogen bonding pattern of a folded β-hairpin can be demonstrated through the shifts of backbone amide protons (Figure 1.2c). While used less frequently in this thesis to demonstrate β-hairpin structure, backbone amide shifts are also excellent indicators of whether the β-hairpin is folded within the correct register and can indicate the overall degree of structure of the hairpin.[10]

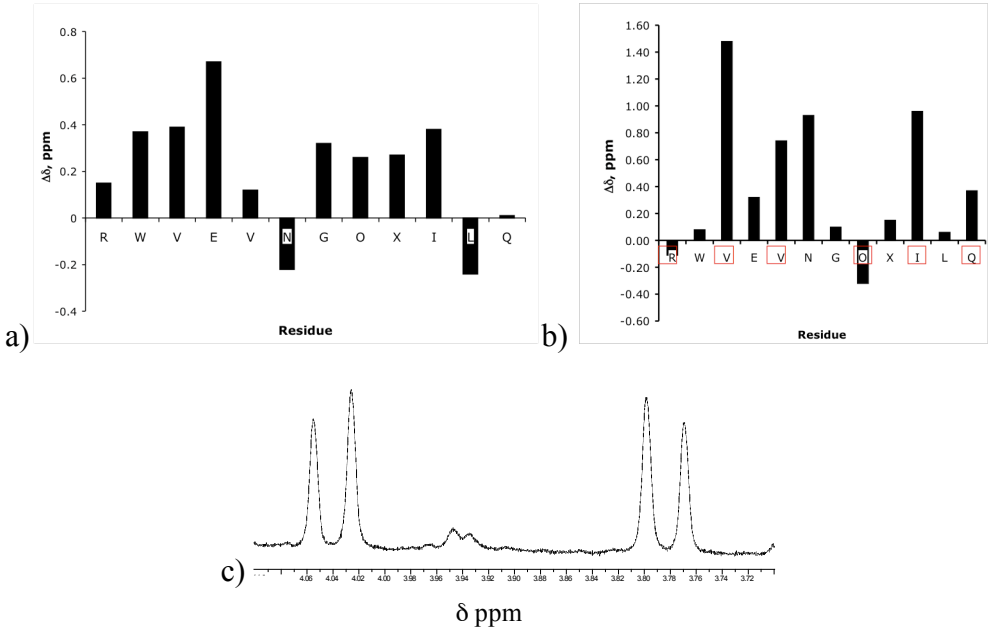

Figure 1.2. (a) Example H_α shifts for a 12-residue β-hairpin peptide. (b) Example backbone amide shifts from a β-hairpin peptide (hydrogen bonded sites in red squares). (c) Example Gly splitting from a Type I' Asn-Gly turn in a β-hairpin.

[9] Searle, M. S.; Griffiths-Jones, S. R.; Skinner-Smith, H. *J. Am. Chem. Soc.* **1999**, *121*, 11615-11620.

[10] Fesinmeyer, R. M.; Hudson, F. M.; Olsen, K. A.; White, G. W. N.; Euser, A.; Andersen, N. H. *Journal of Biomolecular Nmr* **2005,** 33, (4), 213-231.

NOEs are another common indicator of β-hairpin structure. They can show proximity between residues on opposing strands, indicating the presence of a folded state. However, their presence or absence must be evaluated carefully, as the lack of NOEs can be due to a folded, yet highly dynamic β-hairpin structure. As a result, even well-folded β-hairpins typically display critical NOEs and ROEs, but not an overabundance of them, in aqueous solution.

iv. Introduction to the Cation – π interaction. Of the numerous non-covalent interactions discussed in this thesis, the cation-π interaction is the most discussed and its early introduction will therefore serve as a springboard for the discussion of other interactions throughout the text. The presence and functionality of the cation-π interaction in structural biology is now an undisputed fact. This has been established through early statistical analyses by Burley and Petsko and by later, more detailed, work by Dougherty and co-workers.[11] The cation-π interaction is generally defined as a charge-quadrupole interaction between a positively charged species and an aromatic ring that is primarily electrostatic in nature.[11e,12] Additional factors such as charge-transfer, dispersion energies, and polarizabilities can contribute to the interaction, depending on its context.[11e] The electrostatic potential surfaces of both the cationic species and the aromatic species are generally the best way to visualize the potential for cation-π binding

[11] a) Burley, S. K.; Petsko, G. A., *FEBS Letters* **1986,** 203, 139 - 143. b) Burley, S. K.; Petsko, G. A., *Adv. Prot. Chem.* **1988,** 39, 125 - 189. c) Gallivan, J. P.; Dougherty, D. A., *Proc. Natl. Acad. Sci. USA* **1999,** 96, 9459 - 9464. d) Gallivan, J. P.; Dougherty, D. A., *J. Am. Chem. Soc.* **2000,** 122, 870 - 874. e) Ma, J. C.; Dougherty, D. A., *Chem. Rev.* **1997,** 97, 1303 - 1324.

[12] Minoux, H.; Chipot, C. *J. Am. Chem. Soc.* **1999**, *121*, 10366-10372.

(Figure 1.3a).[13] In the gas phase, the interaction has been measured to be stronger than various hydrogen bonding interactions.[11e] Additionally, the cation-π interaction has been demonstrated in the function of ion channels,[14] protein-ligand interactions,[15] and protein-DNA interactions.[16] In protein structures, the cation-π interaction is found between positively charged sidechains (Lys, Arg) and aromatic groups (Phe, Trp, Tyr). Among the potential participants in proteogenic cation-π interactions, Trp has been shown to bind more tightly to cations than either phenylalanine or tyrosine.[17] Specific examples of the cation-π in biology include the operation of acetylcholine esterase and the nicotinic acetylcholine receptor, both of which use pockets of aromatic residues to bind acetylcholine (Figure 1.3b).[11e]

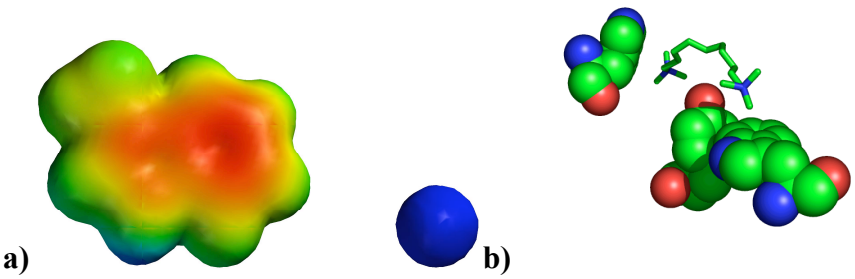

Figure 1.3. a) Electrostatic potential maps showing the predicted binding site of a cation-π binding pair (indole ring and alkali metal cation; MacSpartan 2004; range: -30 to +60 kcal/mol). (b) Key cation-aromatic contacts from structure of decamethonium bound to acetylcholine esterase (PDB ID: 1ACL).

---

[13] Mecozzi, S.; West, A. P.; Dougherty, D. A. *Proc. Nat. Acad. Sci. USA* **1996,** 93, (20), 10566-10571.

[14] Kumpf, R. A.; Dougherty, D. A. *Science* **1993**, *261*, 1708-1710.

[15] a) Susman, J. L.; Harel, M.; Folow, f.; Oefner, C.; Goldman, A.; Toker, L.; Silman, I. *Science* **1991**, *253*, 872-879. b) Zhong, W.; Gallivan, J. P.; Zhang, Y.; Li, L.; Lester, H. A.; Dougherty, D. A. *Proc. Nat. Acad. Sci. USA* **1998**, *95*, 12088-12093. c) Satow, Y.; Cohen, G. H.; Padlan, E. A.; Davis, D. R. *J. Mol. Biol.* **1986**, *190*, 593-604.

[16] Wintjens, R.; Lievin, J.; Rooman, M.; Buisine, E. J. Mol. Biol. **2000**, *302*, 395-410.

[17] a) Shepodd, T. J.; Petti, M. A.; Dougherty, D. A. *J. Am. Chem. Soc.* **1988**, *110*, 1983-1985. b) Okada, A.; Miura, T.; Takeuchi, H. *Biochemistry* **2001**, *40*, 6053-6060.

While the cation-π interaction is a firmly established phenomenon in structural biology, our model systems are useful in demonstrating the magnitude, orientation, and selectivity of the cation-π interaction in a solvent exposed environment. For example, research in the Waters group has demonstrated the orientation and magnitude of cation-π interactions between Lys-Trp, Lys-Phe, and Arg-Trp pairs within β-hairpin and α-helical model systems in aqueous solution.[18]

Model systems enable the quantification of the interaction through studies that might not be feasible using complex proteins. Additionally, computational models tend to overestimate the magnitude of the interaction, so our data is a valuable benchmark for the accuracy of various theoretical models of solvation.[19,12] It is important to note that optimized geometries calculated for cation-π interactions in the gas phase are different than those observed experimentally in aqueous solution (For instance, stacking is observed experimentally between Arg and Trp, while gas phase calculations favor T-shaped orientations) (Figure 1.4a). This phenomenon has been neglected in a number of papers that pair gas-phase optimized geometries with various solvation models in order to estimate binding energies in solution.[11d,20] For instance, the orientation of a methylammonium ion bound to an aromatic ring occurs through N-H----π interactions in the gas phase, but through C-H----π interactions in aqueous solution (Figure 1.4b).

---

[18] a) Tatko, C. D.; Waters, M. L., *J. Am. Chem. Soc.* **2004,** 126, (7), 2028-2034. b) Tatko, C. D.; Waters, M. L., *Protein Science* **2003,** 12, (11), 2443-2452. c) Tsou, L. K.; Tatko, C. D.; Waters, M. L., *J. Am. Chem. Soc.* **2002,** 124, (50), 14917-14921.

[19] Slutsky, M. M.; Marsh, E. N. G. *Prot. Sci.* **2004**, *13*, 2244-2251.

[20] Minoux, H.; Chipot, C. *J. Am. Chem. Soc.* **1999**, *121*, 10366-10372.

Numerous examples of this interaction in aqueous solution are demonstrated within this thesis.

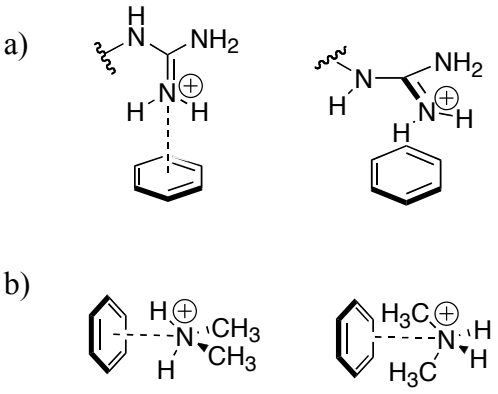

Figure 1.4. a) (above) T-shaped and stacking orientations of Arg with aromatic ring. (b) (below) N-H and C-H orientations of dimethylammonium group with aromatic ring.

v. Introduction to Post-translational Modifications. Since many of the non-covalent interactions explored in this work occur within the biological context of post-translational modifications of proteins and, more specifically, the post-translational modification of histone tails, some attempt will be made to introduce the extremely broad field of post-translational modifications and their relevance to the oft bandied-about "histone code". Post-translation modifications occur in both eukaryotic and prokaryotic organisms, and include phosphorylation, methylation, acylation, ubiquitination, and glycosylation, among others.[21] They run the gamut of functionality, and are involved in processes ranging from signaling (phosphorylation and acylation where reversibility is paramount) to targeting (glycosylation points proteins towards the lysosome) to tagging proteins for degradation (ubiquitination). [22]

[21] Zhang, Y.; Reinberg, D. Genes & Development 2001, 15, 2343-2360.

[22] (a) Strahl, B. D.; Allis, D. C. Nature, 2000, 403, 41-45. (b) Shilatifard, A. Annu. Rev. Biochem. 2006, 75, 243-269.

Histones (H3, H4, H2A, H2B) are the protein framework for packaging genetic material (DNA) (Figure 1.5). Originally thought to be primarily structural, it is now apparent that histone proteins are actively involved in controlling the activity of DNA, and in the switch from inactive genetic material (heterochromatin) to actively transcribed genetic material (euchromatin).[22a] Whilst DNA is wrapped around a core of histone proteins in the nucleosome, peptide tails extend from the histone protein core into solution, making them available for post-translational modification by a variety of enzymatic processes. Modifications of these tails have a number of different effects: Acylation of lysine is thought to negate the favorable electrostatic interaction between lysine and the phosphate backbone of DNA, resulting in the loosening of chromatin structure, making it available for transcription. Other modifications, such as methylation of lysine, cause the recruitment of other proteins through specific binding interactions with the modified histone tail, resulting in further condensation of the chromatin. These modifications do not occur in isolation, and are therefore thought to work together in an elaborate signaling pathway that is commonly deemed the "histone code". The code, as it were, specifies when and where various portions of the genetic material are transcribed. Numerous modifications, functioning in concert, are thought to amplify the transcription signal, thereby increasing the efficiency of this complex process.

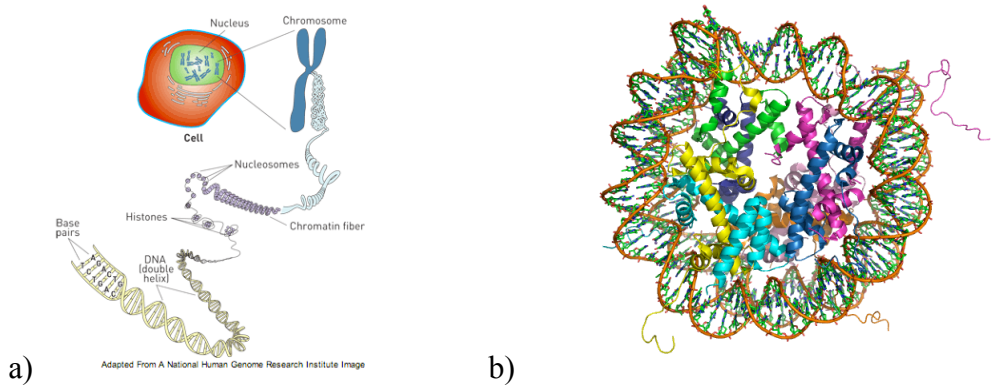

a) b)

Figure 1.5. (a) Packaging of DNA within the nucleus. (b) Crystal structure of a histone-DNA complex (1EQZ).

vi. Conclusion. Since it is clear that non-covalent interactions are important to the function of histone tails, a primary thrust of this thesis is to isolate and study some of the potentially most important interactions within an isolated model system. As described earlier, the β-hairpin peptide provides an ideal framework for such an investigation. Therefore, a number of transcriptionally relevant non-covalent interactions (cation-π, amide-π, etc.) have been selected for investigation within the context of a β-hairpin model system. It is our goal to quantitate the magnitude of these interactions in a solvent exposed environment, and to describe their effects on the two-state folding dynamics of the β-hairpin. Hopefully this leads to a better understanding of the fundamental forces underlying the behaviour of modified histone proteins. Furthermore, this document contains tangentially related studies of the cation-π interaction in a small-molecule model system, and studies on the binding of ATP with a β-hairpin receptor. These studies are also carried out with the same goal, to enhance our understanding of the non-covalent interactions that can determine both orientation and function in molecular systems, and to serve as a source of knowledge and inspiration for the design of future model systems.

CHAPTER II

CATION-π INTERACTIONS AND THE EFFECTS OF N-METHYLATION OF THE CATION

(Reproduced, in part, with permission from Hughes, R.M.; Waters, M.L. *J. Am. Chem. Soc.* **2005**, *127*, 6518 – 6519 *and* Hughes, R.M.; Waters, M.L. *J. Am. Chem. Soc*. **2006**, *128*, 12735 – 12742.)

A. Lysine methylation and the cation-π interaction.

i. Background and significance.

The role of the cation-π interaction between a cationic residue (lysine or arginine) and an aromatic residue (tryptophan, tyrosine, or phenylalanine) in proteins is a topic of continuing interest due to its relevance to protein structure,[1] the mediation of protein-protein interactions,[2] and protein-ligand interactions.[1] These interactions have been observed in statistical analyses of protein structures[1] and even in *de novo* designed proteins.[3] Post-translational modifications of cationic residues in proteins play important roles in cellular processes through the mediation of protein-protein interactions. One

---

[1] (a) Ma, J. C.; Dougherty, D. A. *Chem. Rev.* **1997**, *97*, 1303-1324. (b) Gallivan, J. P.; Dougherty, D. A. *Proc. Nat. Acad. Sci.* **1999**, *96*, 9459-9464.

[2] Crowley, P.B.; Golovin, A. *Prot. Struct. Funct. Bioinform.* **2005**, *59*, 231-239.

[3] Dai, Q.; Tommos, C.; Fuentes, E. J.; Blomberg, M. R. A.; Dutton, P. L.; Wand, A. J. *J. Am. Chem. Soc.* **2002**, *124*, 10952 – 10953.

example of this phenomenon is the methylation of lysine in histone proteins. The methylation of lysine in histone proteins is a post-translational modification that functions in the histone modulated process of chromatin condensation.[4] This phenomenon is associated with epigenetic silencing and, in a broader sense, has implications for designed mediators of protein-protein interactions. In particular, the methylated lysines in histone tails have been shown to trigger protein-protein interactions with several proteins containing the chromodomain. In each case, the binding of the $Lys(Me)_n^+$ (n = 1-3) occurs in an aromatic pocket composed of three aromatic sidechains, suggesting that cation-π interactions are important for selective recognition of the N-methylated sidechain.[4(d)] In general, the binding of small molecules containing quaternary ammonium ions in protein binding pockets lined with aromatic residues, such as the binding of acetylcholine to acetylcholine esterase, is a well known event in structural biology and has been utilized in seminal studies of molecular recognition.[5]

We have previously reported a β-hairpin peptide that is stabilized by a specific cation-π interaction between Trp2 and Lys9 in which the ε-methylene of Lys9 is packed

[4] (a) Lindroth, A. M.; Shultis, D.; Jasencakova, Z.; Fuchs, J.; Johnson, L.; Schubert, D.; Patnaik, D; Pradhan, S.; Goodrich, J.; Schubert, Il; Jenuwein, T.; Khorasanizadeh, S.; Jacobsen, S. E. *Embo. J.* **2004**, *23*, 4286 – 4296. (b) Khorasanizadeh, S. *Biophysical J.* **2003**, *84*, 485A. (c) Jacobs, S.; Harp, J.; Khorasanizadeh, S. *Biophysical J.* **2003**, *84*, 503A. (d) Fischle, W.; Wang, Y. M.; Jacobs, S. A.; Kim, Y. C.; Allis, C. D.; Khorasanizadeh, S. *Genes and Development* **2003**, *17*, 1870 – 1881. (e) Jacobs, S. A.; Khorasanizadeh, S. *Science* **2002**, *295*, 2080 – 2083.

[5] (a) Scharer, K.; Morgenthaler, M.; Paulini, R.; Obst-Sander, U.; Banner, D.W.; Schlatter, D.; Benz, J.; Stihle, M.; Diederich, F. *Angew. Chem. Int. Ed.* **2005**, 44, 2-6. (b) Kearney, P.C.; Mizoue, L.S.; Kumpf, R.A.; Forman, J.E.; McCurdy, A.E.; Dougherty, D.A. *J. Am. Chem. Soc.* **1993**, 115, 9907-9919. (c) McCurdy, A.; Dougherty, D.A. *J. Am. Chem. Soc.* **1992**, 114, 10314-10321.

against the face of the aromatic ring.[6] In our current study, we investigate the effects of lysine methylation on the magnitude of this cation-π interaction and the stability of the designed β-hairpin. We wish to use our designed β-hairpin as a model system for Lys methylation in histone proteins, because, as previously discussed, the methylation of lysine is known to trigger binding to aromatic pockets in chromodomain proteins. By characterizing the interaction between methyl Lys and Trp, and comparing it to our data for the Lys-Trp interaction, we hope to gather more detailed information about the nature of the cation-π interaction in structural biology, and to observe how post-translational modification may alter its dynamics and magnitude in biological systems.

ii. Results and Discussion.

a) Design. Peptides **WK** and **WKMe3** (Figure 2.1) possess a Trp residue that is oriented diagonally with respect to a cationic residue. We have previously shown that when X = Lys, these two residues are in close proximity and interact in a favorable manner via a cation-π interaction, resulting in stabilization of the folded peptide.[6] The overall charge of peptides **WK** and **WKMe3** is +3, lending increased water solubility and decreased aggregation to both. The peptides also include an Asn-Gly sequence, which has been shown to promote hairpin formation via a type I' turn.[7] The peptides were synthesized by Fmoc solid phase peptide synthesis, with the trimethylated lysine hairpin synthesized following the procedure of Kretsinger and Schneider.[8] Peptides were

[6] (a) Tatko, C. D.; Waters, M. L. *Protein Science* **2003**, *12*, 2443 – 2452. (b) Tatko, C. D.; Waters, M. L. *J. Am. Chem. Soc.* **2004**, *126*, 2028 – 2034.

[7] Griffiths-Jones, S. R.; Maynard, A. J.; Sharman, G. J.; Searle, M. S. *Chem. Commun.* **1998**, 789 – 790.

[8] Kretsinger, J. T.; Schneider, J. P. *J. Am. Chem. Soc.* **2003**, *125*, 7907 – 7913.

characterized by MALDI mass spectrometry and NMR as reported previously.[6] Numerous NOEs between cross-strand pairs of sidechains were observed, consistent with β-hairpin formation (See Experimental Information).

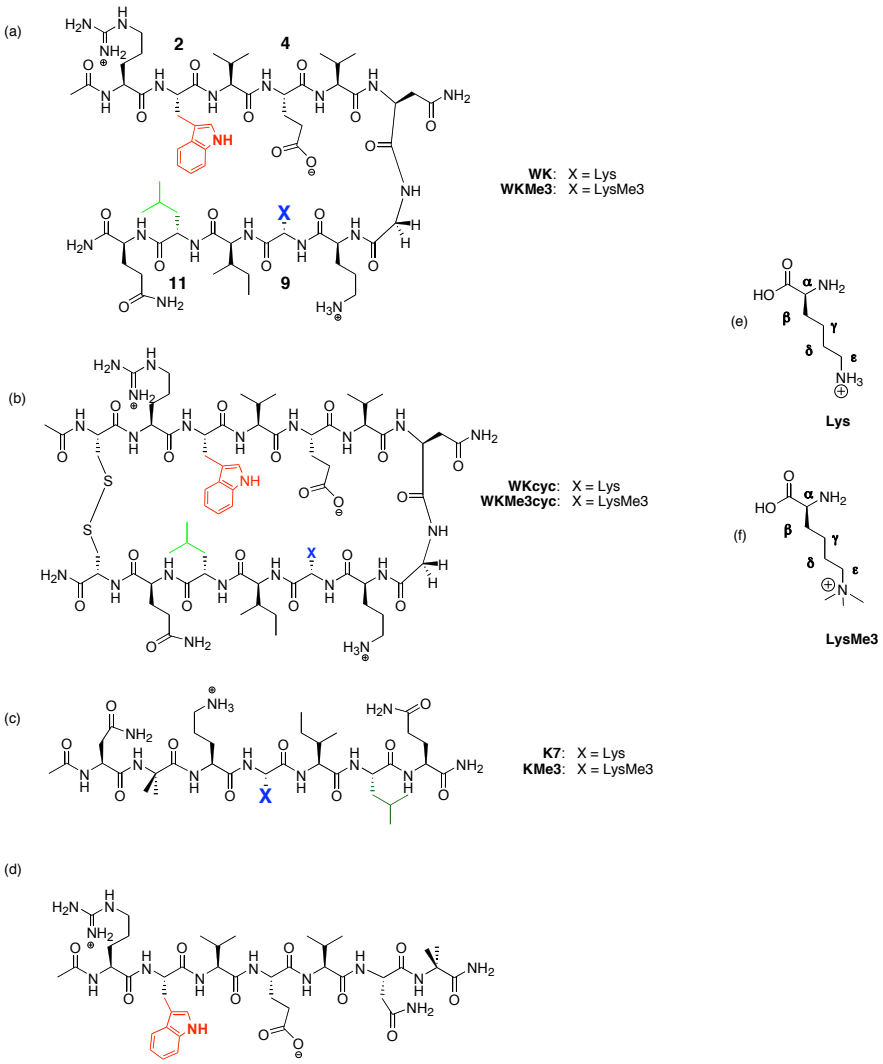

Figure 2.1. (a) β-hairpin peptides **WK** and **WKMe3**. (b) Control peptides for the fully folded state cyclised with a Cys disulfide bond. (c) and (d) Control peptides for the unfolded state. (e) and (f) Lys and LysMe3 sidechains.

Both downfield shifting of the β-sheet H_α protons and the separation of the Gly H_α protons have been shown to correlate with the extent of folding in β-hairpins.[9] Inspection of the H_α chemical shifts relative to unfolded controls indicates that both peptides **WK** and **WKMe3** take on a β-hairpin structure, (Figure 2.2) as downfield shifting of the strand residues by ≥ 0.1 ppm is taken to represent a well-folded β-hairpin.[9b] Moreover, the H_α shifts indicate peptide **WKMe3** is more folded than peptide **WK** at all positions along the strand, with the exception of the residues nearest the termini, which are typically frayed.[10]

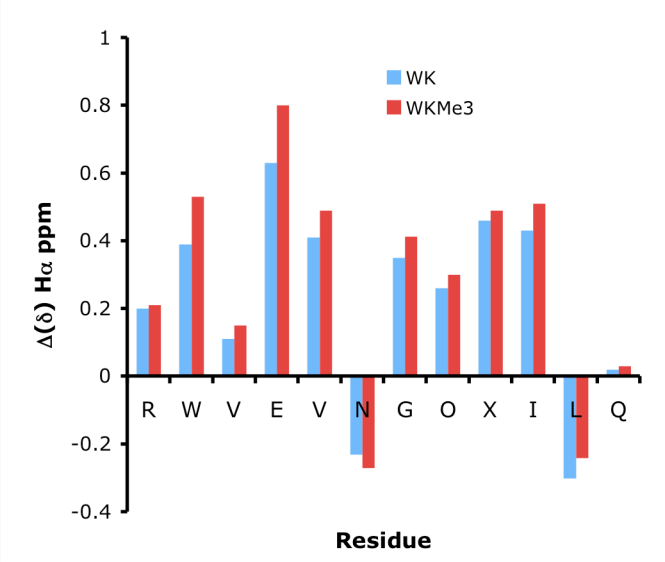

Figure 2.2. H_α shifts of peptides **WK** and **WKMe3**. The Gly bars reflect the H_α separation in the hairpin.

[9] (a) Maynard, A. J.; Sharman, G. J.; Searle, M. S. *J. Am. Chem. Soc.* **1998**, *120*, 1996 – 2007. (b) Griffiths-Jones, S. R.; Maynard, A. J.; Searle, M. S. *J. Mol. Biol.* **1999**, *121*, 11577 – 11578.

[10] Note that H_α for Asn 6 is upfield shifted due to its position in the turn, and H_α for Leu 11 is upfield shifted due to ring current effects by the cross-strand Trp residue.

The extent of folding of peptides **WK** and **WKMe3** was quantified from the Gly H_α splitting relative to the fully folded and random coil control compounds, peptides **3**-**7**, as described previously (Eqn 1).[6] Peptides **WK** and **WKMe3** are found to be 78% and 92% folded, respectively.[11] This translates into ΔG_f values of -0.75 and -1.45 kcal/mol. Hence, methylation increases the overall stability of the β-hairpin by about 0.7 kcal/mol. This is significant given the modest changes in the hairpin structure.

$$\% \text{ folded} = [\delta_{obs} - \delta_0]/ [\delta_{100} - \delta_0] \times 100 \qquad [\mathbf{1}]$$

b) Interaction Energies. Double mutant cycles were performed to determine the magnitude of the sidechain-sidechain interaction in isolation. Double mutant cycles are necessary because in each of the single mutants the Lys···Trp interaction is disrupted, but other changes occur as well, such as the β-sheet propensities of the substituted residues. A double mutant containing corrects for any of the unintentional changes, such that the magnitude of the KMe3···Trp interaction can be determined as shown in Figure 2.3. Using the same substitutions at positions 2 and 9 that were reported previously for the parent peptide, **WK**: Val was substituted for Trp at position 2 and Ser was substituted for KMe3 at position 9 (Figure 2.3).[29] Analysis of the sidechain-sidechain interaction via double mutant cycles,[12] using Val and Ser as the control residues in positions 2 and 9,[6]

[11] The fraction folded as determined by the average Hα shift corresponds very well to that of the Gly splitting, with values of 77% and 90% for peptides **WK** and **WKMe3**, respectively. See reference 6 and Experimental Section.

[12] (a) Blanco, F. J.; Serrano, L. *Eur. J. Biochem.* **1995**, *230*, 634 – 649. (b) Sharman, G. J.; Searle, M. S. *J. Am. Chem. Soc.* **1998**, *120*, 5291 – 5300. (c) Searle, M. S.; Griffiths-

gives a value of -0.3 ± 0.1 kcal/mol for the Lys···Trp interaction and -1.0 ± 0.1 kcal/mol for the $Lys(Me)_3^+$···Trp interaction. Thus, the change in stability of the β-hairpin is primarily due to the increase in the magnitude of the cation-π interaction upon methylation.

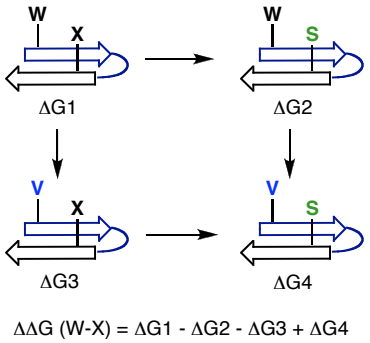

Figure 2.3. Double mutant cycle to measure the interaction energy between Trp and residue X.

c) Analysis of Interaction Geometry. We have previously demonstrated that the Lys residue of peptide **WK** interacts preferentially with the face of the Trp ring through its polarized ε-methylene group (Figure 2.4).[6] Analysis of the KMe3 sidechain upfield shift from peptide **WKMe3** indicates there is significant interaction of both the ε-methylene and its methylammonium group with the indole ring (Figure 2.5). In peptide **WK,** the ε-methylene group is upfield shifted by 0.4 ppm, whereas in peptide **WKMe3**, it is shifted by almost 1 ppm. The methyl groups in KMe3 are also significantly shifted by almost 0.6 ppm, indicating they are also in close proximity to the face of the indole ring. We propose an interaction geometry for the Lys-Trp pairs such as that shown in Figure 2.4.

Jones, S. R.; Skinner-Smith, H. *J. Am. Chem. Soc.* **1999**, *121*, 11615 – 11620. (d) Shi, Z. S.; Olson, C. A.; Kallenbach, N. R. *J. Am. Chem. Soc.* **2002**, *124*, 3284 – 3291.

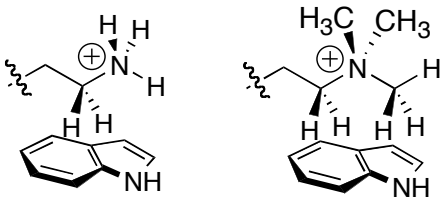

Figure 2.4. Possible interaction geometries for Trp···Lys and Trp···Lys(Me$_3$)$^+$ interactions.

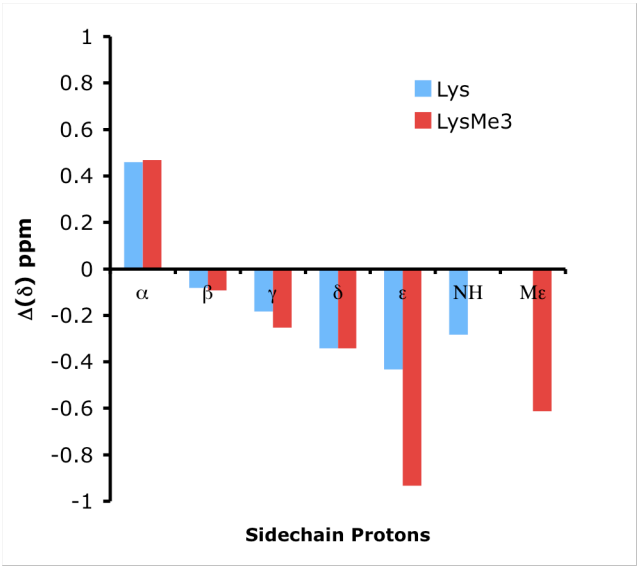

Figure 2.5. Side chain chemical shifts of Lys (peptide **WK**) and Lys(Me)$_3^{\oplus}$ (peptide **WKMe3**).

The Leu11 sidechain, which is cross-strand from Trp, is also significantly upfield shifted at its γ and δ positions, indicating packing against the Trp ring (Figure 2.6). However, the degree of upfield shifting of the Leu changes little between peptides **WK** and **WKMe3**, indicating that, as a whole, the peptide experiences only minor conformational changes upon methylation of the Lys residue.

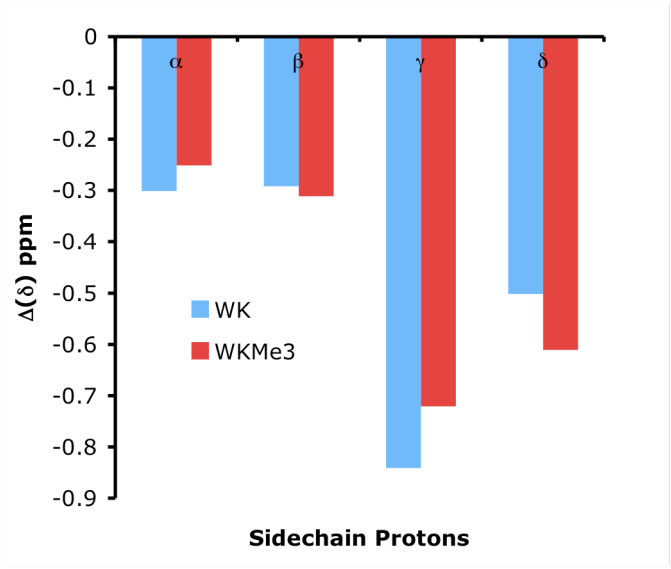

Figure 2.6. Leu sidechain upfield shifts.

Thermal denaturation of peptides **WK** and **WKMe3** reveal that methylation of Lys results in a remarkably thermally stable β-hairpin (Figure 2.7a). Other reported well-folded β-hairpins with high thermal stabilities such as trpzip4 (sequence: GEWTWDDATKTWTWTE-NH_2)[13] and HP5W4 (sequence: KKWTWNPATGKWTWQE)[14] have similar stabilities at 298 K (92% and 96% folded, respectively) to peptide **WKMe3**. However, both denature more quickly at higher temperatures. For example, at 75°C, peptide **WKMe3** is 74% folded, while trpzip 4 is about 40% folded and HP5W4 about 60% folded. This implies that peptide **WKMe3** has a higher melting temperature than either previously reported sequence. Notably, peptide

[13] Cochran, A. G.; Skelton, N. J.; Starovasnik, M. A. *PNAS* **2001**, *98*, 5578 – 5583.

[14] Fesinmeyer, R. M.; Hudson, F. M.; Andersen, N. H. *J. Am. Chem. Soc.* **2004**, *126*, 7238 – 7234.

WKMe3 accomplishes high thermal stability without the four Trp cluster that stabilizes both trpzip4 and HP5W4.

Fitting of the thermal denaturation of peptides **WK** and **WKMe3** with a non-linear form of the van't Hoff equation indicates that the trimethylation of Lys makes the folding of peptide **WKMe3** more entropically favorable and less enthalpically favorable than folding of the unmethylated peptide (Table 2.1).[9] It appears that the methylation of Lys creates a tighter hydrophobic cluster with Trp, resulting in a stonger entropic driving force for folding, as evidenced by the observed enhancement of the cation-π interaction. Additionally, methylation of lysine increases the number of potential sites of favorable interaction with Trp. This is also reflected in the stronger entropic driving force. It is important to note that the folding of **WKMe3** still retains a favorable, though diminished enthalpic term. This would support the notion of hydrophobically-enhanced yet still electrostatically viable cation-π interaction between Trp and KMe3 being the primary source of hairpin stability. The increased strength of the cation-π interaction between tetraalkylammonium guests and cyclophane hosts versus dialkylammonium guests in aqueous solution has been documented by Dougherty and co-workers.[15] This effect has been attributed to the added hydrophobic component to the cation-π interaction upon increased methylation of the cation, which is in agreement with our thermodyamic analysis of peptides **WK** and **WKMe3**.

[15] (a) Kearney, P. C.; Mizoue, L. S.; Kumpf, R. A.; Forman, J. E.; McCurdy, A. E.; Dougherty, D. A. *J. Am. Chem. Soc.* **1993**, *115*, 9907 – 9919. (b) McCurdy, A.; Jimenez, L.; Stauffer, D. A.; Dougherty, D. A. *J. Am. Chem. Soc.* **1992**, *114*, 10314 – 10321.

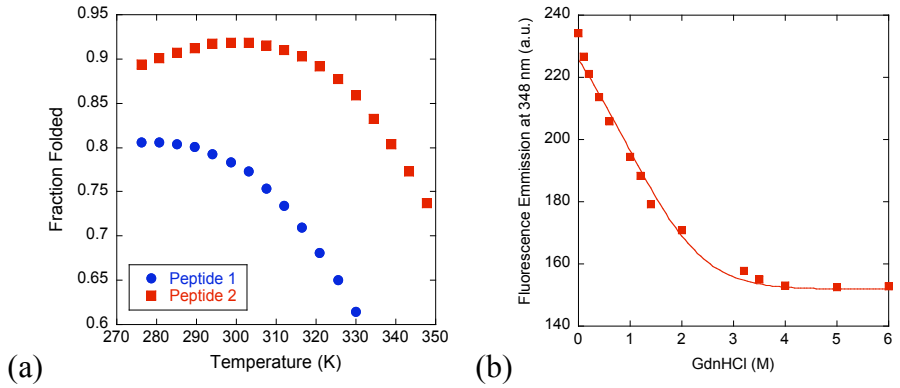

Figure 2.7. (a) Thermal denaturation of peptides **WK** (circles) and **WKMe3** (squares). (b) Chemical denaturation of peptide **WKMe3** as determined by change in Trp fluorescence.

Table 2.1. Thermodynamic Parameters[a] for Folding at 298 K[10]

Peptide	ΔH° (kcal/mol)	ΔS° (cal/mol K)	ΔC_p° (cal/mol K)
WK	-2.8	-6.8	-163
WKMe3	-0.2	4.3	-241

[a] Determined from the temperature dependence of the Gly chemical shift from 0 to 60 °C for peptide **WK** and from 0 to 80 °C for peptide **WKMe3**.

We also performed a chemical denaturation of the β-hairpin with GdnHCl (Figure 2.7b). This denaturation plot clearly demonstrates the two-state nature of folding. Fitting results in a ΔG_f of –1.3 kcal/mol with m = 0.8.[16] This is in reasonable agreement with the ΔG_f determined from Gly chemical shifts, particularly given the error associated with the chemical denaturation.

[16] Kortemme, T.; Ramirez-Alvarado, M.; Serrano, L. *Science* **1998**, *281*, 253 – 256. (b) Pace, C. N. *Methods in Enzymology* **1986**, *131*, 266 – 280.

iii. Conclusions.

In conclusion, an investigation of the influence of Lys methylation on a cation-π interaction has resulted in the synthesis of an extremely stable β-hairpin peptide. Trimethylation enhances the interaction of Lys with Trp by about 0.7 kcal/mol. In agreement with this data, NMR shows enhanced upfield shifting of the Lys sidechain upon methylation, particularly at the ε and N-methylated sites. This indicates that the orientation of the Lys with respect to the Trp remains the same upon methylation, but that the two sidechains form a tighter hydrophobic cluster. This is consistent with our thermal denaturation data, which reveals a greater entropic driving force for folding upon Lys methylation, with the retention some degree of enthalpic favorability. Hence, the methylation of lysine results in a hydrophobically-enhanced cation-π interaction. We expect that further exploration of this sequence will not only help elucidate the role of Lys methylation in the function of histone tails, but also will be of use to the engineering of β-turns in designed proteins and mediators of protein-protein interactions. Investigation of the incremental effects of Lys monomethylation and dimethylation will be discussed later in this chapter.

B. ARGININE METHYLATION AND THE CATION-π INTERACTION

i. Background and significance.

Arginine methylation is a common post-translational modification that has recently been identified as playing a significant role in the regulation of cellular processes.[17] Both arginine (Arg) mono- and dimethylation have been shown to play a role in cell signaling through mediation of protein-protein interactions.[18] In particular, methylated arginines have been shown to function, in concert with other post-translational modifications, in chromatin restructuring and transcriptional activation.[17b] There is still little structural information on record for methylated arginine, and so little is known about how such a subtle change in structure may mediate biomolecular recognition and signaling. However, several recent studies of proteins containing dimethylarginine, DMA, as well as recent structural information on the role of the related posttranslational modification trimethyllysine, KMe3, in protein-protein interactions suggests a possible mechanism for recognition of the modified amino acid: the specific recognition of methylated arginine may depend on its interaction with aromatic rings (Figure 2.8). For example, the Tudor domain, a common 60 amino acid protein domain with highly conserved tryptophan, tyrosine, and phenylalanine residues, has been shown to bind preferentially to symmetrically methylated arginine-containing proteins.[19] In the

---

[17] (a) McBride, A.E.; Silver, P.A. *Cell*, **2001**, *106*, 5-8. (b) Lee, D.Y.; Teyssier, C.; Strahl, B.D.; Stallcup, M.R. *Endocrine Reviews* **2005**, *26*, 147-170. (c) Bedford, M. T.; Richard, S. *Molecular Cell* **2005**, *18*, 263-272.

[18] Cosgrove, M.S.; Boeke, J.D.; Wolberger, C. *Nat. Struct. Mol. Biol.* **2004**, *11*, 1037-1043.

[19] Cote, J.; Richard, S. *J. Biol. Chem.* **2005**, *280*, 28476-28483.

two examples of methylated arginine in the Protein Data Bank, it is found to stack with a tryptophan residue in a histone/chromodomain protein complex (Figure 2.8b)[20] and with an iron-containing heme (not shown).

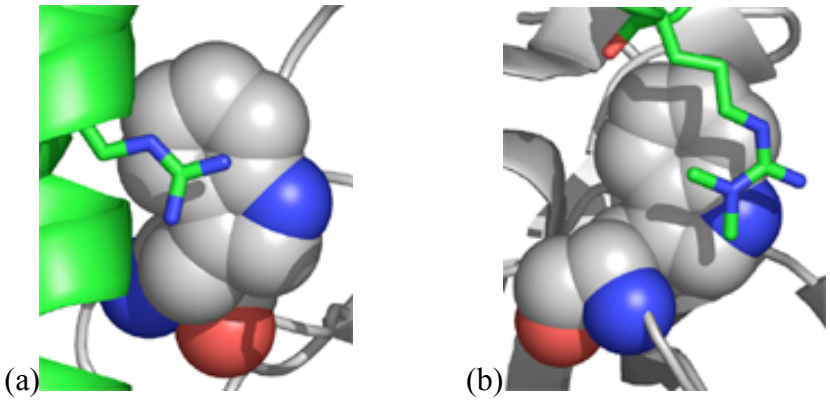

Figure 2.8. (a) Arg-Trp pair in typical cation-π geometry (Human growth hormone and receptor complex: 3HHR).[21] (b) DMAa-Trp pair from histone H3-chromodomain complex (2B2U).[20]

There is significant precedence for Arg stacking with aromatic residues. In surveys of protein crystal structures, cation-π interactions are often observed between the guanidine groups of arginine sidechains and the aromatic rings of tyrosine, tryptophan, and phenylalanine (Figure 2.8a).[22] Gallivan and Dougherty's survey of 593 protein crystal structures found that about 74% of arginine residues are in close proximity to an aromatic

[20] Flanagan IV, J.F.; Mi, L.-Z.; Chruszcz, M.; Cymborowski, M.; Clines, K.L.; Kim, Y.; Minor, W.; Rastinejad, F.; Khorasanizadeh, S. *Nature* **2005**, *438*, 1181-1185.

[21] de Vos, A.M.; Ultsch, M.; Kossiakoff, A.A. *Science* **1992**, *255*, 306-312.

[22] (a) Burley, S.K.; Petsko, G.A. *FEBS Letters* **1986**, *203*, 139-143. (b) Flocco, M. M.; Mowbray, S. L. *J. Mol. Biol.* **1994**, *235*, 709-717. (c) Mitchell, J. B. O.; Nandi, C. L.; McDonald, I. K.; Thornton, J. M.; Price, S. L. *J. Mol. Biol.* **1994**, *239*, 315-331. (d) Gallivan, J. P.; Dougherty, D. A. *Proc. Natl. Acad. Sci. USA* **1999**, *96*, 9459-9464.

sidechain, compared to 43% for Lys.[22d] This statistical preference is due to arginine's unique ability to interact with aromatic rings with a hybrid of the cation-π and π-π stacking interactions, which lends both favorable dispersion and electrostatic character to the interaction without a significant desolvation penalty. Additional surveys of protein structures have identified a specific preference for the stacking of arginine residues with the 6-membered portion of the tryptophan indole ring.[23] Cation-π interactions involving arginine have been identified and investigated within the context of protein structure[22,24] and ligand binding,[25] protein-protein[26] and protein-nucleotide interactions,[27] peptide folding,[28,29] and in model receptor systems.[30] As with Lys, methylation of Arg may

---

[23] (a) Broccheiri, L.; Karlin, S. *Proc. Nat. Acad. Sci. USA* **1994**, *91*, 9297-9301. (b) Karlin, S.; Zuker, M.; Brocchieri, L. *J. Mol. Biol.* **1994**, *239*, 227-248.

[24] (a) Wei, Y.; Horng, J.; Vendel, A.C.; Raleigh, D.P.; Lumb, K.J. *Biochemistry* **2003**, *42*, 7044-7049. (b) Luque, L.E.; Grape, K.P.; Junker, M. *Biochemistry* **2002**, *41*, 13663-13671. (c) St. Charles, R.; Padmanabhan, K.; Arni, R.V.; Padmanabhan, K.P.; Tulinsky, A. *Protein Sci.* **2000**, *9*, 265-272.

[25] (a) Cumpstey, I.; Sundin, A.; Leffler, H.; Nilsson, U. J. *Angew. Chem. Int. Ed.* **2005**, *44*, 5110-5112. (b) Woods, A. S. *J. Proteome Res.* **2004**, *3*, 478-484. (c) Pellequer, J.; Zhao, B.; Kao, H.; Bell, C.W.; Li, K.; Li, Q.X.; Karu, A. E.; Roberts, V.A. *J. Mol. Biol.* **2000**, *302*, 691-699.

[26] Crowley, R.B.; Golovin, A. *Proteins: Struct. Funct. Bioinform.* **2005**, *59*, 231-239.

[27] (a) Kumaki, Y.; Nitta, K.; Hikichi, K.; Matsumoto, T.; Matsushima, N. J. *Biochemistry* **2004**, *136*, 29-37. (b) Wintjens, R.; Lievin, J.; Rooman, M.; Buisine, E. *J. Mol. Biol.* **2000**, *302*, 395-410.

[28] Shi, Z. S.; Olson, C. A.; Kallenbach, N. R. *J. Am. Chem. Soc.* **2002**, *124*, 3284-3291.

[29] Tatko, C. D.; Waters, M. L. *Pro. Sci.* **2003**, *12*, 2443-2452

[30] (a) Ngola, S.M.; Kearney, P.C.; Mecozzi, S.; Russell, K.; Dougherty, D. A. *J. Am. Chem. Soc.* **1999**, *121*, 1192 – 1201. (b) Rensing, S.; Arendt, M.; Springer, A.; Grawe, T.; Schrader, T. *J. Org. Chem.* **2001**, *66*, 5814-5821. (c) Thompson, S.E.; Smithrud, D.B. *J. Am. Chem. Soc.* **2002**, *124*, 442-449. (d) Nishihara, M.; Perret, F.; Takeuchi, T.; Futaki, S.; Lazar, A.N.; Coleman, A.W.; Sakai, N.; Matile, S. *Org. Biomol. Chem.* **2005**, *3*, 1659-1669.

significantly enhance the magnitude of the Arg-π interaction while also making the residue more hydrophobic, thus providing a mechanism to mediate biomolecular recognition.

To probe this possibility, we have investigated the interaction between Trp and symmetrically or asymmetrically dimethylated arginine residues (DMAs and DMAa, respectively) within the context of a β-hairpin peptide (Figure 2.9). This system has previously been shown to be an excellent model system for studying noncovalent interactions in an aqueous environment.[29,31,32] We find that, in comparison to the Arg···Trp interaction, methylation of arginine significantly enhances peptide stability while maintaining the stacked geometry with tryptophan. Thermodynamic analysis of hairpin folding indicates that methylation of Arg results in a decreased entropic penalty for folding with a concomitant decrease in enthalpic driving force. Furthermore, our analysis suggests that inclusion of a temperature-dependent ΔC_p is necessary in some cases for a full accounting of the observed cold denaturation. These results suggest that the enhanced interaction of methyl arginines with aromatic rings may be a key driving force in the mediation of protein-protein interactions by proteins containing methylated arginine.

[31] Tatko, C.D.; Waters, M.L. *J. Am. Chem. Soc*. **2004**, *126*, 2028-2034.

[32] Hughes, R.M.; Waters, M.L. *J. Am. Chem. Soc.* **2005**, *127*, 6518-6519.

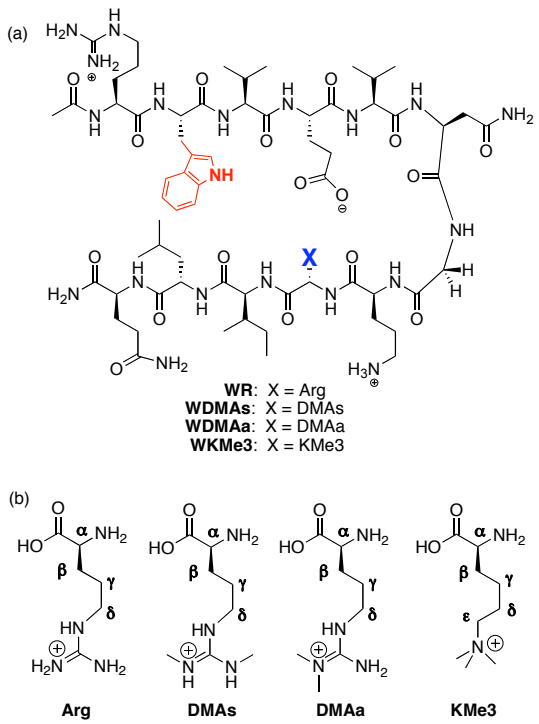

Figure 2.9. (a) β-Hairpin peptides containing arginine (Arg), symmetrically and asymmetrically dimethylated Arg (DMAs and DMAa, respectively), and trimethylated Lys (KMe3); peptides are referred to in the text by their residues in position 2 (Trp) and position 9 (X). (b) Amino acids at position X.

ii. Results and Discussion

(a) Design, Synthesis, and Characterization. To study the Trp-dimethylarginine (DMA) interactions, we utilized the same β-hairpin peptide system that we had previously used to investigate Trp···Lys, Trp···Arg, and Trp···KMe3 interactions (Figure 2.9).[29,31,32] Fmoc-DMAs and Fmoc-DMAa were purchased from Bachem and incorporated into the peptide via standard Fmoc solid phase peptide synthesis. The peptides were characterized by mass spectrometry and NMR as reported previously.[29] α-Hydrogen (Hα) chemical shifts, glycine splitting, amide shifts, and NOEs were used to characterize the hairpins and their respective stabilities.[33] As discussed earlier in this

[33] Maynard, A. J.; Sharman, G. J.; Searle, M. S. *J. Am. Chem. Soc.* **1998**, *120*, 1996-2007.

chapter, the α-hydrogen chemical shifts of the hairpins relative to random coil values (Fig. 2.10a) indicate the degree of β-sheet structure at each position along the strand, where downfield shifting of greater than 0.1 ppm is taken to indicate a β-sheet structure.[34] The magnitude of glycine splitting has also been shown to be a good indicator of overall hairpin stability.[33] The extent of folding can be quantified from both the Hα chemical shift and Gly splitting through comparison to a cyclic peptide which represents the fully folded state. Furthermore, NOEs between cross-strand pairs of sidechains were investigated to confirm β-hairpin formation as well as the specific sidechain-sidechain interaction between Trp and DMA (see Experimental). Lastly, upfield shifting of the DMA sidechain provides information about its proximity to the face of the Trp residue.

(b) Effect of Methylation on Hairpin Stability and Structure. Incorporation of DMAs or DMAa results in an increase in hairpin stability relative to the parent peptide. This is demonstrated by a measurable increase in the α-hydrogen shifts relative to random coil, as shown in Figure 2.10a. Based on the glycine splitting (Table 2.2), fraction folded of **WDMAs** is 94%[35] and **WDMAa** is 93%, versus 84% for the peptide **WR** at 298K, indicating that both symmetric and asymmetric dimethylation enhance hairpin stability similarly, by about 0.6 kcal/mol relative to **WR**. Values determined from the Hα chemical shifts are in good agreement with the values determined from the Gly splitting (Table 2.2). Additionally, the chemical shifts for the arginine sidechains show enhanced upfield shifting upon methylation (Figure 2.10b). The magnitude of upfield

[34] Griffith-Jones, S. R.; Maynard, A. J.; Searle, M. S. *J. Mol. Biol.* **1999**, *292*, 1051-1069.

[35] Percent folded from Ha shifts comes from the average of the percent folded from residues 2-5 and 8-11, excluding the turn residues and the terminal residues. See supporting information.

shifting across the guanidinium functionality is consistent with a stacking interaction between arginine and tryptophan that is enhanced by methylation (Figure 2.10c). Interestingly, for DMAs, the interaction is shifted towards the $NHCH_3$ groups, whereas for DMAa, there is similar upfield shifting at the ε-NH, NH_2, and methyl groups, suggesting a difference in the orientation of stacking for the two different DMA residues.

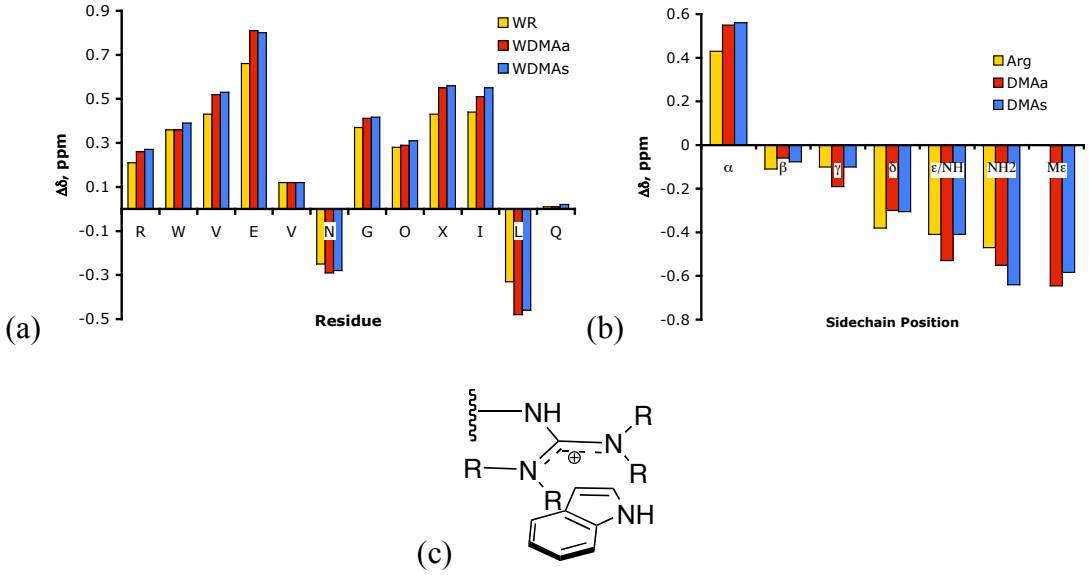

Figure 2.10. (a) **WR**, **WDMAa**, and **WDMAs** αH shifts relative to random coil values. Glycine shifts reflect the splitting. (b) **Arg**, **DMAa**, and **DMAs** sidechain upfield proton shifts relative to random coil values. Conditions: 298K, 50 mM NaOAc buffer, pH 4.0 (uncorrected), referenced to DSS. (c) Proposed geometry for the Trp···DMA interaction.

Table 2.2. Fraction Folded and Stability of Hairpins at 298 K.

Peptide	% Folded (Gly)[a]	% Folded (Hα)[b]	ΔG, kcal/mol[c]
WDMAs	94 (1)	93 (3)	-1.6 (-1.5)
WDMAa	93 (1)	90 (6)	-1.5 (-1.3)
WR	84 (1)	78 (7)	-1.0 (-0.7)

(a) Error is ± 1% as determined from the error in chemical shift. (b) Percent folded from Ha shifts is the average of the values from residues 2-5 and 8-11, excluding the turn residues and the termini. The standard deviation is in parenthesis. (c) Determined from the Gly splitting; values in parentheses are from the Hα data. Error is ± 0.05 kcal/mol, as determined from the error in the chemical shift.

(c) Interaction Energies. Double mutant cycles were performed to determine the magnitude of the sidechain-sidechain interaction in isolation, using the same substitutions at positions 2 and 9 that were reported previously for the parent peptide, **WR**: Val was substituted for Trp at position 2 and Ser was substituted for DMA at position 9 (Figure 2.3).[29] This gave energies of –1.0 (±0.1) kcal/mol for the cation-π interaction with both DMAs and DMAa. Thus, methylation enhances the Arg-Trp interaction by about a factor of two.[29] Interestingly, the interaction between Trp and DMA is equal to that of Trp and KMe3 .[32]

(d) Effects of Arg Methylation on Thermodynamic Analysis and Implications for the Temperature Depencdence of ΔC_p. The thermodynamic driving force for hairpin folding was investigated by performing thermal denaturation studies on each of the peptides, followed by NMR (Figure 2.11). Methylation of Arg resulted in a substantial increase in thermal stability of the hairpin, with no observable difference between **WDMAs** and **WDMAa**. The temperature of maximum stability (T_{max}) for **WR** is about

275 K, versus about 295 K for **WDMAs** and **WDMAa**, amounting to a 20° increase. Moreover, **WDMAa** and **WDMAs** exhibit cold denaturation below 295 K, which is related to the change in buried hydrophobic surface area and is typically associated with a hydrophobic driving force for folding.

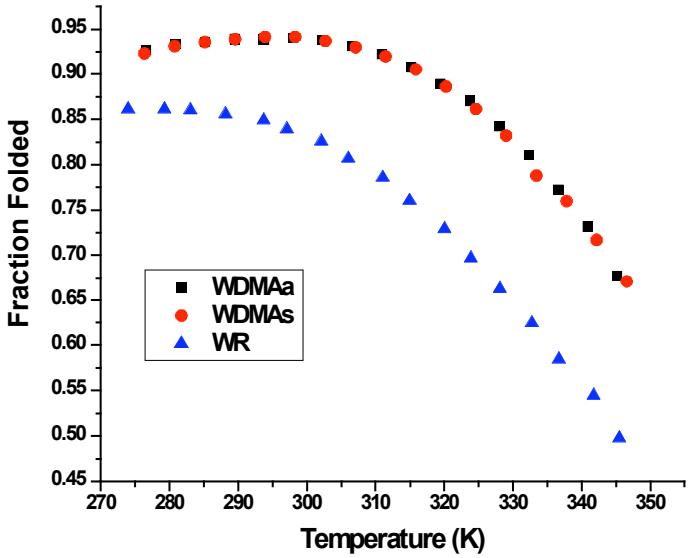

Figure 2.11. Thermal denaturation of peptides **WR, WDMAs**, and **WDMAa** as measured by the temperature dependence of the Gly splitting.

We fit the data to extract $\Delta H°$, $\Delta S°$, and $\Delta C_p°$ of folding using the method reported by Searle (equation [**2**]), which assumes a temperature-independent $\Delta C_p°$:[33]

$$\text{Fraction Folded} = [\exp(x/RT)]/[1 + \exp(x/RT)] \qquad [\mathbf{2}]$$

$$\text{where } x = [T(\Delta S°_{298} + \Delta C°_p \ln (T/298)) - (\Delta H°_{298} + \Delta C°_p (T - 298))]$$

This expression has been shown to fit non-cold denatured β-hairpin data well (see for example **WR** in Figure 2.12a), but for **WDMAa** and **WDMAs**, the fit to the cold-denatured portion of the curve was not as good, based on visual inspection (Figure 2.12b,

c). Andersen has recently shown that the cold-denatured state of a β-hairpin differs from that of the heat-denatured state and that it retains some hydrophobic interactions.[36] The change in heat capacity upon folding, $\Delta C_p°$, is an indicator of the importance of hydrophobic contacts to the folding event (i.e., sidechain interactions), where, a negative $\Delta C_p°$ of folding (or a positive $\Delta C_p°$ of unfolding) is an indication of hydrophobic clustering within the folded state of the hairpin.[37] If there are differences between the cold- and heat-denatured states, such as residual structure, then the $\Delta C_p°$ would be expected to vary with temperature. Hence, we considered the possibility that the $\Delta C_p°$ is not temperature-independent across the entire temperature range. We re-derived the Searle equation assuming a temperature-dependent $\Delta C_p°$, using an empirical expression for the temperature dependence of the heat capacity as shown below.[38]

$$C_{p,m} = a + bT + c/T^2 \quad [\mathbf{3}]$$

$$\Delta H^o = \Delta H^o_{298} + \int C_{p,m}\, dT \quad [\mathbf{4}]$$

$$\int C_{p,m}\, dT = a\,(T - 298) + (b/2)\,(T^2 - 298^2) - c\,(1/T - 1/298) \quad [\mathbf{5}]$$

$$\Delta H^o = \Delta H^o_{298} + a\,(T - 298) + (b/2)\,(T^2 - 298^2) - c\,(1/T - 1/298) \quad [\mathbf{6}]$$

$$\Delta S^o = \Delta S^o_{298} + \int (C_{p,m}/T)\, dT \quad [\mathbf{7}]$$

$$\int (C_{p,m}/T)\, dT = a \ln(T/298) + b\,(T - 298) - (c/2)\,(1/T^2 - 1/298^2) \quad [\mathbf{8}]$$

$$\Delta S^o = \Delta S^o_{298} + a \ln(T/298) + b\,(T - 298) - (c/2)\,(1/T^2 - 1/298^2) \quad [\mathbf{9}]$$

---

[36] Dyer, R. B.; Maness, S. J.; Franzen, S.; Fesinmeyer, R. M.; Olsen, K. A.; Andersen, N. H. *Biochemistry* **2005**, *44*, 10406-10415.

[37] Prabhu, N. V,; Sharp, K. A. *Annu. Rev. Phys. Chem.* **2005**, *56*, 521-48.

[38] Atkins, P. W. Chapter 2, Physical Chemistry, 6th ed.; Oxford University Press: Oxford, U.K., 1998.

Substituting equations [**6**] and [**9**] into equation [**2**] gives the following expression:

$$\text{Fraction Folded} = [\exp(x/RT)]/[1 + \exp(x/RT)] \qquad [\mathbf{10}]$$

where $x = T(\Delta S^{o}_{298} + a \ln(T/298) + b (T - 298) - (c/2) (1/T^2 - 1/298^2)) -$

$(\Delta H^{o}_{298} + a (T - 298) + (b/2) (T^2 - 298^2) - c (1/T - 1/298))]$.

Using equation 10, which allows ΔC_p to vary with temperature, we re-analyzed the data. The effect on **WR** was first investigated, as this peptide does not exhibit noticeable cold denaturation. Fitting of its thermal denaturation data is marginally better using equation 9, based on visual inspection (Figure 2.12a). We performed an F test to determine whether the better fit is significant, and found that it is significant within 95% confidence limits (see Experimental).[39] Nonetheless, equation 10 gives values for $\Delta H°$, $\Delta S°$, within error of those from equation 2 in this case, with a somewhat more negative $\Delta C_p°$ (Table 2.3). This indicates that in the absence of noticeable cold denaturation, the assumption that $\Delta C_p°$ is independent of temperature is generally reasonable, and the simplified equation reported by Searle is satisfactory.

[39] (a) Shoemaker, D. Pl, Garland, C. W., and Nibler, J. W. Experiments in Physical Chemistry, 4th Ed.; McGraw Hill; 1981, 727-730. (b) Moore, D. S. The Basic Principles of Statistics, W. H. Freeman and Co.: New York, NY, 1995, 630-633. (c) Foster, J. E.; Holmes, S. F.; Erie, D. A. *Cell*, **2001**, *106*, 243-252.

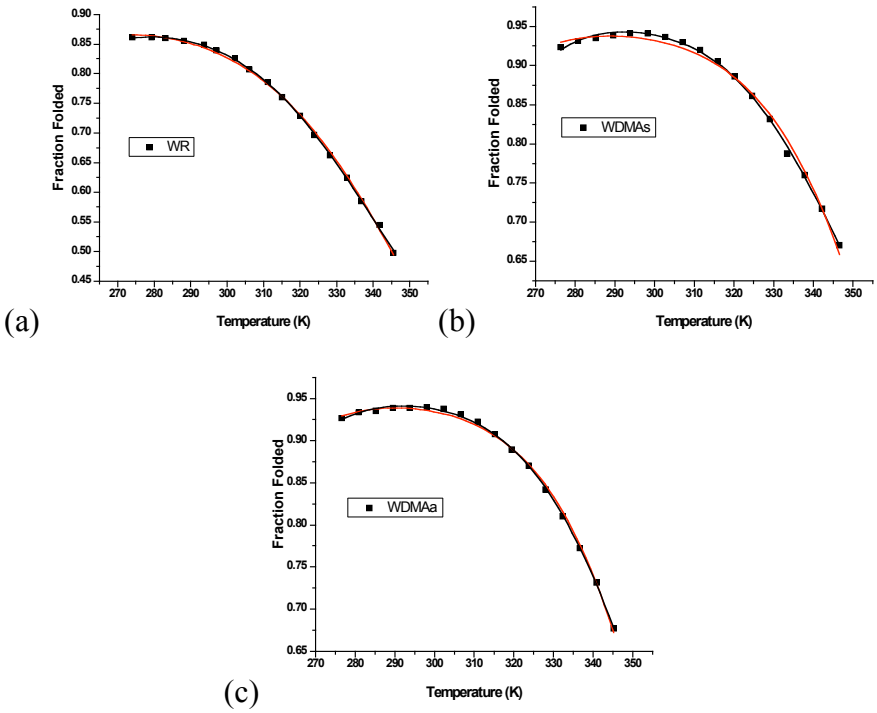

Figure 2.12. Fitting of thermal denaturation profiles of (a) **WR**, (b) **WDMAs**, and (c) **WDMAa** peptides using equation 1 with a temperature independent $DC_p°$ (red line) and equation 9 which allows ΔCp to vary with temperature (black line). The fraction folded was determined from the Gly splitting. Error is ±0.5 K in temperature and ±1% in fraction folded. Conditions: 50 mM NaOAc-*d4* buffer, pD 4.0 (uncorrected).

Table 2.3. Thermodynamic Parameters[a] for Hairpin Folding at 298 K Peptides **WR**, **WDMAs**, and **WDMAa** using Equation 1 (temperature-independent $\Delta C_p°$) and Equation 9 (temperature-dependent $\Delta C_p°$).

	Equation 1			Equation 9		
Peptide	ΔH°	ΔS°	$\Delta C_p°$	ΔH°	ΔS°	$\Delta C_p°$
WR	-3.6 (0.1)	-8.8 (0.3)	-152 (6)	-3.7 (0.1)	-9.1 (0.2)	-193 (29)
WDMAs	-2.4 (0.3)	-2.9 (1.2)	-260 (18)	-2.4 (0.2)	-2.6 (0.8)	-409 (61)
WDMAa	-2.2 (0.2)	-2.1 (0.6)	-280 (10)	-2.3 (0.1)	-2.1 (0.4)	-355 (53)

(a) Determined from the temperature dependence of the Gly chemical shift from 0 to 80 °C. Units are: DH°: kcal/mol; DS°: cal/mol K; $DC_p°$: cal/mol K. Errors (in parentheses) are determined from the fit. Error for $DC_p°$ values from equation 10 estimated at 15%.

Comparison of fits for **WDMAs** and **WDMAa** with equations 2 and 10 indicates that in these cases, in which cold denaturation is observed, a noticeably better fit is obtained with equation 10 (Figures 2.12b and c). This was verified using the F-test. Nonetheless, fitting with equation 10 has no significant effect on the values of $\Delta H°$ and $\Delta S°$ (Table 2.3). In each case, the errors for $\Delta H°$ and $\Delta S°$ are smaller using equation 10, and the values for $\Delta C_p°$ are more negative than with equation 2. This is likely due to a better accounting of the cold denatured state.[37]

Comparison of the thermodynamics of hairpin folding for **WDMAs** and **WDMAa** obtained from equation 10 indicates that the two hairpins are very similar, with a reduced enthalpic driving force for folding relative to **WR** and with a lower entropic cost for folding, as well as a more negative $\Delta C_p°$ (Table 2.3). This data suggests that methylation of Arg results in a reduced electrostatic driving force for interaction with Trp and an enhanced hydrophobic component.[37]

Examination of the electrostatic potential maps of arginine and methylated arginine sidechains provides additional insight into the observed effects (Figure 2.13). Upon methylation, two changes are apparent: the surface area of the guanidinium group is significantly increased and the positive charge (indicated by the blue regions) is further distributed across the methyl functionality. For example, on the central carbon of the guanidinium group, the charge decreases from = +1.16 for Arg to +0.54 for DMAs and +0.76 for DMAa, as determined from the Merz-Kollman atomic charges (Figure 2.14).

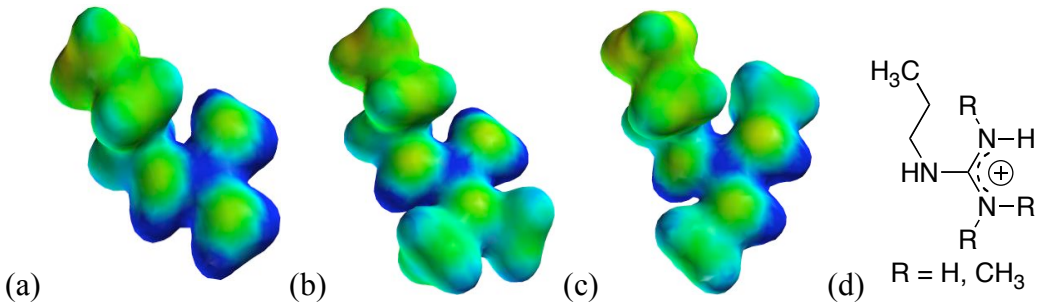

Figure 2.13. Electrostatic potential maps of sidechains: (a) Arg; (b) DMAa; (c) DMAs; (d) Structure of the Arg sidechain indicating its orientation in the electrostatic potential maps. Electrostatic potential maps were generated with MacSpartan: HF/6-31g*; Isodensity value = 0.02; range = 50 (red, electron rich) to 200 kcal/mol (blue, electron poor).

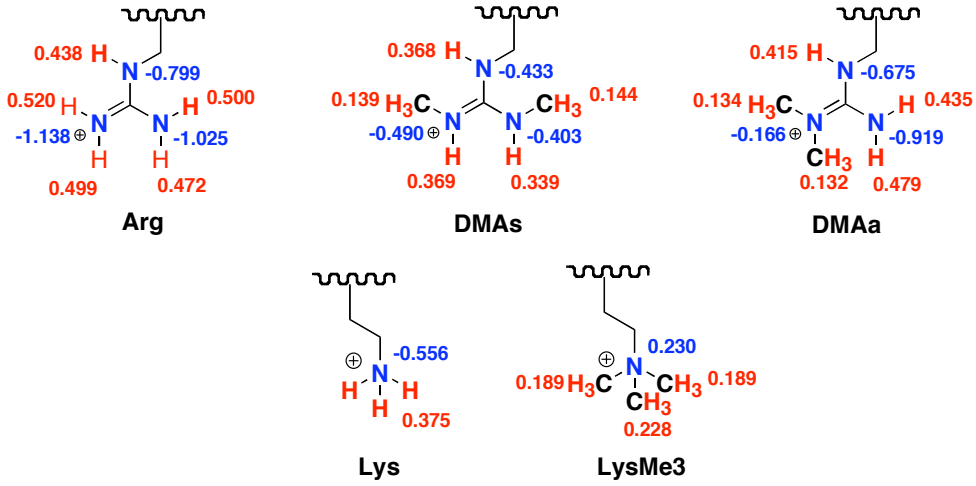

Figure 2.14. Changes in Merz-Kollman charges upon methylation of lysine and arginine (G03: HF/6-31g**).[40]

[40] Gaussian 03, Revision B.04, Frisch, M. J.; Trucks, G. W.; Schlegel, H. B.; Scuseria, G. E.; Robb, M. A.; Cheeseman, J. R.; Montgomery, Jr., J. A.; Vreven, T.; Kudin, K. N.; Burant, J. C.; Millam, J. M.; Iyengar, S. S.; Tomasi, J.; Barone, V.; Mennucci, B.; Cossi, M.; Scalmani, G.; Rega, N.; Petersson, G. A.; Nakatsuji, H.; Hada, M.; Ehara, M.; Toyota, K.; Fukuda, R.; Hasegawa, J.; Ishida, M.; Nakajima, T.; Honda, Y.; Kitao, O.; Nakai, H.; Klene, M.; Li, X.; Knox, J. E.; Hratchian, H. P.; Cross, J. B.; Bakken, V.; Adamo, C.; Jaramillo, J.; Gomperts, R.; Stratmann, R. E.; Yazyev, O.; Austin, A. J.; Cammi, R.; Pomelli, C.; Ochterski, J. W.; Ayala, P. Y.; Morokuma, K.; Voth, G. A.; Salvador, P.; Dannenberg, J. J.; Zakrzewski, V. G.; Dapprich, S.; Daniels, A. D.; Strain, M. C.; Farkas, O.; Malick, D. K.; Rabuck, A. D.; Raghavachari, K.; Foresman, J. B.; Ortiz, J. V.; Cui, Q.; Baboul, A. G.; Clifford, S.; Cioslowski, J.; Stefanov, B. B.; Liu, G.; Liashenko, A.; Piskorz, P.; Komaromi, I.; Martin, R. L.; Fox, D. J.; Keith, T.; Al-Laham, M. A.; Peng, C. Y.; Nanayakkara, A.; Challacombe, M.; Gill, P. M. W.; Johnson, B.;

This distribution of charge is expected to diminish the electrostatic interaction between the arginine guanidinium and the tryptophan indole ring, resulting in a reduced enthalpic driving force, as is observed. The increased surface area may increase the dispersion forces between the two systems, which would be enthalpically favorable, counteracting the effect of the greater charge distribution. However, it will also make the residue more hydrophobic, such that folding would be more entropically favorable. The fact that the entropy of folding becomes more favorable upon methylation and that the $\Delta C_p°$ for folding becomes more negative argues in favor of an increased hydrophobic effect relative to the parent Arg···Trp interaction (Table 2.3).

(e) Comparison to Trimethylated Lysine. The peptide **WKMe3** has been previously reported to be a highly thermally stable β-hairpin due to a methylation-enhanced Lys···Trp interaction (see Chapter 2, section A).[32] Its comparison to the dimethylated arginine peptides is particularly interesting since trimethylation of lysine is also a common post-translational modification, and has been shown to induce binding to an aromatic pocket in the protein chromodomain.[41] While the DMA- and KMe3-containing

---

Chen, W.; Wong, M. W.; Gonzalez, C.; and Pople, J. A.; Gaussian, Inc., Wallingford CT, 2004.

[41] (a) Lachner, M.; Jenuwein, T. *Curr. Opin. Cell. Biol.* **2002**, *14*, 286 – 298. (b) Lindroth, A. M.; Shultis, D.; Jasencakova, Z.; Fuchs, J.; Johnson, L.; Schubert, D.; Patnaik, D; Pradhan, S.; Goodrich, J.; Schubert, Il; Jenuwein, T.; Khorasanizadeh, S.; Jacobsen, S. E. *Embo. J.* **2004**, *23*, 4286 – 4296. (c) Fischle, W.; Wang, Y. M.; Jacobs, S.

peptides are of similar stability at 298 K (Figure 2.16a), they have distinctly different modes of interaction with tryptophan. The trimethylated lysine interacts with tryptophan primarily by packing its ε-CH_2 and terminal methyl groups into the face of the indole ring with the predominant site for interaction at the ε-CH_2 group, as evidenced by the upfield shifting of the ε-CH_2 by nearly 1 ppm (Figure 2.15b).[32] In contrast, the dimethylated arginine derivatives undergo stacking interactions, as evidenced by the relatively even distribution of proton upfield shifting across the guanidinium and methyl groups (Figure 2.15b).

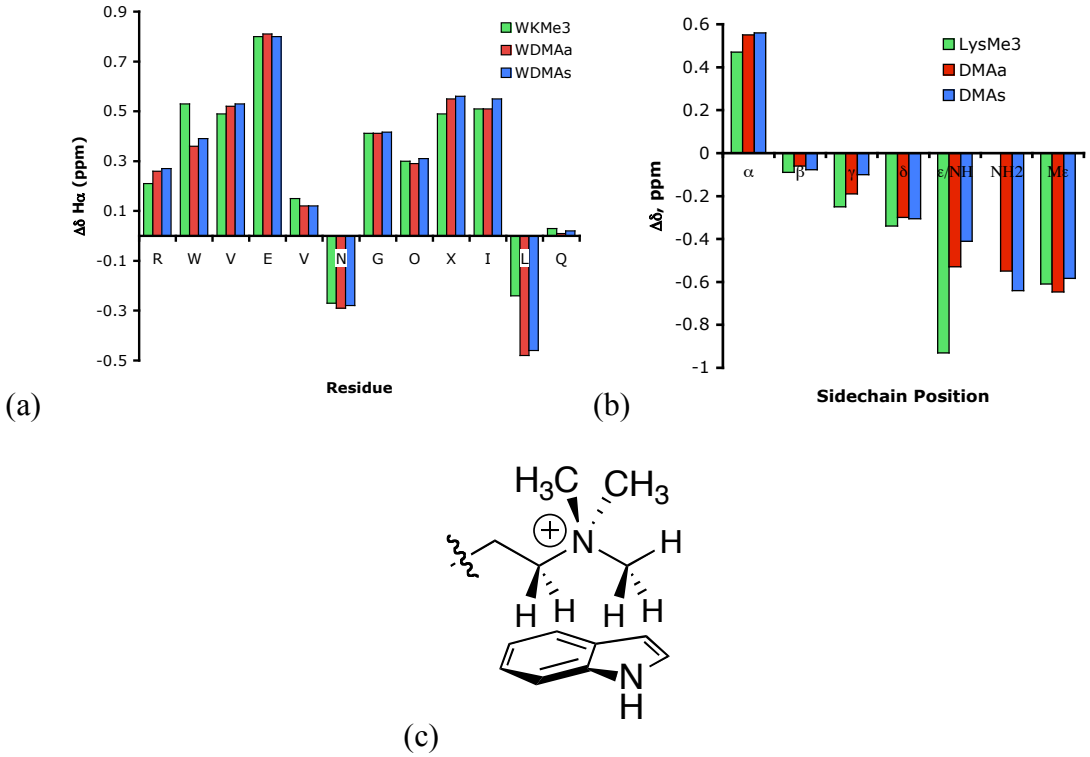

Figure 2.15. (a) **WDMAa**, **WDMAs**, and **WKMe3** αH shifts relative to random coil values. Glycine shifts reflect the splitting. (b) DMAa, DMAs, and KMe3 sidechain upfield proton shifts relative to random coil values. Conditions: 298K, 50 mM NaOAc-*d4* buffer, pD 4.0 (uncorrected), referenced to DSS. (c) Proposed geometry for the Trp···KMe3 interaction.

A.; Kim, Y. C.; Allis, C. D.; Khorasanizadeh, S. *Genes and Development* **2003**, *17*, 1870 – 1881. (d) Jacobs, S. A.; Khorasanizadeh, S. *Science* **2002**, *295*, 2080 – 2083.

Both sets of peptides demonstrate high thermal stability, with melting temperatures (T_m) greater than 75° C, although NMR studies indication that **WKMe3** remains more folded at high temperatures (Figure 2.16). Since **WKMe3** exhibits significant cold denaturation, we re-fit its thermal denaturation data using equation 10, and also re-fit the parent peptide **WK** for comparison.[42] In the case of **WK**, which shows no cold denaturation, the fit with Equation 10 was no better than the fit with Equation 2 according to the F test (Figure 2.16b). However, a better fit was obtained for **WKMe3** with Equation 10 than Equation 2 (Figure 2.16c), as was found with **WDMAa** and **WDMAs**. Interestingly, in this case the temperature-dependent fit resulted in variation of the values for $\Delta H°$ and $\Delta S°$, but with no change in $\Delta C_p°$ (Table 2.4). This may be because equation 2 appears to overestimate the cold denaturation in this case.

[42] The values for $\Delta H°$, $\Delta S°$, and $\Delta C_p°$ reported for **WKMe3** with equation 2 differ slightly from those in reference 29 because the data here comes from the average of four runs rather than the average of two runs in reference 29. Nonetheless, the difference in fraction folded in any one data point in the thermal denaturation from different data sets was less than 1%.

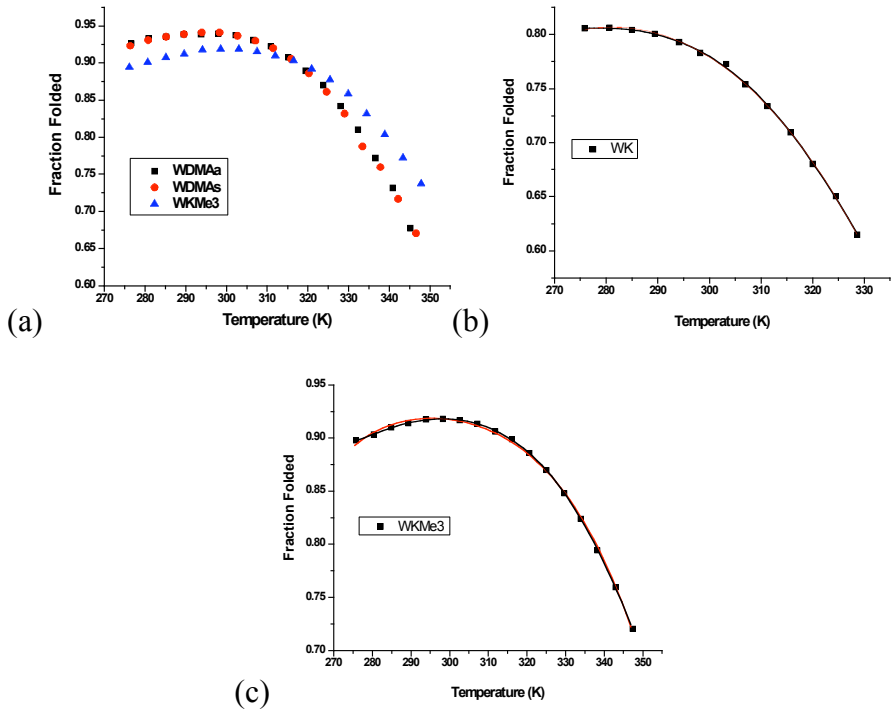

Figure 2.16. (a) Comparison of thermal denaturation profiles of **WDMAa**, **WDMAs, and WKMe3** peptides. (b and c) Fitting of the thermal denaturation profiles of **WK** and **WKMe3** using Equation 2 with a temperature-independent $\Delta C_p°$ (red lines) and Equation 10 which allows ΔC_p to vary with temperature (black lines). The fraction folded was determined from the Gly splitting. Error is ±0.5 K in temperature and ±1% in fraction folded. Conditions: 50 mM NaOAc-*d4* buffer, pD 4.0 (uncorrected).

Table 2.4. Thermodynamic Parameters[a] for Hairpin Folding at 298 K for Peptides **WK** and **WKMe3** using Equation 2 (temperature-independent $\Delta C_p°$) and Equation 10 (temperature-dependent $\Delta C_p°$).

	Equation 2			Equation 10		
Peptide	$\Delta H°$	$\Delta S°$	$\Delta C_p°$	$\Delta H°$	$\Delta S°$	$\Delta C_p°$
WK	-2.8 (0.1)	-6.7 (0.1)	-166 (4)	-2.6 (0.1)	-6.2 (0.2)	-182 (27)
WKMe3	-0.6 (0.1)	+2.7 (0.3)	-237 (5)	-0.1 (0.1)	+4.5 (0.3)	-243 (36)

(a) Determined from the temperature dependence of the Gly chemical shift from 0 to 80 °C. Units are: $\Delta H°$: kcal/mol; $\Delta S°$: cal/mol K; $\Delta C_p°$: cal/mol K. Errors (in parentheses) are determined from the fit. Error for $\Delta C_p°$ values from equation 10 estimated at 15%.

Whereas methylation of Arg has a modest effect on ΔH° and ΔS° of hairpin folding, methylation of Lys has a more considerable effect, resulting in a less favorable enthalpy of folding and a more favorable entropy (Tables 2.3 and 2.4). [32,42] The more favorable entropy of folding for WKMe3 can be explained by the greater conformational freedom of the KMe3-Trp interaction versus that of a DMA-Trp interaction, where the rotor-like KMe3 has more sites of interaction with planar Trp than DMA, which is confined primarily to a stacked orientation with Trp in the folded state. Additionally, $\Delta C_p°$ of folding, which is generally recognized as a better indicator of the hydrophobic driving force in proteins than ΔS°,[37] is more favorable for DMA than for KMe3. The greater hydrophobic driving force for the DMA-Trp interaction over the KMe3-Trp interaction is consistent with our electrostatic potential maps (Figures 2.13 and 2.17) and our calculated Merz-Kollman atomic charges (Figure 2.14), which both show greater polarization of the KMe3 methyl hydrogens versus the DMA methyl hydrogens. Another likely component of the more favorable $\Delta C_p°$ of folding for DMA may be due to differences in the solvent-accessible surface area of KMe3 and DMA in the folded state. Finally, the greater enthalphic driving force of the DMA···Trp interaction versus that of KMe3 is likely due to the π-system of the guanidinium functionality, which results in less charge distribution onto the methyl groups (see Figures 2.13 and 2.17) and lends an additional π-π stacking component to the interaction with Trp. [22d,29]

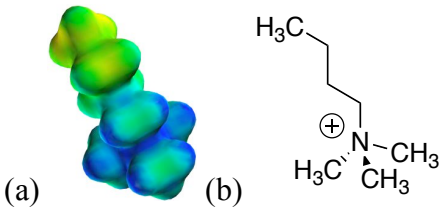

Figure 2.17. (a) Electrostatic potential map of the KMe3 sidechain. (b) Structure KMe3 sidechain indicating its orientation in the electrostatic potential map. The electrostatic potential map was generated with MacSpartan: HF/6-31g*; Isodensity value = 0.02; range = 50 (red, electron rich) to 200 kcal/mol (blue, electron poor).

iii. Conclusions

Using a β-hairpin model system we have found that methylation of Arg enhances its interaction with a neighboring aromatic residue. The interaction involves the stacking of DMA residue with the face of the Trp sidechain. The interaction provides –1.0 kcal/mol in stability to the hairpin, about twice as much as that of the unmethylated Arg, and equal to that of the interaction of Trp with KMe3. The methylation of Arg results in a decreased enthalpic driving force for folding with a concomitant decrease in entropic cost, , consistent with an increased hydrophobic component to the Arg···Trp interaction. Inclusion of the temperature-dependent $\Delta C_p°$ term improves the thermodynamic analysis for peptides exhibiting cold denaturation, and may better account for hydrophobic interactions in the cold denatured state. It is noteworthy that such subtleties in ΔCp° are observable in this system. Indeed, this system may prove to be a useful model system for addressing questions about the role of heat capacity in protein folding.

In comparison to KMe3, DMA has less charge dispersion onto the methyl groups and can interact with a larger portion of the Trp indole ring, but with fewer possible orientations. This has clear implications for the observed trends in ΔS° and $\Delta C_p°$. The fact that such subtleties seem to be well accounted for in our highly stable model system

indicates that they may indeed be useful for correlating thermodynamic properties such as $\Delta S°$ and $\Delta C_p°$ with concepts such as conformational freedom and hydrophobicity.

The role of Arg methylation in biological systems is just beginning to be determined, and these findings suggest a possible role for enhanced Arg···Trp interactions in the mediation of protein-protein interactions by Arg methylation. Although Arg methylation may not provide a large change in interaction energy with Trp, noncovalent interactions rarely function in isolation. Hence, we expect that a binding pocket which can accommodate a polarized methyl group in DMA via enhanced cation-π interactions, but would not provide hydrogen-bonding sites for an unmethylated Arg, provides the high selectivity necessary for such a subtle post-translational modification to act as a chemical switch for mediating a protein-protein interaction. While our data does not explain the preference, in some cases, for the recognition of asymmetrically methylated arginine over symmetrically methylated arginine, it is clear that DMAs and DMAa interact with Trp in different geometries, which implies that differently shaped binding sites could easily provide specificity for one form of methylation over the other. We expect that this work will have relevance to the role of Arg methylation in the "histone code".

C. DISTANCE DEPENDENCE STUDY OF THE CATION-π INTERACTION

i. Introduction.

In a section 1A, we have shown that the trimethylation of lysine significantly increases the magnitude of the cation-π interaction between a lysine and a tryptophan residue in the context of a well-folded β-hairpin peptide.[43] Our current study has two aims: (1) to systematically explore both the effect of mono, di, and trimethylation of lysine on the magnitude of the interaction; and (2) study the influence of proximity of the methylated ammonium group to tryptophan with the lysine (Lys) analogues ornithine (Orn) and diaminobutyric acid (Dab), in which the alkyl chain is shortened by one and two methylenes, respectively (Figure 2.18). By incrementally methylating the Orn and Dab sidechains in the same manner as Lys, we investigated the optimal length for interaction of the unmethylated cationic sidechain with tryptophan and determined whether the same chain length was still optimal upon methylation. As a result, this study allows us to investigate the maximal interaction energy of the cation-π interaction within our model system. Additionally, this study reveals the interplay between the contributions of sidechain-sidechain interactions and β-sheet propensity to overall β-hairpin stability. Both β-sheet propensity, which is the statistical preference for a particular amino acid to adopt a β-sheet conformation, and sidechain-sidechain interactions have been shown to contribute to β -hairpin stability.[44] In this study, we find that while β -sheet propensity

[43] Hughes, R.M.; Waters, M.L. *J. Am. Chem. Soc.* **2005**, 127, 6518-6519.

[44] (a) Stotz, C. E.; Topp, E. M. *J. Pharm. Sci.* **2004**, *93*, 2881 – 2894. (b) Gellman, S. H. *Curr. Opin. Chem. Biol.* **1998**, *2*, 717 – 725, (c) Ramirez-Alvarado, M.; Kortemme, T.; Blanco, F. J.; Serrano, L. *Biorg. Med. Chem.* **1999**, *7*, 93 – 103.

decreases in the order Lys > Orn > Dab, the magnitude of the cation-π interaction between the truncated cationic residues and Trp still increases with N-methylation, lending stability to the hairpin and offsetting much of the destabilizing effects of low β-sheet propensity.

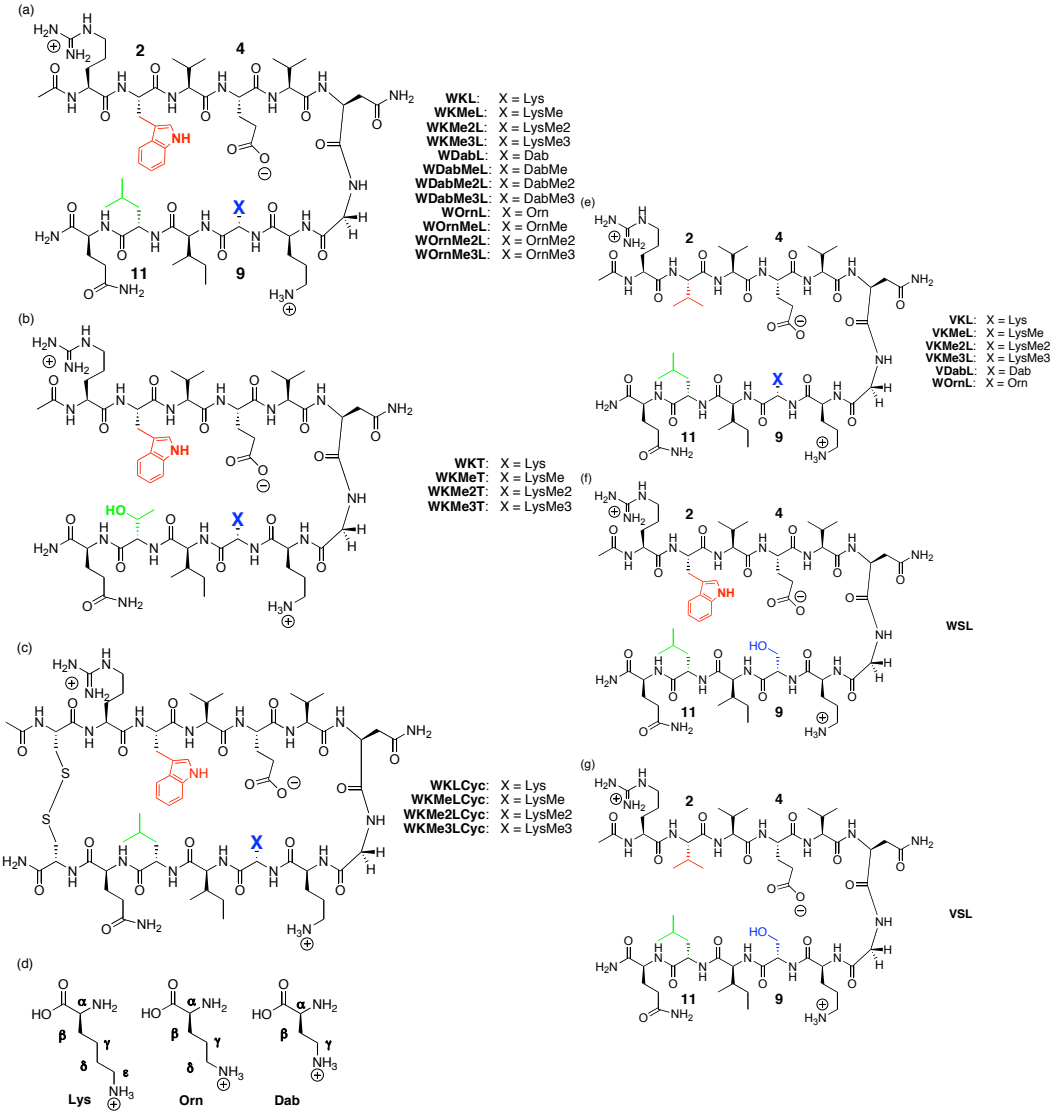

Figure 2.18. (a) β-Hairpin peptides **WXL** containing Lys, Orn, and Dab at position 9, and their methylated analogues. (b) β-hairpin peptides **WXT** containing Lys and its methylated analogues at position 9, with Leu 11 mutated to Thr. (c) Cyclic peptides **WXLcyc** are disulfide bridged at the hairpin termini to represent the fully folded state. 7mers (not shown) are used to determine the random coil chemical shifts (see Supporting Information). (d) Structure of Lys, Orn, and Dab. (e) Single mutant peptides **VXL**, in which Trp 2 has been replaced with Val. (f) Single mutant peptide **WSL** in which residue X at position 9 has been replaced with Ser. (g) Double mutant peptide **VSL** in which Trp 2 has been replaced by Val and residue X at position 9 has been replaced with Ser.

ii. Results and Discussion

(a) Design, Synthesis, and Characterization. Peptides were designed to exploit a known energetically favorable cation-π interaction between Lys and Trp in diagonally oriented non-hydrogen bonded positions on the same face of the β-hairpin (Figure 2.17).[45] Due to the right-handed twist of the hairpin fold, the cross strand diagonal positions 2 (Trp) and 9 (Lys) place their respective sidechains in closer proximity than the diagonal positions 4 (Glu) and 11 (Leu).[44] This creates a favorable environment for the sidechains to interact if an attractive force exists between them. We initially studied peptides with Leu and position 11, laterally cross-strand from Trp 2 (Figure 2.17a). Due to the very high stability of the original Leu-containing peptide series (and therefore small differences in fraction folded, which result in large differences in ΔG when near fully folded), Leu was mutated to Thr to create a less stable series of β-hairpins (Figure 2.17b), such that variation in hairpin stability could be measured more accurately.

Methylated amino acids were synthesized as shown in Schemes 2.1 and 2.2. Monomethylated species were synthesized starting with either Boc-Orn-OH (**1a**) or Boc-Dab-OH (**1b**) (Scheme 2.1). Following protection of the sidechain with o-nitrobenzene sulfonic acid, amino acid **2** was selectively methylated in the presence of NaOH with dimethyl sulfate. Deprotection of **3** with TFA and reprotection with Fmoc-Cl gave **4**. After solid phase peptide synthesis, the o-nitrobenzenesulfonyl moiety was selectively

[45] (a) Tatko, C. D.; Waters, M. L. *Protein Science* **2003**, *12*, 2443 – 2452. (b) Tatko, C.D.; Waters, M.L. *J. Am. Chem. Soc*. **2004**, *126*, 2028-2034.

cleaved in the presence of 2-mercaptoethanol and DBU[46], followed by cleavage from the resin with TFA. Boc-dimethyl Orn (**6a**) and Boc-dimethyl Dab (**6b**) were prepared from Boc-Orn (**1a**) and Boc-Dab (**1b**) by reductive methylation in the presence of formaldehyde and H_2/Pd/C (Scheme 2.2).[47] The Boc-protected amino acids were deprotected with TFA, reprotected with Fmoc-OSu, and incorporated into peptides via standard Fmoc solid-phase peptide synthesis. Trimethylated species were achieved by methylation of dimethyllysine with methyl iodide and MTBD (7-Methyl-1,5,7-triazabicyclo[4.4.0]dec-5-ene) after peptide synthesis, followed by cleavage from the resin.[48]

Peptides were characterized by mass spectrometry and NMR as reported previously.[45] Alpha hydrogen (H_α) chemical shifts, glycine splitting, and NOEs were used to characterize the hairpin structure and their respective stabilities. The degree of H_α chemical shifts of the hairpins relative to random coil values (Figure 2.17c-d) are used as indicators of the degree of β-sheet structure at each position along the strand.[49] In the folded state, H_α are shifted downfield relative to random coil due to the inductive effects of the amide-carbonyl cross-strand hydrogen bonds present in β-sheets.[50] Hence, increased downfield H_α shifting is evidence of increased hairpin stability. Also, the magnitude of glycine splitting has been shown to be a good indicator of overall hairpin

---

[46] Miller, S.C.; Scanlan, T.S. *J. Am. Chem. Soc.* **1997**, *119*, 2301-2302.

[47] (a) Benoiton, L. *Can. J. Chem.***1964**, *42*, 2043.(b)Lamar, J., et al. *Bioorg. & Med. Chem. Lett.* **2004**, *14*, 239 – 243.

[48] Kretsinger, J.K.; Schneider, J.P. *J. Am. Chem. Soc.* **2003**, 125, 7907-7913.

[49] Griffith-Jones, S. R.; Maynard, A. J.; Searle, M. S. J. Mol. Biol. 1999, 292, 1051-1069.

[50] Guo, H.; Karplus, M. *J. Phys. Chem.* **1994**, *98*, 7104 – 7105.

stability.[51] The extent of folding can be quantified by calculating the fraction folded, as shown by the following equation: fraction folded (**f**) = $[\delta_{obs} - \delta_0]/[\ \delta_{100} - \delta_0]$, where δ_0 represents the random coil chemical shift determined from 7mer peptides and δ_{100} the fully folded chemical shift determined from the cyclic peptides (Figure 2.17). Free energy of folding is determined from the fraction folded value by the equation $\Delta G = -RT\ln(\mathbf{f}/(1-\mathbf{f}))$.

Sidechain chemical shifts were used to evaluate the proximity of the cationic sidechain to the Trp indole ring. Due to the anisotropy of the aromatic ring, protons that are in close proximity to the electron rich face of an aromatic ring are shifted upfield. As a result, the degree of Lys sidechain upfield shifting is an indicator of the degree of contact between the alkyl side chain and the face of the tryptophan ring. Finally, NOEs between cross-strand pairs of sidechains provide evidence for hairpin folding within the correct register. These are provided in the experimental section.

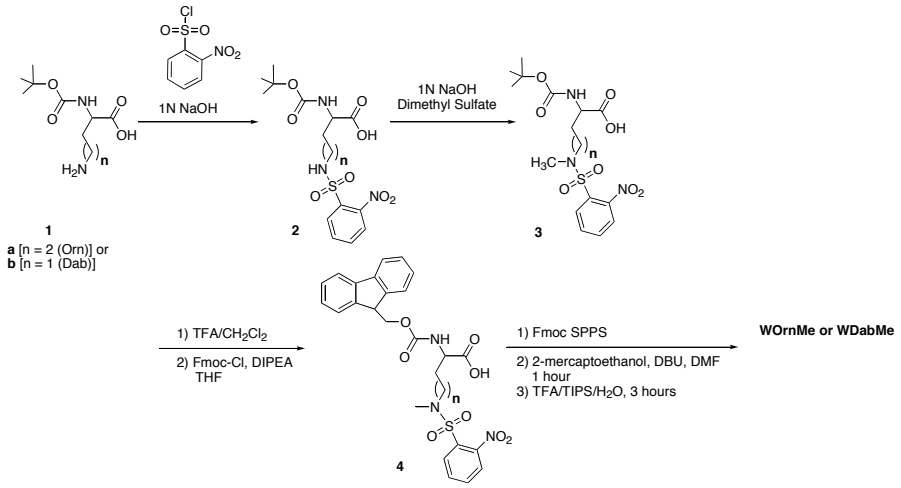

Scheme 2.1. Synthesis of Monomethylated Orn and Dab containing peptides.

[51] Maynard, A. J.; Sharman, G. J.; Searle, M. S. *J. Am. Chem. Soc.* **1998**, *120*, 1996-2007.

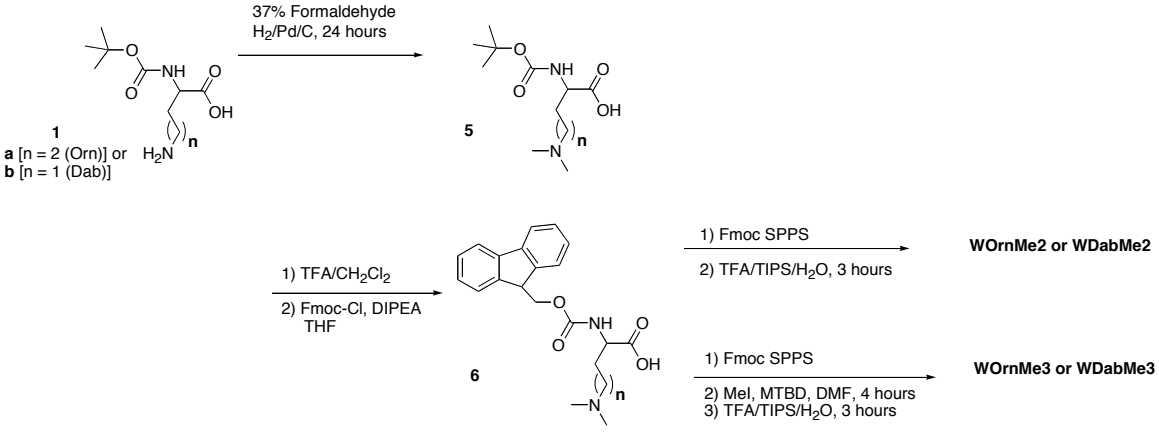

Scheme 2.2. Synthesis of Di- and Trimethylated Orn and Dab containing peptides.

Effects of Chain Length in Unmethylated Sidechains. Comparison of **WKL**, **WOrnL**, and **WDabL** allows for the influence of the chain length on the cation-π interaction to be determined. To correct for differences in β-sheet propensities of Dab, Orn, and Lys, double mutant cycles were performed,[52] indicating that the cation-π interactions for **WKL** and **WOrnL** are –0.3 and –0.2 (± 0.1) kcal/mol, respectively. Due to the instability of the Dab single mutant hairpin **VKL** (fraction folded = 13%), large errors in the double mutant cycles complicate a direct analysis of the contribution of the sidechain-Trp interaction to hairpin stability for **WDabL**. However, based on the trends in upfield shifting of the Lys, Orn, and Dab sidechains (Figure 2.19), the available evidence suggests that the cation-π component of the sidechain-Trp interaction decreases with each truncation of the sidechain. Indeed, for Dab it appears that there is little or no interaction with Trp, as the upfield shifting is < 0.05 ppm at any position in the Dab sidechain (Figure 2.19). This suggests that Dab is too short to interact with Trp in a diagonal orientation. The upfield shifting of Orn suggests that the δ-position is the most

[52] Hunter, C. A.; Tomas, S. *Chemistry and Biology* **2003**, *10*, 1023-1032.

favorable for interaction with Trp, but that it is not as favorable as the ε-position of Lys. Hence, Lys appears to be of the optimal length for a diagonal cation-π interaction.

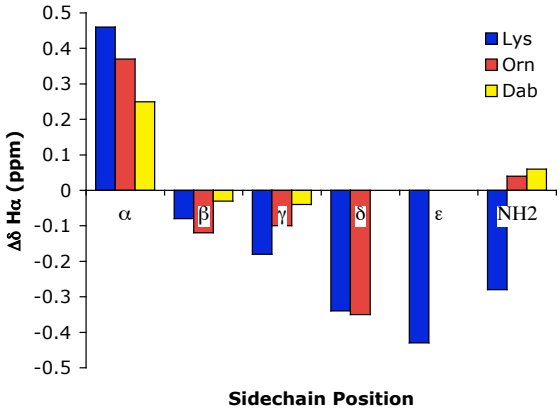

Figure 2.19. Upfield shift profiles of Lys, Orn, and Dab sidechains.

The fraction folded of the control peptides, **VKL**, **VOrnL**, and **VDabL**, in which a cation-π interaction is not possible, provides information about the inherent β-sheet propensity of Orn and Dab relative to Lys. As the sidechain is shortened, its β-sheet propensity decreases, resulting in a decreased fraction folded [from 37% for **VKL** to 29% for **VOrnL** to 13% for **VDabL**]. Hence, mutation of Lys to Orn and Dab results in destabilization of the β-hairpin due to the reduced β-sheet propensity even in the absence of a cation-π interaction. Additionally, the fraction folded of the single mutant peptides does not change significantly upon methylation [for example, **VKL** (37%) and **VKMe3L** (38%)]. This indicates that in the case of the WXL peptides, it is indeed enhancement of the sidechain-sidechain interaction via methylation, and not a change in β-sheet propensity upon methylation , that lends added stability to the peptide (see discussions of methylated peptides below).

Effects of Lysine Methylation: Peptides WK(Me)$_n$L (n = 0-3). The lysine-containing peptides **WKL, WKMeL, WKMe$_2$L, and WKMe$_3$L** show an increase in hairpin stability with each addition of a methyl group to the lysine sidechain, revealing that even monomethylation significantly stabilizes the folded peptide (Table 2.5 and Figure 2.20a). This trend is also evident in the H_α shifts, which are further downfield upon methylation, with the exception of the frayed terminal residues arginine and glutamine, which are not significantly affected by methylation, and Asn in the β-turn (Figure 2.20b).

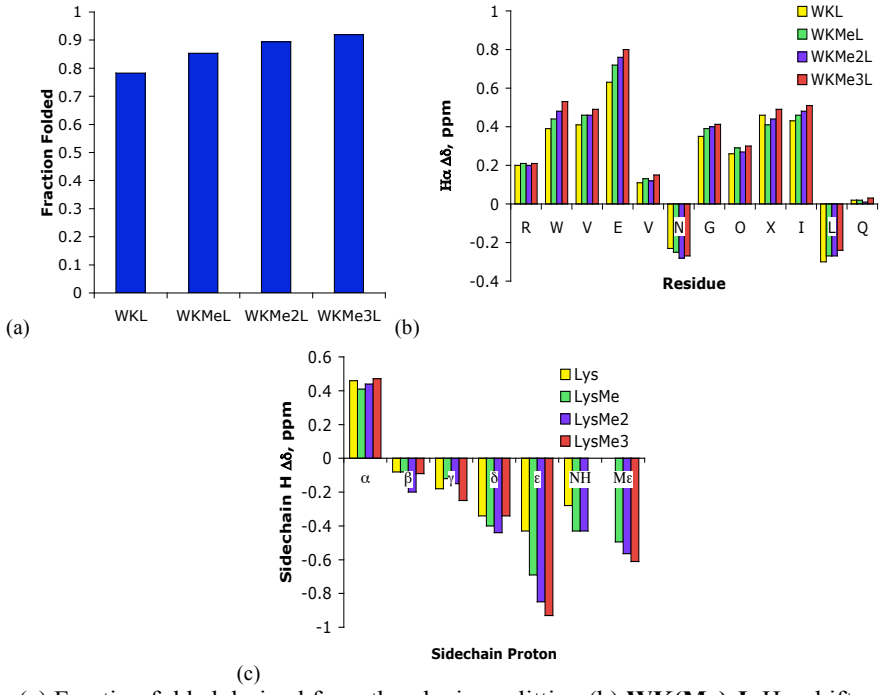

Figure 2.20. (a) Fraction folded derived from the glycine splitting (b) **WK(Me)$_n$L** Hα shifts relative to random coil values. Glycine shifts reflect the splitting. (c) **WK(Me)$_n$L** sidechain upfield proton shifts relative to random coil values.

Table 2.5. Fraction Folded and Stability of Hairpins at 298 K.

Peptide	% Folded (Gly)[a]	% Folded (Ha)[b]	DG, kcal/mol[c]
WKL	78 (1)	76 (1)	-0.76 (-0.7)
WKMeL	86 (1)	84 (13)	-1.06 (-1.0)
WKMe$_2$L	89 (1)	84 (16)	-1.26 (-1.0)
WKMe$_3$L	92 (1)	91 (15)	-1.45 (-1.4)

(a) Error is ± 1% as determined from the error in chemical shift. (b) Percent folded from Ha shifts is the average of the values from residues 2-5 and 8-11, excluding the turn residues and the termini. The standard deviation is in parenthesis. (c) Determined from the Gly splitting; values in parentheses are from the Ha data. Error is ± 0.05 kcal/mol, as determined from the error in the chemical shift; Average error for Ha data (as calculated from the standard deviation) is ± 0.4 kcal/mol.

The lysine sidechain also exhibits increased upfield shifting with each additional methylation, indicating a greater degree of interaction with the tryptophan indole ring (Figure 2.20c). The ε-methylene is the most upfield shifted portion of the sidechain in each peptide, indicating its close proximity to the indole ring. In the case of Lys, the ε-protons are polarized by the neighboring cationic ammonium group, which creates a site of favorable interaction with the face of the aromatic ring (Figure 2.21). This is consistent with the orientation of Lys-Trp pairs commonly observed in protein crystal structures.[53]

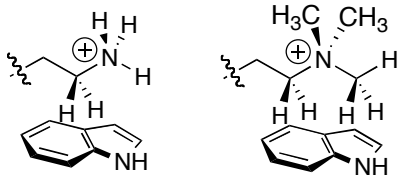

Figure 2.21. Possible interaction geometries for Trp-Lys and Trp-KMe3 interactions.

[53] Gallivan, J.P.; Dougherty, D.A. *Proc. Natl. Acad. Sci.* **1999**, *96*, 9459-9464.

To quantitatively assess the Lys-Trp interaction, double mutant cycles were performed, using the non-interacting residues Ser and Val in place of Trp and Lys, respectively (Figure 2.18).[45] Double mutant cycles isolate the interaction energy of the residues in question (in this case, Lys and Trp), and extracts the contribution of this interaction to the overall ΔG of hairpin folding. The single mutant peptides (Trp2Ser and Lys9Val) account for the contribution of each residue in the interacting pair (Trp or Lys) to β-hairpin stability, while the double mutant peptide accounts for changes in stability that may be due to differences in β-sheet propensities, etc. between the native and mutant sidechains. Double mutant cycles provide Lys-Trp interaction energies for **WKL**, **WKMeL**, **WKMe$_2$L**, and **WKMe$_3$L** of -0.3, -0.5, -0.7, and -1.0 kcal/mol (+/-0.1 kcal/mol), respectively. This amounts to an enhancement of the cation-π interaction of about 0.2 - 0.3 kcal/mol per methylation. The value of -1.0 kcal/mol for the interaction of trimethylated lysine with tryptophan compares well with other literature values for the binding of tetra-alkyl ammonium species to aromatic rings in water: approximately 0.9 kcal/mol per aromatic residue in Diederich's study of a Factor Xa binder[5a], and approximately 1.1 kcal/mol per aromatic residue in Dougherty's cyclophane receptor.[54b]

The methylated hairpins **WKMeL**, **WKMe$_2$L**, and **WKMe$_3$L** show a significant increase in thermal stability in comparison to the parent peptide **WKL** (Figure 2.22a). By NMR, **WKMe$_3$L** appears to be ~72% folded at 70 °C. Interestingly, the trimethylated peptide **WKMe$_3$L** shows little or no thermal denaturation by CD over the range 0 to 90 °C (Figure 2.22b). The peptide **WKMe$_3$L** also shows no unfolding transition over the 20

[54] (a) Stauffer, M.; Dougherty, D.A. *Tett. Lett.* **1988**, 29, 6039.; (b) Stauffer, M; Dougherty, D.A. *Science* **1990**, 250, 1558.

to 90 °C range when monitored by DSC. These results corroborate a recent FTIR study of the thermal denaturation of the β-hairpin peptide **trpzip2**, which maintains substantial residual native structure when heated to 82 °C.[55] Taken together, these results support the notion that the global β-sheet structure of **WKMe$_3$L** changes little over a wide temperature range, making it impractical to measure a thermal transition with traditional calorimetry techniques such as DSC. The CD spectrum gives insight into global stability of the hairpin, while the NMR spectrum can reveal detailed structural changes indistinguishable by CD. Notable exceptions to this are the **trpzip** peptides, which display large exciton couplings, enabling accurate determination of thermodynamic parameters from thermal CD studies.[56]

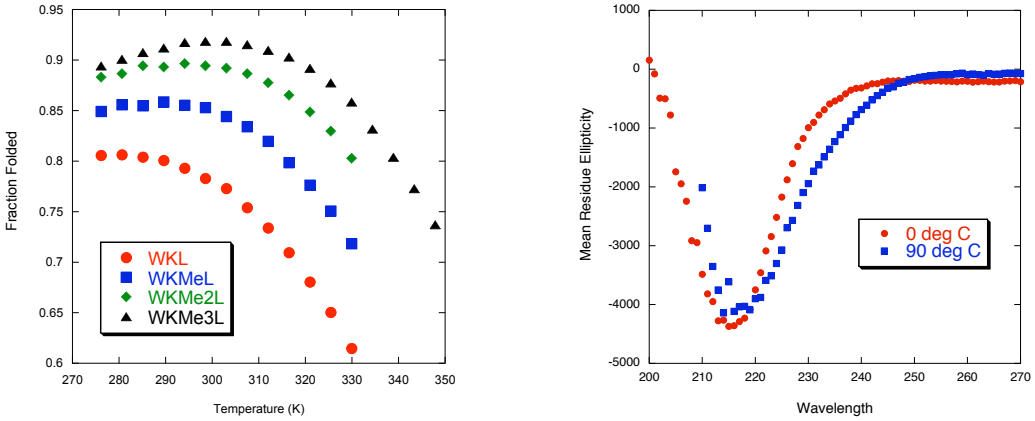

Figure 2.22. (a) Thermal denaturation profiles of WK(Me)$_n$L peptides by NMR. (b) CD spectra of **WKMe$_3$L** at 0 and 90° C.

Analysis of the thermodynamics of folding derived from NMR thermal denaturation reveals increasingly favorable entropy of folding and increasingly

[55] Smith, A.W.; Chung, H.S.; Ganim, Z.; Tokmakoff, A. *J. Phys. Chem. B* **2005**, 109, 17025-17027.

[56] Cochran, A. G.; Skelton, N. J.; Starovasnik, M. A. *Proc. Nat. Acad. Sci.* **2001**, *98*, 5578 – 5583.

unfavorable enthalpy of folding with each methylation step (Table 2.6). The decrease in enthalpic favorability can be explained by the greater dispersion of the positive charge across the N-methyl groups in KMe3, as can be seen from the electrostatic potential maps in Figure 2.23. The increase in entropic favorability is consistent with additional sites of interaction with the aromatic ring with each additional methyl group: while the lysine sidechain in hairpin **WKL** has one preferred site of interaction (the polarized ε-methylene), the methylated peptides **WKMeL, WKMe$_2$L,** and **WKMe$_3$L** have additional polarized methyl groups that can interact favorably with the aromatic ring. In addition, the enhanced hydrophobicity of the sidechain upon methylation is also reflected by the trend in ΔS. There is also a trend of increasingly favorable ΔCp° with each methylation, which is usually associated with an increased hydrophobic effect and may be the result of increased burial of the lysine sidechain with each methylation.[57]

Table 2.6. Thermodynamic Parameters[a] for **WK(Me)$_n$L** (n = 0-3) peptides at 298 K[10]

Peptide	ΔH° (kcal/mol)	ΔS° (cal/mol K)	ΔC$_p$° (cal/mol K)
WKL	-2.8 (0.03)	-6.8 (0.1)	-163 (3)
WKMeL	-1.7 (0.1)	-2.2 (0.3)	-221 (33)
WKMe$_2$L	-0.7 (0.1)	+1.8 (0.4)	-207 (31)
WKMe$_3$L	-0.1 (0.1)	+4.5 (0.3)	-243 (36)

[a] Determined from the temperature dependence of the Gly chemical shift from 0 to 60 °C for peptide **WKL**, **WKMeL**, and **WKMe$_2$L** and from 0 to 80 °C for the peptide **WKMe$_3$L**. Conditions: 50 mM sodium acetate-d$_4$, pH 4.0 (uncorrected) at 298 K, referenced to DSS. Errors (in parentheses) are determined from the fit.

[57] Loladze, V.V.; Ermolenko, D.N.; Makhatadze, G.I. *Prot. Sci.* **2001**, 10, 1343-1352.

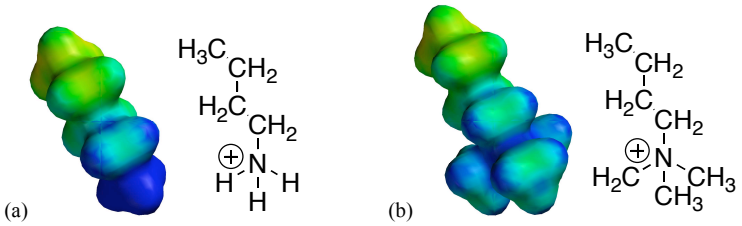

Figure 2.23. Electrostatic potential maps of (a) lysine sidechain analogue and (b) trimethylated lysine sidechain analogue (Spartan: HF/6-31g*; Scale = 50 to 200 kcal/mol).[58] Chemdraw structures are included to show the orientation of the sidechain.

WK(Me)$_n$T (n = 0-3) Peptides. Because the series of methylated **WK(Me)$_n$L** peptides are so well folded, we had some concern about the accuracy of the ΔG's determined from the fraction folded, since near 100% folded, small changes in fraction folded result in larger changes in ΔG than near 50% folded. Hence, we reinvestigated the Trp-Lys(Me)$_n$ (n = 1-3) interactions using a peptide series in which the fraction folded of the peptide containing unmethylated Lys was only modestly folded. In addition to the cation-π interaction, another stabilizing structural feature of this family of β-hairpins is the hydrophobic packing of the Trp residue with the cross-strand Leu. This interaction stabilizes the hydrophobic core of the folded peptide, as demonstrated by a series of lysine-containing peptides in which Leu is mutated to Thr (Figure 2.18b), leading to a less well-folded family of β-hairpins (Figure 2.24). Thr has been observed to have a lower β-sheet propensity than Leu in other β-hairpin model systems.[59] It is also clear from the chemical shifts of the Thr and Leu sidechains from **WK(Me)$_n$T** and **WK(Me)$_n$L** peptides that Thr does not interact with Trp as strongly as does Leu (Figure 2.25).

[58] MacSpartan 2004 (Wavefunction, Inc.)

[59] (a) Cochran, A.G.; Tong, R. T.; Starovasnik, M. A.; Park, E. J.; McDowell, R. S.; Theaker, J. E.; Skelton, N. J. *J. Am. Chem. Soc.* **2001**, *123*, 625 – 632. (b) Russell, S. J.; Blandl, T.; Skelton, N.; Cochran, A. G. *J. Am. Chem. Soc.* **2003**, *125*, 388 – 395.

Hence, the observed destabilization of the hairpin appears to be a combination of sidechain-sidechain interaction and β-sheet propensity effects.

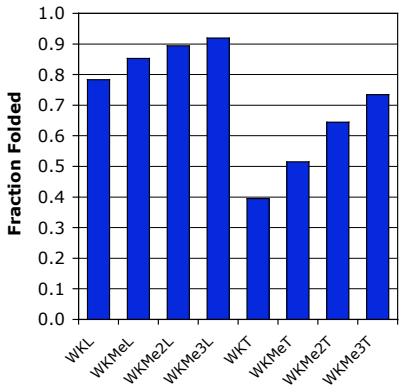

Figure 2.24. Fraction Folded (based on glycine splitting) of **WK(Me)$_n$T** and **WK(Me)$_n$L** (n=0-3) β-hairpins.

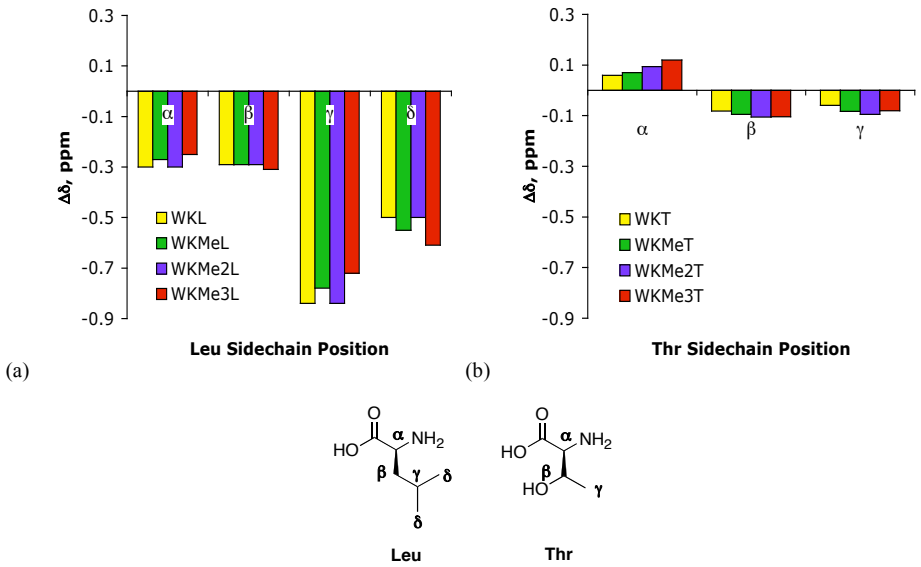

Figure 2.25. (a) Upfield shifts of Leu in **WK(Me)$_n$L** peptides (n=0-3). (b) Upfield shifts of Leu in **WK(Me)$_n$T** peptides (n=0-3). (c) Labeled sidechains of Leu and Thr. (c) Structures of Leu and Thr with sidechain positions labeled.

Comparison of the free energies of folding from the **WK(Me)$_n$L** series of peptides and the **WK(Me)$_n$T** series indicate that the differences in energy upon each

methylation are within error in the two series (Table 2.7). This indicates that the values determined from the **WK(Me)$_n$L** series are reliable, and hence, the double mutant data discussed above for the **WK(Me)$_n$L** series is correct. Moreover, this demonstrates the modular nature of these systems for studying noncovalent interactions, in that two different peptide systems provide the same information on cation-π interactions.

Table 2.7. Comparison of Hairpin Stabilities in the **WKL** and **WKT** Series.

Peptide	Fraction Folded	ΔG° (kcal/mol)	ΔΔG°[a] (kcal/mol)
WKL	0.78	-0.76	--
WKMeL	0.85	-1.04	-0.28
WKMe2L	0.89	-1.26	-0.22
WKMe3L	0.92	-1.44	-0.18
WKT	0.39	0.27	--
WKMeT	0.50	-0.01	-0.27
WKMe2T	0.63	-0.32	-0.31
WKMe3T	0.73	-0.58	-0.26

(a) $\Delta\Delta G° = \Delta G°(WK(Me)_nX) - \Delta G°(WK(Me)_{n-1}X)$, where n = 0-3 and X = Leu or Thr.

WOrn(Me)$_n$L Peptides (n = 0-3). From the ornithine-containing peptide series (**WOrnL, WOrnMeL, WOrnMe$_2$L, WOrnMe$_3$L**), it is apparent that shortening the length of the sidechain by one methylene destabilizes the folded peptide (Figure 2.26a). The ΔG° of folding for **WKL** is -0.77 kcal/mol, while the ΔG° of **WOrnL** is -0.42 kcal/mol. As seen with the lysine series, hairpin stability increases with each methylation of Orn, so that the stability of the trimethylated Orn hairpin **WOrnMe$_3$L** is approximately that of the unmethylated lysine hairpin **WKL** (Figure 2.26b). As

compared to the methylated lysine series, the methylated Orn sidechains show similar trends in their upfield shifting relative to random coil due to their proximity to the aromatic ring (Figure 2.26c). However, with ornithine the polarized δ position is the most upfield shifted portion of the sidechain, indicating that it is the preferred side of interaction with the indole ring. This is directly analogous to the Lys-Trp interaction, where the methylene adjacent to the ammonium group is the preferred site of interaction with Trp. As seen in the methylated lysines, the N-terminal methyl groups are significantly upfield shifted, but less so than the δ protons (Figure 2.26c).

Double mutant cycles performed for the peptides **WOrnL** and **WOrnMe$_3$L** show that methylation of the Orn sidechain lends added stability to the Trp-Orn interaction, just as in the case of the Lys-Trp interaction, with the cation-π interaction worth -0.2 kcal/mol in **WOrnL** and -0.8 kcal/mol in **WOrnMe$_3$L** (±0.1 kcal/mol). That the cation-π interaction is worth slightly less in the Orn peptides versus the Lys peptides is born out by the upfield shifting profiles, which show less upfield shifting for the Orn sidechains than for the Lys sidechains (Figure 2.27).

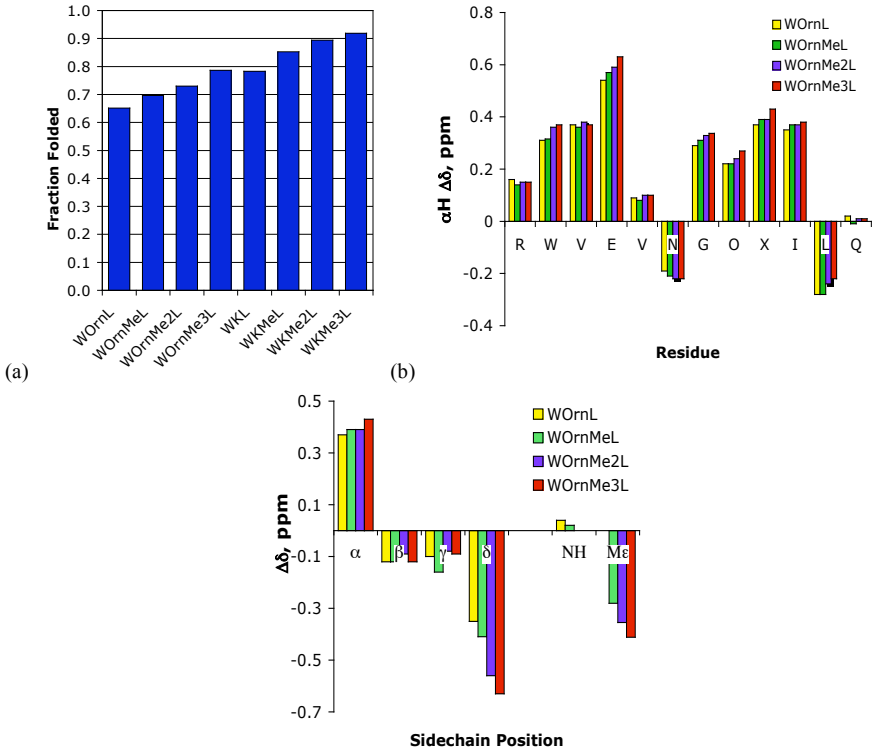

Figure 2.26. (a) **WOrn(Me)$_n$L** and **WK(Me)$_n$L** fraction folded from the glycine splitting (b) **WOrn(Me)$_n$L** H_α shifts relative to random coil values. Glycine shifts reflect the splitting. (c) **WOrn(Me)$_n$L** sidechain upfield proton shifts relative to random coil values.

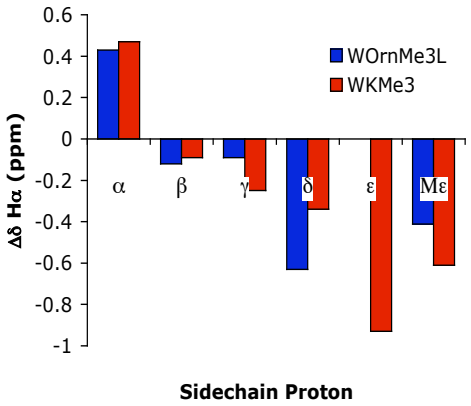

Figure 2.27. Comparison of $OrnMe_3$ and $LysMe_3$ sidechain upfield shifting profiles.

WDab(Me)$_n$L Peptides (n = 0-3). In the diaminobutyric acid (Dab)-containing peptides (**WDabL, WDabMeL, WDabMe$_2$L, and WDabMe$_3$L**), the trends in global hairpin stability observed for the methylation of Lys and Orn continue (Figure 2.28a):

Dab is less stable than Orn or Lys. This is evident from both the fraction folded derived from the glycine splitting and the H_α downfield shifts (Figure 2.28b). However, due to the shortened sidechain of Dab, the preferred site of interaction with Trp changes in comparison to Orn and Lys. While there is some upfield shifting along the Dab sidechain (Figure 2.28c), the magnitude of the methylene shifts proximal to the cation is minor compared to those observed for both the Lys and Orn peptides (-0.95 ppm for the ε-methylene of **WKMe$_3$L** and -0.72 ppm for the δ-methylene of **WOrnMe$_3$L** versus -0.1 ppm for the γ-methylene of **WDabMe$_3$L**). Additionally, while the N-methyl groups of Orn(Me)$_n$ and Lys(Me)$_n$ are less upfield shifted than their δ and ε-methylenes, respectively (Orn: -0.4 ppm versus -0.7 ppm; Lys: -0.6 ppm versus -1.0 ppm), the Dab(Me)$_n$ methyl groups are by far the most upfield shifted portion of the Dab sidechain (-0.4 ppm). The Dab N-methyl groups are at the same location as the Lys ε-methylene. Thus, it appears that due to length restriction, the Dab N-terminal methyl groups are the only portion of the sidechain to experience significant contact with the indole ring. Double mutant cycles for the Trp-Dab interaction possess higher error (0.2 kcal/mol) due to the instability of the Trp to Val single mutant peptides in the Dab series (fraction folded ~ 14%). Thus, they give numbers that are within error for those of the Orn and Lys peptides ($\Delta\Delta G$ = -0.3 kcal/mol for Trp-Dab interaction in WDabL and $\Delta\Delta G$ = -0.9 kcal/mol for Trp-DabMe3 interaction in WDabMe3L, all values ±0.2 kcal/mol). Nonetheless, the magnitude of the Trp-DabMe3 interaction, despite the decreased upfield shifting relative to LysMe3 and OrnMe3 sidechains, suggests that it may be able to interact with the Trp sidechain in a non-specific, hydrophobic fashion (i.e., packing against the side of the ring) in addition to undergoing a cation-π interaction with the face

of the indole ring via its N-terminal methyl groups. Additionally, given the similarity of the interaction magnitudes of the cationic residues with Trp, the trends in overall hairpin stability suggest that the Dab residues also have lower β-sheet propensities than their Orn and Lys analogues.

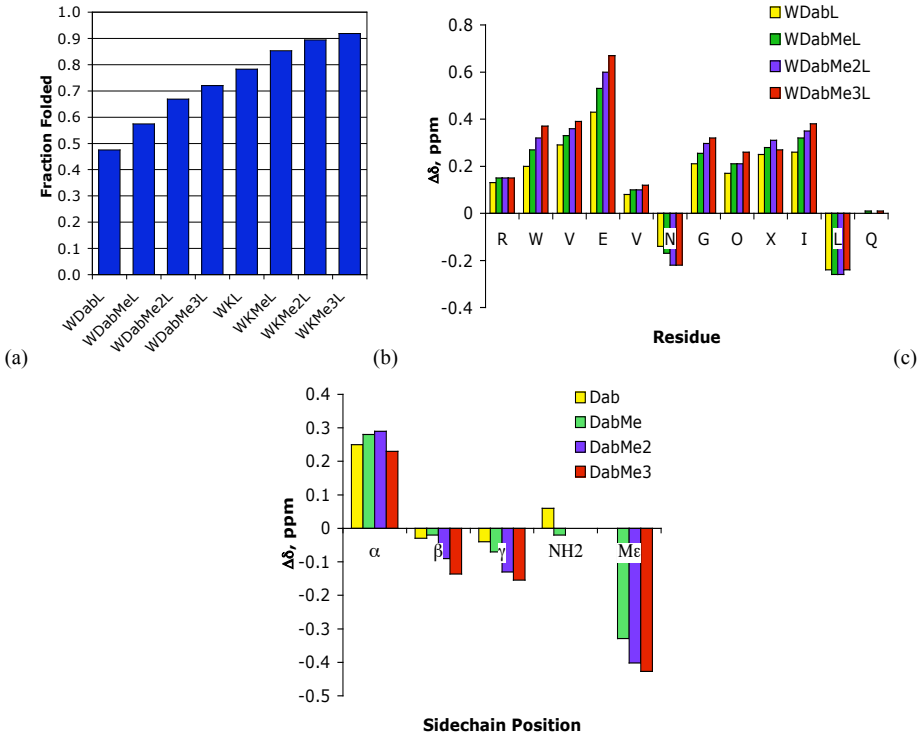

Figure 2.28. (a) WDab(Me)$_n$L and WK(Me)$_n$L fraction folded comparison (b) WDab(Me)$_n$L αH shifts relative to random coil values. Glycine shifts reflect the splitting. (c) WDab(Me)$_n$L sidechain upfield proton shifts relative to random coil values.

pH Studies. It is conceivable that the shortening of the lysine sidechain to diaminobutyric acid might actually favor the formation of a salt bridge with the cross strand glutamic acid (Figure 2.18a). We have previously demonstrated the effect of protonating the Glu in **WKL** by showing that lowering the pH increases hairpin stability.[45] Consistent with our initial observations, all peptides in the series show an

increase in stability upon lowering the pH, which is consistent with hydrophobic packing of the alkyl chains of Lys, Orn, and Dab with the alkyl group of the Glu sidechain, rather than the formation of a traditional salt-bridge (Figure 2.29). Furthermore, mutation of Glu to Gln eliminates the pH dependence of stability. Similar hydrophobic interactions between lysine and glutamic acid have been observed in related coiled-coil systems.[60,61]

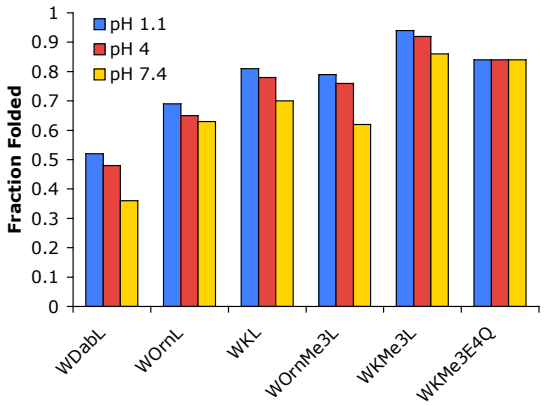

Figure 2.29. pH study of hairpin stability (based on glycine splitting).

NMR Structure Calculation. The calculation of NMR solution structures was undertaken in order to further confirm our experimental observations. Using the program CNSSolve, a simulated annealing protocol was used in conjuction with NMR chemical shift and NOE data to generate a number of low energy structures for the β-hairpins **WKL** and **WKMe$_3$L**.[62] Shown below are selected 10 lowest energy structures from the simulated annealing runs (Figure 2.30). The superimposed backbone structures show the

[60] Ciani, B.; Jordan, M.; Searle, M.S. *J. Am. Chem. Soc.* **2003**, 125, 9038-9047.

[61] Tsou, K.; Tatko, C. D.; Waters, M. L. *J. Am. Chem. Soc.* **2002**, 124, 14917-14921.

[62] Brunger, A.T.; Adams, P.D.; Clore, G.M.; Delano, W.L.; Gros, P.; Grosse-Kunstleve, R.W.; Jiang, J.-S.; Kuszewski, J.; Nilges, N.; Pannu, N.S.; Read, R.J.; Rice, L.M.; Simondson, T.; Warren, G.L. *ACTA CRYST.* **1998**, *D54*, 905-921.

hydrogen-bonding pattern expected for β-hairpin structure and the experimentally observed fraying at the termini (Figure 2.30a-b). The sidechain orientations in the average structure shown in Figure 2.31 also reflect what has been observed experimentally: orientation of the lysine sidechain near the face of the tryptophan ring, with the ε-CH_2 packed into the ring, packing of the leucine with the tryptophan residue, and packing of the glutamic acid sidechain against the lysine methylenes, with the carboxyl functionality directed away from the hydrophobic cluster. Unrestrained molecular dynamics simulations of these average structures in explicit water with the AMBER package indicates that these structures are stable over several nanoseconds of simulation time and are therefore not overly biased by the experimental restraints in our NMR structure calculations (Figure 2.32). The overall conclusion from the computational data is that 1) our initial hypothesis regarding the orientation of the lysine sidechain with respect to the tryptophan is correct and 2) these hairpins contain a tightly packed hydrophobic cluster between residues in the non-hydrogen bonding sites that is accurately described by both experimental and computational data.

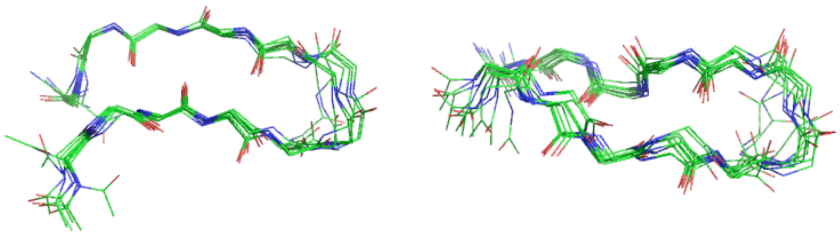

Figure 2.30. Backbones of superimposed NMR structures from simulated annealing runs. (a) **WKL** and (b) **WKMe3L**.

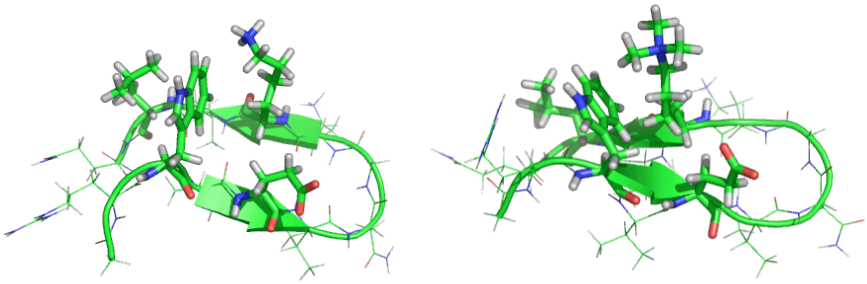

Figure 2.31. Averages of selected NMR structures from simulated annealing runs. (a) **WKL** and (b) **WKMe3L**.

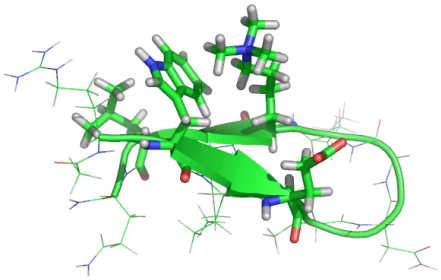

Figure 2.32. Low energy structure of peptide **WKMe3L** from a 2 nanosecond MD simulation in AMBER.

iii. Conclusion

The enhancement of the cation-π interaction via N-methylation within the context of a β-hairpin has been thoroughly investigated. Shortening the sidechain decreases the magnitude of the observed interaction and substantially decreases hairpin stability. Other key factors of fold stability, including the formation of a hydrophobic cluster between Trp, Leu, Glu, and the methylated cationic sidechain, have been shown to contribute substantially to the overall stability of the peptides studied. The incremental modulation of the thermodynamic profile of hairpin folding with increasing methylation reveals the contribution of each additional methyl group to the interaction and suggests a thermodynamic basis for discrimination between mono-, di-, and trimethylation in

biological systems, as seen in the preferential binding of trimethylated lysines by PhD domains and chromodomains.[63] On a fundamental level, this study shows the ability of the Lys, Orn, and Dab sidechains to maintain a favorable interaction with Trp, even as the geometry of the interaction appears to be changing. This is due in part to the flexibility of our β-hairpin model system, and due to the broad recognition surface of Trp, which makes it an easy target to hit. Furthermore, the examination of Orn and Dab residues versus Lys presents another means of stability control in designed proteins and receptors via the cation-π interaction. One can imagine the use of these three interactions to lend varying degrees of strength and specificity to designed systems. Studying these effects in a less solvent-exposed environment might lead to even better control of the interaction. Finally, this study highlights the interplay between β-sheet propensities, specific, and non-specific hydrophobic interactions in determining the overall stability of β-hairpin model systems.

[63] Wysocka, J.; Swigut, T.; Xiao, H.; Milne, T. A.; Kwon, SY; Landry, J.; Kauer, M.; Tackett, A. J.; Chait, B. T.; Badenhorst, P.; Wu, C.; Allis, C. D. *Nature* **2006**, *442*, 86-90.(b) Li, H. T.; Ilin, S.; Wang, W. K.; Duncan, E. M.; Wysocka, J.; Allis, C. D.; Patel, D. J. *Nature* **2006**, *442*, 91-95. (c) Shi, X. B.; Hong, T.; Walter, K. L.; Ewalt, M.; Michishita, E.; Hung, T.; Carney, D.; Pena, P.; Lan, F.; Kaadige, M. R.; Lacoste, N.; Cayrou, C.; Davrazou, F.; Saha, A.; Cairns, B. R.; Ayer, D. E.; Kutateladze, T. G.; Shi, Y.; Cote, J.; Chua, K. F.; Gozani, O. *Nature* **2006**, *442*, 96-99.

D. Experimental Section

i. Small Molecule and Peptide Synthesis

Synthesis of Fmoc-Monomethyl-(oNBS)-Ornithine and Fmoc-Monomethyl-(oNBS)-Diaminobutyric Acid 4. Boc-ornithine-OH (0.358g; 1.5 mmol) was taken up into 15 mL of 1N NaOH in a 100 mL round bottom flask and cooled in an ice bath. O-nitrobenzenesufonyl chloride (2.05g; mmol) was dissolved in 30 mL of diethyl ether and added dropwise over a ten minute period with stirring to the chilled aqueous solution via separatory funnel. After addition was complete, the two-phase solution was allowed to warm slowly to room temperature with vigorous stirring over 14 hours. Next, the reaction mixture was transferred to a separatory funnel, and the aqueous and organic layers separated. The aqueous layer was washed with ether (2 X 25mL), and then chilled to 0 °C. Gradual addition of 1N HCl to pH 4 resulted in the formation of a white precipitate. The chilled aqueous mixture was extracted with several volumes of ethyl acetate (3 X 50 mL). The ethyl acetate was dried with $MgSO_4$ and rotovapped to dryness, yielding a clear oil (0.327g). The oil was subsequently taken up in 10 mL of 1N NaOH with stirring in a 100 mL roundbottom flask. Dimethyl sulfate (1 mL) was added and the solution was allowed to stir for 3 hours. The reaction was followed by TLC (10:1 CH_2Cl_2: MeOH). The resulting aqueous solution was chilled to 0 °C and carefully acidified to pH 4 with 1N HCl, resulting in the formation of a white precipitate. The acidic mixture was extracted with several volumes of ethyl acetate, which was dried with $MgSO_4$ and evaporated in vacuo to give a yellowish oil, which was purified vi silica gel chromatography (10:1 CH_2Cl_2:MeOH) to give compound **3**. (Yield: 0.215g, 0.5 mmol,

33% yield). NMR (600 MHz, CDCl3): 7.96 (d, 1H), 7.68 (m, 2H), 7.60 (d, 1H), 5.27 (broad s, 1H), 4.2 (m, 1H), 3.26 (m, 2H). 2.87 (s, 3H), 1.68 (m, 4H), 1.43 (s, 9H). ESI-MS: calculated = 431.14 actual = 431.2

Compound **3** was taken up into a solution of 5mL of trifluoroacetic acid in 15 mL of methylene chloride and stirred for 30 minutes to remove the BOC group. After removing the solvent in vacuo, the remaining residue was triturated with ether, resulting in a white solid. The material was extracted into water (10 mL), frozen, and lyophilized. The resulting compound was dissolved in 25 mL THF and chilled to ice temperature. DIPEA was added (causing compound to precipitate out of solution), followed by gradual addition of Fmoc-Cl in THF (20 mL). Upon completion of addition of Fmoc-Cl, the precipitated compound disappeared and the solution was removed from the ice bath and stirred for 10 hours. The resulting solution was rotovapped and the residue was washed with several volumes of ether, which was carefully decanted. The remaining residue was taken up into ethyl acetate (50 mL) and washed with water (2 X 10 mL). The resulting organic solution was dried with $MgSO_4$ and evaporated to dryness, resulting in a clear oil. Compound **4** was purified via silica gel chromatography (column flushed with 100 mL methylene chloride; product eluted with 10:1 methylene chloride:methanol) to give 0.200 g of a white solid (0.362 mmol; 72% yield for two steps). ESI-MS: calculated = 553.15; actual = 553.2 NMR (600 MHz): 7.954 (d, 1H), 7.748 (d, 2H), 7.652 (m, 2H), 7.58 (m, 3H), 7.384 (dd, 2H), 7.299 (dd, 2H), 5.325 (d, 1H), 4.405 (s, 2H), 4.208 (t, 1H), 3.320 (m, 1H), 3.238 (m, 1H), 2.862 (s, 1H), 2.00 – 1.80 (m, 4H).

An identical procedure was followed for the synthesis of Fmoc-monomethyldiaminobutyric acid (oNBS), using Boc-diaminobutyric acid (0.358 g; 1.64

mmol). The product was isolated as a clear oil (0.180 g; 0.334 mmol). ESI-MS: calculated = 539.14; actual = 539.2 NMR (600 MHz): 8.027 (d, 1H), 7.748 (d, 2H), 7.652 (m, 2H), 7.58 (m, 3H), 7.384 (dd, 2H), 7.299 (dd, 2H), 5.427 (d, 1H), 4.403 (s, 2H), 4.170 (t, 1H), 3.269 (m, 1H), 3.153 (m, 1H), 2.822 (s, 1H), 2.125 (m, 2H).

Synthesis of Fmoc-Dimethyl Ornithine and Fmoc-Dimethyl Diaminobutyric Acid 7. Boc-ornithine **5** (0.175 g; 0.75 mmol) was taken up in 10 mL of methanol in a 100 mL round bottom flask with stirring. 340 μL of 37% formaldehyde (11 mmol) was added to the solution, which was then allowed to stir for 5 minutes. The flask was flushed with N2, followed by the addition of 0.33 g of 10% Pd/C. Next, the flask was plugged with a rubber septum and flushed with H_2 gas. A balloon of H_2 was attached, and the reaction stirred for 24 hours. The contents of the flask were then filtered to remove the catalyst and rotovapped to dryness to give compound **6a**. The reaction was monitored by TLC (5:1 CH_2Cl_2: MeOH) with ninhydrin staining. Reaction completion was confirmed with RP-HPLC (C18 column; gradient of 5% CH_3CN – 60% CH_3CN in water over 30 minutes). ESI-MS: calculated = 260.17; actual = 260.2 NMR (600 MHz,CDCl3): 5.70 (s, 1H), 4.08 (s, 1H), 2.98 (t, 1H), 2.80 (t, 1H), 2.70 (s, 6H), 1.81-1.59 (m, 4H), 1.42 (s, 9H). Compound **6a** was taken up into a solution of 5 mL of trifluoroacetic acid and 250 mL of triisopropylsilane in 15 mL of methylene chloride and stirred for 30 minutes to remove the BOC group. After removing the solvent in vacuo, the remaining residue was triturated with ether, resulting in an oily precipitate. The material was extracted into water (10 mL), frozen, and lyophilized to dryness. The resulting oil was then dissolved in water (10 mL) and added to a 100 mL round bottom flask equipped with a stirbar. Sodium carbonate (2.3 mmol; 0.240 g) was added to the solution, followed by 5 mL of dioxane. The

resulting solution was stirred for 10 minutes at 0 °C. Fmoc-OSu (0.825 mmol; 0.278 g) was dissolved in 5 mL dioxane and added dropwise to the ice-cold solution over 10 minutes. The resulting mixture was stirred for 1 hour at 0 °C and 16 hours at room temperature. The reaction was followed by TLC (10:1 CH_2Cl_2:MeOH; Ninhydrin staining). The mixture was then washed with ether (2 X 25 mL) and acidified with 1N HCl to pH 3. The acidic solution was extracted with ethyl acetate (4 X 50 mL), dried with sodium sulfate, and the solvent was removed in vacuo to give 0.252 g (0.659 mmol; 88% yield for two steps) of compound **7a** as an amorphous white solid. ESI-MS: calculated = 382.19; actual = 382.3 NMR (600 MHz,CDCl3): 7.711 (d, 2H), 7.559 (m, 2H), 7.346 (dd, 2H), 7.252 (dd, 2H), 6.149 (s, 1H), 4.304 (m, 2H), 4.150 (t, 1H), 3.111 (m, 1H), 2.984 (m, 1H), 2.746 (s, 6H), 1.95 – 1.80 (m, 4H).

An identical procedure was followed for the synthesis of Fmoc-dimethyldiaminobutyric acid, using Boc-diaminobutyric acid (0.164 g; 0.75 mmol), 30% formaldehyde (340 uL), Pd/C (0.033 g) in MeOH (10 mL) and H_2O (1 mL). ESI-MS: calculated = 246.16; actual = 246.2 NMR (600 MHz,CDCl3): 5.89 (s, 1H), 3.99 (s, 1H), 3.15 (t, 1H), 3.00 (t, 1H), 2.72 (s, 6H), 2.19-2.14 (m, 2H), 1.44 (s, 9H). Deprotection with TFA and reprotection with Fmoc-OSu via an identical procedure gave 0.173 g of compound **7b** as a clear oil (0.47 mmol; 63% yield for two steps). ESI-MS: calculated = 368.17; actual = 368.2 NMR (600 MHz,CDCl3): 7.737 (d, 2H), 7.590 (m, 2H), 7.374 (dd, 2H), 7.289 (dd, 2H), 6.239 (s, 1H), 4.331 (m, 2H), 4.185 (t, 1H), 3.160 (m, 1H), 3.045 (m, 1H), 2.739(s, 6H), 2.28 – 2.16 (m, 2H).

Synthesis of Trimethylated Lysine, Ornithine, and Diaminobutyric acid. Trimethylated amino acids were synthesized following the procedure of Kretsinger and

Schneider.[64] The peptides were synthesized using Fmoc-Lys$(Me)_2$-OH purchased from either Anaspec or Bachem or Fmoc-Orn$(Me)_2$-OH or Fmoc-Dab$(Me)_2$-OH synthesized by methods described above. The dimethylated amino acid-containing peptides (0.100 mmol scale) were reacted prior to cleavage from the resin with MTBD (18 μL, 0.125 mmol) and methyl iodide (62 μL, 1 mmol) in DMF (5 mL) for 4 hours with bubbling N_2 in a peptide synthesis flask stoppered with a vented septum. After washing the resin with DMF (3X), CH_2Cl_2 (3X), and drying, the peptide was cleaved with a cocktail of 90% TFA/5% Triisopropylsilane/5% H_2O for 3 hours. The peptide was then purified by standard HPLC methods.

Peptide Synthesis and Purification. Peptide synthesis was performed on an Applied Biosystems Pioneer peptide synthesizer using standard FMOC solid phase peptide synthesis methodology. Non-commercially available amino acids were in some cases coupled by hand. Peptides were purified with reverse phase HPLC, lyophilized, and characterized by MALDI or ESI-TOF mass spectroscopy and NMR.

ii. NMR Spectroscopy.

NMR samples were made in concentrations of approximately 1 mM and analyzed on a Varian Inova 600 MHz spectrometer. Samples were dissolved in D_2O buffered to pD 4.0 (uncorrected) with 50 mM NaOAc-d_3, unless otherwise noted. Amine and amide resonances were assigned in 60% H_2O solutions. 1D NMR spectra were collected using 32K data points and between 8 and 64 scans using a 1-3 sec presaturation. All 2D NMR experiments used pulse sequences from the Chempack software including TOCSY, DQCOSY, gCOSY, and NOESY. 2D NMR scans were taken with 16-64 scans in the first

[64] Kretsinter, J. K.; Schneider, J. P. *J. Am. Chem. Soc.* **2003**, *125*, 7907 – 7913.

dimension and 64-256 scans in the 2nd dimension. All spectra were analyzed using standard window functions (sinebell and gaussian). Mixing times of 0.5 or 0.6 sec were used in the NOESY spectra. Assignments were made using standard methods as described by Wurthrich (ref). Temperature calibrations were made using methanol and ethylene glycol standards.

iii. pH Studies.

Three buffer solutions in D_2O were used to analyze the sensitivity of peptide stability to changes in pH: pH 7.4 (10 mM Sodium Phosphate buffer), pH 4 (50 mM Sodium Acetate buffer), and pH1.10 (Phosphoric Acid buffer). pH values uncorrected for deuterium isotope effects.

iv. NMR Structure Calculation and MD Simulation.

NOEs were classified as strong, medium, or weak by visual inspection. Accordingly, upper bounds for distance restraints were set at 5.0, 3.5, or 2.5 Å.[65] NMR structures were calculated using a simulated annealing protocol within the program CNS_Solve.[62] Hydrogen bonds were enforced with upper limits of 2.0 Å and assigned based on backbone amide shifts. 23 non-sequential NOEs were used in the calculation of **WKL** and 34 non-sequential NOEs were used in the calculation of the structure of **WKMe3L**. All available backbone amide, H_α, and sidechain ^1H chemical shifts were also employed in the calculations via a harmonic potential with a primary chemical shift force value of 10 (61 observed chemical shifts; random coil values taken from 7mers). Two rounds of simulated annealing were employed in each calculation. In the first, 200 structures were generated from an extended starting structure. In the second, 50 structures

[65] Mahalakshmi, R.; Raghothama, S.; Balaram, P. *J. Am. Chem. Soc.* **2006**, *128*, 1125-1138.

were generated starting from an averaged folded structure taken from the initial run. The best structures were selected from the second run based on total energy and visual inspection and averaged. The average structures were subjected to an additional unconstrained conjugate gradient minimization.

The resulting average structure for **WKMe3L** was used as the starting structure for an MD run in explicit water in AMBER.[66] Non-natural residues were constructed in xLeap and parameterized based on existing residues with scaled Merz-Kollman atomic charges. The starting structure was solvated in an octahedral box using TIP3P water and the system charge neutralized with two chloride ions. The solvated system was equilibrated by heating from 0 to 300K over 20 ps. Finally, production MD were run at 300K using PME electrostatics and periodic boundary conditions within Amber ff99. The lowest energy structure was selected from the 2 ns run for demonstrative purposes.

Atomic charges of trimethylated lysine for use in Amber ff99 were parameterized using Merz-Kollman charge calculated with Gaussian 03 [b3lyp/cc-pvDZ SCF=Tight Test Pop=MK iop(6/33=2,6/41=10,6/42=10) Nosymm] and processed using Antechamber. Charges were averaged for equivalent groups (i.e., methyls on ammonium headgroup) and are shown below (Figure 2.33):

[66] D.A. Case, T.A. Darden, T.E. Cheatham, III, C.L. Simmerling, J. Wang, R.E. Duke, R. Luo, K.M. Merz, B. Wang, D.A. Pearlman, M. Crowley, S. Brozell, V. Tsui, H. Gohlke, J. Mongan, V. Hornak, G. Cui, P. Beroza, C. Schafmeister, J.W. Caldwell, W.S. Ross, and P.A. Kollman (**2004**), AMBER 8, University of California, San Francisco.

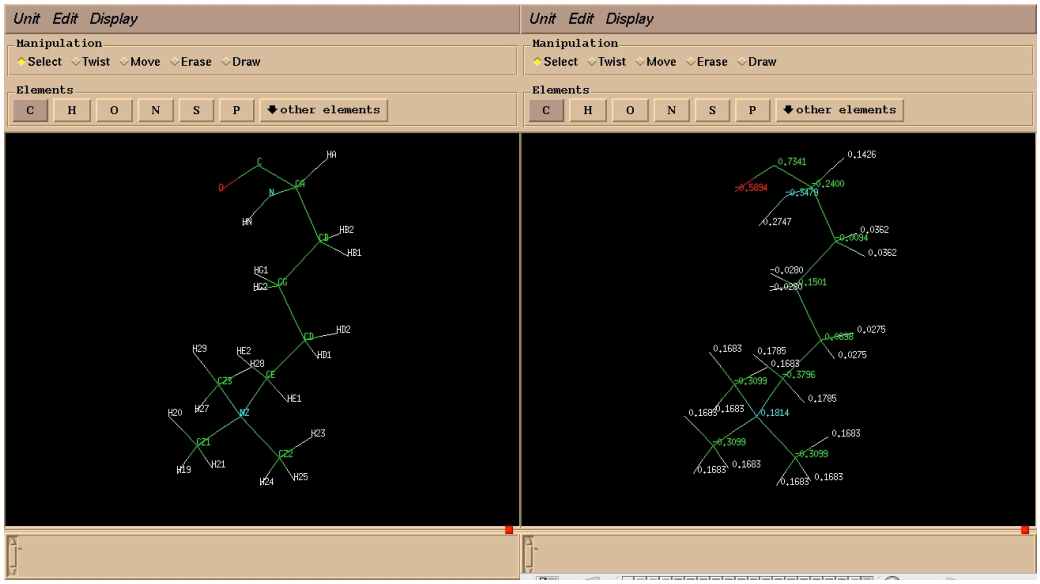

Figure 2.33. Xleap visualization of KMe3 atomic charges calculated for Amber ff99.

Pre-production runs included minimization of the solvent (TIP3P water) and counterions, minimization of the entire system, and heating of the system from 0 to 300K over 20 ps.The 2 ns MD simulation was run under constant temperature (300K; Langevin temperature) and pressure (1 atm), using the SHAKE algorithm and a timestep of 2 fs. Plots of Energy, Temperature, and Pressure from the simulation are shown below (Figure 2.34).

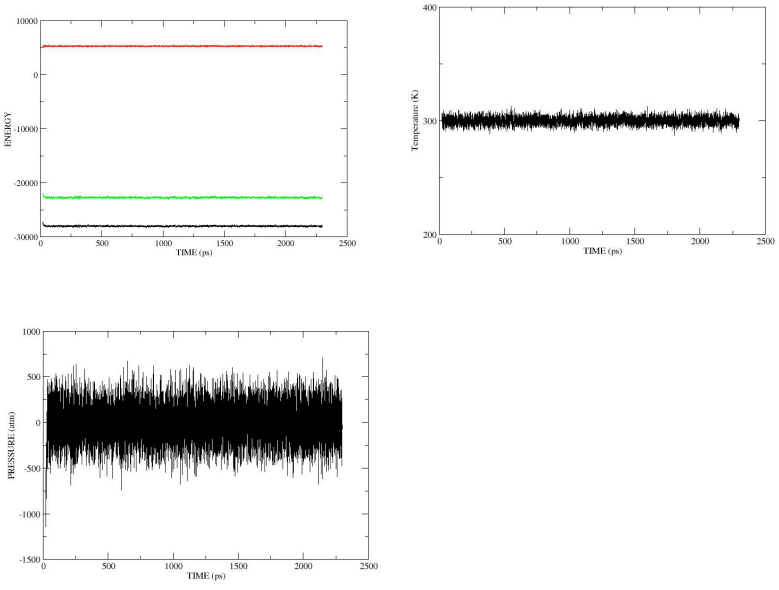

Figure 2.34. (a) Energy plots from the 2 ns simulation (Kinetic Energy: Red; Potential Energy: Black;

Total Energy: Green) (b) Temperature during the simulation. (c) Pressure fluctuation during the simulation.

v. Determination of Fraction Folded.

To determine the chemical shifts of the fully folded state, 14-residue disulfide-linked analogs of peptides were synthesized with the sequence of Ac-CRWVEVNGO**X**ILQC-NH_2, where **X** = cationic residue (Arg, DMAa, DMAs, K, KMe, KMe2, KMe3, etc.) and characterized by NMR. The disulfide bond between Cys1 and Cys14 constrains the peptide to a β-hairpin. To determine the unfolded chemical shifts, 7-mers were synthesized with sequences Ac-RWVEVNG-NH_2 and Ac-NGO**X**ILQ-NH_2, where **X** = (Arg, DMAa, DMAs, K, KMe, KMe2, KMe3, etc.). The chemical shifts for residues in the strand and one turn residue were obtained from each 7-mer peptide. The fraction folded was determined from equation [11].

$$\text{Fraction Folded} = [\delta_{obs} - \delta_0]/[\delta_{100} - \delta_0], \quad [11]$$

where δ_{obs} is the observed chemical shift, δ_{100} is the chemical shift of the cyclic peptide, and δ_0 is the chemical shift of the unfolded 7-mers.

The free energy of folding can be calculated using equation [12]

$$\Delta G = -RT\ln(f/(1-f)), \text{ where } T = 298K;\ f = \text{fraction folded} \quad [12]$$

vi. Double Mutant Cycles.

Single and double mutants of β-hairpin peptides were synthesized by mutating Trp to Val and the cationic residue (Arg, DMAa, DMAs, K, KMe, KMe2, KMe3, etc.) to Ser. This resulted in the following peptides, where **X** = (Arg, DMAa, DMAs, K, KMe, KMe2, KMe3, etc.): Ac-R**V**VEVNGO**X**ILQ-NH_2, Ac-CR**V**VEVNGO**X**ILQC-NH_2, Ac-R**W**VEVNGO**S**ILQ-NH_2, and Ac-R**V**VEVNGO**S**ILQ-NH_2. The stability of each mutant hairpin was determined from equations 10 and 11 as described above, using the following

cyclic peptides as controls for the fully folded state: Ac-CR**V**VEVNGO**X**ILQC-NH2, Ac-CR**W**VEVNGO**S**ILQC-NH_2, and Ac-CR**V**VEVNGO**S**ILQC-NH_2. The magnitude of the sidechain-sidechain interaction was then determined as shown in Figure 1.4.

vii. Thermal Denaturations.

Thermal denaturations were conducted following the change in glycine splitting with a 600 MHz Varian NMR spectrometer. Samples were allowed to equilibrate for seven minutes at each temperature. Spectra were acquired using 16-32 scans with 72000 data points at each temperature. Solvent suppression was achieved using presaturation. Denaturation experiments were run in duplicate, and the temperature was calibrated using methanol and ethylene glycol standards. Thermodynamic data was determined using a non-linear least squares fitting algorithm to equations [2] and [10] using Origin 7.5.[67]

An F test was performed to determine if the improvement in fit from Equation [10] was statistically significant.[39] In this case, one cannot rely on comparison of the chi-squared values, since the fit from Equation [10] will necessarily be better because it contains two more parameters than Equation [2]. F is defined by equation [13]:

$$F = 1/2[(N-3)\chi_1^2/\chi_9^2 - (N-5)] \qquad [13]$$

where N is the number of points in the data set and χ_1^2 and χ_9^2 are the chi-squared values for Equations [2] and [10], respectively. For data sets containing 12 or more data points (the smallest number of points in any of the data sets), an F value of > 3.9 indicates that the fit from Equation [10] is better than with Equation [2] within 95% confidence limits, and a value of > 6.8 indicates > 99% confidence.[39b] For the peptides

[67] Origin 7.5, OriginLab Corporation, One Roundhouse Plaza, Northampton, MA 01060, U.S.A.

reported here, only WKL gave an F value of less than 3.9, indicating that Equation [2] is satisfactory. Of the other peptides, all gave F values at the > 95% confidence level.

viii. Characterization of Structure.

Methods used to indicate the formation of β-hairpin structure in peptide **WK*L**, **WK*T**, **WOrn*L**, **WDab*L, WR, and WDMA*** include the analysis of Hα shifting relative to random coil, backbone amide shifts relative to random coil, and the identification of cross strand NOEs. The β-hairpin should have backbone hydrogen bonded amides between cross-strand residue pairs Arg-Gln, Val-Ile, and Val-Orn in all hairpin peptides. The presence of these hydrogen bonds is readily demonstrated by downfield shifting of the amide hydrogens in these positions relative to random coil. As seen below, the selected peptides exhibit significant downfield shifting at key positions along the strand (Figure 2.35). As expected for β-hairpins, the termini are frayed and show little or no amide shifting. The Asn amide shows significant downfield shifting as expected for a Type I' turn.

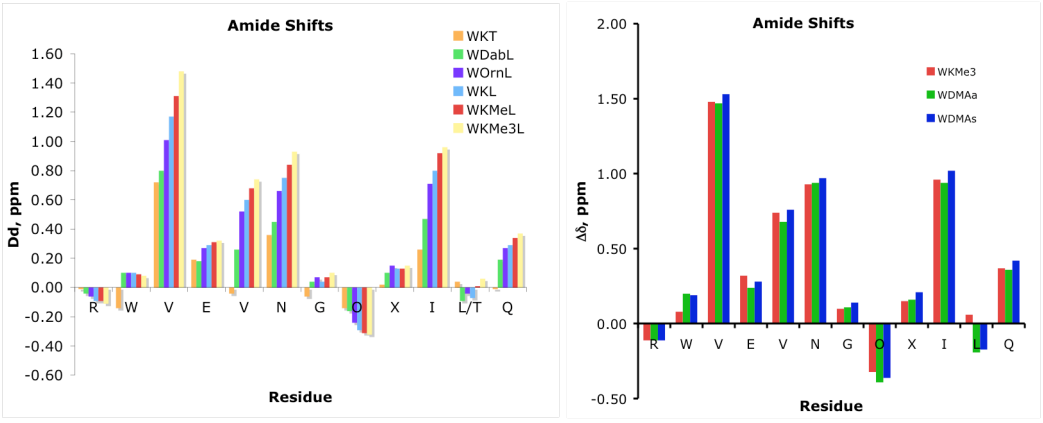

Figure 2.35. Backbone amide shifts for selected β-hairpin peptides.

Furthermore, analysis of the H_α fraction folded plot for selected peptides WKL, WKMeL, WKMe3L, WOrnL, WDabL, WKT, WR, and WDMA* as calculated by equation [11]**,** shows cooperative folding along the entire strand, with the exception of fraying at the termini.

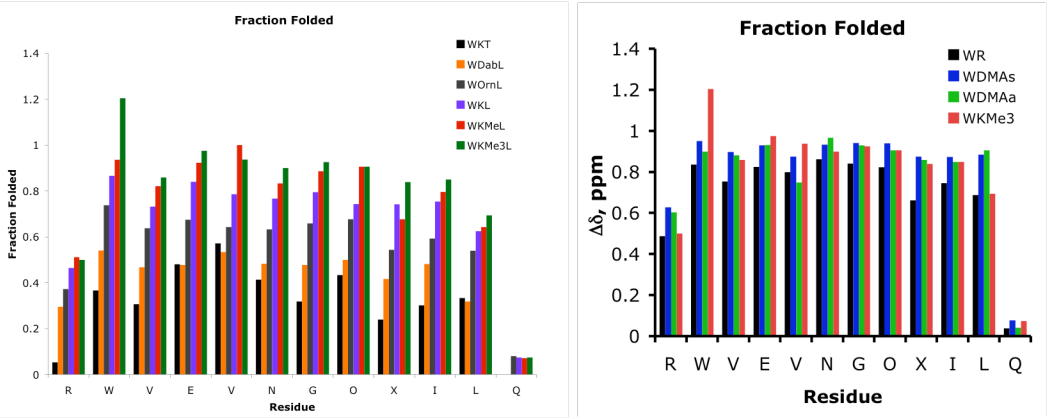

Figure 2.36. Fraction folded data for selected β-hairpin peptides.

Finally, the identification of numerous cross-strand NOEs indicates that all peptides have β-hairpin structure.

Figure 2.37. **WKL** Cross-strand NOEs.

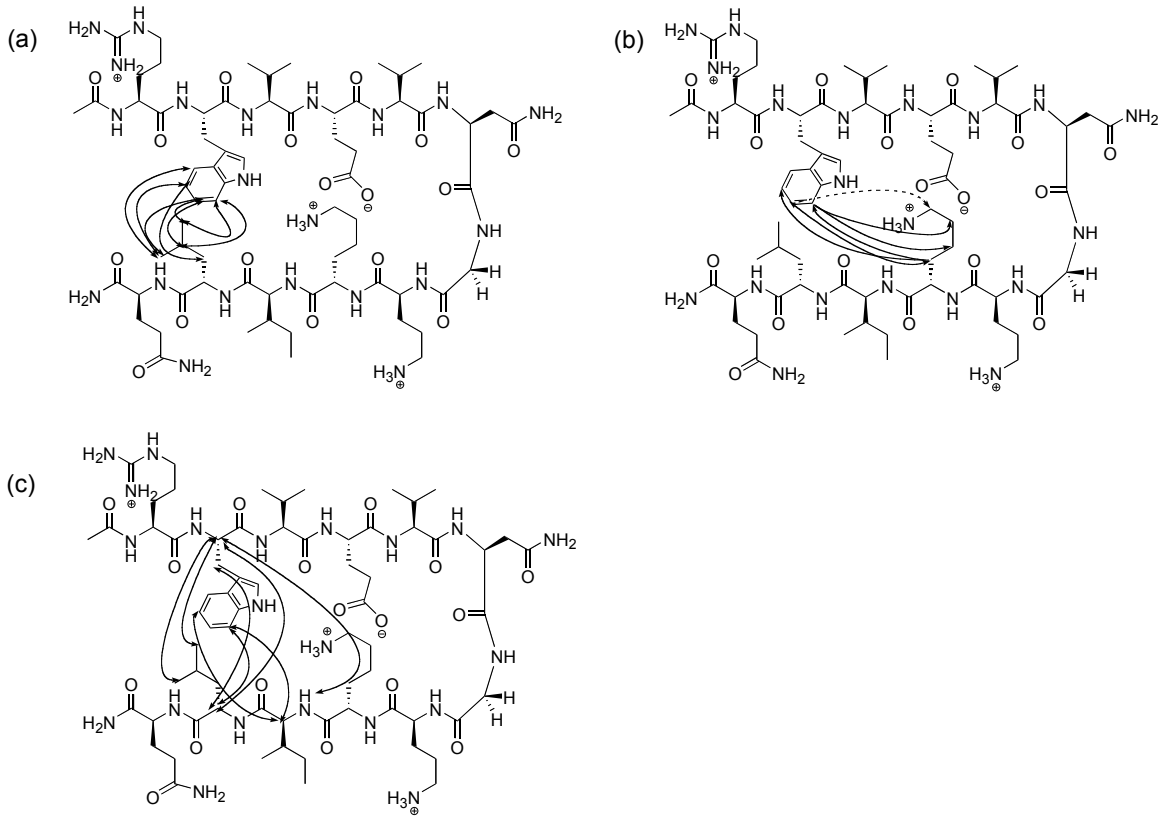

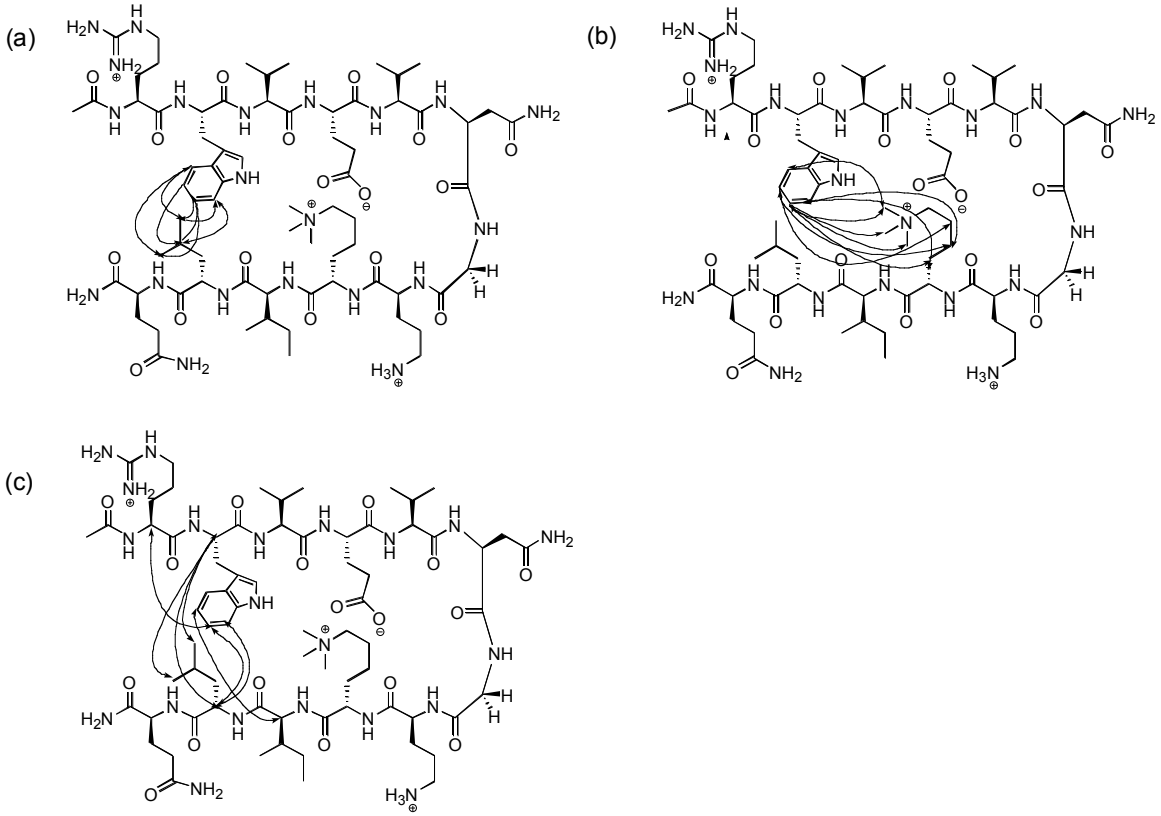

Figure 2.38. **WKMe3L** Cross-strand NOEs.

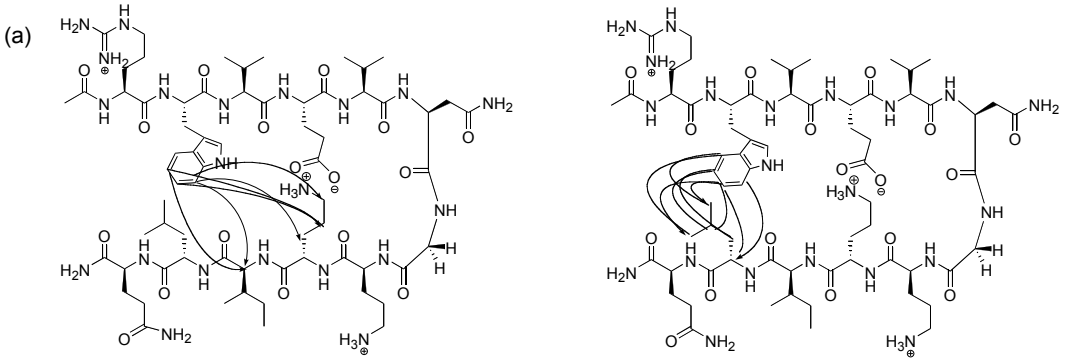

Figure 2.39. WOrnL Cross-strand NOEs.

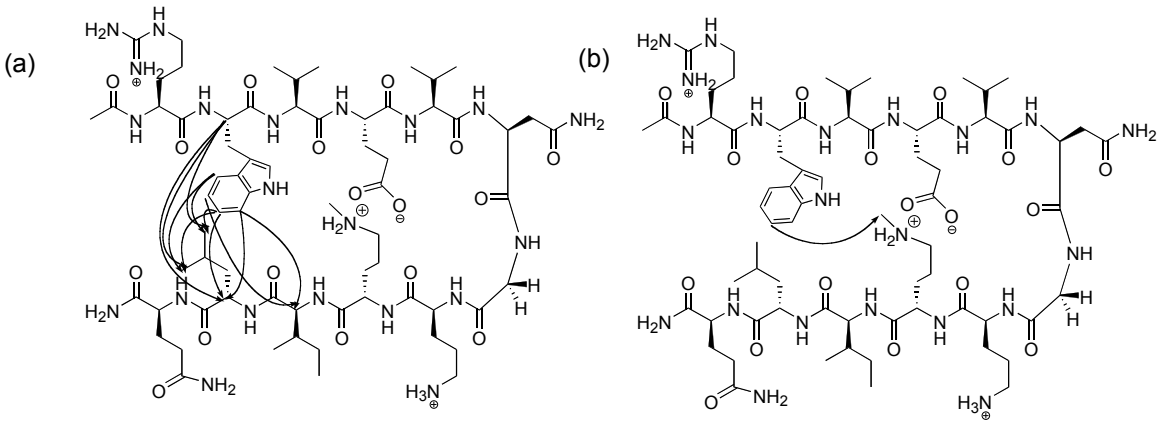

Figure 2.40. WOrnMeL Cross-strand NOEs.

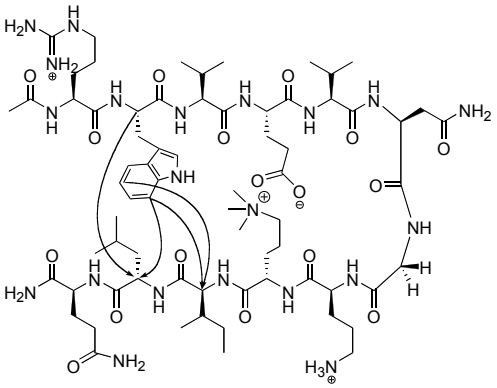

Figure 2.41. WOrnMe3L Cross-strand NOEs.

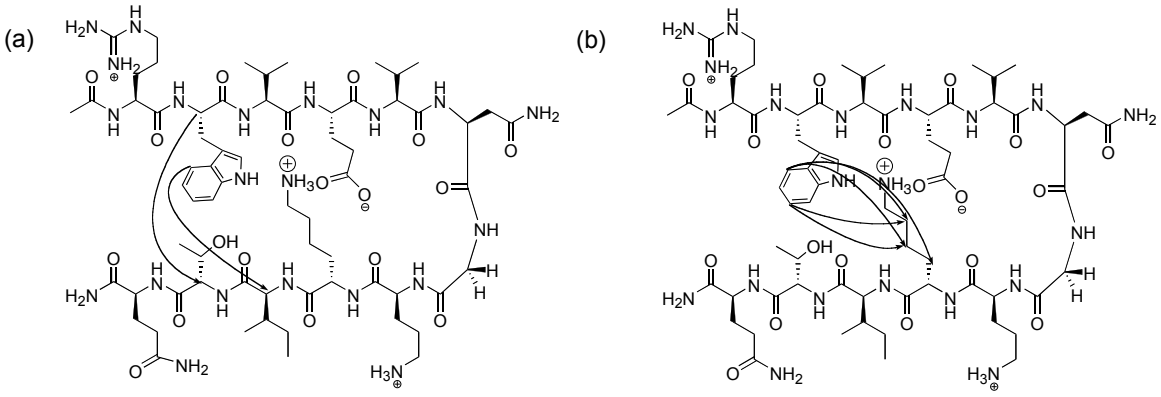

Figure 2.42. WKT Cross-strand NOEs.

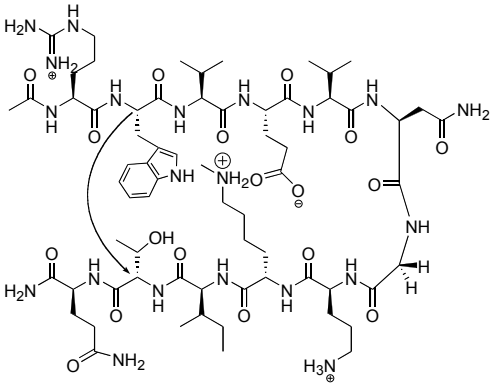

Figure 2.43. **WKMeT** Cross-strand NOEs.

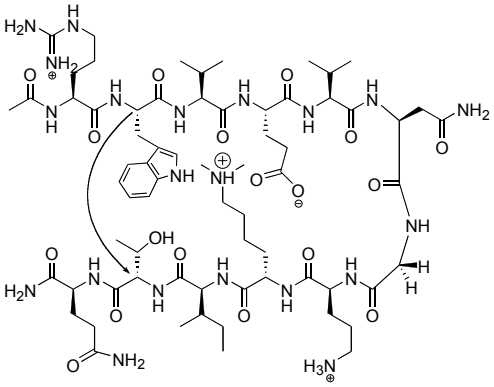

Figure 2.44. WKMe2T Cross-strand NOEs.

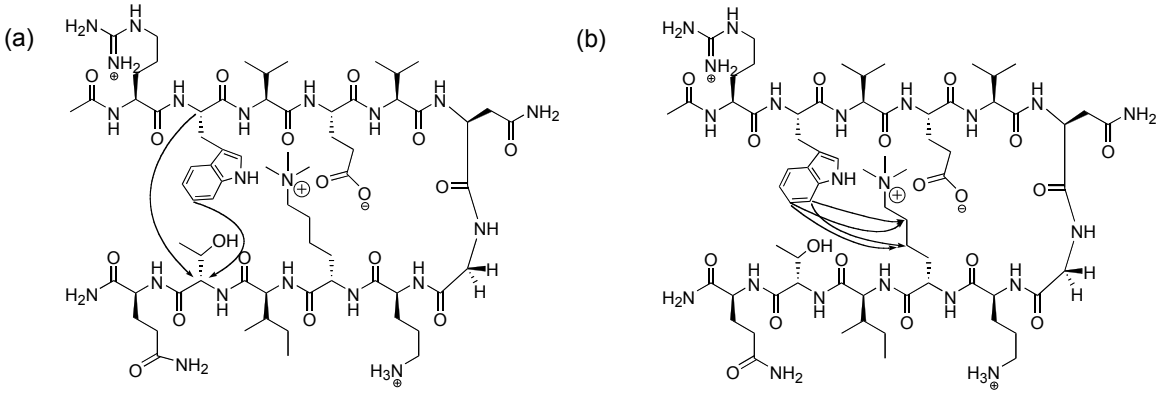

Figure 2.45. WKMe3T Cross-strand NOEs.

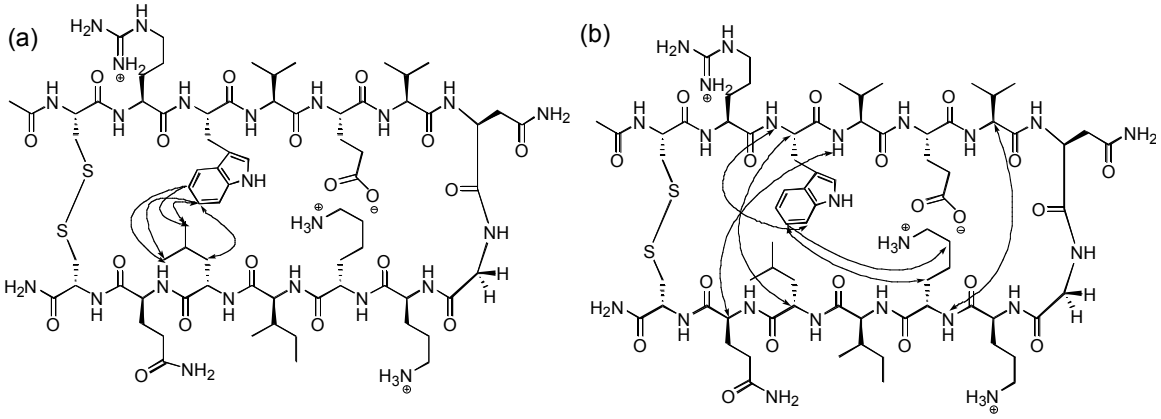

Figure 2.46. WKLcyc Cross-strand NOEs.

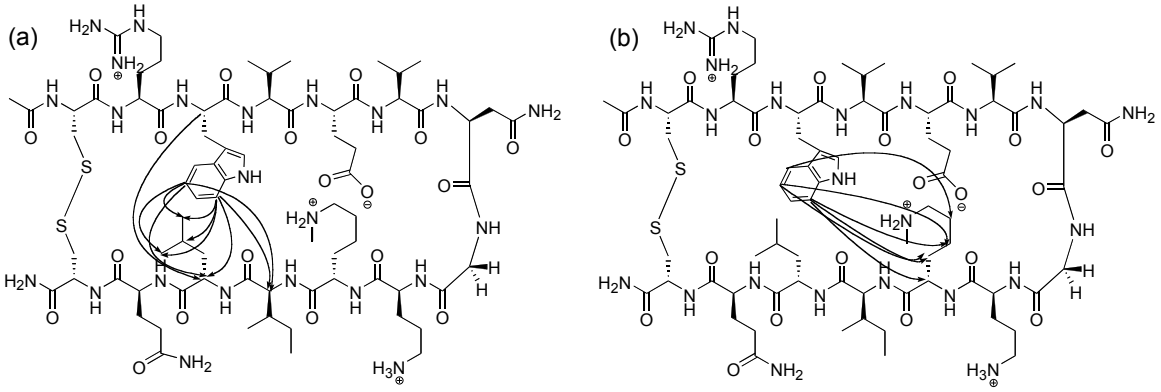

Figure 2.47. WKMeLcyc Cross-strand NOEs.

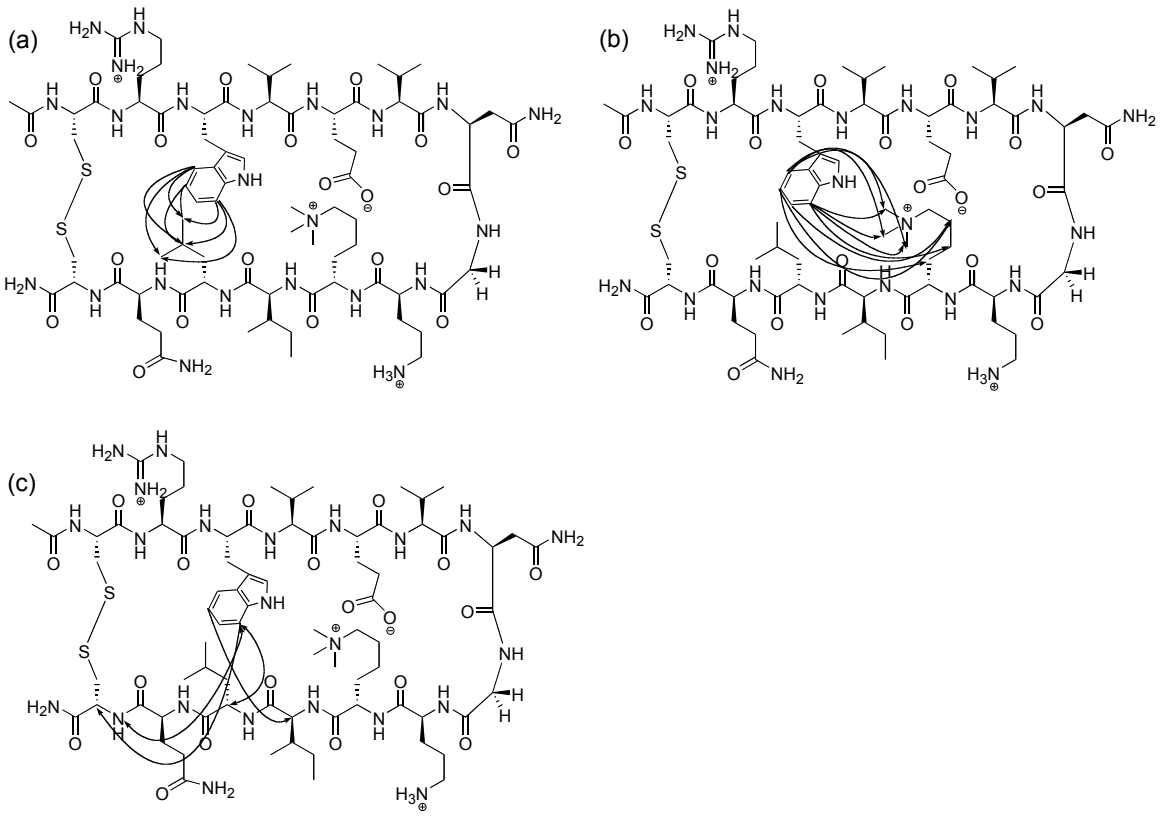

Figure 2.48. WKMe3Lcyc Cross-strand NOEs.

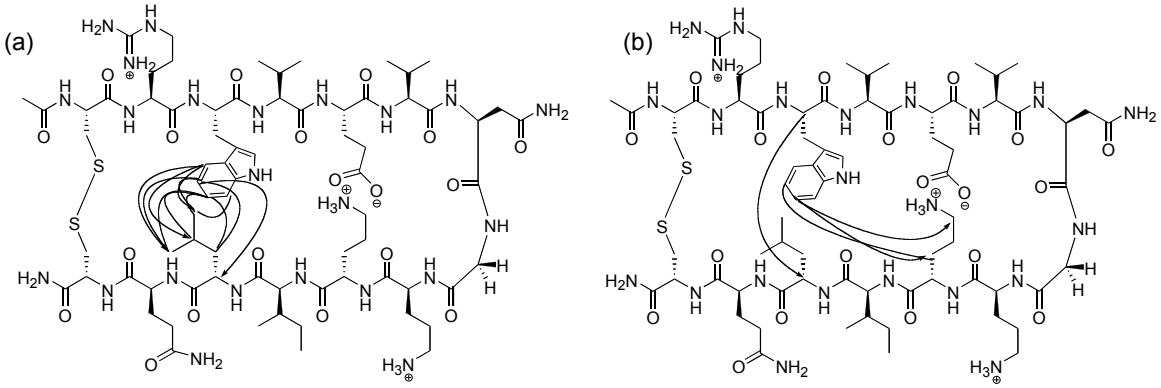

Figure 2.49. WOrnLcyc Cross-strand NOEs.

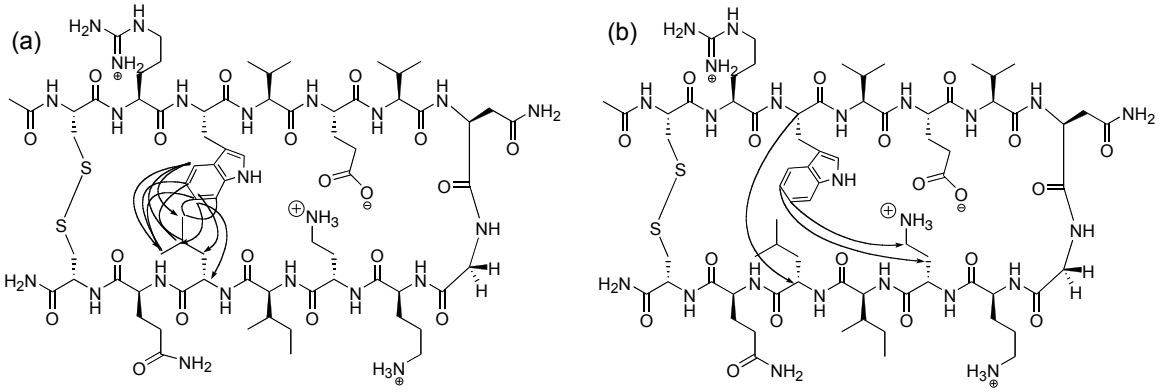

Figure 2.50. WDabLcyc Cross-strand NOEs.

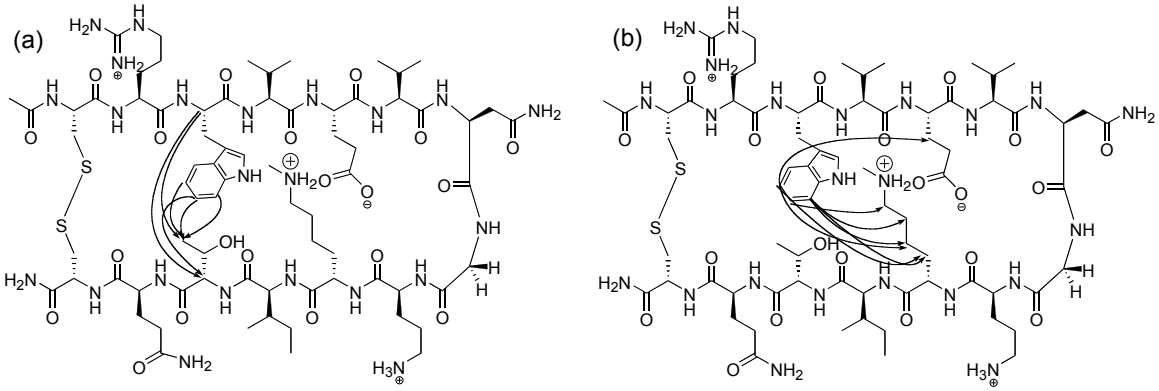

Figure 2.51. WKMeTcyc Cross-strand NOEs.

Figure 2.52. WDMAaCyc Intra- and Interstrand NOEs.

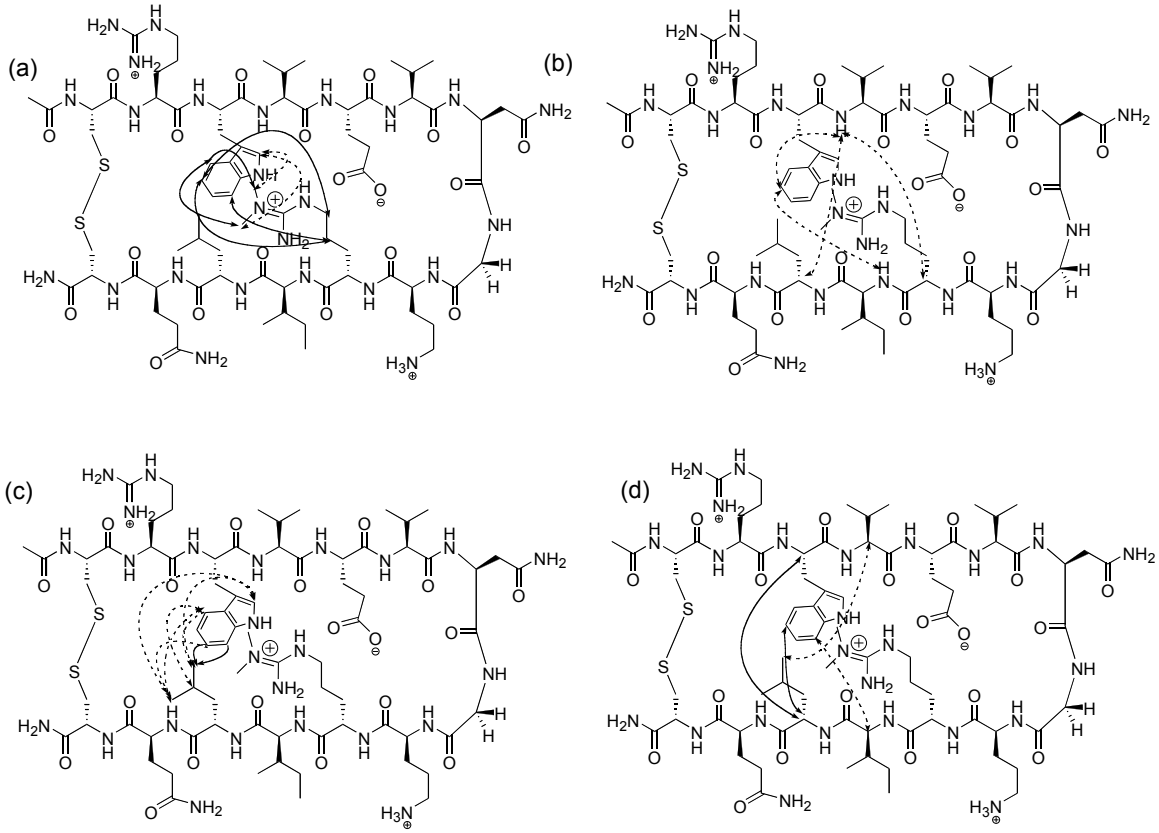

(a) Trp – DMAa NOEs
(b) Cross-strand NOEs
(c) Trp – Leu NOEs
(d) Cross-strand NOEs
Solid line = Strong or Medium NOE
Dashed line = Weak NOE

Figure 2.53. WDMAsCyc Intra- and Interstrand NOEs.

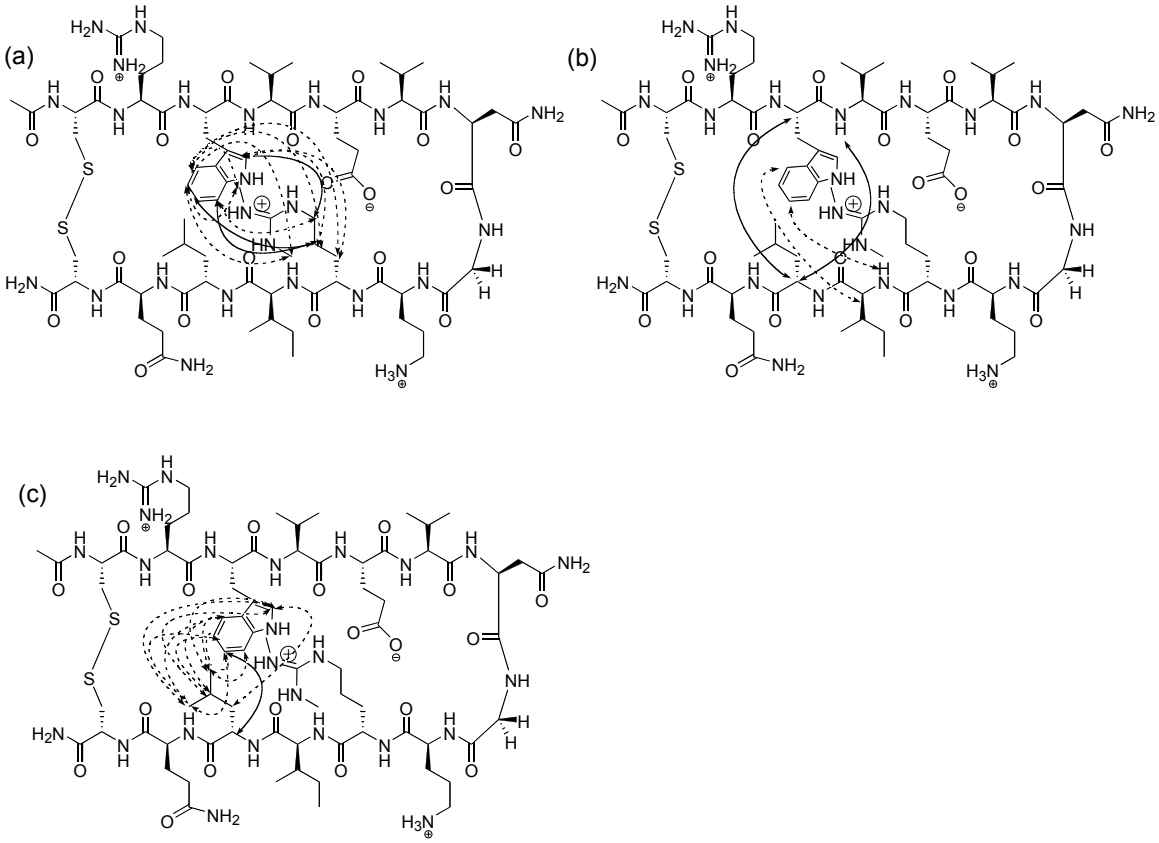

(a) Trp – DMAa NOEs
(b) Cross-strand NOEs
(c) Trp – Leu NOEs
Solid line = Strong or Medium NOE
Dashed line = Weak NOE

Tables 2.8 a-f. NOEs observed in Peptides **WKL**, **WKMe3L**, **WKLCyc**, **WKMe3LCyc**, **WDMAaCyc**, **WDMAsCyc** at 298 K (S=Strong; M=Medium; W=Weak).

Table 2.8a. Peptide **WKL:** Ac-RWVEVNGOKILQ-NH_2

Trp 2	Ar 5	Ile 10	α	M
Trp 2	Ar 5	Lys 9	β	W
Trp 2	Ar 5	Leu 11	β	W
Trp 2	Ar 6	Lys 9	ε	VW
Trp 2	Ar 5	Leu 11	δ	M
Trp 2	Ar 6	Lys 9	β	W
Trp 2	Ar 6	Leu 11	γ	M
Trp 2	Ar 6	Leu 11	δ	M
Trp 2	Ar 7	Ile 10	α	M
Trp 2	Ar 7	Leu 11	α	M
Trp 2	Ar 7	Lys 9	β	S
Trp 2	Ar 7	Lys 9	δ	M
Trp 2	Ar 7	Lys 9	γ	M
Trp 2	Ar 4	Leu 11	δ	W
Trp 2	α	Leu 11	α	S
Trp 2	α	Leu 11	δ	M
Ile 10	α	Trp 2 Ar 7		W
Ile 10	α	Trp 2 Ar 5		W
Leu 11	α	Trp 2	β	W
Leu 11	α	Trp 2	α	S
Leu 11	α	Trp 2 Ar 7		W
Ile 10	NH	Trp 2	α	M

Table 2.8b. Peptide **WKMe3L:** Ac-RWVEVNGOK$(Me)_3^{\oplus}$ILQ-NH_2

Trp 2	Ar 5	Ile 10	α	M
Trp 2	Ar 5	Lys 9	γ	M
Trp 2	Ar 5	Lys 9	δ	M
Trp 2	Ar 5	Leu 11	γ	W
Trp 2	Ar 6	Arg 1	α	M
Trp 2	Ar 6	Leu 11	α	W
Trp 2	Ar 6	Lys 9	$(CH_3)_3$	M
Trp 2	Ar 6	Lys 9	β	W
Trp 2	Ar 6	Lys 9	δ	W
Trp 2	Ar 6	Lys 9	γ	W
Trp 2	Ar 6	Leu 11	γ	W
Trp 2	Ar 6	Leu 11	δ	W
Trp 2	Ar 7	Leu 11	α	M
Trp 2	Ar 7	Leu 11	δ	W
Trp 2	Ar 7	Lys 9	β	S
Trp 2	Ar 7	Lys 9	δ	S
Trp 2	Ar 7	Lys 9	γ	S
Trp 2	Ar 4	Leu 11	δ	M
Trp 2	Ar 4	Lys 9	$(CH_3)_3$	M
Trp 2	α	Leu 11	α	S
Trp 2	α	Leu 11	δ	W
Trp 2	α	Val 3	α	W
Leu 11	α	Trp 2	α	S
Val 3	NH	Trp 2	α	S
Val 5	NH	Glu 4	α	S

Table 2.8c. Peptide **WKLcyc:**
Ac-CRWVEVNGOKILQC-NH_2

Trp 3	Ar 7	Trp 3	NH2 M
Trp 3	Ar 6	Leu 12	α M
Trp 3	Ar 6	Lys 10	δ M
Trp 3	Ar 6	Leu 12	δ W
Trp 3	Ar 6	Lys 10	β M
Trp 3	Ar 5	Leu 12	δ M
Trp 3	α	Leu 12	α S
Val 4	NH	Trp 3	α S
Ile 11	NH	Lys 10	α S
Val 6	NH	Gln 13	α S
Gln 13	NH	Leu 12	α S
Arg 2	NH	Cys 14	α M
Arg 2	NH	Cys 14	β W
Trp 3	NH	Arg 2	α M
Trp 3	NH	Arg 2	β W
Lys 10	NH	Val 4	α W

Table 2.8d. Peptide **WKMe3Lcyc:**
Ac-CRWVEVNGOK$(Me)_3^{\oplus}$ILQC-NH_2

Trp 3	Ar 4	Lys 10	$(CH_3)_3$ M
Trp 3	Ar 4	Leu 12	δ M
Trp 3	Ar 4	Leu 12	γ M
Trp 3	Ar 7	Cys 14	NH M
Trp 3	Ar 7	Lys 10	$(CH_3)_3$ M
Trp 3	Ar 7	Leu 12	δ M
Trp 3	Ar 7	Val 4	NH M
Trp 3	Ar 7	Cys 14	α W
Trp 3	Ar 7	Leu 12	α M
Trp 3	Ar 7	Lys 10	γ S
Trp 3	Ar 6	Lys 10	δ M
Trp 3	Ar 6	Cys 14	β W
Trp 3	Ar 5	Ile 11	α W
Trp 3	Ar 7	Lys 10	δ S
Trp 3	Ar 5	Lys 10	β W
Trp 3	Ar 5	Lys 10	δ S
Trp 3	Ar 7	Leu 12	γ M
Trp 3	Ar 7	Lys 10	NH M
Trp 3	Ar 5	Leu 12	γ S
Trp 3	Ar 5	Leu 12	δ W
Val 6	NH	Cys 14	α S
Asn 7	NH	Trp 3	α M
Ile 11	NH	Val 4	NH M
Ile 11	NH	Lys 10	α M
Val 6	NH	Glu 5	α S
Val 6	NH	Leu 12	α S
Val 6	NH	Glu 5	β M
Val 6	NH	Leu 12	δ M
Arg 2	NH	Cys 14	α S
Arg 2	NH	Cys 14	β M
Arg 2	NH	Leu 12	δ M
Trp 3	NH	Arg 2	α M
Cys 14	NH	Trp 3	Ar 6 M
Cys 14	NH	Arg 2	α S
Cys 14	NH	Arg 2	β M
Leu 12	NH	Ile 11	β M
Orn 9	NH	Gln 13	NH W

Table 2.8e. Peptide **WDMAaCyc:**
Ac-CRWVEVNGOR$(Me)_2^{\oplus}$ILQC-NH_2

Residue	Proton	Residue	Proton	Intensity
Trp 3	Ar 2	DMAa 10	$(CH_3)_2$	M
Trp 3	Ar 2	Trp 3	α	W
Trp 3	Ar 2	Val 4	α	W
Trp 3	Ar 2	Leu 12	δ	W
Trp 3	Ar 4	DMAa 10	$(CH_3)_2$	W
Trp 3	Ar 4	Leu 12	δ	W
Trp 3	Ar 4	Leu 12	γ	W
Trp 3	Ar 5	DMAa 10	δ	S
Trp 3	Ar 5	DMAa 10	γ	S
Trp 3	Ar 5	Trp 3	α	S
Trp 3	Ar 5	Leu 12	α	S
Trp 3	Ar 6	Leu 12	δ	M
Trp 3	Ar 7	DMAa 10	γ	M
Trp 3	Ar 7	Ile 11	α	W
Trp 3	Ar 7	Leu 12	δ	M
Val 4	NH	Trp 3	α	S
Val 4	NH	Trp 3	5H	W
Val 4	NH	Arg 2	α	W
Val 4	NH	Leu 12	α	W
Val 4	NH	Trp 3	β	W
Ile 11	NH	DMAa 10	α	S
Ile 11	NH	Trp 3	5H	W
Gln 13	NH	Leu 12	α	M
Trp 3	α	Leu 12	α	S
Trp 3	α	Val 4	NH	S
Trp 3	α	Val 4	γ	W
DMAa 10	α	Ile 11	α	S
Val 4	α	Leu 12	δ	W
Leu 12	α	Trp 3	α	S
Leu 12	α	Val 4	NH	M
Leu 12	α	Gln 13	NH	M
Leu 12	α	Trp 3	5H	W

Table 2.8f. Peptide **WDMAsCyc:**
Ac-CRWVEVNGOR$(Me)_2^{\oplus}$ILQC-NH_2

Residue	Proton	Residue	Proton	Intensity
Trp 3	Ar 2	DMAa 10	δ	S
Trp 3	Ar 2	DMAa 10	β	W
Trp 3	Ar 2	DMAa 10	γ	W
Trp 3	Ar 2	Leu 12	β	W
Trp 3	Ar 2	Leu 12	γ	W
Trp 3	Ar 2	Leu 12	δ	W
Trp 3	Ar 4	DMAa 10	$(CH_3)_2$	W
Trp 3	Ar 4	Leu 12	δ	W
Trp 3	Ar 4	Leu 12	γ	W
Trp 3	Ar 5	DMAa 10	$(CH_3)_2$	W
Trp 3	Ar 5	DMAa 10	γ	W
Trp 3	Ar 5	DMAa 10	β	W
Trp 3	Ar 5	Leu 12	γ	W
Trp 3	Ar 5	Leu 12	δ	W
Trp 3	Ar 6	Trp 3	α	S
Trp 3	Ar 6	Trp 3	β	S
Trp 3	Ar 6	Leu 12	α	S
Trp 3	Ar 6	DMAa 10	δ	S
Trp 3	Ar 6	Leu 12	δ	W
Trp 3	Ar 7	DMAa 10	γ	M
Trp 3	Ar 7	DMAa 10	δ	W
Trp 3	Ar 7	Leu 12	δ	W
Val 4	NH	Trp 3	α	S
Val 4	NH	Trp 3	2H	M
Val 4	NH	Leu 12	α	M
Ile 11	NH	DMAa 10	α	S
Ile 11	NH	Trp 3	6H	W
Val 6	NH	Glu 5	α	M
Gln 13	NH	Leu 12	α	S
Gln 13	NH	Leu 12	δ	W
Gln 13	NH	Leu 12	γ	W
Arg 2	NH	Cys 1	α	S
Arg 2	NH	Cys 1	β	W
Trp 3	α	Leu 12	α	S

ix. Thermodynamic Analysis

Peptides were analyzed assuming a two-state system. The equilibrium constant was determined from the fraction folded (f) by K = f/(1-f). The free energy was then calculated from $\Delta G° = - RT\ln K$. In order to determine the thermodynamic parameters, $\Delta H°$, $\Delta S°$, and $\Delta Cp°$, the temperature dependence of the Gly chemical shift difference was fit to one of the following equations, as described earlier in the text:[68]

$$\text{Fraction folded} = [\exp(x/RT)]/[1 + \exp(x/RT)]$$

$$\text{Where } x = [T(\Delta S°298 + \Delta Cp° \ln(T/298)) - (\Delta H°298 + \Delta Cp°(T - 298))] \qquad [2]$$

Or

$$\text{Fraction folded} = [\exp(x/RT)]/[1 + \exp(x/RT)]$$

$$\text{where } x = T(\Delta S°_{298} + a \ln(T/298) + b (T - 298) - (c/2) (1/T^2 - 1/298^2)) - (\Delta H°_{298} + a (T - 298) + (b/2) (T^2 - 298^2) - c (1/T - 1/298))]. \qquad [10]$$

[68] Maynard, A.J. Sharman, G. J. and Searle, M. S. *J. Am. Chem. Soc.* **1998**, *120*, 1996-2007.

Table 2.9. Temperature Dependence of the Fraction Folded from Glycine Chemical Shift Data for the **WKL** series peptides:

WKL:		**WKMeL:**		**WKMe2L:**		**WKMe3L:**	
Temp (K)	fraction folded	Temp (K)	fraction folded	Temp (K)	fraction folded	Temp (K)	fraction folded
276	0.806	276	0.849	276	0.883	276	0.894
281	0.806	281	0.856	281	0.886	281	0.901
285	0.804	285	0.855	285	0.894	285	0.908
289	0.801	289	0.859	289	0.893	290	0.912
294	0.793	294	0.855	294	0.896	294	0.918
298	0.783	298	0.853	298	0.894	299	0.919
302	0.773	302	0.844	302	0.892	303	0.919
307	0.754	307	0.834	307	0.886	308	0.915
311	0.734	311	0.820	311	0.878	312	0.910
316	0.709	316	0.798	316	0.865	317	0.903
320	0.680	320	0.776	320	0.849	321	0.892
324	0.650	324	0.751	324	0.830	325	0.878
329	0.615	329	0.718	329	0.803	330	0.859
						334	0.832
						339	0.804
						343	0.773
						348	0.737

Table 2.10. Temperature Dependence of the Fraction Folded from Glycine Chemical Shift Data for the **WOrnL** and **WDabL** peptides:

WOrnL:		**WDabL:**	
Temp (K)	fraction folded	Temp (K)	fraction folded
275	0.722	275	0.557
280	0.717	280	0.547
284	0.711	284	0.533
289	0.701	289	0.514
293	0.688	293	0.492
298	0.671	298	0.468
303	0.649	303	0.441
307	0.622	307	0.410
312	0.594	312	0.380
316	0.564	316	0.346
321	0.530	321	0.315
325	0.493	325	0.279
330	0.454	330	0.244

Table 2.11. Temperature Dependence of the Fraction Folded from Glycine Chemical Shift Data for WK*T series peptides:

	WKT	WKMeT	WKMe2T	WKMe3T
Temp (K)	fraction folded	fraction folded	fraction folded	fraction folded
276	0.453	0.583	0.706	0.784
280	0.449	0.573	0.701	0.780
285	0.438	0.564	0.692	0.778
289	0.426	0.549	0.680	0.769
294	0.414	0.531	0.664	0.760
298	0.398	0.514	0.647	0.744
303	0.379	0.491	0.624	0.729
307	0.358	0.467	0.602	0.707
312	0.337	0.441	0.571	0.684
316	0.315	0.420	0.542	0.656
321	0.292	0.388	0.510	0.626
326	0.270	0.359	0.477	0.595
330	0.245	0.331	0.445	0.559

Table 2.12. Parameters Derived from Fitting of Thermal Denaturation Data for Peptides WK*T at 298 K(Errors shown in parenthesis):

	WKT	WKMeT	WKMe2T	WKMe3T
ΔS (cal/mol*K)	-10.2 (0.04)	-10.4(0.1)	-10.1(0.1)	-8.3 (0.1)
ΔC_p(cal/mol*K)	-99 (2)	-98 (3)	-116 (3)	-134 (3)
ΔH (kcal/mol)	-2.8 (0.01)	-3.1(0.02)	-3.4(0.03)	-3.11 (0.03)

Table 2.13. Temperature Dependence of the Fraction Folded from Glycine Chemical Shift Data for **WDMAa**, **WDMAs**, and **WKMe3**:

WDMAa: **WDMAs:** **WKMe3:**

Temp (K)	fraction folded	Temp (K)	fraction folded	Temp (K)	fraction folded
277	0.927	276	0.923	276	0.894
281	0.933	281	0.931	281	0.901
285	0.936	285	0.936	285	0.908
289	0.939	290	0.939	290	0.912
294	0.939	294	0.941	294	0.918
298	0.940	298	0.941	299	0.919
302	0.938	303	0.937	303	0.919
307	0.931	307	0.930	308	0.915
311	0.922	311	0.920	312	0.910
315	0.907	316	0.905	317	0.903
319	0.889	320	0.886	321	0.892
324	0.870	325	0.861	325	0.878
328	0.842	329	0.832	330	0.859
332	0.810	333	0.788	334	0.832
337	0.772	338	0.760	339	0.804
341	0.731	342	0.717	343	0.773
345	0.677	347	0.670	348	0.737

Table 2.14. Temperature Dependence of the Fraction Folded from Glycine Chemical Shift Data for WR:

WR:

Temp (K)	fraction folded
276	0.870
281	0.868
285	0.865
290	0.860
294	0.850
299	0.830
303	0.810
308	0.780
312	0.740

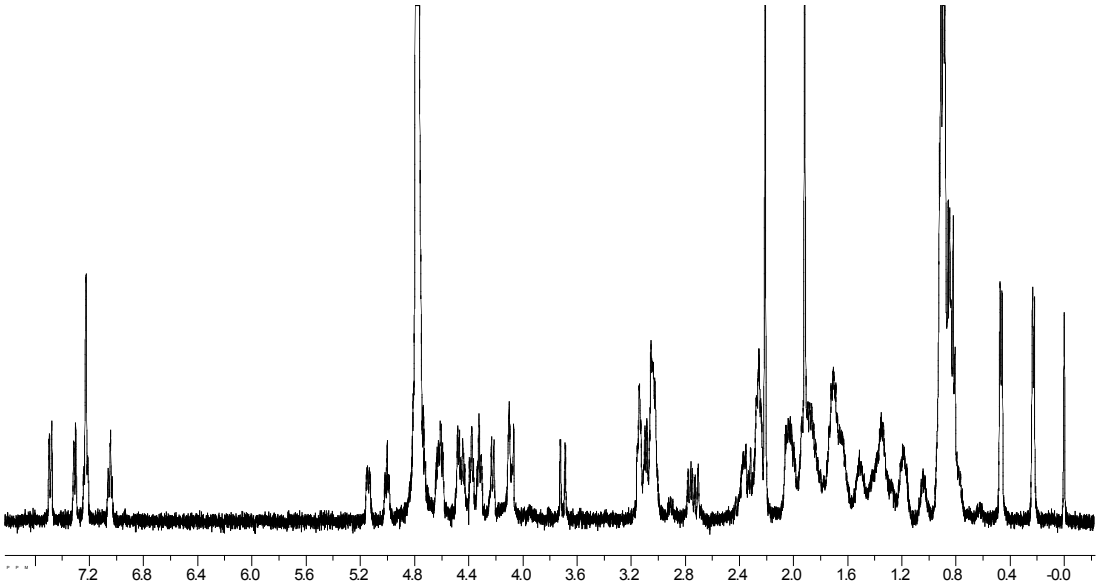

Figure 2.54. [1]HNMR of Peptide **WKL**: Ac-Arg-Trp-Val-Glu-Val-Asn-Gly-Orn-Lys-Ile-Leu-Gln-NH2

Table 2.15. Proton Chemical Shift Assignments for Peptide **WKL**.

	α	β	γ	δ	ε	Amide	Amine
R	4.38	1.69	1.51, 1.65	3.14		8.05	6.62,7.09
W	5.09	3.10	7.23,7.49	7.07,7.23	7.23	8.29	10.17
V	4.43	2.03	0.87			8.92	
E	4.92	2.02,1.91	2.28			8.49	
V	4.21	1.95	0.91			8.82	
N	4.47	3.05,2.76				9.35	
G	4.08,3.73					8.59	
O	4.61	1.86	1.75	3.04		7.84	7.64
K	4.77	1.69	1.24	1.35	2.56	8.46	7.28
I	4.57	1.88	0.89,1.42,1.19	0.89		9.05	
L	4.08	1.36,1.06	0.77	0.3,0.51		8.30	
Q	4.32	2.04,1.88	2.27			8.62	

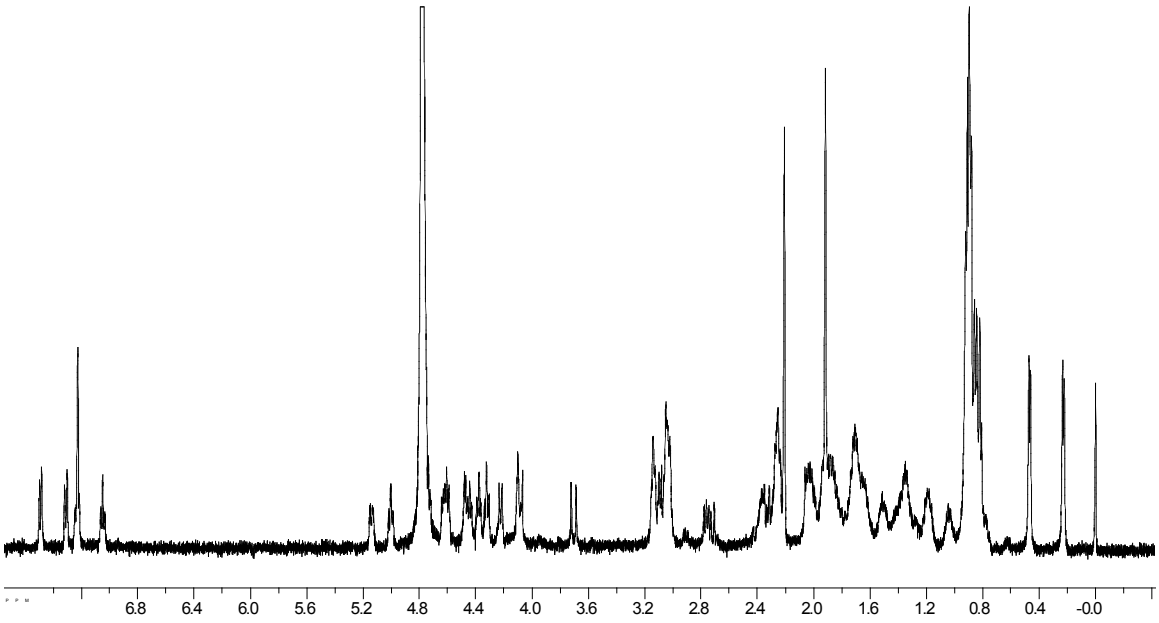

Figure 2.55. [1]HNMR of Peptide **WKMeL**: Ac-Arg-Trp-Val-Glu-Val-Asn-Gly-Orn-Lys(Me)-Ile-Leu-Gln-NH2

Table 2.16. Proton Chemical Shift Assignments for Peptide **WKMeL**.

	α	β	γ	δ	ε	Amide	Amine
R	4.39	1.72	1.53	3.14		8.05	7.11,6.64
W	5.14	3.08				8.28	10.19
V	4.48	2.03	0.87			9.06	
E	5.01	1.97	2.28			8.51	
V	4.23	1.93	0.91			8.90	
N	4.45	3.06,2.75				9.44	
G	4.09,3.70					8.63	
O	4.64	1.83	1.75	3.03		7.82	7.62
K(Me)	4.73	1.67	1.28	1.28	2.33 **CH3**=2.21	8.46	7.66
I	4.58	1.88	0.87,1.43,1.18	0.87		9.16	
L	4.11	1.36,1.06	0.87	0.34		8.37	
Q	4.32	1.93	2.23			8.66	

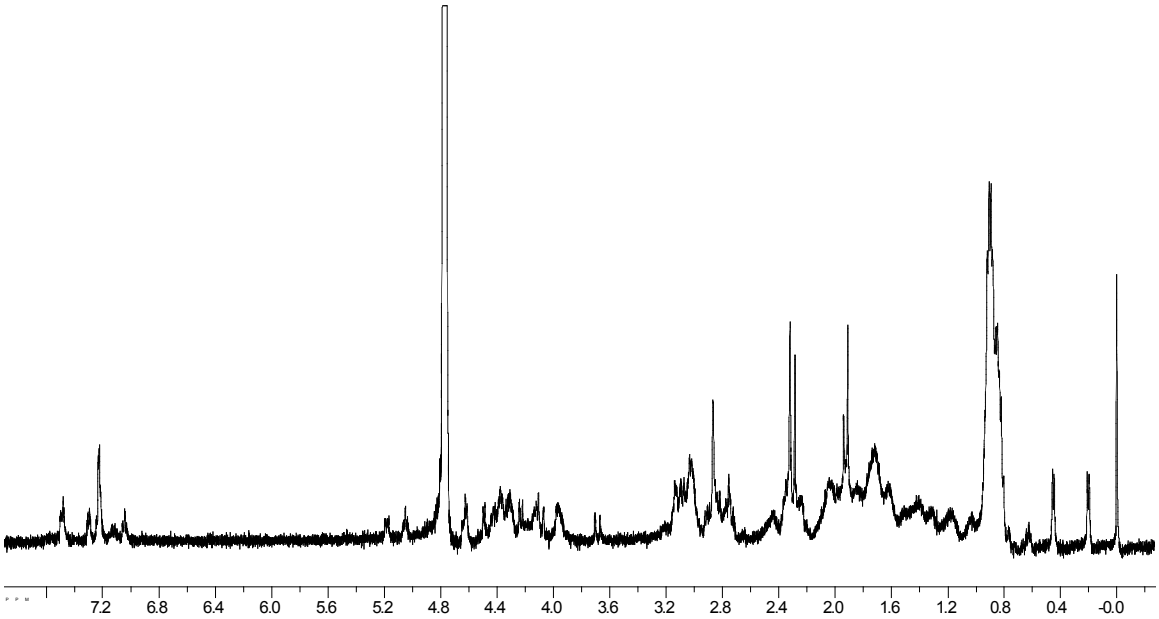

Figure 2.56. [1]HNMR of Peptide **WKMe2L**: Ac-Arg-Trp-Val-Glu-Val-Asn-Gly-Orn-Lys(Me)$_2$-Ile-Leu-Gln-NH2

Table 2.17. Proton Chemical Shift Assignments for Peptide **WKMe2L**.

	α	β	γ	δ	ε	Amide	Amine
R	4.38	1.73	1.59	3.08		8.05	7.10
W	5.18	3.08				8.27	10.21
V	4.48	2.02	0.86			9.16	
E	5.05	1.96	2.27			8.54	
V	4.22	1.92	0.90			8.91	
N	4.42	3.00				9.51	
G	4.08,3.68					8.64	
O	4.62	1.78	1.78	3.00		7.81	7.66
K(Me)$_2$	4.75	1.67	1.25	1.25	2.27 **(CH3)$_2$**=2.32, 2.29	8.47	8.40
I	4.62	1.80	0.88,1.43,1.18	0.88		9.22	
L	4.11	1.37	0.89	0.36		8.42	
Q	4.31	1.96	2.27			8.68	

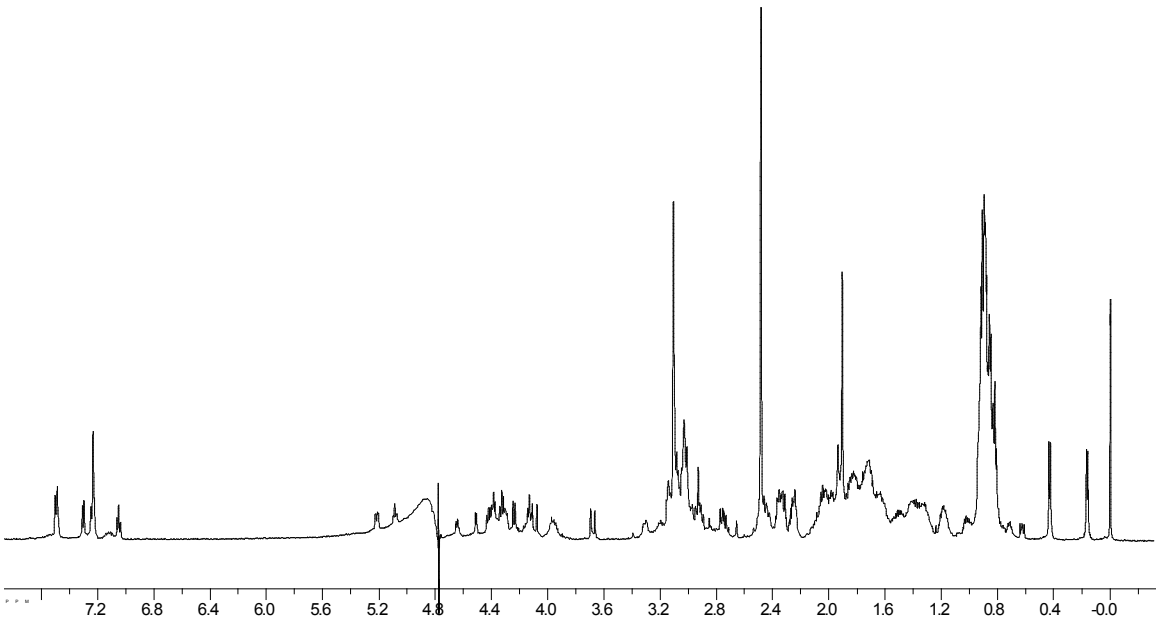

Figure 2.57. ^{1}HNMR of Peptide **WKMe3L**: Ac-Arg-Trp-Val-Glu-Val-Asn-Gly-Orn-Lys(Me)$_3^{\oplus}$-Ile-Leu-Gln-NH2

Table 2.18. Proton Chemical Shift Assignments for Peptide **WKMe3L**.

	α	β	γ	δ	ε	Amide	Amine
R	4.39	1.72	1.63, 1.52	3.14		8.03	7.11,6.64
W	5.23	3.12,2.96	7.05,7.23,7.30,7.5			8.27	10.22
V	4.51	2.05	0.87			9.23	
E	5.09	1.96	2.30			8.52	
V	4.25	1.92	0.91			8.96	
N	4.43	3.10,2.76				9.53	
G	4.095					8.65	
	3.675						
O	4.65	1.83	1.76	3.04		7.79	7.64
K(Me)$_3$	4.8	1.7	1.18	1.32	2.37	8.48	**(CH$_3$)$_3$**=2.49
I	4.65	1.83	1.42,1.20,0.89	0.89		9.26	
L	4.14	1.39	0.92,0.86	0.44,0.17		8.43	
Q	4.33	2.01,1,86	2.26			8.70	

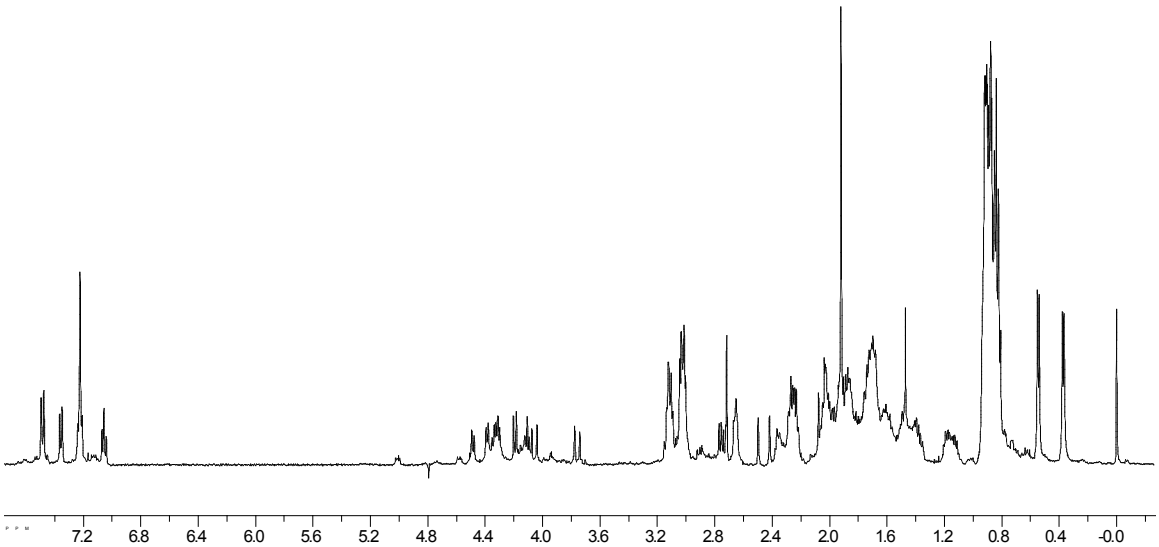

Figure 2.58. [1]HNMR of Peptide **WOrnL**: Ac-Arg-Trp-Val-Glu-Val-Asn-Gly-Orn-Orn-Ile-Leu-Gln-NH2

Table 2.19. Proton Chemical Shift Assignments for Peptide **WOrnL**.

	α	β	γ	δ	ε	Amide	Amine
R	4.34	1.65	1.51	3.13		8.08	6.63,7.12
W	5.01	3.12	7.22,7.49	7.06,7.22	7.36	8.29	10.17
V	4.39	2.02	0.86			8.76	
E	4.83	1.97	2.24			8.47	
V	4.19	1.96	0.91			8.74	
N	4.51	3.02,2.75				9.26	
G	4.06,3.77					8.59	
O	4.58	1.89	1.7	3.03		7.91	7.66
O	4.73	1.72	1.60	2.67		8.55	7.66
I	4.47	1.84	0.88,1.41,1.18	0.88		8.96	
L	4.12	1.39	1.11,0.86	0.55,0.41		8.33	
Q	4.33	2.04	2.27			8.59	

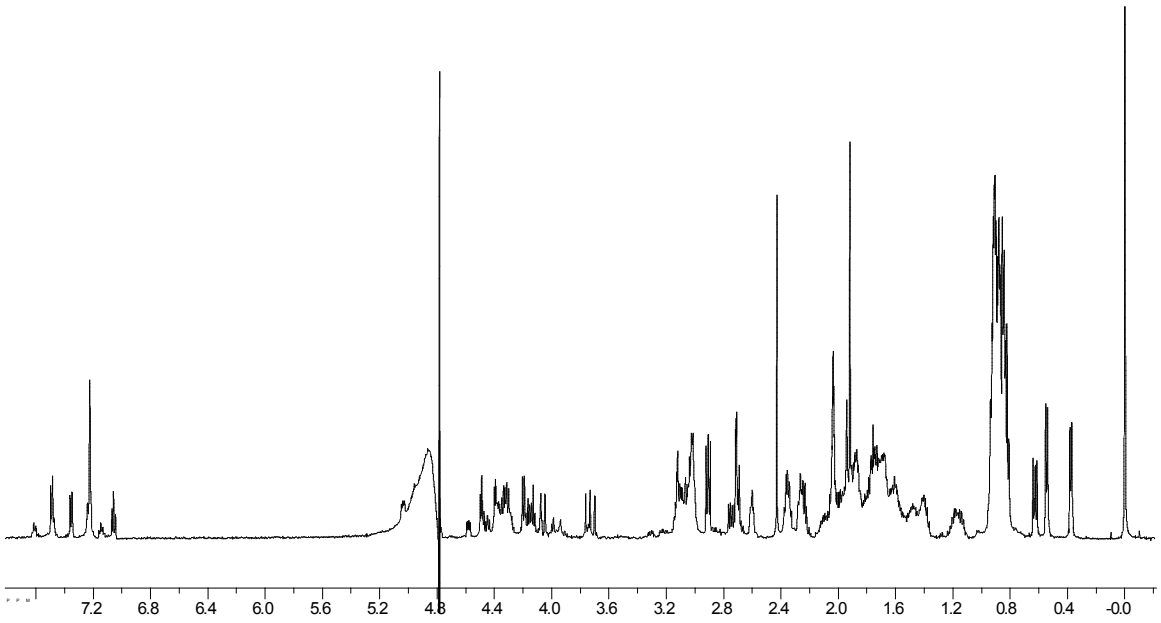

Figure 2.59. [1]HNMR of Peptide **WOrnMeL**: Ac-Arg-Trp-Val-Glu-Val-Asn-Gly-Orn-Orn(Me)-Ile-Leu-Gln-NH2

Table 2.20. Proton Chemical Shift Assignments for Peptide **WOrnMeL**.

	α	β	γ	δ	ε	Amide	Amine
R	4.32	1.70	1.50	3.12		8.07	6.63,7.11
W	5.04	3.13				8.29	10.20
V	4.38	2.03	0.91			8.77	
E	4.82	1.97	2.23			8.50	
V	4.18	1.94	0.91			8.72	
N	4.48	3.03,2.75				9.29	
G	4.03,3.72					8.60	
O	4.56	1.82	1.72	3.03		7.90	7.65
O(Me)	4.74	1.72	1.60	2.61	**CH_3**=2.43	8.56	8.16
I	4.50	1.84	0.87,1.42	0.87		8.97	
L	4.10	1.39	1.15,0.90	0.54,0.38, 0.90		8.36	
Q	4.28	1.98	2.33			8.60	

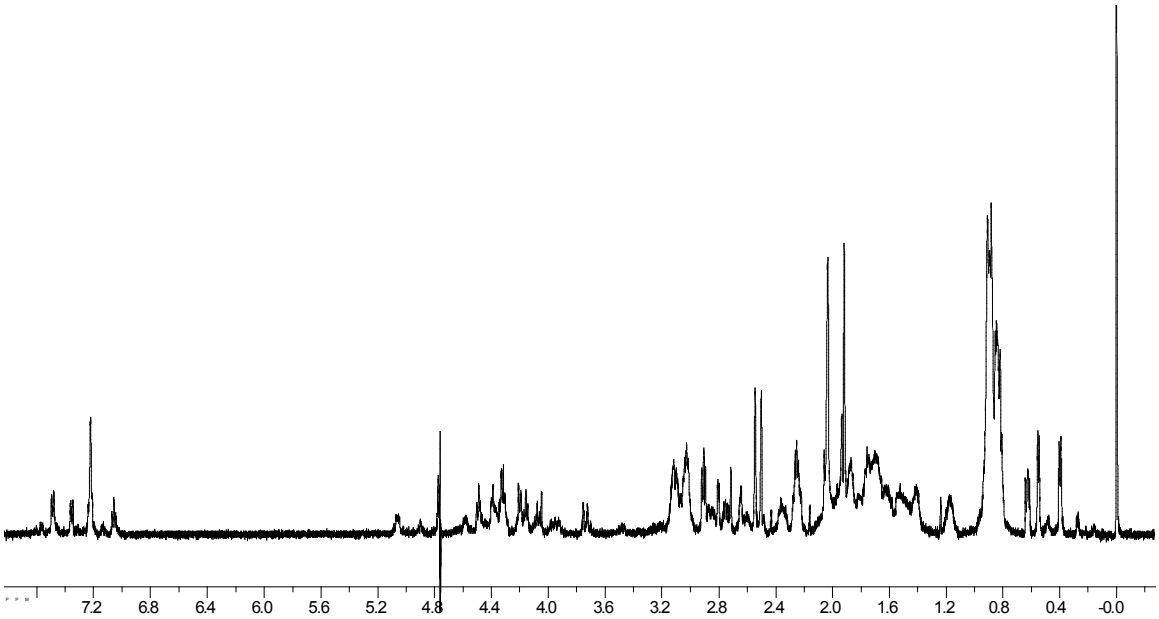

Figure 2.60. [1]HNMR of Peptide **WOrnMe2L**: Ac-Arg-Trp-Val-Glu-Val-Asn-Gly-Orn-Orn(Me)$_2$-Ile-Leu-Gln-NH2

Table 2.21. Proton Chemical Shift Assignments for Peptide **WOrnMe2L.**

	α	β	γ	δ	ε	Amide	Amine
R	4.33	1.61	1.52	3.12		8.07	6.61,7.10
W	5.06	3.10				8.25	10.21
V	4.40	2.02	0.86			8.82	
E	4.88	1.94	2.23			8.51	
V	4.20	1.92	0.89			8.73	
N	4.47	3.04,2.75				9.32	
G	4.06,3.74					8.59	
O	4.58	1.84	1.72	3.03		7.86	7.64
O(Me)$_2$	4.77	1.68	1.57	2.61	**(CH$_3$)$_2$**=2.54,2.50	8.57	8.16
I	4.51	1.86	0.87,1.43,1.18	0.87		9.00	
L	4.14	1.4	1.14,0.92	0.56, 0.38		8.38	
Q	4.32	2.05,1.87	2.28			8.59	

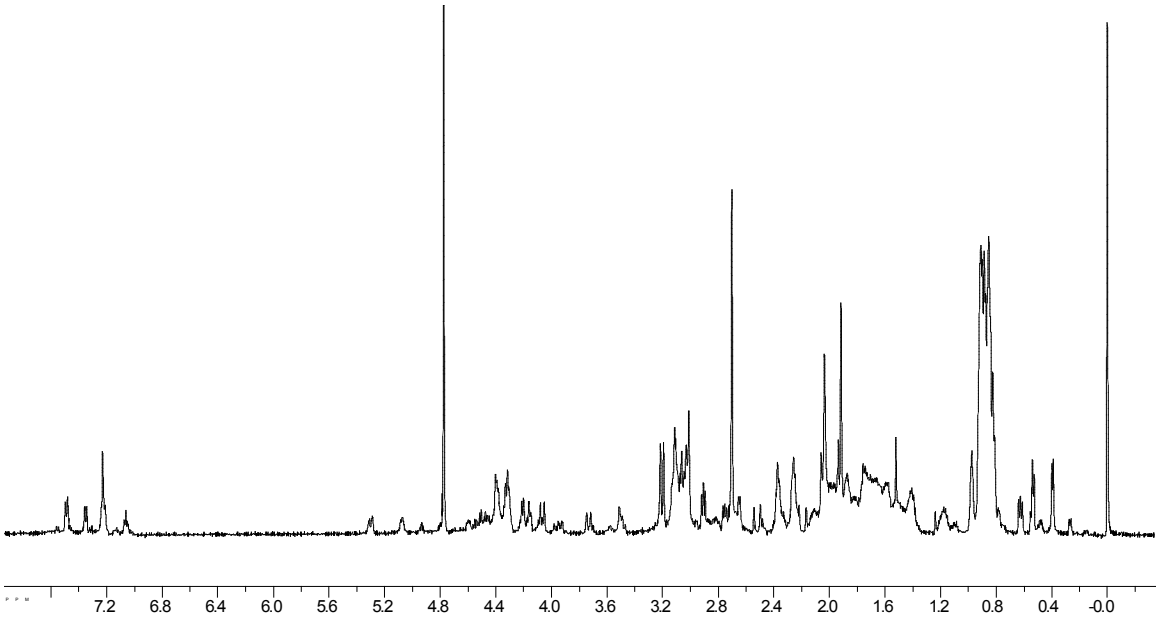

Figure 2.61. [1]HNMR of Peptide **WOrnMe3L**: Ac-Arg-Trp-Val-Glu-Val-Asn-Gly-Orn-Orn(Me)$_3$-Ile-Leu-Gln-NH2

Table 2.22. Proton Chemical Shift Assignments for Peptide **WOrnMe3L.**

	α	β	γ	δ	ε	Amide	Amine
R	4.33	1.64	1.52	3.12			
W	5.07	3.10					
V	4.39	2.03	0.87				
E	4.92	1.96	2.24				
V	4.20	1.94	0.91				
N	4.47	3.01,2.76					
G	4.07,3.73						
O	4.60	1.83	1.75	3.02			
O(Me)$_3$	4.81	1.69	1.60	2.71	**(CH$_3$)$_3$**=2.70		
I	4.51	1.85	0.89,1.43,1.2	0.89			
L	4.15	1.61	1.17,1.39,0.92	0.57,0.40,0.92			
Q	4.31	1.97	2.30				

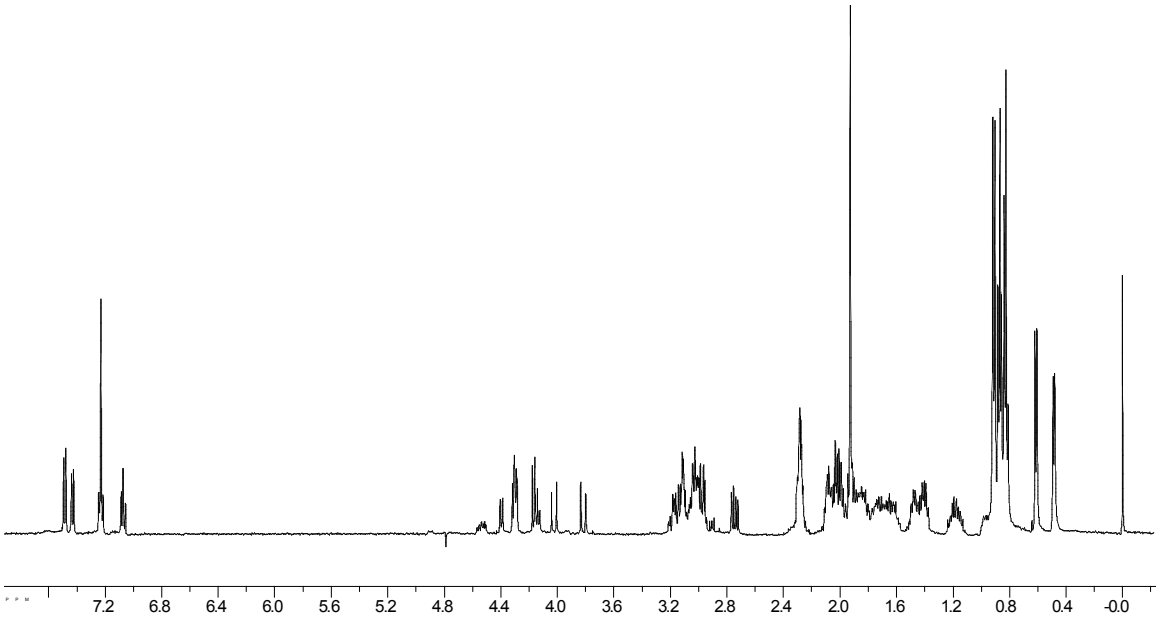

Figure 2.62. [1]HNMR of Peptide **WDabL**: Ac-Arg-Trp-Val-Glu-Val-Asn-Gly-Orn-Dab-Ile-Leu-Gln-NH2

Table 2.23. Proton Chemical Shift Assignments for Peptide **WDabL.**

	α	β	γ	δ	ε	Amide	Amine
R	4.31	1.66	1.48	3.12		8.10	7.11,6.62
W	4.90	3.16	7.23,7.49	7.07,7.23	7.43	8.29	10.17
V	4.31	2.02	0.85			8.55	
E	4.72	2.00	2.29			8.38	
V	4.18	1.98	0.92			8.48	
N	4.56	2.97,2.76				9.05	
G	4.02,3.81					8.54	
O	4.52	1.83	1.76	3.02		8.01	7.66
Dab	4.72	2.09	3.03			8.64	7.66
I	4.4	1.85	0.87,1.42,1.17	0.87		8.76	
L	4.14	1.39	1.20,0.97	0.61,0.49		8.33	
Q	4.31	2.05,1.9	2.30			8.54	

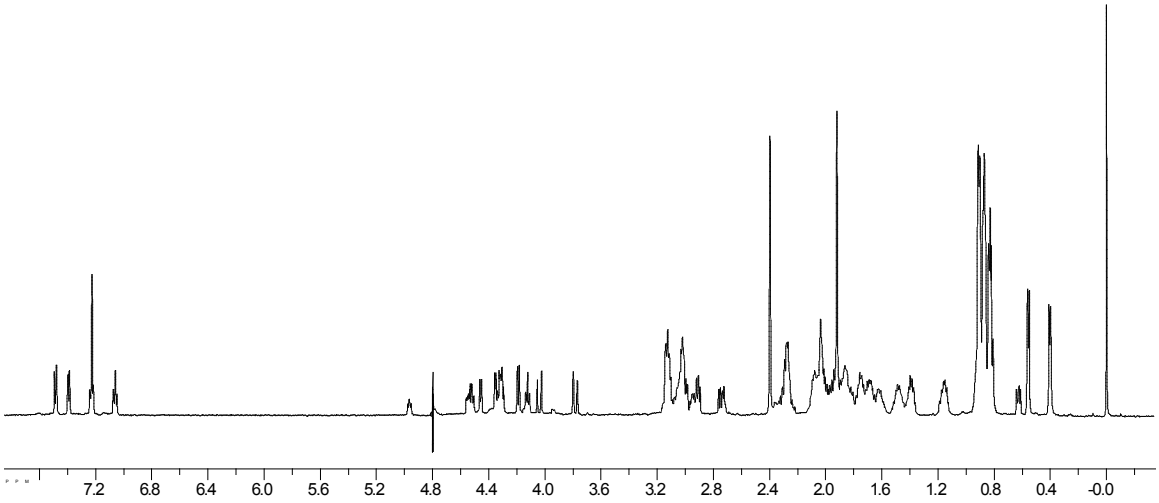

Figure 2.63. [1]HNMR of Peptide **WDabMeL**: Ac-Arg-Trp-Val-Glu-Val-Asn-Gly-Orn-Dab(Me)-Ile-Leu-Gln-NH2

Table 2.24. Proton Chemical Shift Assignments for Peptide **WDabMeL.**

	α	β	γ	δ	ε	Amide	Amine
R	4.33	1.64	1.52	3.13		8.09	7.11, 6.63
W	4.97	3.14	7.62,7.39,7.23,7.23,7.06			8.30	10.16
V	4.20	1.96	0.92			8.63	
E	4.82	1.98	2.29			8.42	
V	4.35	2.03	0.86			8.68	
N	4.53	3.02, 2.76				9.17	
G	4.05, 3.80					8.57	
O	4.56	1.81	1.81	3.02		7.98	7.65
Dab(Me)	4.76	2.09	3.02	**CH3**=2.40		8.68	8.58
I	4.46	1.86	1.43,1.16,0.87	0.87		8.89	
L	4.14	1.40	1.17,0.92	0.50		8.36	
Q	4.32	1.92	2.30			8.57	

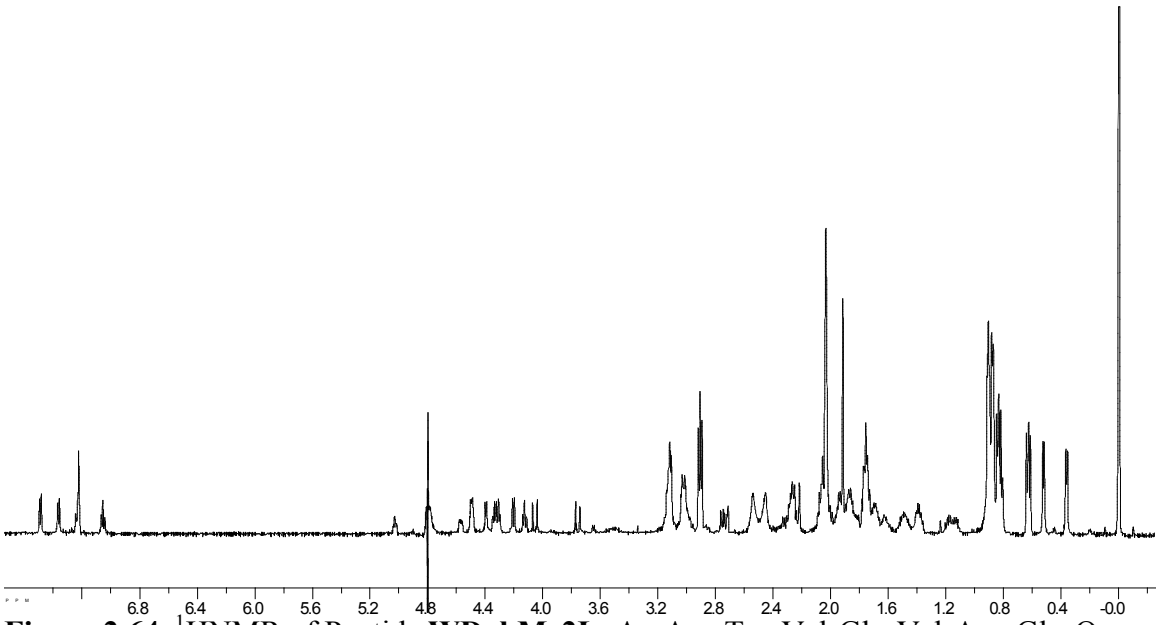

Figure 2.64. ^{1}HNMR of Peptide **WDabMe2L**: Ac-Arg-Trp-Val-Glu-Val-Asn-Gly-Orn-Dab(Me)$_2$-Ile-Leu-Gln-NH2

Table 2.25. Proton Chemical Shift Assignments for Peptide **WDabMe2L.**

	α	β	γ	δ	ε	Amide	Amine
R	4.33	1.63	1.51	3.12			
W	5.02	3.11					
V	4.38	2.04	0.85				
E	4.89	1.97	2.27				
V	4.20	1.95	0.90				
N	4.48	3.04,2.69					
G	4.047, 3.750						
O	4.55	1.77	1.77	3.02			
Dab(Me)$_2$	4.77	2.06	3.07	**(CH3)$_2$**=2.457, 2.542			
I	4.48	1.87	0.87,1.38,1.17	0.87			
L	4.13	1.38	1.13,0.90	0.45			
Q	4.30	1.96	2.27				

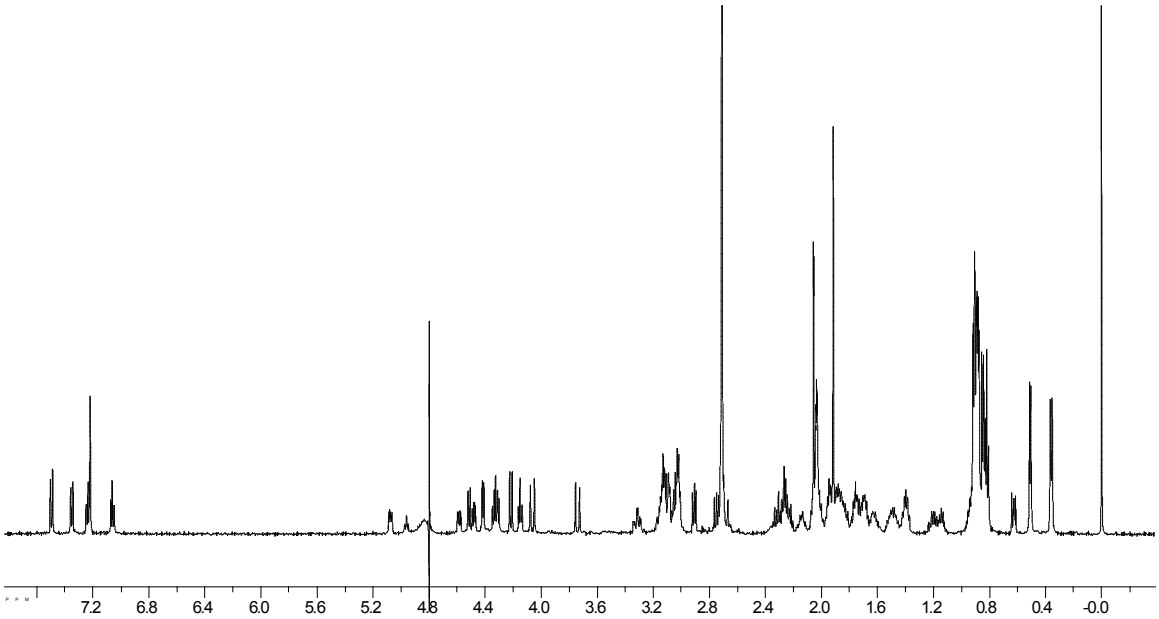

Figure 2.65. [1]HNMR of Peptide **WDabMe3L**: Ac-Arg-Trp-Val-Glu-Val-Asn-Gly-Orn-Dab(Me)$_3$-Ile-Leu-Gln-NH2

Table 2.26. Proton Chemical Shift Assignments for Peptide **WDabMe3L.**

	α	β	γ	δ	ε	Amide	Amine
R	4.33	1.66	1.54	3.12			
W	5.07	3.13					
V	4.41	2.06	0.87				
E	4.96	1.98	2.30				
V	4.22	1.92	0.91				
N	4.48	3.06,2.73					
G	4.062,3.742						
O	4.59	1.79	1.79	3.03			
Dab(Me)$_3$	4.79	2.11	3.24	**(CH3)$_3$**= 2.715			
I	4.51	1.88,1.51	0.88, 1.26	0.88			
L	4.16	1.40	0.95	0.46			
Q	4.31	1.93	2.27				

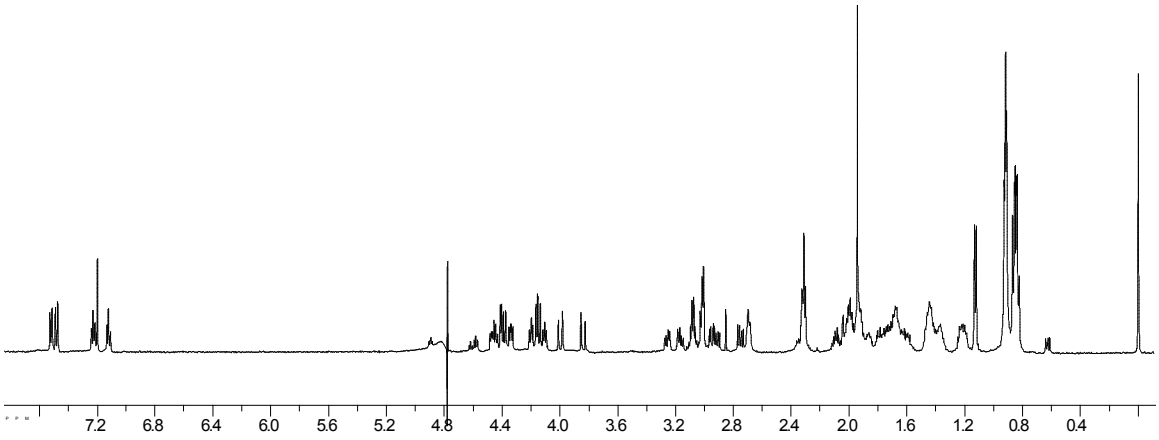

Figure 2.66. [1]HNMR of Peptide **WKT**: Ac-Arg-Trp-Val-Glu-Val-Asn-Gly-Orn-Lys-Ile-Thr-Gln-NH2

Table 2.27. Proton Chemical Shift Assignments for Peptide **WKT.**

	α	β	γ	δ	ε	Amide	Amine
R	4.20	1.58	1.50	3.08		8.13	7.07
W	4.92	3.25,3.19				8.05	10.14
V	4.17	2.01	0.92			8.47	
E	4.66	1.98	2.37			8.39	
V	4.18	2.00	0.87			8.18	
N	4.58	2.76,2.96				8.96	
G	4.00,3.86					8.49	
O	4.49	1.81	1.75	3.02		7.98	7.64
K	4.45	1.69	1.25	1.37	2.68	8.39	7.35
I	4.40	1.92	0.91	0.91		8.60	
T	4.42	4.11	1.15			8.30	
Q	4.34	1.95	2.33			8.39	

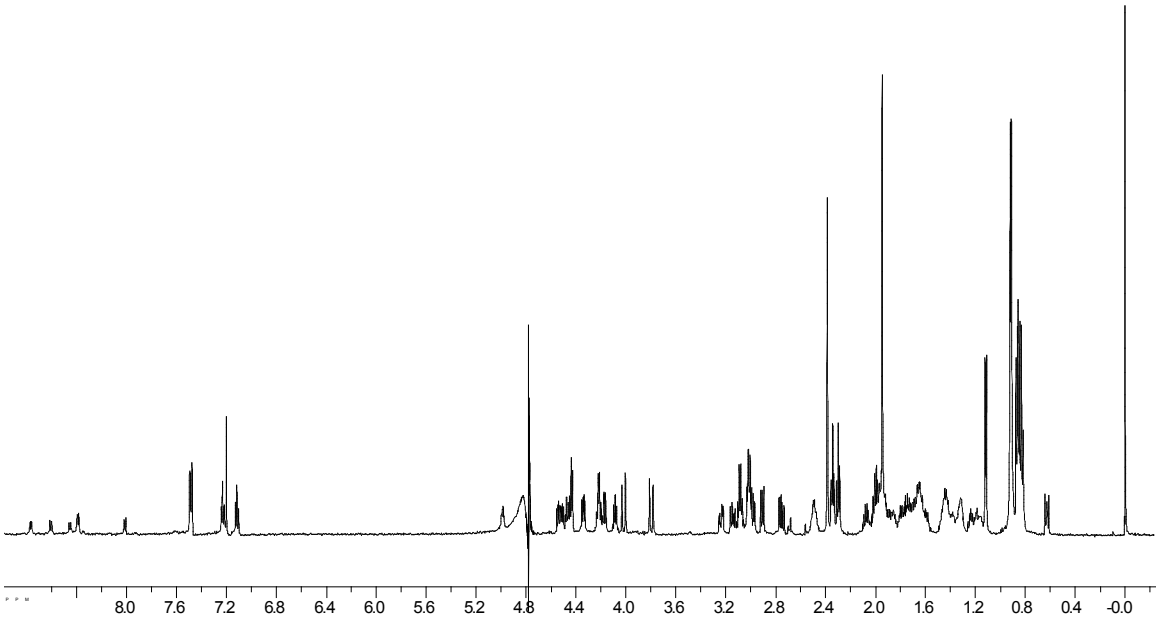

Figure 2.67. [1]HNMR of Peptide **WKMeT**: Ac-Arg-Trp-Val-Glu-Val-Asn-Gly-Orn-Lys(Me)-Ile-Thr-Gln-NH2

Table 2.28. Proton Chemical Shift Assignments for Peptide **WKMeT.**

	α	β	γ	δ	ε	Amide	Amine
R	4.21	1.61	1.45	3.08			
W	4.99	3.20				8.00	
V	4.23	1.99	0.86			8.38	
E	4.76	1.97	2.35				
V	4.17	1.98	0.92			8.60	
N	4.54	2.76,2.97					
G	4.02,3.80					8.55	
O	4.51	1.77	1.77	3.01			
K(Me)	4.47	1.65	1.17	1.33	2.50 **CH3**=2.39		
I	4.44	1.94	0.91	0.91		8.77	
T	4.44	4.10	1.12				
Q	4.34	2.09,1.91	2.30				

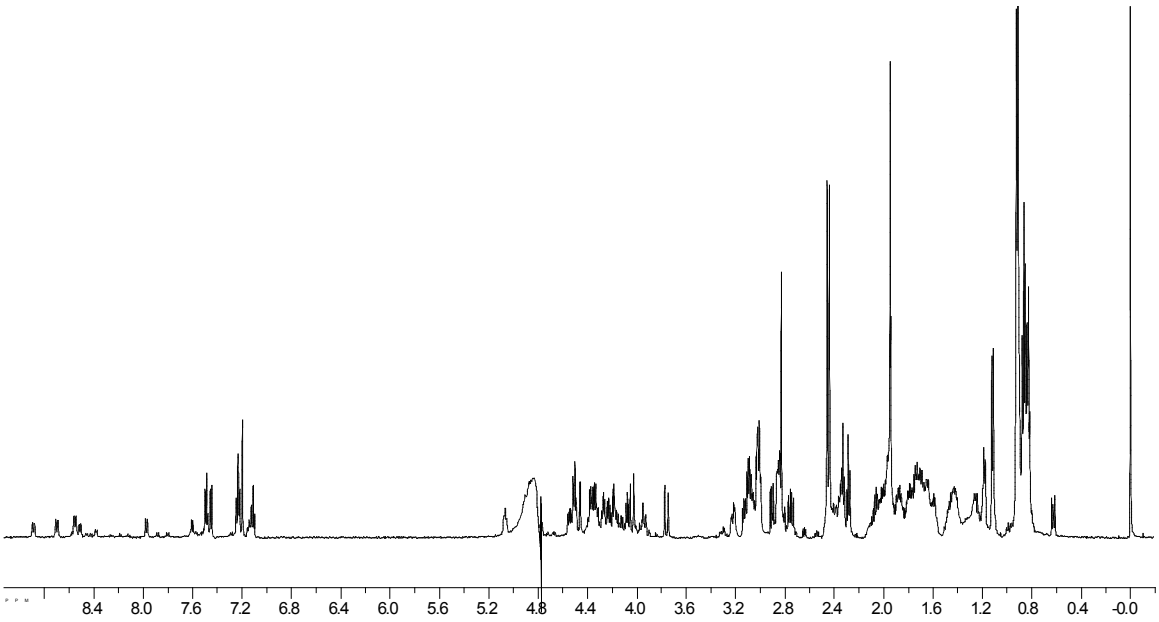

Figure 2.68. [1]HNMR of Peptide **WKMe2T**: Ac-Arg-Trp-Val-Glu-Val-Asn-Gly-Orn-Lys(Me)$_2$-Ile-Thr-Gln-NH2

Table 2.29. Proton Chemical Shift Assignments for Peptide **WKMe2T.**

	α	β	γ	δ	ε	Amide	Amine
R	4.23	1.62	1.46	3.09			
W	5.06	3.14				7.97	
V	4.27	2.01	0.87			8.53	
E	4.87	1.97	2.33				
V	4.19	1.96	0.92			8.69	
N	4.51	2.75,3.00					
G	4.04,3.76						
O	4.54	1.79	1.73	3.02			
K(Me)$_2$	4.51	1.65	1.11	1.29	2.44 **(CH3)$_2$**=2.46, 2.44		
I	4.50	1.95	0.91	0.91		8.86	
T	4.38	4.19	1.18				
Q	4.33	1.95	2.30				

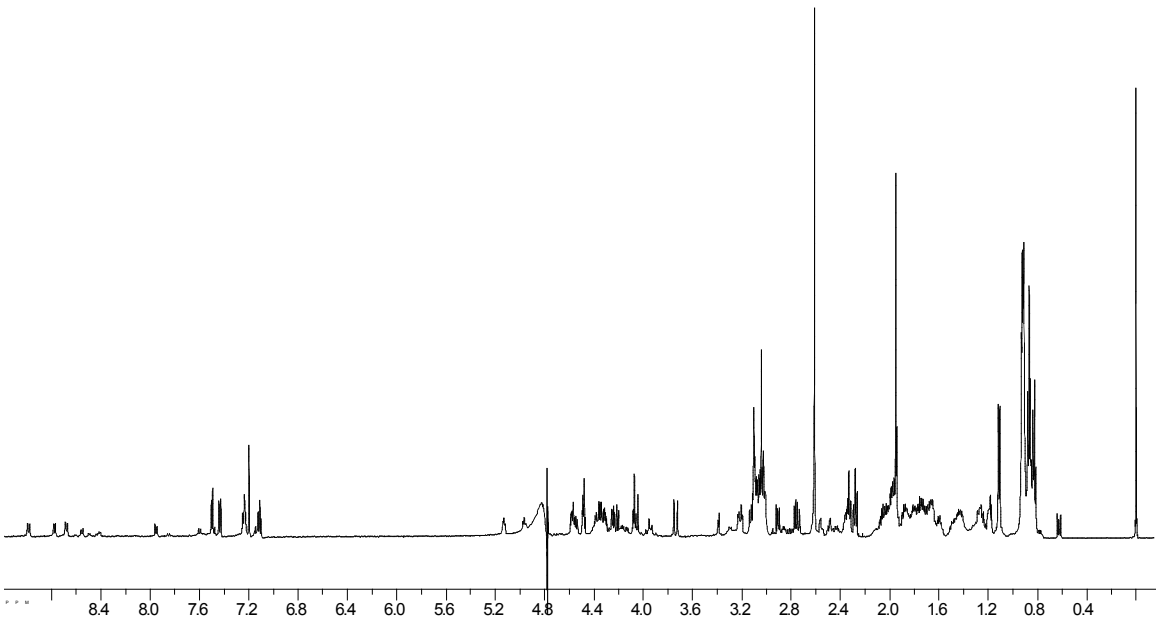

Figure 2.69. [1]HNMR of Peptide **WKMe3T**: Ac-Arg-Trp-Val-Glu-Val-Asn-Gly-Orn-Lys(Me)$_3$-Ile-Thr-Gln-NH2

Table 2.30. Proton Chemical Shift Assignments for Peptide **WKMe3T.**

	α	β	γ	δ	ε	Amide	Amine
R	4.25	1.62	1.48	3.09			
W	5.12	3.14				7.95	
V	4.31	2.02	0.86			8.68	
E	4.96	1.97	2.33			8.55	
V	4.22	1.94	0.92			8.77	
N	4.49	2.75,3.04					
G	4.05,3.73					8.62	
O	4.57	1.81	1.71	3.02			
K(Me)$_3$	4.57	1.67	1.11	1.28	2.52 **(CH3)$_2$**=2.61		
I	4.55	1.99	0.91	0.91		8.97	
T	4.49	4.09	1.11				
Q	4.36	1.88	2.28				

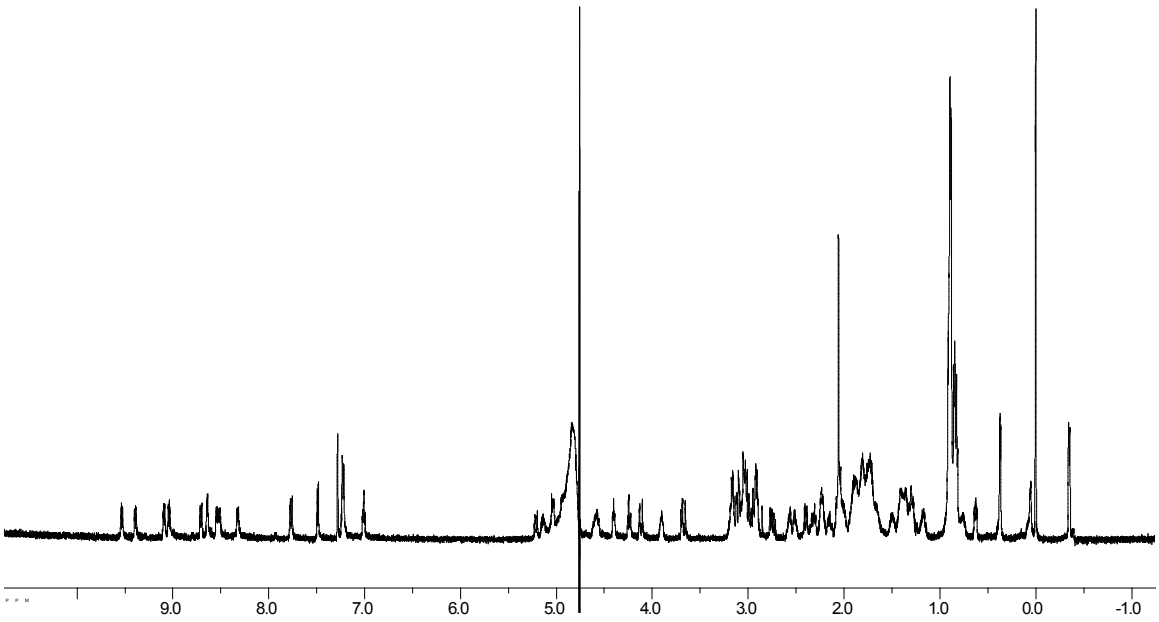

Figure 2.70. 1HNMR of Peptide **WKLcyc**: Ac-Cys-Arg-Trp-Val-Glu-Val-Asn-Gly-Orn-Lys-Ile-Leu-Gln-Cys-NH2

Table 2.31. Proton Chemical Shift Assignments for Peptide **WKLcyc.**

	α	β	γ	δ	ε	Amide	Amine
C	5.04	2.95				8.91	
R	4.61	1.80	1.66,1.51	3.18		8.71	7.11,6.67
W	5.15	3.09,2.94	7.00,7.23,7.28,7.49			8.64	
V	4.58	2.05	0.87			9.54	
E	5.04	2.00,1.93	2.27			8.54	
V	4.24	1.92	0.89			9.09	
N	4.40	3.10,2.75				9.6	
G	4.115, 3.675					8.68	
O	4.70	1.85	1.71	3.05		7.76	7.66
K	4.93	1.72	1.29	1.38	2.53	8.52	7.21
I	4.71	1.85	1.43,1.16,0.87	0.87		9.40	
L	3.90	1.29,0.76	0.37	0.07, -0.35		8.32	
Q	4.57	2.07,1.82	2.24,2.16			9.04	
C	5.22	3.00,2.40				8.36	

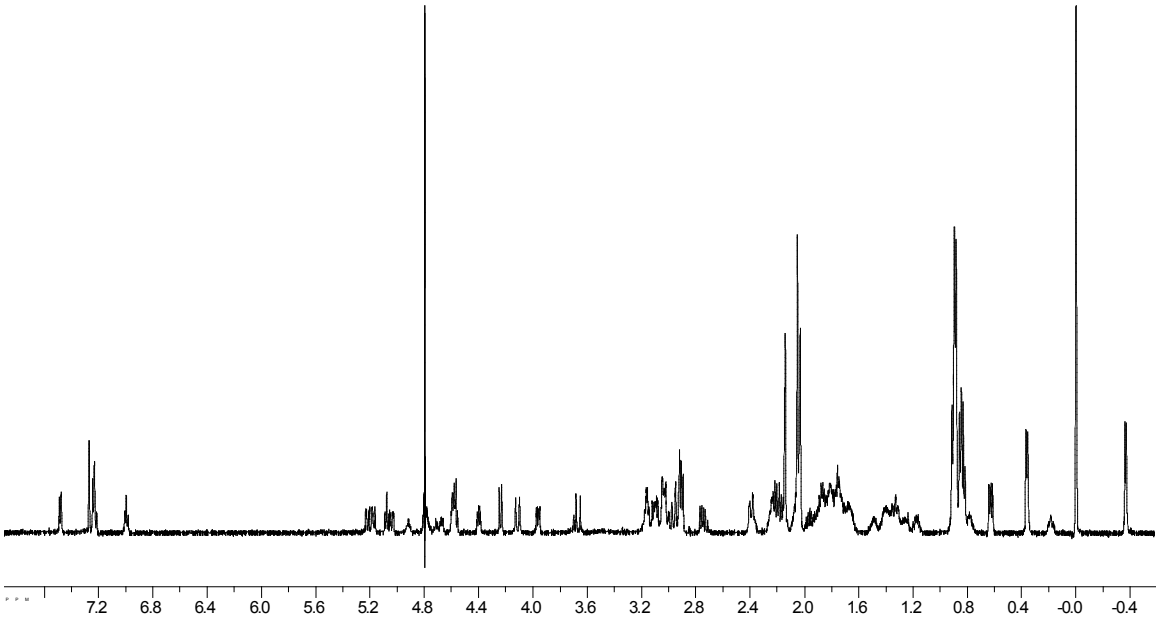

Figure 2.71. [1]HNMR of Peptide **WKMeLcyc**: Ac-Cys-Arg-Trp-Val-Glu-Val-Asn-Gly-Orn-Lys(Me)-Ile-Leu-Gln-Cys-NH2

Table 2.32. Proton Chemical Shift Assignments for Peptide **WKMeLcyc.**

	α	β	γ	δ	ε	Amide	Amine
C	5.04	2.95					
R	4.59	1.73	1.50	3.16		8.72	
W	5.17	3.09,2.97				8.61	
V	4.58	2.07	0.87			9.53	
E	5.07	1.93	2.19			8.51	
V	4.23	1.91	0.89			9.05	
N	4.40	3.10,2.75					
G	4.115, 3.668						
O	4.67	1.81	1.77	3.04		7.76	7.27
K(Me)	4.92	1.71	1.33	1.33		2.36, 2.24	(**CH_3**)=2.14
I	4.72	1.86	1.41,1.17	0.87		9.40	
L	3.96	1.33	0.79,0.35	0.19, -0.38		8.38	
Q	4.58	1.87	2.16			9.04	
C	5.21	2.97,2.41					

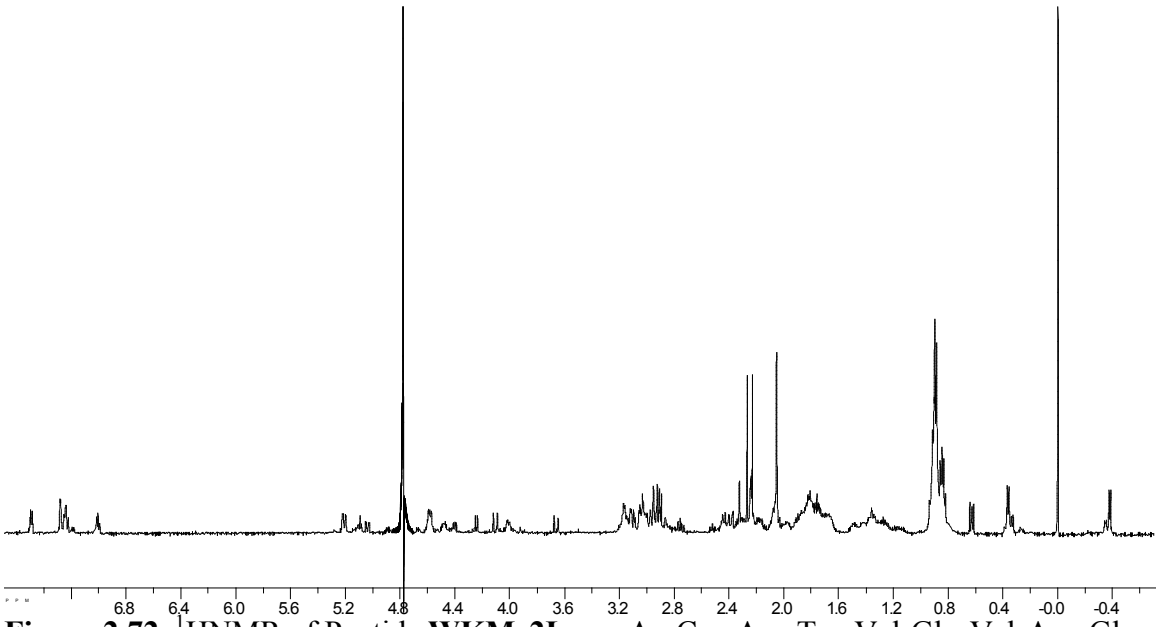

Figure 2.72. ^{1}HNMR of Peptide **WKMe2Lcyc**: Ac-Cys-Arg-Trp-Val-Glu-Val-Asn-Gly-Orn-Lys(Me)$_2$-Ile-Leu-Gln-Cys-NH2

Table 2.33. Proton Chemical Shift Assignments for Peptide **WKMe2Lcyc.**

	α	β	γ	δ	ε	Amide	Amine
C	5.04	2.92					
R	4.60	1.86	1.70	3.16			
W	5.12	3.03					
V	4.49	1.96	0.89				
E	5.11	1.93	2.28				
V	4.25	1.94	0.91				
N	4.40	3.04,2.75					
G	4.11,3.66						
O	4.75	1.79	1.79	3.00			
K(Me)$_2$	4.90	1.72	1.31	1.31	2.25		**(CH$_3$)$_2$**= 2.27, 2.23
I	4.83	1.88	0.89	0.89			
L	4.01	1.34	0.81,0.41,0.31	-0.36			
Q	4.59	1.93	2.17				
C	5.22	3.05					

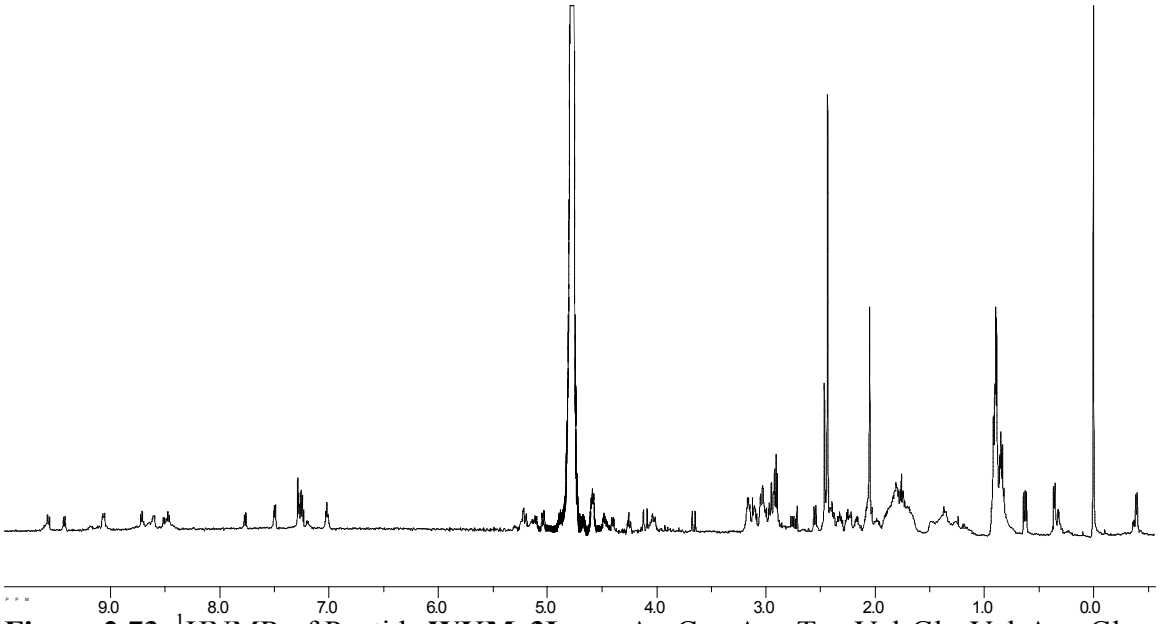

Figure 2.73. ^{1}HNMR of Peptide **WKMe3Lcyc**: Ac-Cys-Arg-Trp-Val-Glu-Val-Asn-Gly-Orn-Lys(Me)$_3^{\oplus}$-Ile-Leu-Gln-Cys-NH2

Table 2.34. Proton Chemical Shift Assignments for Peptide **WKMe3Lcyc.**

	α	β	γ	δ	ε	Amide	Amine
C	5.04	2.92,3.10				8.92	
R	4.6	1.80	1.68,1.48	3.16		8.71	6.64,7.10
W	5.14	2.96,3.11	7.02,7.25,7.28	7.50		8.64	10.17
V	4.59	2.08	0.87			9.57	
E	5.11	1.93	2.29			8.50	
V	4.26	1.91	0.90			9.05	
N	4.40	3.09,2.75				9.61	
G	4.105, 3.660					8.70	
O	4.68	1.84	1.74	3.03		7.76	7.65
K(Me)$_3$	4.89	1.77	1.22	1.35	2.36	8.48	**(CH$_3$)$_3$**=2.46,2.44
I	4.74	1.87	1.17,1.42,0.88	0.88		9.42	
L	4.03	1.35,0.79	0.32	-0.39		8.46	
Q	4.58	2.08,1.82	2.20			9.06	
C	5.21	2.96,3.11				8.59	

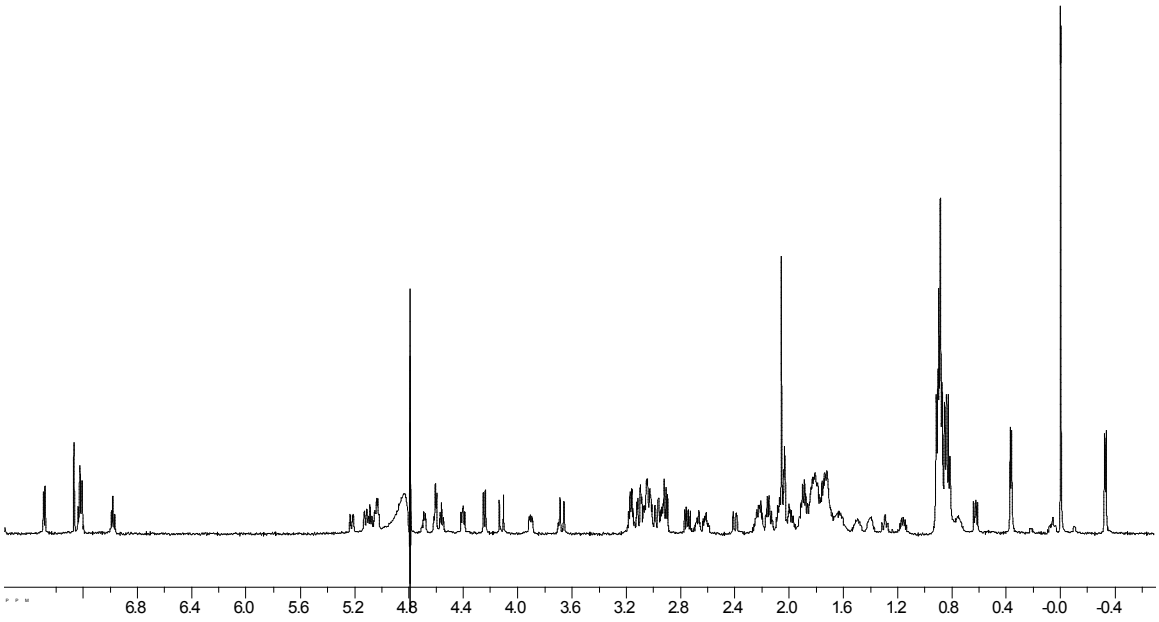

Figure 2.74. [1]HNMR of Peptide **WOrnLcyc**: Ac-Cys-Arg-Trp-Val-Glu-Val-Asn-Gly-Orn-Orn-Ile-Leu-Gln-Cys-NH2

Table 2.35. Proton Chemical Shift Assignments for Peptide **WOrnLcyc.**

	α	β	γ	δ	ε	Amide	Amine
C	5.04	2.91					
R	4.61	1.79	1.65,1.50	3.16		8.73	
W	5.12	3.09	7.00,7.23,7.27,7.49	6.99		8.67	
V	4.60	2.07	0.86			9.51	
E	5.09	1.97	2.17				
V	4.24	1.90	0.90			9.04	
N	4.40	3.09,2.75					
G	4.12,3.67						
O	4.69	1.83	1.83	3.04			
Orn	5.04	1.78	1.67	2.64			
I	4.69	1.83	1.39,1.16,0.87	0.87		9.40	
L	3.89	1.29	0.74,0.37	0.059, -0.33		8.35	
Q	4.56	2.05,1.82	2.18				
C	5.22	2.99,2.40					

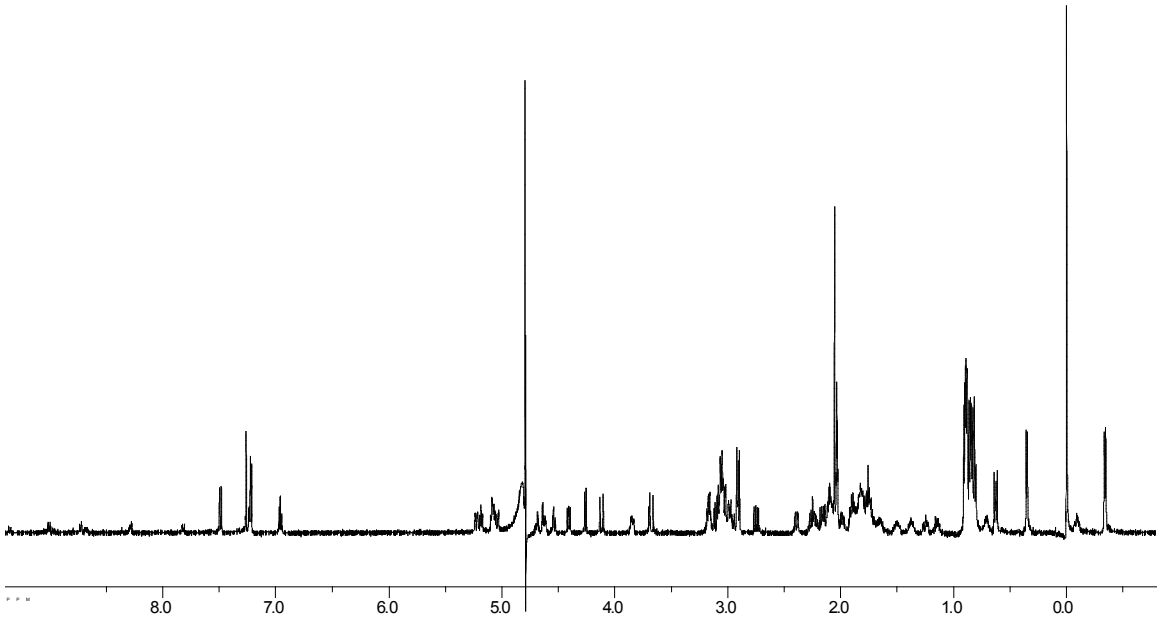

Figure 2.75. [1]HNMR of Peptide **WDabLcyc**: Ac-Cys-Arg-Trp-Val-Glu-Val-Asn-Gly-Orn-Dab-Ile-Leu-Gln-Cys-NH2

Table 2.36. Proton Chemical Shift Assignments for Peptide **WDabLcyc.**

	α	β	γ	δ	ε	Amide	Amine
C	5.04	2.94					
R	4.62	1.80	1.67,1.50	3.17		8.72	
W	5.07	3.05	7.00,7.23,7.27,7.49	6.96		8.68	
V	4.64	2.09	0.86			9.53	
E	5.19	1.97	2.21				
V	4.25	1.89	0.89			8.98	
N	4.41	3.11,2.74					
G	4.11,3.67						
O	4.69	1.88	1.75	3.04		7.82	
Dab	5.07	2.11	3.05				
I	4.68	1.83	1.37,1.15,0.84	0.84		9.35	
L	3.84	1.24	0.71,0.35	-0.09, -0.34		8.28	
Q	4.54	2.09,1.82	2.15			9.01	
C	5.22	2.99,2.39					

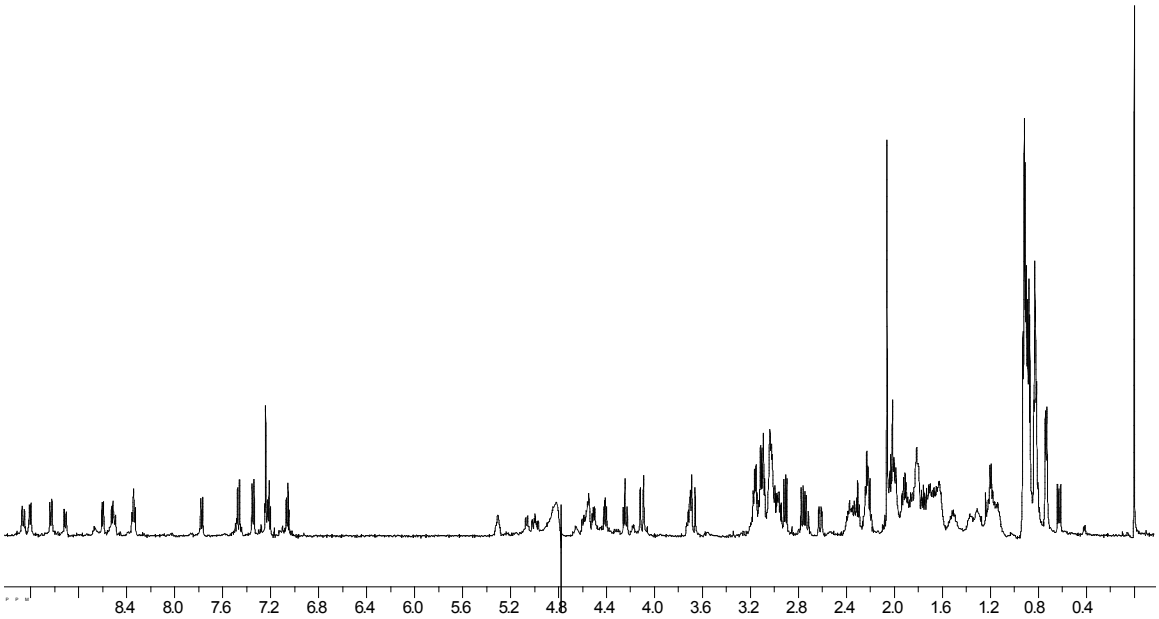

Figure 2.76. [1]HNMR of Peptide **WKTcyc**: Ac-Cys-Arg-Trp-Val-Glu-Val-Asn-Gly-Orn-Lys-Ile-Thr-Gln-Cys-NH2

Table 2.37. Proton Chemical Shift Assignments for Peptide **WKTcyc.**

	α	β	γ	δ	ε	Amide	Amine
C	5.00	2.95,2.62					
R	4.56	1.82	1.50	3.16			
W	5.30	3.08				8.33	10.10
V	4.51	2.03	0.85			9.19	
E	5.06	1.97	2.25			8.59	
V	4.24	1.90	0.90			9.02	
N	4.41	3.10,2.76					
G	4.11,3.67						
O	4.66			3.03		7.77	7.66
K	4.80	1.62	1.17	1.25	2.36		
I	4.77	1.99	0.92	0.92		9.25	
T	4.54	3.71	0.73			8.33	
Q	4.57	2.02,1.83	2.21			8.91	
C	4.98	3.08,2.96					

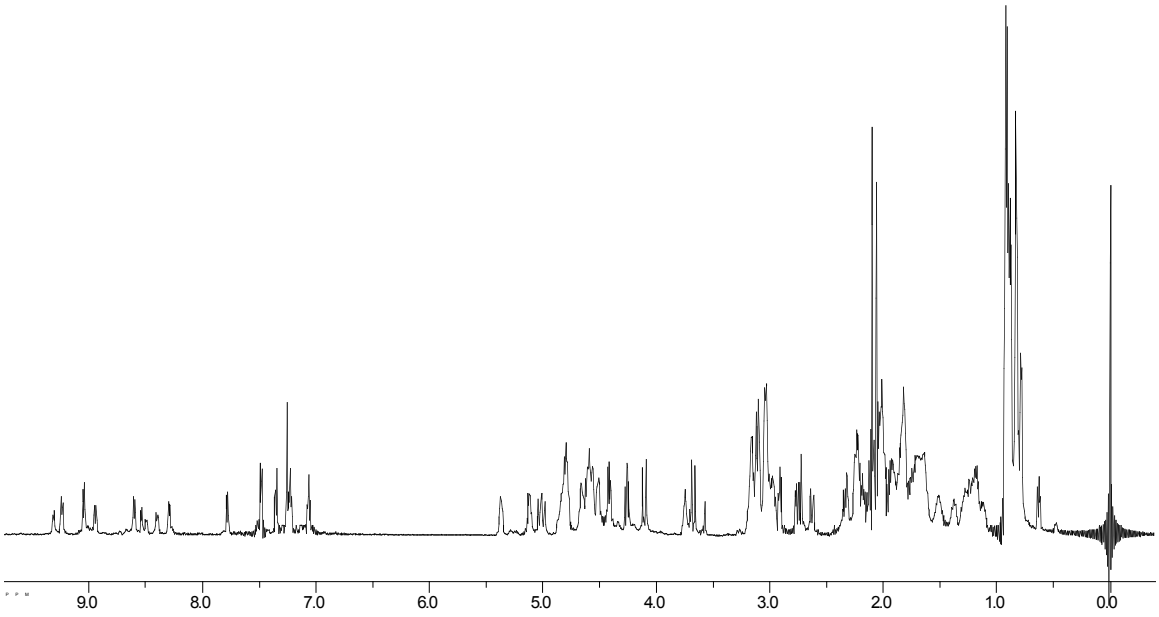

Figure 2.77. [1]HNMR of Peptide **WKMeTcyc**: Ac-Cys-Arg-Trp-Val-Glu-Val-Asn-Gly-Orn-Lys(Me)-Ile-Thr-Gln-Cys-NH2

Table 2.38. Proton Chemical Shift Assignments for Peptide **WKMeTcyc.**

	α	β	γ	δ	ε	Amide	Amine
C	5.03	2.96,2.63					
R	4.55	1.82	1.51	3.16			
W	5.36	3.08					
V	4.51	2.03	0.85				
E	5.11	1.98	2.28				
V	4.25	1.90	0.91				
N	4.41	3.10,2.76					
G	4.10,3.67						
O	4.66	1.82	1.73	3.03			
K	4.80	1.64	1.19	1.21	2.13	**CH3=** 2.09	
I	4.80	2.00	0.92	0.92			
T	4.59	3.74	0.78				
Q	4.60	2.03,1.84	2.22				
C	4.98	3.09,2.97					

Table 2.39. Proton Chemical Shift Assignments for Peptide **KL7**: Ac-Asn-Gly-Orn-Lys-Ile-Leu-Gln-NH2

	α	β	γ	δ	ε	Amide	Amine
N	4.67	2.82				8.44	
G	3.94					8.55	
O	4.35	1.88,1.78	1.7	3.01		8.13	7.64
K	4.31	1.77	1.42	1.69	2.99	8.33	7.56
I	4.14	1.85	1.48,1.20,0.89	0.89		8.25	
L	4.38	1.65	1.61	0.93,0.88		8.37	
Q	4.3	2.12,1.99	2.37			8.33	

Table 2.40. Proton Chemical Shift Assignments for Peptide **KMeL7**: Ac-Asn-Gly-Orn-Lys(Me)-Ile-Leu-Gln-NH2

	α	β	γ	δ	ε	Amide	Amine
N	4.68	2.81				8.43	
G	3.94					8.56	
O	4.35	1.78	1.68	3.01		8.13	7.61
K(Me)	4.30	1.75	1.40	1.68	3.02 CH3=2.701	8.33	8.05
I	4.13	1.85	1.49,1.23,0.89	0.89		8.24	
L	4.38	1.63	1.63	0.86		8.36	
Q	4.3	2.10,1.96	2.37			8.32	

Table 2.41. Proton Chemical Shift Assignments for Peptide **KMe2L7**: Ac-Asn-Gly-Orn-Lys$(Me)_2$-Ile-Leu-Gln-NH2

	α	β	γ	δ	ε	Amide	Amine
N	4.7	2.81				8.54	
G	3.96					8.58	
O	4.36	1.75	1.75	3.02		8.12	7.60
K$(Me)_2$	4.30	1.95,1.79	1.40	1.69	3.12 $(CH3)_2$=2.87	8.34	8.83
I	4.14	1.84	0.89	0.89		8.28	
L	4.39	1.66	1.66	0.90		8.39	
Q	4.3	2.01	2.33			8.35	

Table 2.42. Proton Chemical Shift Assignments for Peptide **KMe3L7**: Ac-Asn-Gly-Orn-Lys(Me)$_3^{\oplus}$-Ile-Leu-Gln-NH2

	α	β	γ	δ	ε	Amide	Amine
N	4.71	2.81				8.42	
G	3.94					8.55	
O	4.36	1.84	1.69	3.02		8.11	7.64
K(Me)$_3$	4.33	1.84,1.73	1.43	1.66	3.3	8.33	(CH$_3$)$_3$=3.1
I	4.14	1.84	1.49,1.19,0.89	0.89		8.30	
L	4.39	1.7	1.61	0.92		8.37	
Q	4.31	2.04	2.36			8.33	

Table 2.43. Proton Chemical Shift Assignments for Peptide **W7**: Ac-Arg-Trp-Val-Glu-Val-Asn-Gly-NH2

	α	β	γ	δ	ε	Amide	Amine
R	4.18	1.60	1.48	3.08		8.14	6.63,7.12
W	4.70	3.27				8.19	10.11
V	4.02	1.96	0.85			7.75	
E	4.29	1.99	2.43			8.20	
V	4.10	2.07	0.94			8.22	
N	4.70	2.82				8.60	
G	3.91					8.38	

Table 2.44. Proton Chemical Shift Assignments for Peptide **OrnL7**: Ac-Asn-Gly-Orn-Orn-Ile-Leu-Gln-NH2

	α	β	γ	δ	ε	Amide	Amine
N	4.69	2.80				8.41	
G	3.95					8.52	
O	4.35	1.85	1.72	3.02		8.15	7.6
O	4.36	1.84	1.70	3.02		8.40	7.6
I	4.15	1.85	1.35,1.14,0.90	0.90		8.25	
L	4.39	1.71	1.71	0.90		8.37	
Q	4.31	2.04	2.35			8.32	

Table 2.45. Proton Chemical Shift Assignments for Peptide **OrnMeL7**: Ac-Asn-Gly-Orn-Orn(Me)-Ile-Leu-Gln-NH2

	α	β	γ	δ	ε	Amide	Amine
N	4.69	2.80				8.45	
G	3.93					8.55	
O	4.35	1.84	1.76	3.04		8.16	7.6
O(Me)	4.35	1.84	1.76	3.00	CH3=2.71	8.45	8.14
I	4.13	1.83	1.48,1.13,0.89	0.89		8.31	
L	4.38	1.64	1.59,0.93,0.86	0.86		8.39	
Q	4.29	2.09,1.97	2.34			8.36	

Table 2.46 Proton Chemical Shift Assignments for Peptide **OrnMe2L7**: Ac-Asn-Gly-Orn-Orn$(Me)_2$-Ile-Leu-Gln-NH2

	α	β	γ	δ	ε	Amide	Amine
N	4.69	2.82				8.45	
G	3.94					8.56	
O	4.34	1.77	1.65	3.01		8.16	7.63
$O(Me)_2$	4.38	1.77	1.65	3.17	$(CH3)_2$=2.88,2.87	8.44	8.16
I	4.14	1.84	1.48,1.1,0.90	0.90		8.33	
L	4.38	1.63	1.63	0.90		8.40	
Q	4.31	2.10,1.98	2.36			8.36	

Table 2.47. Proton Chemical Shift Assignments for Peptide **OrnMe3L7**: Ac-Asn-Gly-Orn-Orn$(Me)_3$-Ile-Leu-Gln-NH2

	α	β	γ	δ	ε	Amide	Amine
N	4.67	2.80					
G	3.93						
O	4.33	1.79	1.65	3.01			
$O(Me)_3$	4.38	1.81	1.69	3.34	$(CH3)_3$=3.11		
I	4.13	1.84	1.48,1.1,0.88	0.88			
L	4.37	1.69	1.69	0.90			
Q	4.30	2.09,1.97	2.36				

Table 2.48. Proton Chemical Shift Assignments for Peptide **DabL7**: Ac-Asn-Gly-Orn-Dab-Ile-Leu-Gln-NH2

	α	β	γ	δ	ε	Amide	Amine
N	4.69	2.81				8.41	
G	3.95					8.5	
O	4.35	1.85	1.69	3.01		8.17	7.6
Dab	4.47	2.12	3.06			8.54	7.6
I	4.14	1.81	1.37,1.1,0.90	0.90		8.29	
L	4.28	1.66	1.66	0.98,0.84		8.42	
Q	4.31	2.12,1.99	2.38			8.35	

Table 2.49. Proton Chemical Shift Assignments for Peptide **DabMeL7**: Ac-Asn-Gly-Orn-Dab(Me)-Ile-Leu-Gln-NH2

	α	β	γ	δ	ε	Amide	Amine
N	4.68	2.81					
G	3.95						
O	4.35	1.88	1.70	3.01			
Dab(Me)	4.47	2.11	3.09		CH3=2.73		
I	4.14	1.85	1.47,1.17,0.90	0.90			
L	4.39	1.63	0.91	0.91			
Q	4.31	1.99	2.37				

Table 2.50. Proton Chemical Shift Assignments for Peptide **DabMe2L7**: Ac-Asn-Gly-Orn-Dab(Me)$_2$-Ile-Leu-Gln-NH2

	α	β	γ	δ	ε	Amide	Amine
N	4.68	2.83					
G	3.95						
O	4.34	1.82	1.73	3.02			
Dab(Me)$_2$	4.48	2.20	3.20		(CH3)$_2$=2.901		
I	4.13	1.85	1.45,0.91	0.91			
L	4.40	1.65	0.92	0.92			
Q	4.305	2.03	2.35				

Table 2.51. Proton Chemical Shift Assignments for Peptide **DabMe3L7**: Ac-Asn-Gly-Orn-Dab(Me)$_3$-Ile-Leu-Gln-NH2

	α	β	γ	δ	ε	Amide	Amine
N	4.68	2.84					
G	3.94						
O	4.32	1.77	1.77	3.01			
Dab(Me)$_3$	4.51	2.246	3.395		(CH3)$_3$=3.142		
I	4.14	1.74	0.91	0.91			
L	4.39	1.644	1.644, 0.926	0.926			
Q	4.29	2.00	2.36				

Table 2.52. Proton Chemical Shift Assignments for Peptide **KT7**: Ac-Asn-Gly-Orn-Lys-Ile-Thr-Gln-NH2

	α	β	γ	δ	ε	Amide	Amine
N	4.69	2.81				8.44	
G	3.94					8.55	
O	4.36	1.84	1.72	3.01		8.12	7.60
K	4.34	1.87	1.43	1.70	3.01	8.37	7.53
I	4.24	1.89	1.50,1.21,0.93	0.90		8.34	
T	4.36	4.19	1.20			8.26	
Q	4.34	2.14,2.00	2.37			8.40	

Table 2.53. Proton Chemical Shift Assignments for Peptide **KMeT7**: Ac-Asn-Gly-Orn-Lys(Me)-Ile-Thr-Gln-NH2

	α	β	γ	δ	ε	Amide	Amine
N	4.69	2.80					
G	3.94					8.55	
O	4.37	1.76	1.76	3.01		8.11	
K(Me)	4.34	1.75	1.42	1.70	3.01 CH3=2.70		
I	4.24	1.89	1.49,1.22,0.91	0.91		8.33	
T	4.37	4.19	1.20			8.26	
Q	4.34	2.00	2.37			8.39	

Table 2.54. Proton Chemical Shift Assignments for Peptide **KMe2T7**: Ac-Asn-Gly-Orn-$Lys(Me)_2$-Ile-Thr-Gln-NH2

	α	β	γ	δ	ε	Amide	Amine
N	4.70	2.81				8.43	
G	3.94					8.55	
O	4.37	1.76	1.76	3.01		8.12	
$K(Me)_2$	4.33	1.77	1.41	1.70	3.10 CH3=2.87		
I	4.24	1.89	0.90	0.90		8.35	
T	4.37	4.19	1.20			8.25	
Q	4.33	2.00	2.37			8.40	

Table 2.55. Proton Chemical Shift Assignments for Peptide **KMe3T7**: Ac-Asn-Gly-Orn-$Lys(Me)_3$-Ile-Thr-Gln-NH2

	α	β	γ	δ	ε	Amide	Amine
N	4.67	2.80				8.42	
G	3.94					8.55	
O	4.37	1.78	1.78	3.01			
$K(Me)_3$	4.36	1.79	1.40	1.79	3.31 CH3=3.10		
I	4.24	1.89	1.50,1.18,0.91	0.91		8.36	
T	4.37	4.19	1.19			8.24	
Q	4.33	2.09,2.00	2.37			8.39	

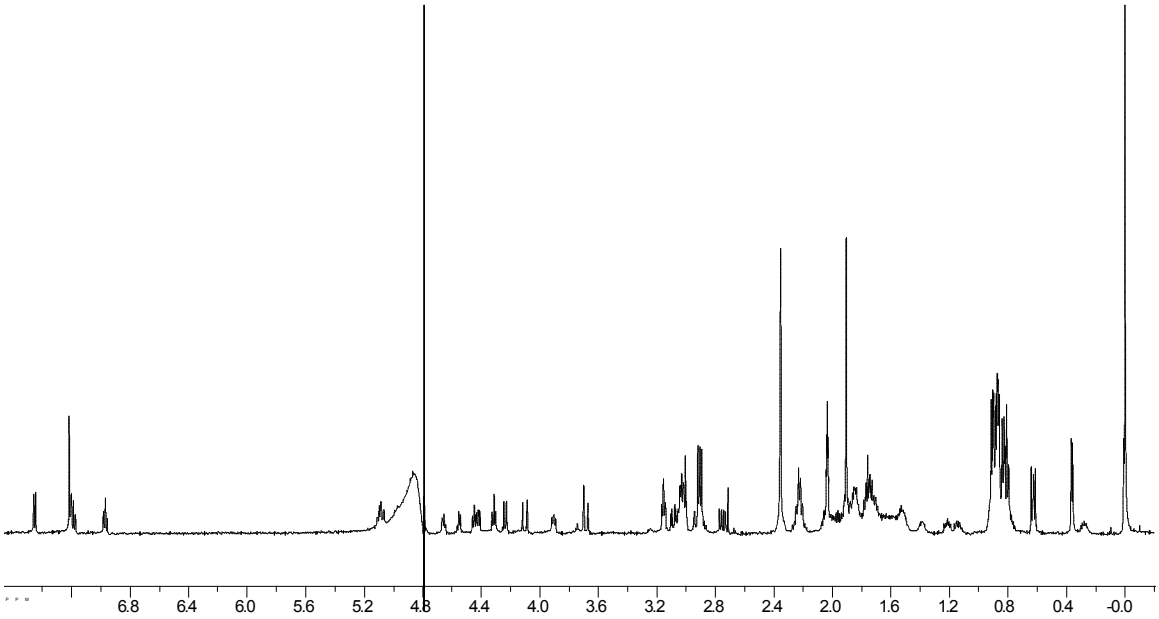

Figure 2.78. [1]HNMR of Peptide **WDMAa**: Ac-Arg-Trp-Val-Glu-Val-Asn-Gly-Orn-Arg(Me)$_2$-Ile-Leu-Gln-NH2

Table 2.56. Proton Chemical Shift Assignments for Peptide **WDMAa.**

	α	β	γ	δ	ε	Amide	Amine
R	4.44	1.66	1.53	3.14		8.03	7.12,6.74,6.60
W	5.06	3.01,2.93				8.39	10.11
V	4.54	2.05	0.84			9.22	
E	5.10	1.93	2.21			8.44	
V	4.22	1.91	0.88			8.90	
N	4.41	3.08,2.74				9.54	
G	4.10,3.69					8.69	
O	4.65	1.80	1.80	3.02		7.77	7.65
R(Me)$_2$	4.87	1.71	1.58	2.95	**(CH3)$_2$**=2.356	8.52	6.26,6.21
I	4.65	1.80	0.85	0.85		9.24	
L	3.91	1.21	0.79	0.37,0.25, -0.05		8.19	
Q	4.31	1.89	2.21			8.70	

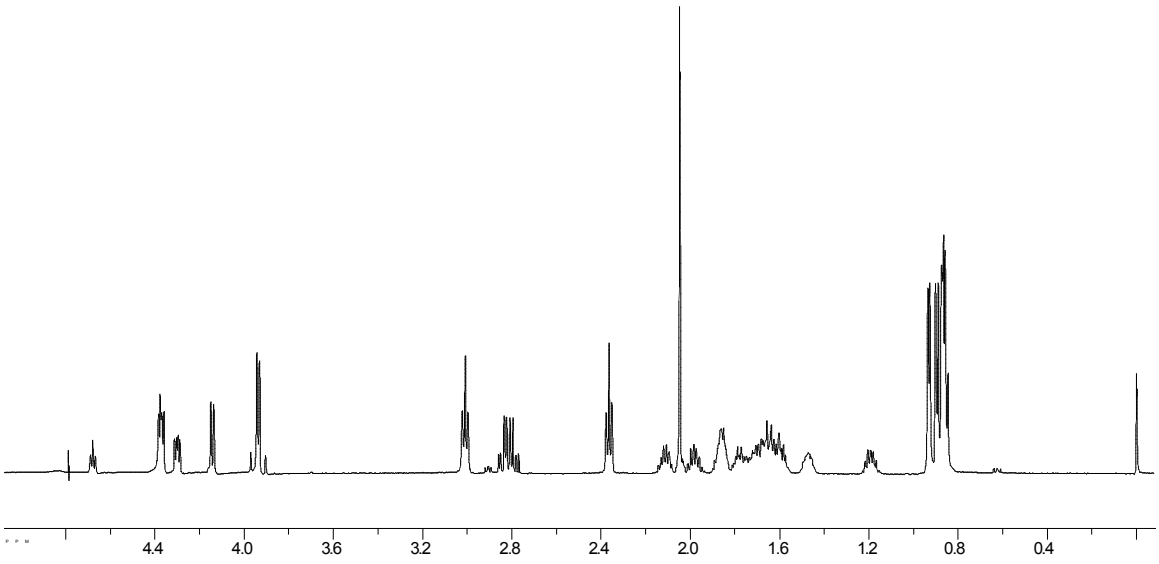

Figure 2.79. ^{1}HNMR of Peptide **DMAa7**: Ac-Asn-Gly-Orn-Arg(Me)$_2$-Ile-Leu-Gln-NH2

Table 2.57. Proton Chemical Shift Assignments for Peptide **DMAa7.**

	α	β	γ	δ	ε	Amide	Amine
N	4.67	2.80				8.46	
G	3.93					8.58	
O	4.36	1.65	1.60	3.01		8.16	7.64
R(Me)$_2$	4.32	1.77	1.77	3.25	**(CH3)$_2$**=3.002	8.36	6.79,6.76
I	4.14	1.84	1.49,1.18, 0.89	0.89		8.30	
L	4.39	1.88	1.64	0.92,0.85		8.38	
Q	4.30	2.11,1.98	2.36			8.34	

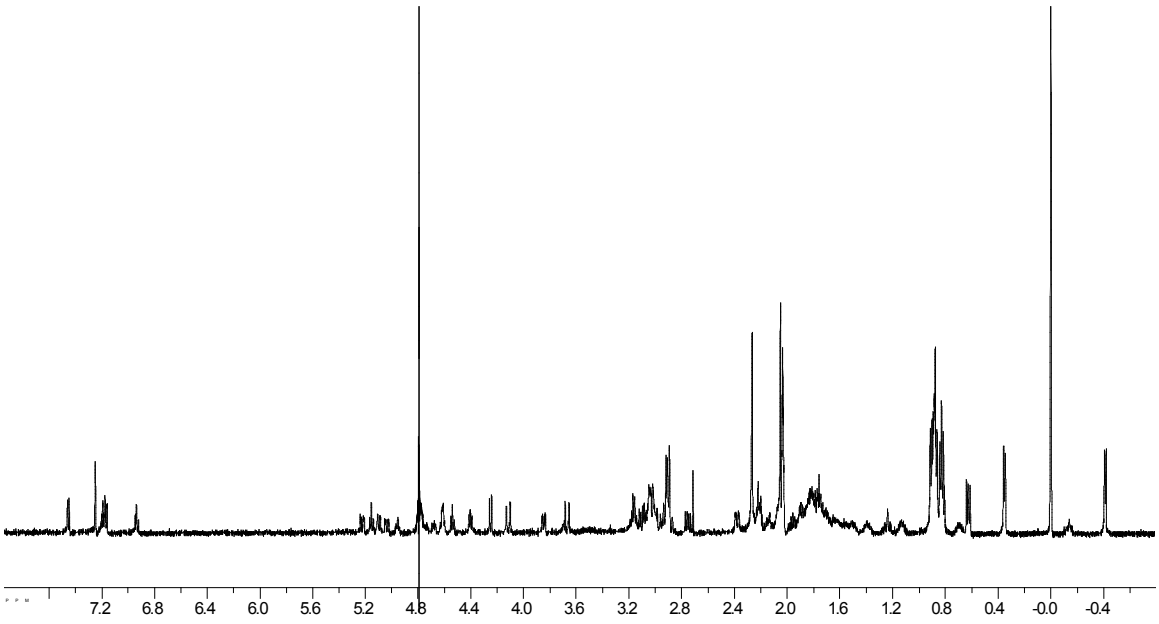

Figure 2.80. [1]HNMR of Peptide **WDMAaCyc**: Ac-Cys-Arg-Trp-Val-Glu-Val-Asn-Gly-Orn-Arg(Me)$_2$-Ile-Leu-Gln-Cys-NH2

Table 2.58. Proton Chemical Shift Assignments for Peptide **WDMAaCyc.**

	α	β	γ	δ	ε	Amide	Amine
C	5.23	2.98, 2.32					
R	4.61	1.79	1.66,1.51	3.16		8.73	
W	5.10	2.96	7.45,7.25	7.19,7.17	6.94	8.64	
V	4.61	2.07	0.86			9.54	
E	5.16	1.93	2.22			8.46	
V	4.26	1.91	0.90			9.05	
N	4.40	3.13, 2.76					
G	4.115, 3.672						
O	4.68	1.85	1.73	3.04		7.79	
R(Me)$_2$	4.96	1.82	1.59	3.07,2.92	**(CH$_3$)$_2$**=2.27		
I	4.74	1.82	1.40,1.13	0.86		9.41	
L	3.86	1.24	0.7,0.35	-0.13,-0.4		8.24	
Q	4.54	1.80	2.15,2.09			9.02	
C	5.04	2.94				9.05	

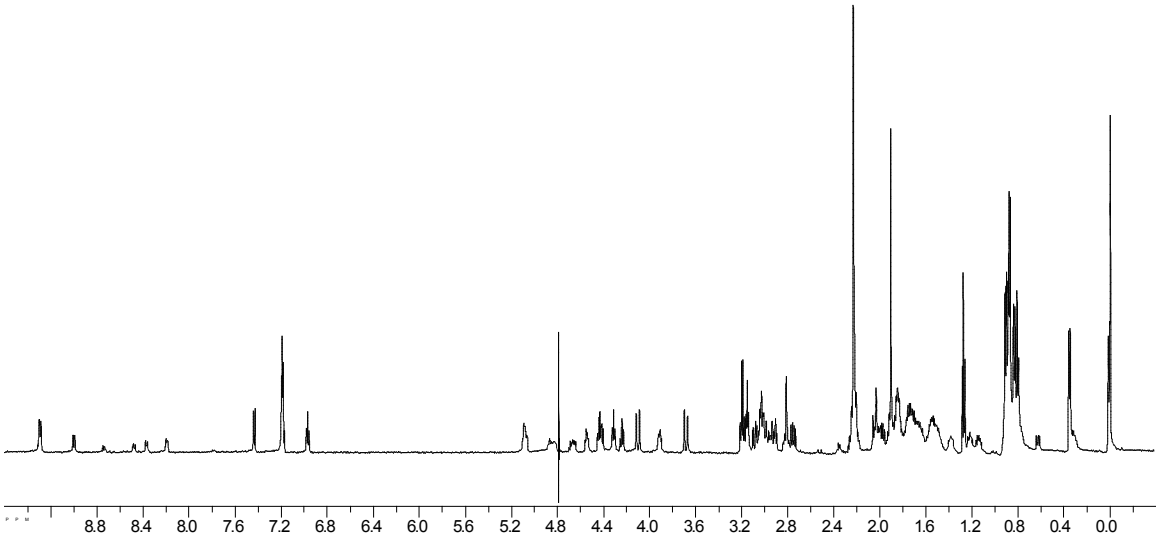

Figure 2.81. [1]HNMR of Peptide **WDMAs**: Ac-Arg-Trp-Val-Glu-Val-Asn-Gly-Orn-Arg(Me)$_2$-Ile-Leu-Gln-NH2

Table 2.59. Proton Chemical Shift Assignments for Peptide **WDMAs.**

	α	β	γ	δ	ε	Amide	Amine
R	4.45	1.66	1.54	3.15		8.03	7.13,6.61
W	5.09	3.02,2.93				8.38	10.07
V	4.55	2.06	0.85			9.28	
E	5.10	1.94	2.23			8.48	
V	4.24	1.91	0.91			8.98	
N	4.42	3.09,2.77				9.57	
G	4.102,3.685					8.70	
O	4.66	1.84	1.73	3.04		7.77	7.66
R(Me)$_2$	4.88	1.766,1.68	1.52	2.96,2.83	**(CH$_3$)$_2$**=2.229	8.53	6.34,6.17
I	4.69	1.85	1.39, 1.14,0.88	0.88		9.29	
L	3.92	1.22	0.79	0.35,0.016		8.20	
Q	4.32	2.01,1.84	2.23			8.73	

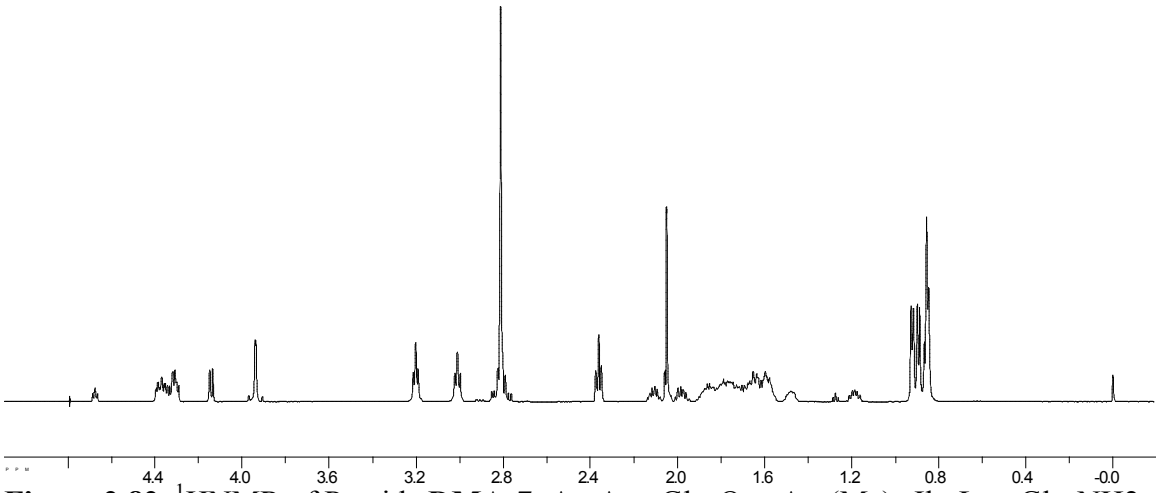

Figure 2.82. ^{1}HNMR of Peptide **DMAs7**: Ac-Asn-Gly-Orn-Arg(Me)$_2$-Ile-Leu-Gln-NH2

Table 2.60. Proton Chemical Shift Assignments for Peptide **DMAs7.**

	α	β	γ	δ	ε	Amide	Amine
N	4.68	2.80				8.43	
G	3.94					8.56	
O	4.35	1.77	1.77	3.01		8.13	7.60
R(Me)$_2$	4.32	1.80	1.62	3.20	**(CH$_3$)$_2$**=2.812	8.32	6.81,6.75
I	4.14	1.84	1.48,1.18, 0.88	1.00,0.89		8.27	
L	4.38	----	1.63	0.88		8.37	
Q	4.30	1.99	2.36			8.31	

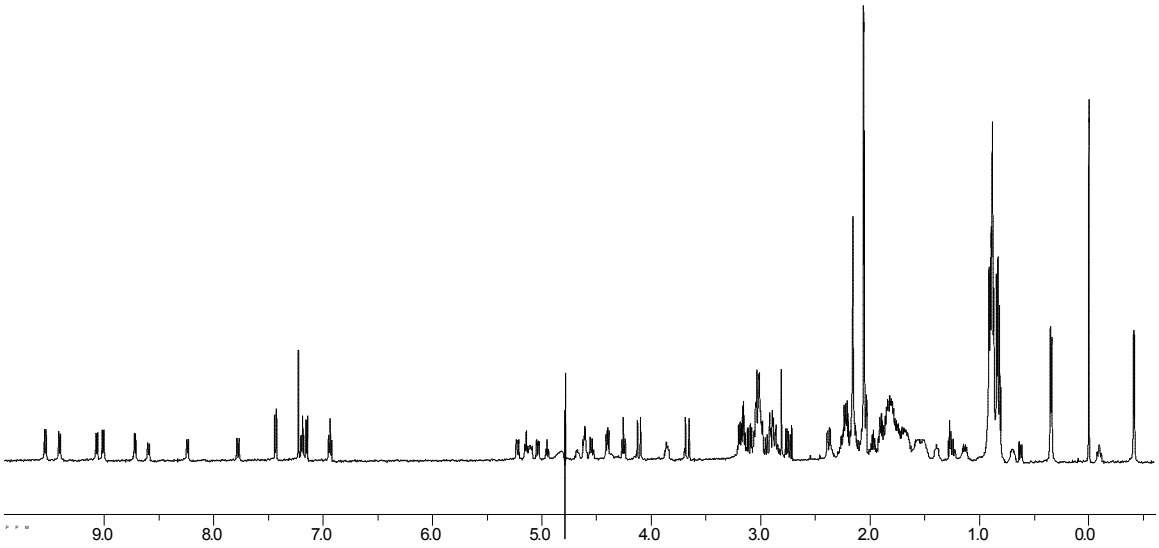

Figure 2.83. [1]HNMR of Peptide **WDMAsCyc**: Ac-Cys-Arg-Trp-Val-Glu-Val-Asn-Gly-Orn-Arg(Me)$_2$-Ile-Leu-Gln-Cys-NH2

Table 2.61. Proton Chemical Shift Assignments for Peptide **WDMAsCyc.**

	α	β	γ	δ	ε	Amide	Amine
C	5.23	2.95, 2.38					
R	4.61	1.79	1.67,1.50	3.17		8.72	
W	5.11	3.00,2.89				8.60	
V	4.61	2.07	0.87			9.54	
E	5.15	1.93	2.23				
V	4.26	1.91	0.90			9.07	
N	4.40	3.11,2.77					
G	4.115, 3.672						
O	4.68	1.85	1.73	3.04		7.79	
R(Me)$_2$	4.96	1.82	1.68,1.56	2.996,2.879	**(CH$_3$)$_2$**=2.059		
I	4.77	1.84	1.40,1.13	0.88		9.41	
L	3.86	1.25	0.71,0.35	-0.07,-0.4		8.24	
Q	4.56	1.81	2.21,2.10			9.02	
C	5.04	3.03					

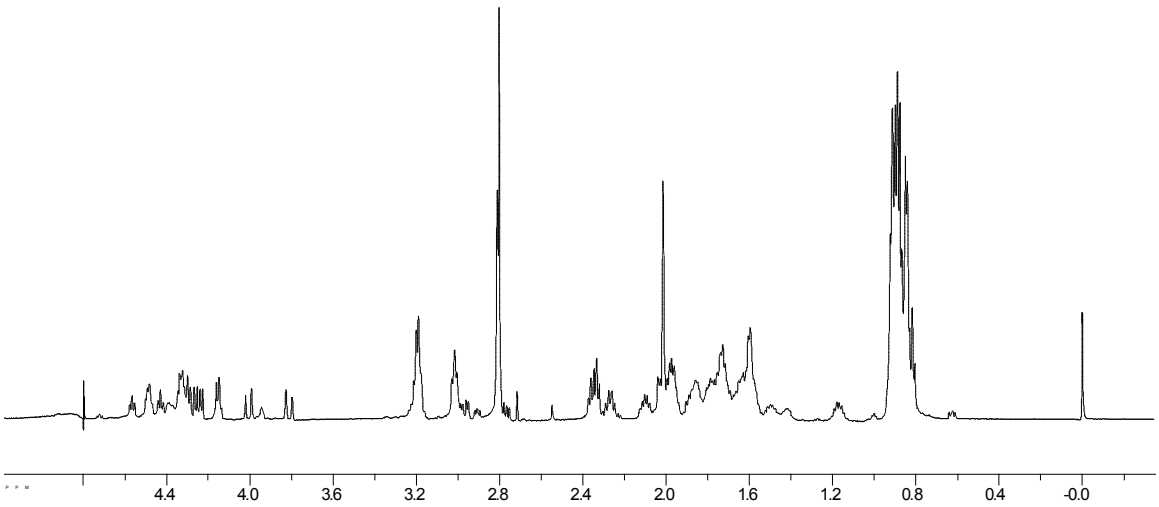

Figure 2.84. [1]HNMR of Peptide **VDMAs**: Ac-Arg-Val-Val-Glu-Val-Asn-Gly-Orn-Arg(Me)$_2$-Ile-Leu-Gln-NH2

Table 2.62. Proton Chemical Shift Assignments for Peptide **VDMAs.**

	α	β	γ	δ	ε	Amide	Amine
R	4.32	1.74	1.63	3.19			
V	4.29	1.98	0.88				
V	4.23	2.02	0.88				
E	4.72	1.91	2.27				
V	4.15	1.96	0.90				
N	4.56	2.93,2.80					
G	4.006,3.812						
O	4.48	1.82	1.65	3.02			
R(Me)$_2$	4.42	1.79	1.63	3.20	**(CH$_3$)$_2$**=2.802		
I	4.25	1.85	1.42,1.16,0.87	0.87			
L	4.48	1.66	0.87	0.87			
Q	4.33	2.06	2.34				

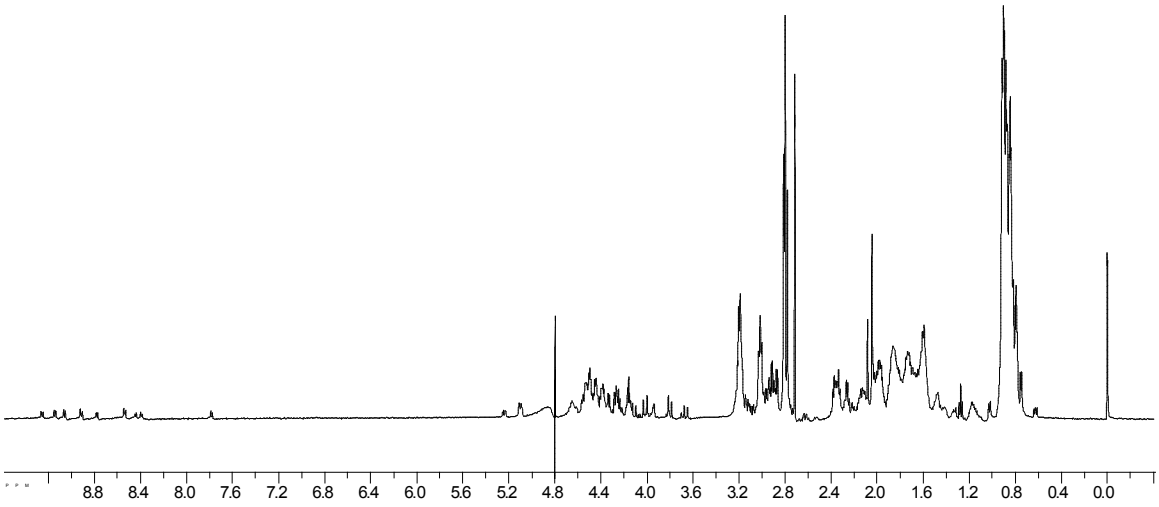

Figure 2.85. [1]HNMR of Peptide **VDMAsCyc**: Ac-Cys-Arg-Val-Val-Glu-Val-Asn-Gly-Orn-Arg(Me)$_2$-Ile-Leu-Gln-Cys-NH2

Table 2.63. Proton Chemical Shift Assignments for Peptide **VDMAsCyc.**

	α	β	γ	δ	ε	Amide	Amine
C	5.24	3.16,2.61					
R	4.64	1.84	1.65	3.17		8.76	
V	4.64	1.87	0.79			8.52	
V	4.47	1.99	0.81			9.05	
E	5.09	1.88	2.14			8.43	
V	4.22	1.87	0.87			8.90	
N	4.52	2.90					
G	4.112, 3.662						
O	4.65	1.82	1.71	3.02		7.78	
R(Me)$_2$	4.44	1.82	1.64	3.17		**(CH$_3$)$_2$**=2.801	
I	4.49	1.86	1.12,0.83	0.83		9.14	
L	4.73	1.49	0.77	0.77		8.38	
Q	4.66	2.06	2.19			9.25	
C	5.09	3.06					

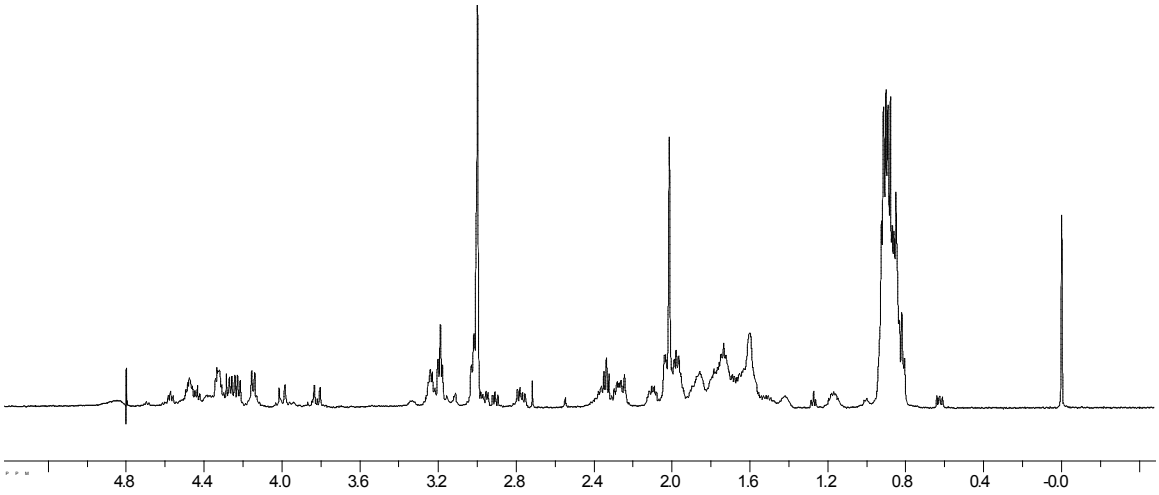

Figure 2.86. [1]HNMR of Peptide **VDMAa**: Ac-Arg-Val-Val-Glu-Val-Asn-Gly-Orn-Arg(Me)$_2$-Ile-Leu-Gln-NH2

Table 2.64. Proton Chemical Shift Assignments for Peptide **VDMAa.**

	α	β	γ	δ	ε	Amide	Amine
R	4.33	1.76	1.65	3.20			
V	4.27	1.96	0.89				
V	4.23	2.02	0.89				
E	4.70	1.92	2.28				
V	4.15	1.98	0.91				
N	4.58	2.96,2.79					
G	4.001,3.821						
O	4.48	1.80	1.65	3.02			
R(Me)$_2$	4.43	1.78	1.62	3.24	**(CH$_3$)$_2$**=2.998		
I	4.25	1.86	1.43,1.17,0.87	0.87			
L	4.47	-----	0.88	0.88			
Q	4.33	2.00	2.35				

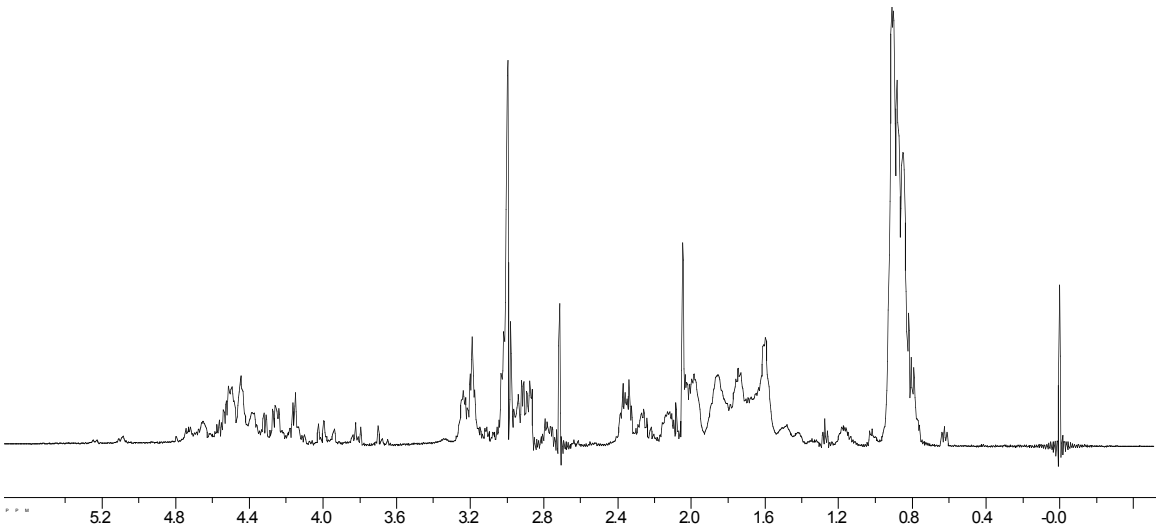

Figure 2.87. [1]HNMR of Peptide **VDMAaCyc**: Ac-Cys-Arg-Val-Val-Glu-Val-Asn-Gly-Orn-Arg(Me)$_2$-Ile-Leu-Gln-Cys-NH2

Table 2.65. Proton Chemical Shift Assignments for Peptide **VDMAaCyc.**

	α	β	γ	δ	ε	Amide	Amine
C	5.23	3.13,2.61					
R	4.61	1.76	1.76	3.26		8.79	
V	4.65	1.85	0.79			8.52	
V	4.48	1.98	0.81			9.05	
E	5.08	1.88	2.13			8.41	
V	4.21	1.86	0.87			8.91	
N	4.52	2.90					
G	4.113, 3.663						
O	4.63	1.82	1.65	3.02		7.76	
R(Me)$_2$	4.44	1.78	1.64	3.20		**(CH$_3$)$_2$**=2.997	
I	4.48	1.86	1.17,0.82	0.82		9.13	
L	4.72	1.50	0.79	0.79		8.38	
Q	4.64	2.08	2.27			9.24	
C	5.09	3.02					

CHAPTER III

LYSINE ACYLATION AND AMIDE-π INTERACTIONS

(Reproduced, in part, with permission from Hughes, R.M.; Waters, M.L. *J. Am. Chem. Soc.* **2006**, *128*, 13586 – 13591.)

A. Background and significance.

The acylation of lysine is a common post-translational modification of histone proteins. Lysine acylation can weaken the histone-DNA complex in chromatin by neutralizing the electrostatic interaction between unmodified lysine in histones and the negatively charged phosphate backbone of DNA, thereby activating transcription.[1] Additionally, lysine acylation is commonly found in cells with DNA damage, where it is also thought to weaken the DNA-histone complex to make DNA accessible to repair enzymes,[2] and can play a role in protein stability by preventing lysine ubiquitination, which tags proteins for proteolysis.[3] The bromodomain, a protein domain with a specific affinity for acetylated lysine, is found in most acyltransferases and in many proteins associated with the

---

[1] Hong, L.; Schroth, G. P.; Matthews, H.; Yau, P.; Bradbury, E. M. *J. Biol. Chem.* **1993**, *268*, 305-314.

[2] Masumoto, H.; Hawke, D.; Kobayashi, R.; Verreault, A. *Nature* **2005**, *436*, 294.

[3] Caron, C.; Boyault, C.; Khochbin, S. *BioEssays* **2005**, *27*, 408-415. (b) Simonsson, M.; Heldin, C.; Ericsson, J.; Gronroos, E. *J. Biol. Chem.* **2005**, *280*, 21797-21803.

regulation of chromatin structure.[4] The bromodomain binding pocket contains highly conserved aromatic residues that appear to interact with acetylated lysine through amide-π interactions (Figure 3.1).[5]

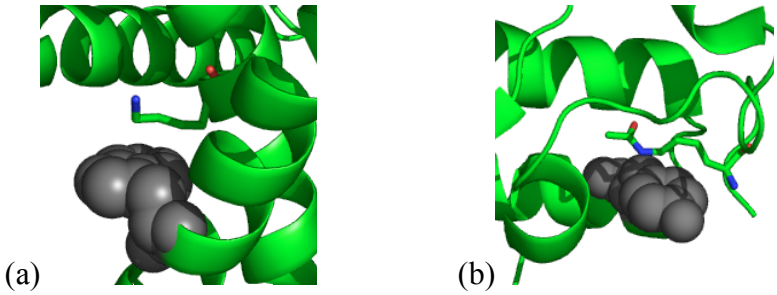

Figure 3.1. (a) Lys-Trp pair in typical cation-π geometry (PDB code: 1ONR). (b) KAc-Tyr pair in typical amide-π geometry (Bromodomain from GCN5 complexed with acetylated H4 peptide; PDB code: 1E6I).

The importance of amide-π interactions in structural biology has been long established through data-mining studies of protein crystal structures, in which amide-containing sidechains (Gln, Asn) were found to have statistical preference for packing near the faces of aromatic rings.[6] Additional investigations have identified numerous backbone amide-π

[4] Zeng, L.; Zhou, M. M. *FEBS Letters* **2002**, 513, 124-128.

[5] (a) Dhalluin, C.; Carlson, J. E.; Zeng, L.; He, C.; Aggarwal, A.; Zhou, M. *Nature* **1999**, *399*, 491-496. (b) Owen, D.J., Ornaghi, P., Yang, J.C., Lowe, N., Evans, P.R., Ballario, P., Neuhaus, D., Filetici, P., Travers, A.A. *EMBO J.* **2000**, *19,* 6141-6149.

[6] (a) Burley, S.K.; Petsko, G.A. *FEBS Letters* **1986**, 203, 139-143. (b) Burley, S.K.; Petsko, G.A. *Adv. Prot. Chem.* **1988**, 39, 125-189. (c) Singh, J.; Thornton, J. M. *J. Mol. Biol.* **1990**, *211*, 595-615. (d) Steiner, T.; Koellner, G. *J. Mol. Biol.* **2001**, *305*, 535 – 557.

interactions in protein and peptide structures,[6d,7] as well as a number of amide-π interactions that occur in the binding of ligands.[8] For example, backbone amide-π interactions have been identified between Gly/Phe and Gly/Trp pairs in analyses of pair-wise residue preferences in antiparallel β-sheets,[9] and amide-π interactions have been identified in the binding of the drug bezafibrate by human deoxyhemoglobin.[10] Amide-π interactions have also been utilized in the selective binding of guests by model systems in organic solution.[11] Additional theoretical studies have been conducted to demonstrate both the orientation and magnitude of the amide-π interaction, using variously the formamide-benzene interaction[12] and the ammonia-benzene interaction[13] in the gas phase

---

[7] (a) van der Spoel, D.; van Buuren, A. R.; Tieleman, P.; Berendsen, H. J. C. *J. Biomol. NMR* **1996**, *8*, 229 – 238. (b) Honda, S.; Kobayashi, N.; Munekata, E. *J. Mol. Biol.* **2000**, *295*, 269-278. (c) Duan, G.; Smith, V.H.; Weaver, D.F. *Int. J. Quant. Chem.* **2000**, *80*, 44-60. (d) Toth, G.; Watts, C.R.; Murphy, R.F.; Lovas, S. *Prot. Struct. Func. Gen.* **2001**, *43*, 373-381. (e) Toth, G.; Murphy, R.F.; Lovas, S. *Prot. Eng.* **2001**, *14*, 543-547. (f) Toth, G.; Murphy, R.F.; Lovas, S. *J. Am. Chem. Soc.* **2001**, *123*, 11782-11790. (g) Toth, G.; Kover, K.E.; Murphy, R.F.; Lovas, S. *J. Phys. Chem. B.* **2004**, *108*, 9287-9296. (h) Meyer, E.A.; Castellano, R.K.; Diederich, F. *Angew. Chem. Int. Ed.* **2003**, *42*, 1211-1250. (i) Sengupta, A.; Mahalakshmi, R.; Shamala, N.; Balaram, P. *J. Pept. Res.* **2005**, *65*, 113-129. (j) Mahalakshmi, R.; Raghothama, S.; Balaram, P. *J. Am. Chem. Soc.* **2006**, *128*, 1125-1138.

[8] Perutz, M.F. *Phil. Trans. Phys. Sci. Eng.* **1993**, *345*, 105-112.

[9] (a) Hutchinson, E. G.; Sessions, R. B.; Thornton, J. M.; Woolfson, D. N. Prot. Sci. **1998**, *7*, 2287 – 2300. (b) Merkel, J. S.; Regan, L. *Folding & Design* **1998**, 3, 449 - 455.

[10] Perutz, M. F.; Fermi, G.; Abraham, D. J.; Poyart, C.; Bursaux, E. *J. Am. Chem. Soc.* **1986**, *108*, 1064-1078.

[11] (a) Bisson, A. P.; Lynch, V. M.; Monahan, M. C.; Anslyn, E. V. *Angew. Chem. Int. Ed.* **1997**, 36, 2340 – 2342. (b) Snowden, T. S.; Bisson, A. P.; Anslyn, E. V. *J. Am. Chem. Soc.* **1999**, *121*, 6324 – 6325.

[12] (a) Duan, G.; Smith, V.H.; Weaver, D.F. *J. Phys. Chem. A* **2000**, *104*, 4521-4532. (b) Duan, G.; Smith, V.H.; Weaver, D.F. *Chem. Phys. Lett.* **1999**, *310*, 323-332.

as models for the amide-π interaction in proteins. Notably, a recent study investigated both amide- and cation-π interactions using implicit solvent models and predicted the amide-π interaction of Asn and Gln sidechains with an adenine ring (Ade) to be intermediate in magnitude (-4 kcal/mol) between the cation-π interactions Arg-Ade (-7 kcal/mol) and Lys-Ade (-2 kcal/mol).[14] In addition, Burley and Pestko's survey of 33 protein crystal structures found higher fractions of polar amide residues interacting with aromatic sidechains (31% Asn, 40% Gln) than for Lys (26%), but lower than that of Arg (47%).[6a] These findings suggest that the amide-π interaction may be more favorable than the cation-π interaction between lysine and an aromatic ring (Figure 3.1).

To explore the efficacy of amide-π interactions, and in particular their role in the recognition of KAc, we have investigated the effects of acylation of lysine and its interaction with tryptophan within the context of a β-hairpin peptide (Figure 3.2). This is a useful model system to study non-covalent interactions in water within a biologically relevant context and has previously been used to study cation-π interactions.[15] Two analogs of acyl lysine (KAc), formyl lysine (KFm) and trifluoroacetyl lysine (KFAc), were studied to explore the effects of changes in hydrophobic and electronic character of the acyl group. In our investigation, we find that the interaction between acylated lysine and tryptophan consists of a polar-π interaction that occurs primarily between the

---

[13] Tsuzuki, S.; Honda, K.; Uchimaru, T.; Mmikami, M.; Tanabe, K. *J. Am. Chem. Soc.* **2000**, *122*, 11450-11458.

[14] Biot, C.; Buisine, E.; Rooman, M. *J. Am. Chem. Soc*. **2003**, *125*, 13988-13994.

[15] (a) Tatko, C.D.; Waters, M.L. *Prot. Sci.* **2003**, *12*, 2443-2452. (b) Tatko, C.D.; Waters, M.L. *J. Am. Chem. Soc*. **2004**, *126*, 2028-2034. (c) Hughes, R.M.; Waters, M.L. *J. Am. Chem. Soc.* **2005**, *127*, 6518-6519.

polarized amide of acyl lysine and the electron rich face of the tryptophan indole ring. Despite the loss of the positive charge upon N-acylation, the KAc···Trp interaction is as strong as the unmodified Lys···Trp interaction previously reported in the same model system.[15a,b] This indicates that the polar-π interaction is energetically competitive with the cation-π interaction, likely due to a reduced desolvation penalty of interaction between lysine and tryptophan upon acylation of the lysine sidechain while maintaining the electrostatic and van der Waals components of the interaction via NH(δ+)···π(δ-) and π-π stacking.

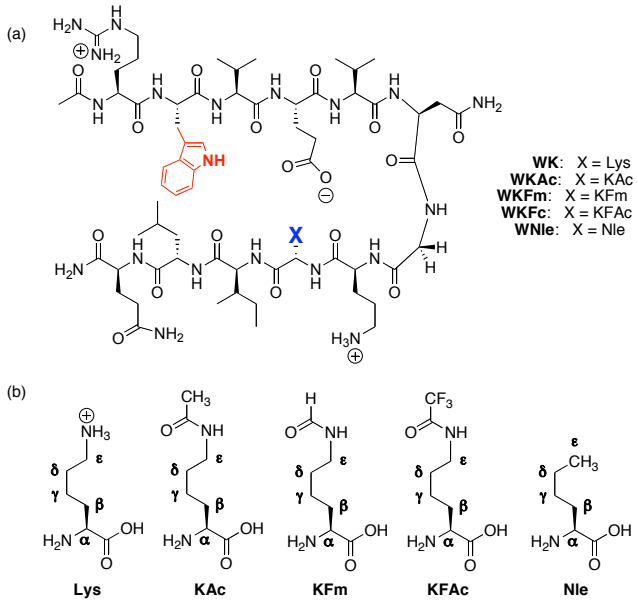

Figure 3.2. (a) β-hairpin peptide structure. (b) Amino acids at position X: Lysine (Lys), Acyl Lysine (KAc), Formyl Lys (KFm), Trifluoroacetylated Lysine (KFAc), and Norleucine (Nle).

B. Results and Discussion

i. Design. The 12-residue β-hairpin sequence used in this study is based on a sequence that has been previously described (Figure 3.2).[15] Key design features include a good turn-nucleating sequence (Val-Asn-Gly-Val) and a number of hydrophobic interactions to

stabilize the hairpin, including Val3, Val5, Ile10 on one face of the hairpin, and Trp2 and Leu11 on the opposite face of the hairpin. The diagonal interaction between Trp2 and position 9 (residue X in Figure 3.2) is the site of interest for this study. A Lys residue at position 9 has been previously been shown to interact favorably with Trp2 via a cation - π interaction between the ε-CH_2 of Lys and the face of the aromatic ring. To explore the relative favorability of an amide-π interaction, we investigated the effect of Lys acylation.

ii. Characterization. As discussed in Chapter 1, the beta-hairpin structure and stability was characterized by a number of standard NMR techniques, including α-hydrogen (Hα) chemical shifts, glycine splitting (Δδ Gly), and cross-strand NOEs.[15,16] The degree of Hα downfield shifting and Gly splitting relative to random coil values is used as an indicator of the degree of β-sheet structure at each position along the strand and in the turn, respectively.[17] The fraction folded is calculated with the following equation: $\%_{folded} = (d_{obs} - d_U)/(d_F - d_U)$, where the unfolded state (U) is represented by random coil control peptides and the fully folded state (F) by cyclic peptides (see Experimental). Furthermore, numerous NOEs between cross-strand pairs of sidechains were observed for all peptides, consistent with β-hairpin formation (see Experimental).

iii. Effects of Lysine Acylation. Acylation of lysine results in a modest enhancement in stability of the β-hairpin peptide. This is demonstrated by an increase in the α-hydrogen shifts relative to random coil, as shown in Figure 3.3a. Based on the

---

[16] Maynard, A. J.; Sharman, G. J.; Searle, M. S. *J. Am. Chem. Soc.* **1998**, *120*, 1996-2007.

[17] Griffith-Jones, S. R.; Maynard, A. J.; Searle, M. S. *J. Mol. Biol.* **1999**, *292*, 1051-1069.

glycine splitting, fraction folded of **WKAc** is 87% (± 1%) (Sidechain $H\alpha_{avg}$ = 83 ± 8%)[18], versus 78% (± 1%) for the peptide **WK** at 298 K (Sidechain $H\alpha_{avg}$ = 76 ± 7%),[18] indicating that acylation enhances hairpin stability ($\Delta\Delta G$ = 0.38 kcal/mol, ± 0.05 kcal/mol). Because acylation of Lys may change its beta-sheet propensity, we performed a double mutant cycle to quantitatively asses the interaction energy between Trp and KAc. Val and Ser were used as controls for Trp and Lys, respectively.[15] Double mutant cycles give the magnitude of the Trp···X sidechain-sidechain interaction for **WK** and **WKAc** to be -0.30 and -0.34 kcal/mol (± 0.1 kcal/mol), respectively. While the differences in the two interaction energies are within experimental error, this is significant in that acylation does not *decrease* the magnitude of the interaction with Trp, despite the loss of the positive charge. Rather, the conversion of the ammonium group to an amide provides an interaction with Trp of comparable magnitude.

Although the interaction energies for Trp···KAc and Trp···Lys are similar, the upfield shifting patterns of the lysine and acyl lysine sidechains indicate a *change in the interaction geometry* with Trp for KAc relative to Lys (Figure 3.3b). While the unmodified lysine is most upfield shifted at the ε-CH_2 protons, KAc is most upfield shifted at its amide proton. The ε-CH_2 of KAc exhibits some upfield shifting as well, wheareas the acetyl methyl group is less shifted. Thus, although it is difficult to determine if the amide group is stacked with the Trp or interacting via an NH···π interaction, it is clear that it interacts in a different geometry than Lys. The preference for interaction at the amide NH in KAc versus the ε-CH_2 in Lys may arise from differences in the desolvation cost for an amide relative to an ammonium group. If the amide in KAc

[18] Sidechain $H\alpha_{avg}$ values were calculated excluding the terminal residues (Arg,Gln) and the turn residues (Asn,Gly).

is stacked with the Trp residue, the NH group may still be able to hydrogen bond with water, such that there is minimal desolvation penalty, as has been proposed for the interaction of Arg with Trp.[19] In proteins, the stacked conformation for Asn and Gln sidechains with aromatic residues is favored by a factor of about 2.5. [6d] Given that the Trp···KAc interaction is highly solvent exposed in this peptide model system, a stacked conformation is likely.

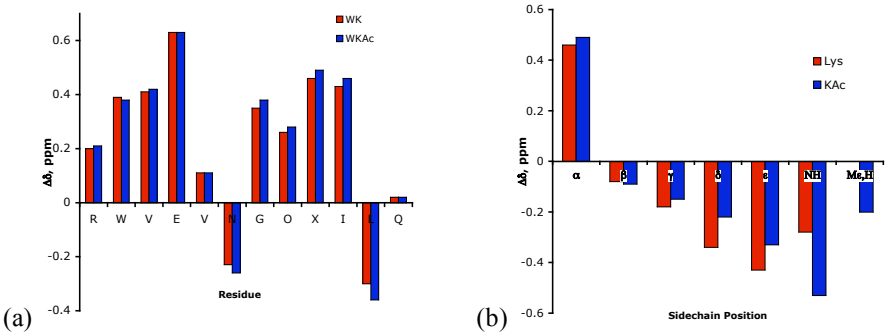

Figure 3.3. (a) **WK** and **WKAc** αH shifts relative to random coil values. Glycine shifts reflect the splitting. (b) WK and WKAc sidechain upfield proton shifts relative to random coil values. Conditions: 298K, 50 mM NaOAc-d_3 in D_2O, pH 4.0 (uncorrected), referenced to DSS.

The thermodynamics of hairpin folding for **WKAc** are consistent with hairpin stabilization due to a polar-π interaction (Figure 3.4 and Table 3.1).[20] The driving force for folding of **WKAc** is similar to **WK**, with an enthalpic driving force for the folding and an associated entropic cost, despite the difference in charge. In contrast, comparison with a peptide containing a nonpolar alkyl sidechain, **WNle**, at position X shows that the

[19] (a) Mitchell, J. B. O.; Nandi, C. L.; McDonald, I. K.; Thornton, J. M. *J. Mol. Biol.* **1994**, *239*, 315-331. (b) Gallivan, J. P., Dougherty, D. A. *Proc. Natl. Acad. Sci. USA* **1999**, *96*, 9459-9464.

[20] Hughes, R. M.; Waters, M. L., *J. Am. Chem. Soc.*, *in press*.

driving force folding of **WKAc** is much more enthalpically favorable than the nonpolar Nle sidechain.[15b] This is consistent with significant interaction between the polarized amide NH and tryptophan in **WKAc** as seen in Figure 3.3b.

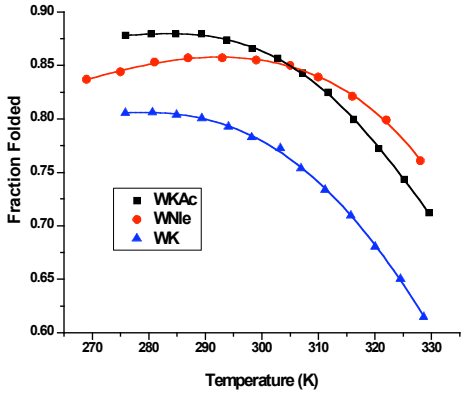

Figure 3.4. Thermal denaturation profiles of **WK**, **WKAc**, and **WNle** peptides as determined by NMR. The fraction folded was determined from the Gly splitting. Error is ±0.5 K in temperature and ±1% in fraction folded. Conditions: 50 mM NaOAc-d_3 buffer, pD 4.0 (uncorrected).

Table 3.1. Thermodynamic Parameters[a] for Folding at 298 K[10]

Peptide	ΔH° (kcal/mol)	ΔS° (cal/mol K)	ΔC_p° (cal/mol K)	Reference
WK	-2.8 (0.03)	-6.8 (0.1)	-163 (3)	15a,b
WKAc	-2.91 (0.07)	-6.1 (0.2)	-250 (40)	*this work*
WNle	-0.85 (0.07)	-0.7 (0.2)	-170 (25)	15b

[a] Determined from the temperature dependence of the Gly chemical shift from 0 to 60 °C. Errors (in parentheses) are determined from the fit. Error is ±0.5 K in temperature and ±1% in fraction folded. Conditions: 50 mM NaOAc-d_3 buffer, pD 4.0 (uncorrected).

iv. Effects of Acyl Lysine Analogs. Acyl lysine analogs, formyl lysine (KFm) and trifluoroacetyl lysine KFAc), were used to further examine the effects of acylation.

KFm was investigated in order to determine the contribution of hydrophobic or van der Waals interactions, and KFAc was studied to examine electronic effects on the interaction with Trp interaction. With these analogs, subtle changes were detected in the geometry of the interaction, but there was little effect on stability and driving force for folding. **WKAc** and its analogs **WKFm** and **WKFAc** are approximately equistable at 298K: 87, 86, and 87% folded (± 1%), respectively, based on the glycine splitting (83, 82, and 83% ± 8% folded based on the average sidechain Ha fraction folded).[18] This is supported by the consistency of the Hα shifts relative to random coil (Figure 3.5a). While these hairpins are of similar stabilities, comparison of the sidechain upfield shifting profiles for KAc, FAc, and Fm indicates differences in the mode of interaction (Figure 3.5b). The KFm sidechain has a similar profile to the KAc sidechain. Both are most upfield shifted at the amide NH position. However, the KFm has both polarized amide and aldehyde protons (Figure 3.6), both of which can interact favorably with the tryptophan ring. As a result, the upfield shifting is distributed more evenly over the two sites, while the KAc sidechain has a definite preference for interacting with tryptophan through the amide position. In contrast, the KFAc sidechain exhibits significant upfield shifting at the δ- and ε-CH_2 groups and very little shifting of the amide nitrogen (Figure 3.5b). Indeed, it has an interaction profile more similar to lysine (Fig. 3.5c).

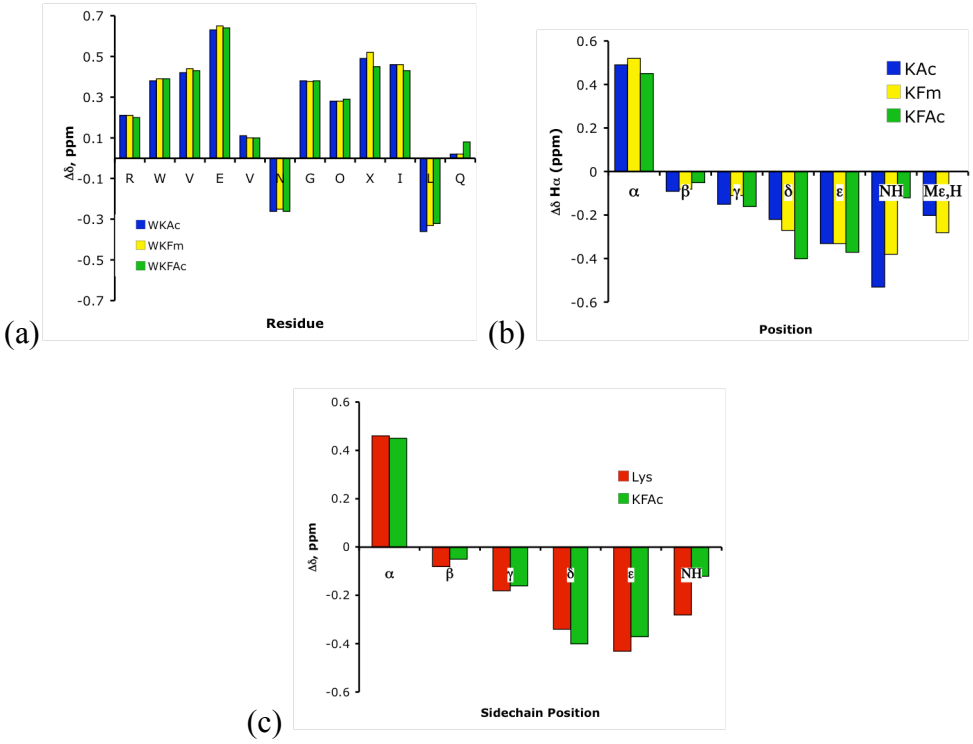

Figure 3.5. (a) **WKAc**, **WKFm**, and **WKFAc** Hα shifts relative to random coil values. Glycine shifts reflect the splitting. (b) KAc, Kfm, and KFAc sidechain upfield proton shifts relative to random coil values. (c) Lys and KFAc sidechain upfield proton shifts relative to random coil. Conditions: 298K, 50 mM NaOAc-d_3 buffer, pH 4.0 (uncorrected), referenced to DSS.

The differences in interaction geometries can be elucidated through a comparison of electrostatic potential maps of the three sidechains (KAc, KFm, and KFAc) as shown in Figure 3.6. Clearly the amide proton is the most polarized site on each of the three sidechain analogs, with the carbonyl carbon on the KFAc analog also highly polarized due to the inductive effects of the fluorines. However, the fluorines in the KFAc analog may present both a steric and electronic barrier to interaction of the amide NH with the indole ring. The CF_3 group in KFAc is the largest of the groups on the carbonyl, thus obscuring the amide proton. Additionally, CF···π interactions have been shown to have weak repulsive character in fluoromethane-benzene model systems, lending some

repulsive electronic character to the KFAc···Trp interaction.[21] Due to long-range inductive effects of the fluorines, the δ and ε positions of the KFAc sidechain are more polarized than the corresponding positions in the KAc and KFm sidechains (Figure 3.6). This, in combination with the electronic and steric repulsion of the trifluoro group, would explain the upfield shifting pattern seen in Figure 3.5c, where the most intense shifts are seen at the δ and ε positions of the KFAc sidechain.

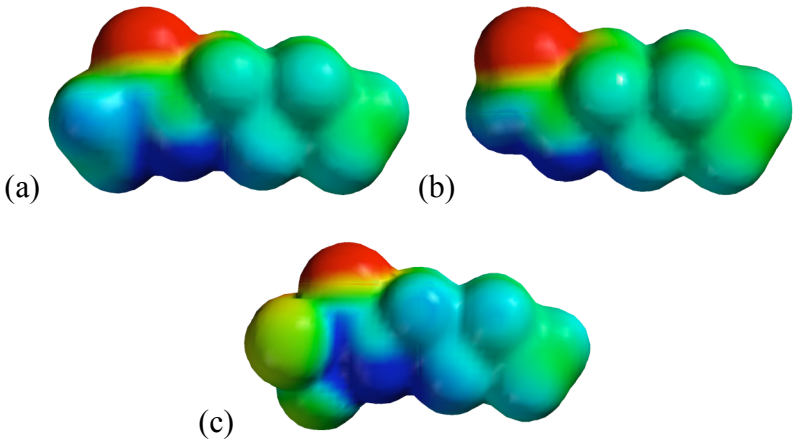

Figure 3.6. Electrostatic potential maps of amino acid sidechains: (a) KAc, (b) KFm, (c) KFAc. Electrostatic potential maps generated with MacSpartan (HF/6-31g*; Isodensity value = 0.02; range = -30 to 30 kcal/mol).

The thermal denaturation for each of the three peptides **WKAc**, **WKFm**, and **WKFAc** were found to be close to or within error (Figure 3.7), resulting in very similar values for ΔH°, ΔS°, and ΔCp° (Table 3.2). Thus, although changing the sterics and electronics of the amide group influences the geometry of the interaction, there is very little effect on its driving force. This suggests a level of control of the interaction geometry that is not often achieved with noncovalent interactions. Moreover, it provides insight into the

[21] Kawahara, S.; Tsuzuki, S.; Uchimaru, T. *J. Phys. Chem. A*. **2004**, *108*, 6744.

subtle factors that may influence the folding of a protein into a single, low energy structure.

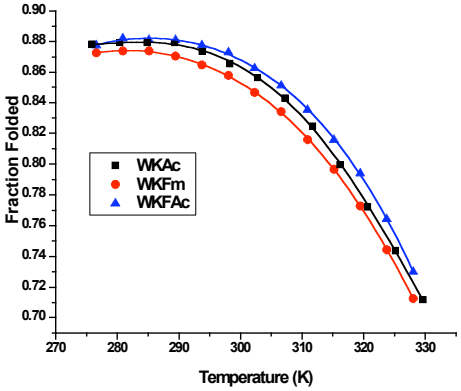

Figure 3.7. Thermal denaturation profiles of **WKAc**, **WKFm**, and **WKFAc** peptides as determined by NMR. The fraction folded was determined from the Gly splitting. Error is ±0.5 K in temperature and ±1% in fraction folded. Conditions: 50 mM NaOAc-d_3 buffer, pD 4.0 (uncorrected).

Table 3.2. Thermodynamic Parameters[a] for Folding at 298 K

Peptide	ΔH° (kcal/mol)	ΔS° (cal/mol K)	ΔC_p° (cal/mol K)
WKAc	-2.91 (0.07)	-6.1 (0.2)	-250 (40)
WKFm	-3.06 (0.03)	-6.7 (0.1)	-195 (30)
WKFAc	-2.68 (0.07)	-5.2 (0.2)	-220 (30)

[a] Determined from the temperature dependence of the Gly chemical shift from 0 to 60 °C. Errors (in parentheses) are determined from the fit.

C. Conclusion.

We have utilized a β-hairpin model system to investigate the nature of an amide-π interaction between Trp and an acylated Lys residue and compared it to the interaction of Trp with the unmodified Lys. Our system demonstrates both the geometric and energetic effects of acylation upon the Trp···Lys interaction. Surprisingly, while the geometry of

the interaction changes upon acylation, the magnitude of the interaction does not decrease, despite the loss of a positive charge. NMR chemical shifts indicate that the amide NH is in close proximity to the face of the aromatic ring, rather than between the ε-CH_2 and Trp that is observed with the unmodified Lys. The change in geometry is likely due to differences in desolvation costs for the Lys and KAc sidechains. The thermodynamics for folding indicate that the amide-π interaction contains significant polar-π character. Acylated lysine analogs KFm and KFAc have further elucidated our understanding of this interaction through manipulation of both electronic and sterics of the Lys sidechain. These changes in sterics and electronics result in subtle changes in the geometery of interaction, indicating the fine tuning that is possible in such noncovalent interactions. These findings provide insight into the specific recognition of acylated lysine that plays a significant biological role in chromatin condensation via the "histone code" as well as the general role of amide-π interactions in protein structure and function.

D. Experimental Section

i. Characterization of Structure. Methods used to indicate the formation of β-hairpin structure include the analysis of Hα shifting relative to random coil, backbone amide shifts relative to random coil, and the identification of cross strand NOEs. The β-hairpin should have backbone hydrogen bonded amides between cross-strand residue pairs Arg-Gln, Val-Ile, and Val-Orn in all hairpin peptides. The presence of these hydrogen bonds is readily demonstrated by downfield shifting of the amide hydrogens in these positions relative to random coil. As seen below, both peptides exhibit significant downfield shifting at key positions along the strand. As expected for β-hairpins, the termini are frayed and show little or no amide shifting. The Asn amide shows significant downfield shifting as expected for a Type I' turn.

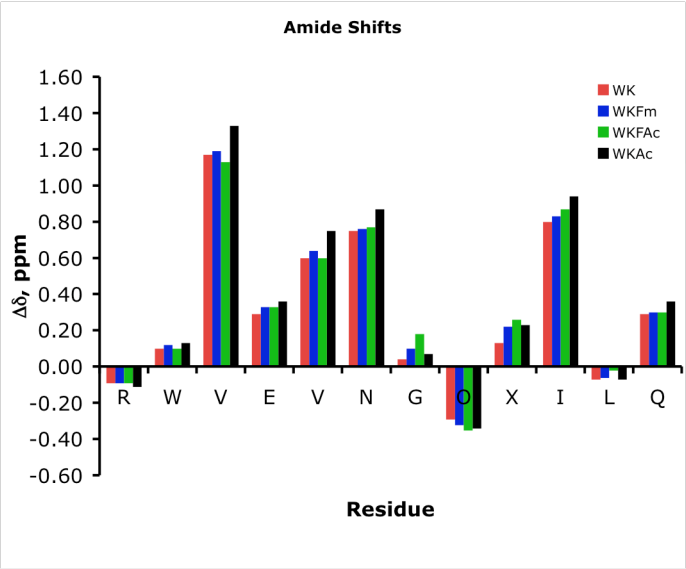

Figure 3.8. Backbone amide shifts for selected β-hairpin peptides.

Furthermore, analysis of the H_α fraction folded plot for selected peptides **WK**, **WKMe3**, **WKAc**, **WKFam**, and **WKTFAc**, as calculated by equation [**11],** shows cooperative folding along the entire strand, with the exception of fraying at the termini.

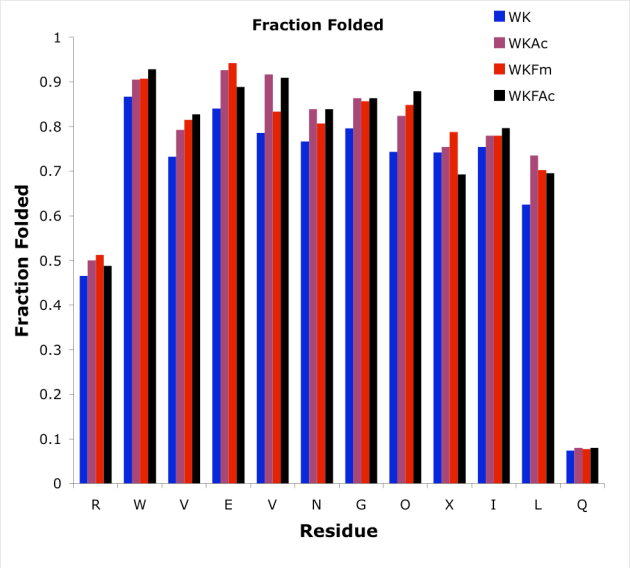

Figure 3.9. Fraction folded data for selected β-hairpin peptides.

Finally, the identification of numerous cross-strand NOEs in all hairpin peptides indicates that all peptides have β-hairpin structure.

Figure 3.10. WKAc Cross-strand NOEs:

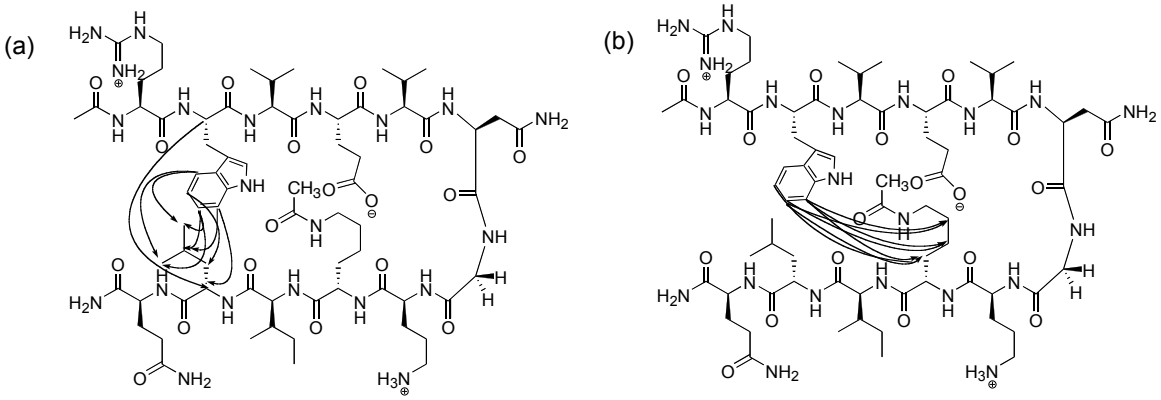

Figure 3.11. WKAcCyc Cross-strand NOEs:

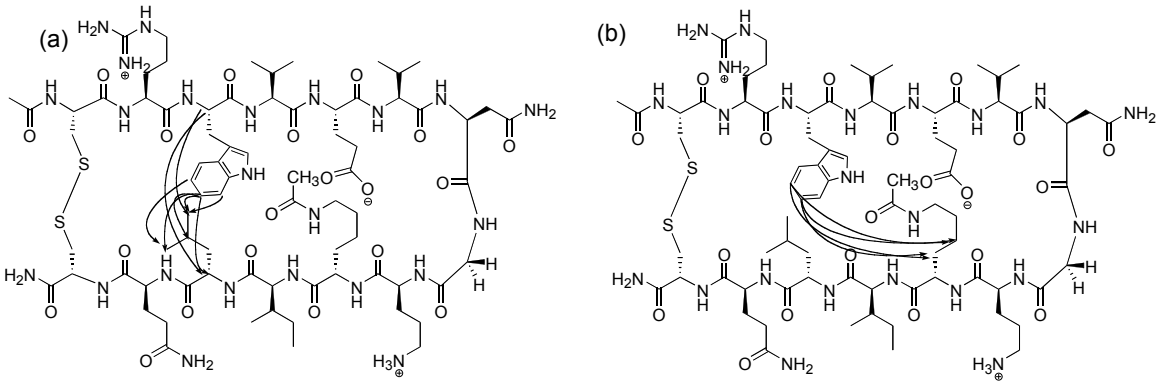

Figure 3.12. WKFmCyc Cross-strand NOEs:

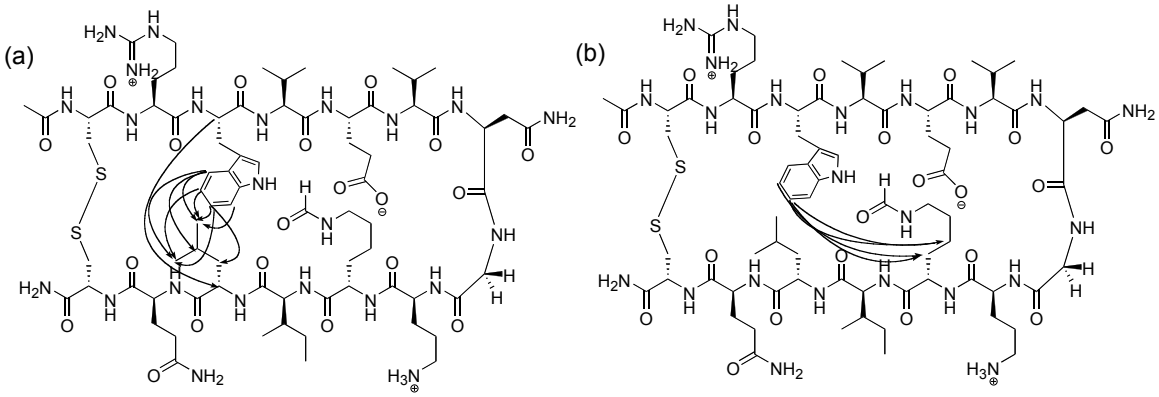

Figure 3.13. WKFAcCyc Cross-strand NOEs:

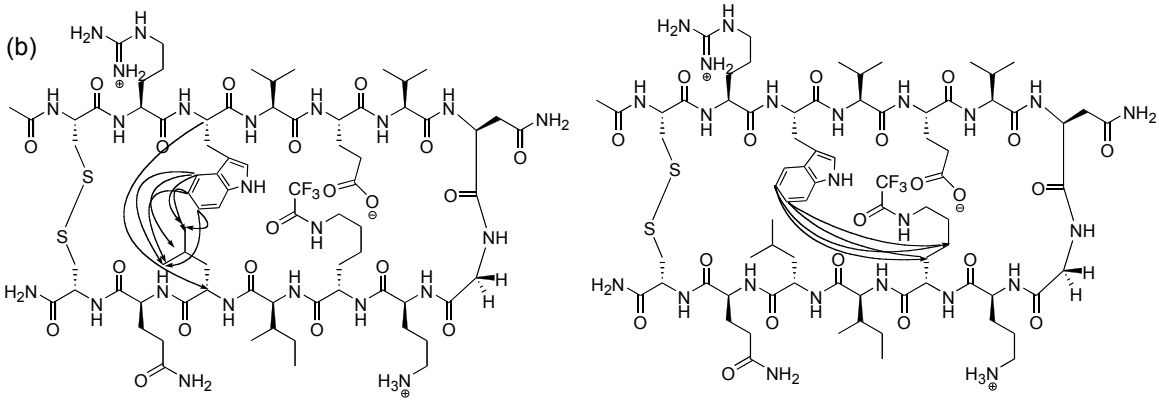

Tables 3.3a-c. NOEs observed in peptides **WKFAc**, **WKFAcCyc**, **WKFmCyc** at 298 K (S=Strong; M=Medium; W=Weak)

Table 3.3a. Peptide **WKFAc:**
Ac-RWVEVNGO(KFAc)ILQ-NH

Residue	**Proton**	**Residue**	**Proton**	**Intensity**
Trp 2	Ar 4	Leu 11	δ	W
Trp 2	Ar 7	Leu 11	δ	W
Trp 2	Ar 7	KFAc 9	β	S
Trp 2	Ar 7	KFAc 9	γ	M
Trp 2	Ar 7	KFAc 9	δ	M
Trp 2	Ar 7	Ile 10	α	M
Trp 2	Ar 7	Leu 11	α	M
Trp 2	Ar 7	Arg 1	α	M
Trp 2	Ar 7	Ile 10	α	W
Trp 2	Ar 7	Leu 11	α	M
Trp 2	Ar 6	KFAc 9	β	M
Trp 2	Ar 6	KFAc 9	γ	W
Trp 2	Ar 6	KFAc 9	δ	W
Trp 2	Ar 6	Leu 11	δ	W
Trp 2	Ar 5	KFAc 9	β	M
Trp 2	Ar 5	Ile 10	α	M
Trp 2	Ar 5	Leu 11	α	W
Trp 2	Ar 5	Leu 11	β	W
Trp 2	Ar 5	Leu 11	γ	M
Trp 2	α	Leu 11	α	S

Table 3.3b. Peptide **WKFAcCyclic:**
Ac-CRWVEVNGO(KFAc)ILQC-NH_2

Residue	**Proton**	**Residue**	**Proton**	**Intensity**
Trp 3	Ar 4	Leu 12	δ	W
Trp 3	Ar 4	Leu 12	γ	W
Trp 3	Ar 7	Leu 12	δ	W
Trp 3	Ar 6	KFAc10	β	S
Trp 3	Ar 6	KFAc10	γ	S
Trp 3	Ar 6	Leu 12	α	M
Trp 3	Ar 6	Leu 12	δ	M
Trp 3	Ar 6	Leu 12	γ	W
Trp 3	Ar 5	KFAc 10	β	W
Trp 3	Ar 5	KFAc 10	γ	W
Trp 3	Ar 5	Leu 12	δ	M
Trp 3	α	Leu 12	α	S
Trp 3	α	Leu 12	δ	S

Trp 3	NH	Arg 2	α	M
Arg 2	NH	Cys 1	α	M
Gln 13	NH	Leu 12	α	M
Ile 11	NH	KFAc 10	α	M

Table 3.3c. Peptide **WKFmCyclic:**
Ac-CRWVEVNGO(KFm)ILQC-NH_2

Residue	**Proton**	**Residue**	**Proton**	**Intensity**
Trp 3	Ar 4	Leu 12	δ	W
Trp 3	Ar 4	Leu 12	γ	W
Trp 3	Ar 7	Leu 12	δ	M
Trp 3	Ar 6	KFm 10	β	S
Trp 3	Ar 6	KFm 10	γ	S
Trp 3	Ar 6	Leu 12	δ	M
Trp 3	Ar 6	Leu 12	γ	W
Trp 3	Ar 6	Leu 12	β	W
Trp 3	Ar 5	Ile 11	α	M
Trp 3	Ar 5	Leu 12	α	M
Trp 3	Ar 5	KFm 10	β	M
Trp 3	Ar 5	KFm 10	γ	M
Trp 3	Ar 5	Leu 12	δ	M
Trp 3	α	Leu 12	α	S
Trp 3	α	Leu 12	δ	S
Glu 5	α	KFm 10	γ	W

Thermodynamic Analysis

Peptides were analyzed assuming a two-state system. The equilibrium constant was determined from the fraction folded (f) by K = f/(1-f). The free energy was then calculated from $\Delta G° = - RT\ln K$. In order to determine the thermodynamic parameters, $\Delta H°$, $\Delta S°$, and $\Delta Cp°$, the temperature dependence of the Gly chemical shift difference was fit to the following equation:[22]

$$\text{Fraction Folded} = [\exp(x/RT)]/[1 + \exp(x/RT)], \text{ where}$$

$$x = T(\Delta S°_{298} + a \ln(T/298) + b (T - 298) - (c/2) (1/T^2 - 1/298^2)) - (\Delta H°_{298} + a (T - 298) + (b/2) (T^2 - 298^2) - c (1/T - 1/298))].$$

[22] Maynard, A.J. Sharman, G. J. and Searle, M. S. *J. Am. Chem. Soc.* **1998**, *120*, 1996-2007.

Table 3.4. Temperature Dependence of the Fraction Folded from Glycine Chemical Shift Data for the peptides in this study:

WK:		**WKAc:**		**WKFm:**	
Temp (K)	fraction folded	Temp (K)	fraction folded	Temp (K)	fraction folded
276	0.806	276	0.878	277	0.872
281	0.806	280	0.879	281	0.874
285	0.804	285	0.879	285	0.874
289	0.801	289	0.879	290	0.87
294	0.793	294	0.874	294	0.865
298	0.783	298	0.866	298	0.858
302	0.773	303	0.856	302	0.847
307	0.754	307	0.843	307	0.834
311	0.734	312	0.825	311	0.816
316	0.709	316	0.800	315	0.797
320	0.680	321	0.772	320	0.773
324	0.650	325	0.744	324	0.744
329	0.615	330	0.712	328	0.713
		334	0.672		
		339	0.633		
		343	0.595		
		348	0.552		

WKFAc:

Temp (K)	fraction folded
277	0.878
281	0.882
285	0.881
290	0.881
294	0.878
298	0.873
302	0.863
307	0.851
311	0.835
315	0.816
320	0.794
324	0.764
328	0.730

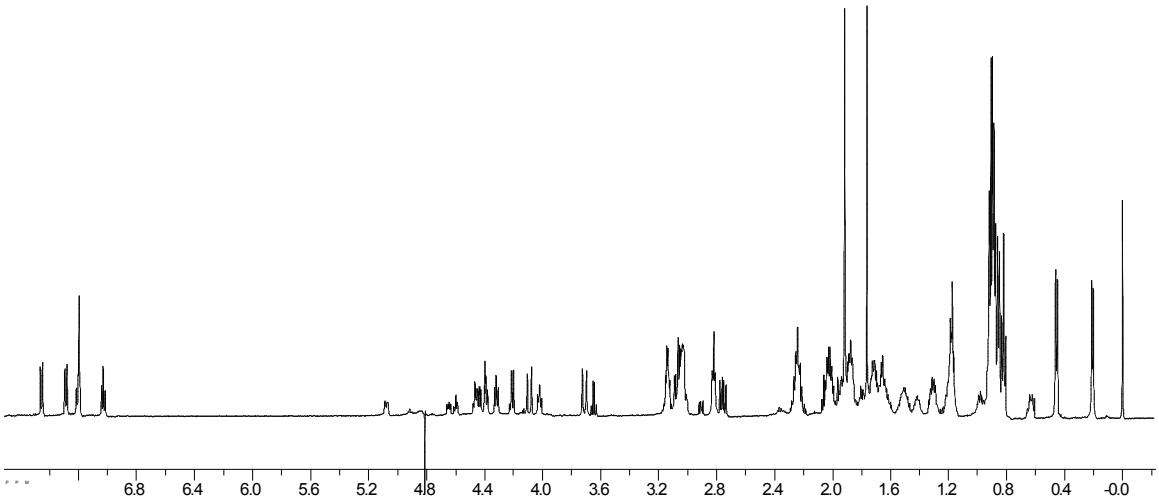

Figure 3.14. ^{1}H NMR of Peptide **WKAc**: Ac-Arg-Trp-Val-Glu-Val-Asn-Gly-Orn-Lys(Ac)-Ile-Leu-Gln-NH2

Table 3.5. Proton Chemical Shift Assignments for Peptide **WKAc**.

	α	β	γ	δ	ε	Amide	Amine
R	4.39	1.71	1.51,1.63	3.14		8.03	7.13,6.65
W	5.08	3.07,3.03	7.46,7.29	7.195,7.20	7.03	8.32	10.13
V	4.44	2.02	0.88			9.08	
E	4.92	2.01,1.89	2.23			8.56	
V	4.21	1.95	0.91			8.97	
N	4.44	3.07,2.75				9.47	
G	4.09,3.71					8.64	
O	4.65	1.80	1.72	3.04		7.79	7.65
K(Ac)	4.76	1.65	1.18	1.29	2.82 Ac=1.76	8.47	Sidechain amide= 7.40
I	4.59	1.88	1.42,1.19,0.89	0.89		9.18	
L	4.02	1.31	0.98,0.64	0.46,0.21		8.26	
Q	4.32	2.03,1.85	2.24			8.69	

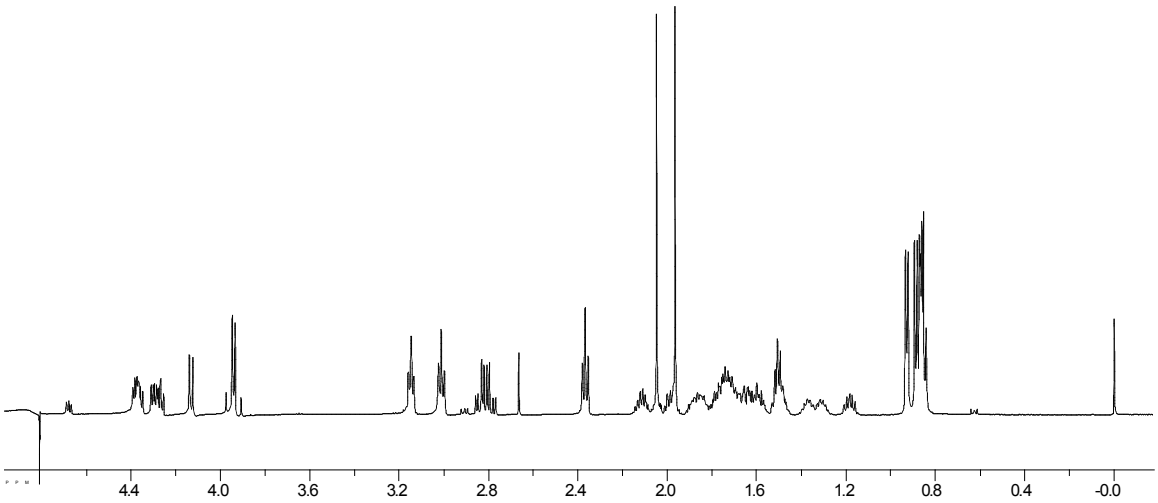

Figure 3.15. ^{1}H NMR of Peptide **KAc7**: Ac-Asn-Gly-Orn- Lys(Ac)-Ile-Leu-Gln-NH2

Table 3.6. Proton Chemical Shift Assignments for Peptide **KAc7.**

	α	β	γ	δ	ε	Amide	Amine
N	4.69	2.81				8.44	
G	3.94					8.57	
O	4.37	1.70	1.70	3.01		8.13	7.68
K(Ac)	4.27	1.74	1.36,1.30	1.51	3.15 Ac=1.96	8.24	Sidechain amide= 7.93
I	4.13	1.84	1.49,1.19, 0.89	0.89		8.24	
L	4.38	1.88	1.62,1.59	0.92,0.85		8.33	
Q	4.30	2.09,1.98	2.37			8.33	

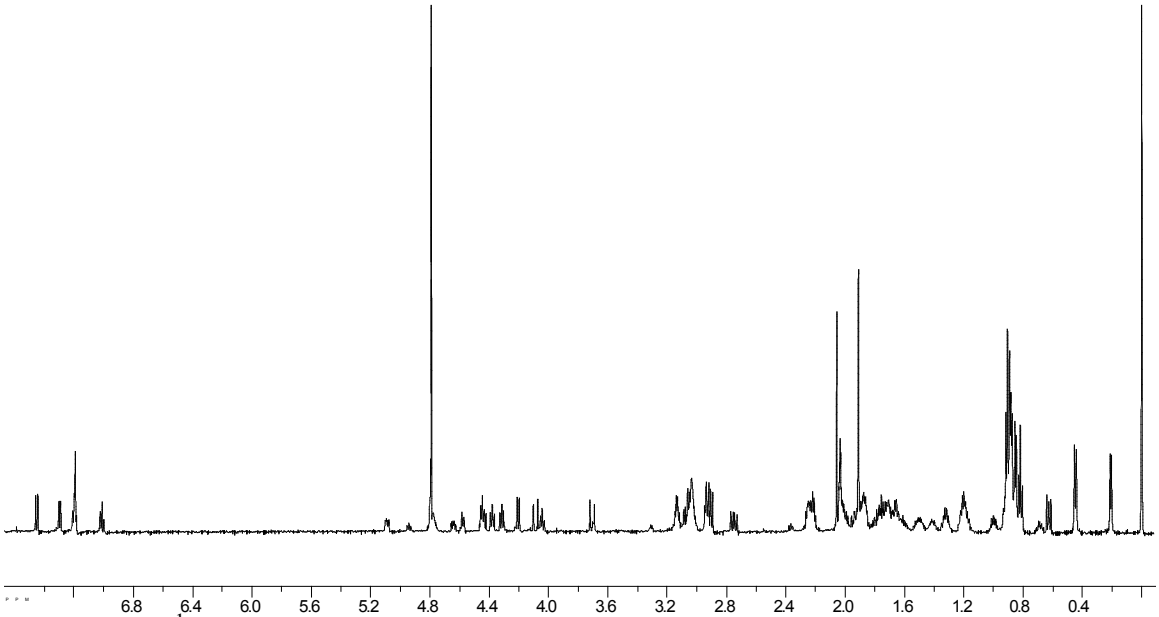

Figure 3.16. ^{1}H NMR of Peptide **WKFAc**: Ac-Arg-Trp-Val-Glu-Val-Asn-Gly-Orn-Lys(TFAc)-Ile-Leu-Gln-NH2

Table 3.7. Proton Chemical Shift Assignments for Peptide **WKFAc.**

	α	β	γ	δ	ε	Amide	Amine
R	4.38	1.66	1.55	3.13		8.05	7.12,6.64
W	5.09	3.06				8.29	10.15
V	4.45	2.02	0.86			8.88	
E	4.93	1.97	2.21			8.53	
V	4.20	1.92	0.90			8.82	
N	4.44	3.08,2.75				9.37	
G	4.08,3.71					8.73	
O	4.64	1.83	1.71	3.03		7.82	7.66
K(FAc)	4.73	1.66	1.22	1.22	2.94	8.50	Sidechain amide= 9.13
I	4.57	1.87	1.19,1.00,0.87	0.87		9.10	
L	4.06	1.32	0.99,0.69	0.46,0.22		8.31	
Q	4.31	1.89	2.24			8.63	

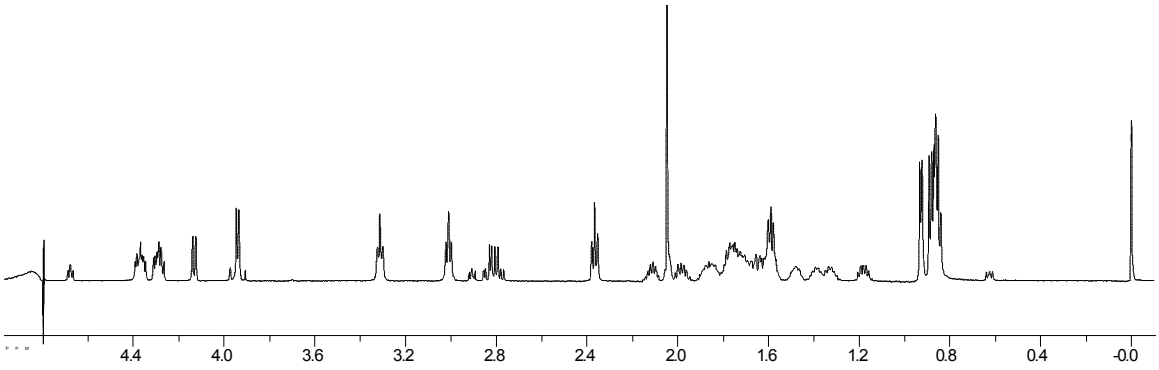

Figure 3.17. ^{1}H NMR of Peptide **KFAc7**: Ac-Asn-Gly-Orn- Lys(TFAc)-Ile-Leu-Gln-NH2

Table 3.8. Proton Chemical Shift Assignments for Peptide **KFAc7.**

	α	β	γ	δ	ε	Amide	Amine
N	4.68	2.81				8.43	
G	3.94						
O	4.35	1.80	1.73	3.02		8,17	
K(FAc)	4.28	1.71	1.38	1.62	3.31	8.24	Sidechain amide= 9.25
I	4.14	1.85	1.52,1.24, 0.88	0.88		8.23	
L	4.38	1.66	1.28	0.91		8.33	
Q	4.29	2.00	2.37			8.33	

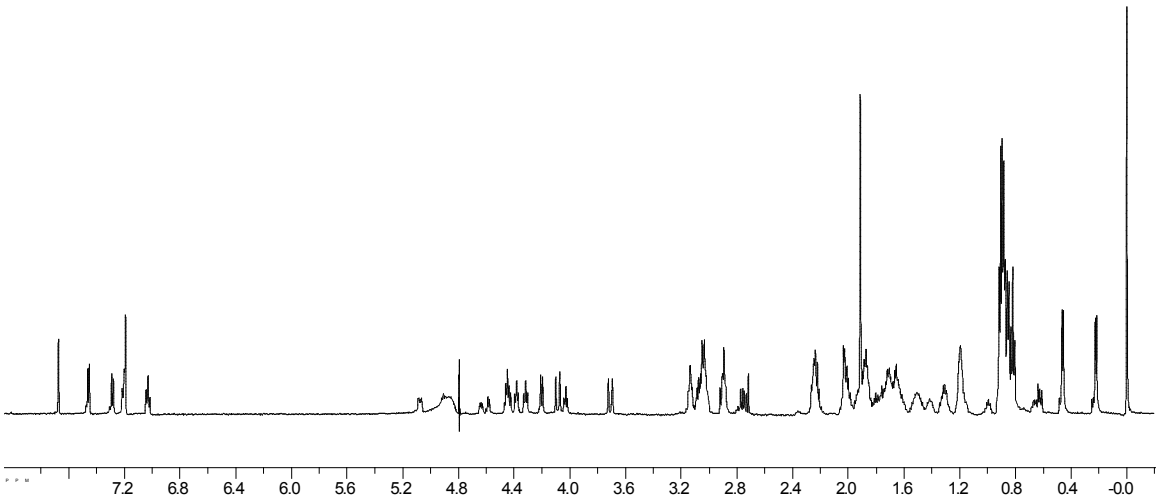

Figure 3.18. ^{1}H NMR of Peptide **WKFam**: Ac-Arg-Trp-Val-Glu-Val-Asn-Gly-Orn-Lys(Fam)-Ile-Leu-Gln-NH2

Table 3.9. Proton Chemical Shift Assignments for Peptide **WKFAm.**

	α	β	γ	δ	ε	Amide	Amine
R	4.39	1.68	1.52	3.13		8.05	7.12
W	5.09	3.06,2.75	7.46,7.29	7.20,7.19	7.03	8.31	10.15
V	4.46	2.01	0.88			8.94	
E	4.94	1.96	2.23			8.53	
V	4.20	1.95	0.91			8.86	
N	4.45	3.08,2.76				9.36	
G	4.09,3.72					8.66	
O	4.64	1.84	1.75	3.05		7.81	7.63
K(Fam)	4.79	1.67	1.25	1.25	2.89	8.46 $_{\text{aldehyde}}$=7.72	Sidechain amide= 7.60
I	4.59	1.88	1.47,1.22,0.88	0.88		9.07	
L	4.04	1.32	1.01,0.67	0.56,0.23		8.28	
Q	4.32	1.90	2.26			8.64	

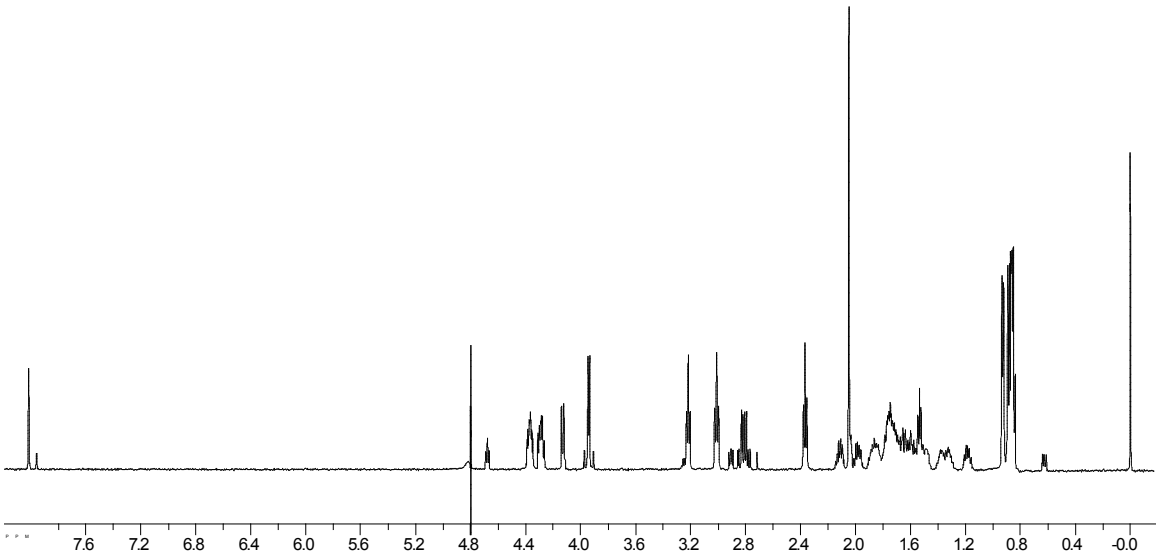

Figure 3.19. ^{1}H NMR of Peptide **KFam7**: Ac-Asn-Gly-Orn-Lys(Fam)-Ile-Leu-Gln-NH2

Table 3.10. Proton Chemical Shift Assignments for Peptide **KFAm7.**

	α	β	γ	δ	ε	Amide	Amine
N	4.67	2.80				8.43	
G	3.94					8.56	
O	4.36	1.79	1.65	3.01		8.13	7.61
K(Fam)	4.27	1.75	1.36	1.52	3.22	8.24 $_{aldehyde}$=8.00	Sidechain amide= 7.98
I	4.13	1.84	1.49,1.17, 0.87	0.87		8.24	
L	4.37	1.65	0.89	0.89		8.34	
Q	4.30	1.99	2.36			8.34	

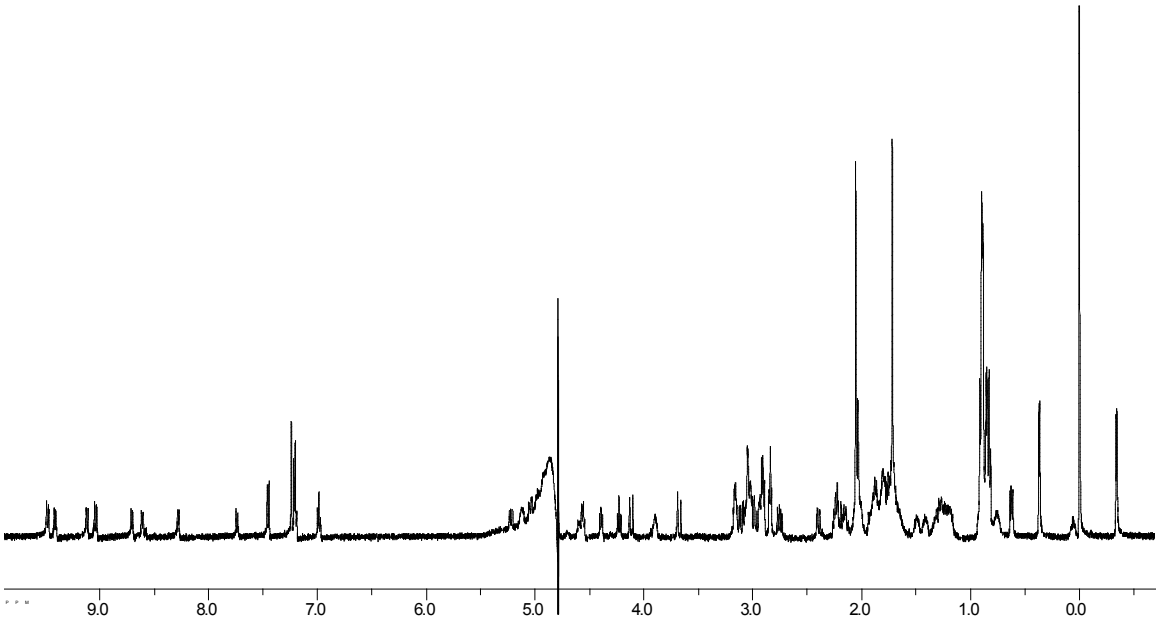

Figure 3.20. ^{1}H NMR of Peptide **WKAcCyc**: Ac-Cys-Arg-Trp-Val-Glu-Val-Asn-Gly-Orn-Lys(Ac)-Ile-Leu-Gln-Cys-NH2

Table 3.11. Proton Chemical Shift Assignments for Peptide **WKAcCyc.**

	α	β	γ	δ	ε	Amide	Amine
C	5.22	2.98,2.39					
R	4.60	1.79	1.49	3.16		8.70	
W	5.12	3.03				8.59	
V	4.55	1.82	0.86			9.48	
E	4.97	2.00	2.21			8.59	
V	4.22	1.91	0.895			9.10	
N	4.39	3.09,2.75					
G	4.11,3.67						
O	4.71	1.80	1.75	3.04		7.73	
K(Ac)	4.92	1.69	1.27	1.30	2.83 Ac= 1.72		
I	4.72	1.85	1.42,1.17,0.88	0.88		9.39	
L	3.89	1.29	0.75,0.36	0.06, -0.34		8.26	
Q	4.55	2.06	2.17			9.03	
C	5.04	2.90					

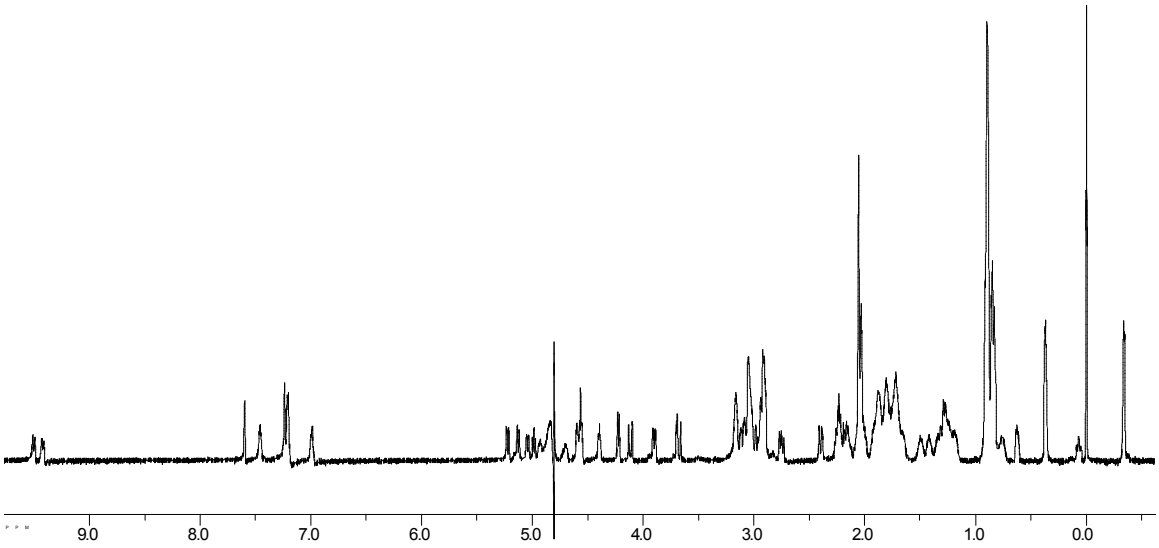

Figure 3.21. ^{1}H NMR of Peptide **WKFamCyc**: Ac-Cys-Arg-Trp-Val-Glu-Val-Asn-Gly-Orn-Lys(Fam)-Ile-Leu-Gln-Cys-NH2

Table 3.12. Proton Chemical Shift Assignments for Peptide **WKFamCyc.**

	α	β	γ	δ	ε	Amide	Amine
C	5.22	2.98,2.40					
R	4.59	1.79	1.66,1.50	3.16			
W	5.13	3.05,2.91					
V	4.56	2.06	0.87			9.50	
E	4.98	2.01,1.88	2.21				
V	4.22	1.91	0.90				
N	4.39	3.09,2.75					
G	4.11,3.67						
O	4.69	1.84	1.76	3.04			
K(Fam)	4.93	1.70	1.26	1.26	2.90	Aldehyde=7.61	
I	4.72	1.87	1.42,1.18,0.89	0.89		9.41	
L	3.90	1.29	0.76,0.36	0.07, -0.35			
Q	4.56	1.82	2.16				
C	5.04	3.04,2.91					

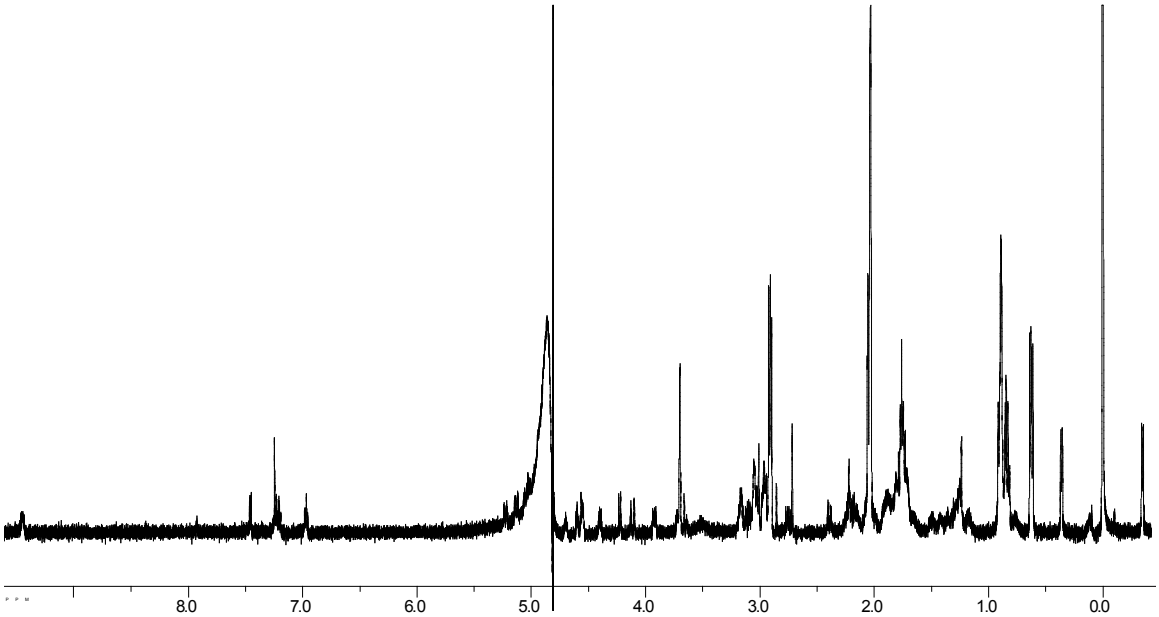

Figure 3.22. ^{1}H NMR of Peptide **WKFAcCyc**: Ac-Cys-Arg-Trp-Val-Glu-Val-Asn-Gly-Orn-Lys(TFac)-Ile-Leu-Gln-Cys-NH2

Table 3.13. Proton Chemical Shift Assignments for Peptide **WKFacCyc.**

	α	β	γ	δ	ε	Amide	Amine
C	5.21	2.97,2.38					
R	4.59	1.79	1.48,1.64	3.16			
W	5.12	3.04,2.99					
V	4.54	2.03	0.86			9.43	
E	5.01	1.99	2.18				
V	4.21	1.90	0.89				
N	4.39	3.10,2.74					
G	4.11,3.66						
O	4.68	1.83	1.77	3.04			
K(TFAc)	4.93	1.70	1.25	1.25	2.95		
I	4.68	1.86	1.41,1.16,0.88	0.88		9.43	
L	3.92	1.30	0.75,0.35	0.11, -0.35			
Q	4.54	1.81	2.16				
C	5.04	3.02,2.91					

Figure 3.23. ^{1}H NMR of Peptide **VKAc**:

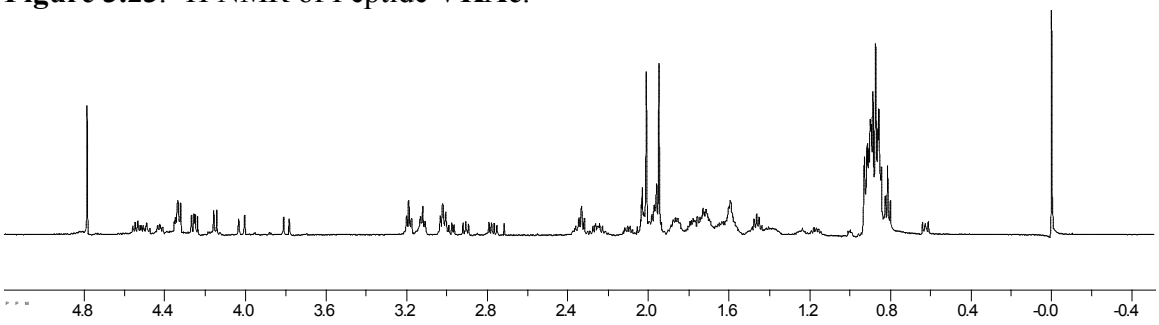

Figure 3.24. ^{1}H NMR of Peptide **VKAcCyc**:

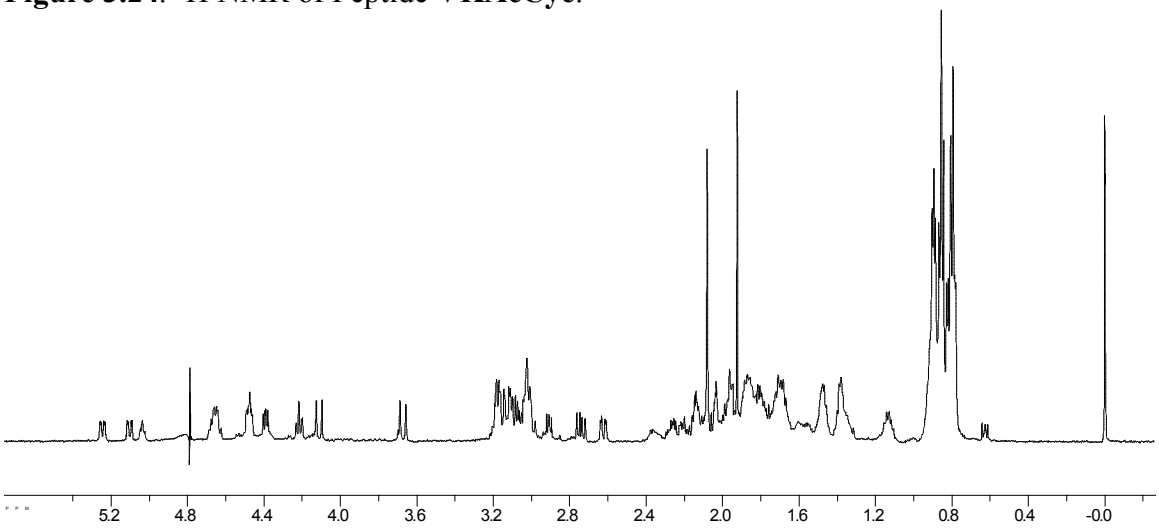

Figure 3.25. ^{1}H NMR of Peptide **VKFac**:

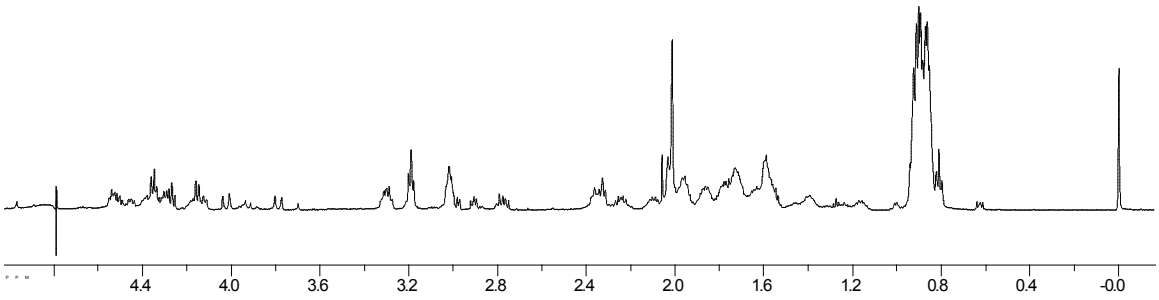

Figure 3.26. ^{1}H NMR of Peptide **VKFacCyc**:

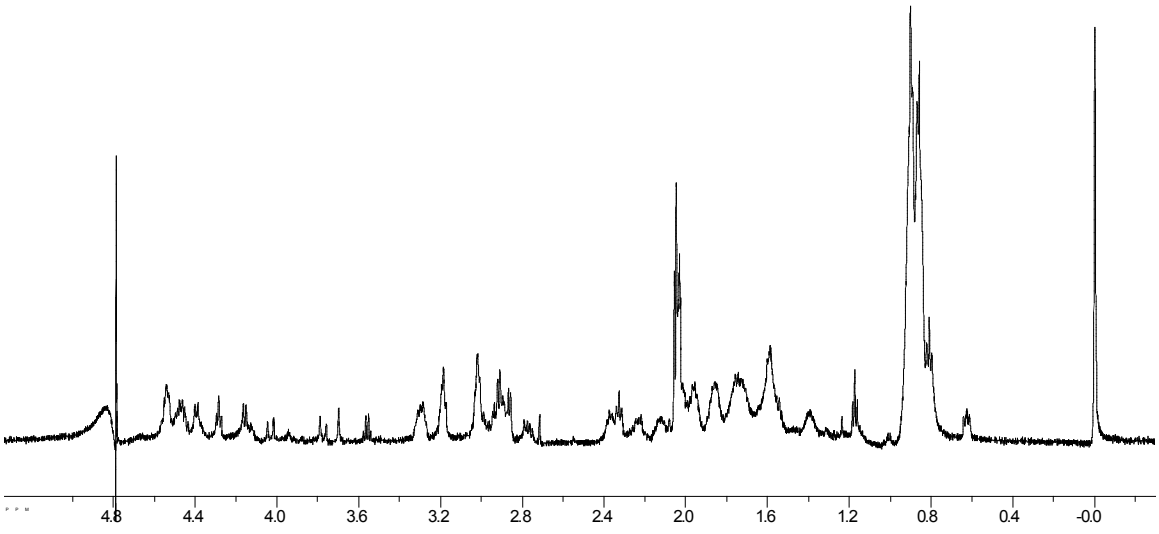

CHAPTER IV

ALKYL-π INTERACTIONS

(Reproduced, in part, with permission from Hughes, R.M.; Wiggins, Kimberly R.; Khorasanizadeh, Sepideh; Waters, M. L. *submitted for publication*.)

A. Tert-butyl norleucine and an alkyl-π interaction.

i. Background and significance.

With rapid advancements in genomics, epigenetics has become the next major challenge in understanding how genetic information is controlled.[1] It is becoming clear that post-translational modifications of proteins are a key component in controlling gene expression. These modifications include a number of subtle structural changes, including Lys and Arg methylation, Lys acylation, and Ser/Thr/Tyr phosphorylation, which act as chemical switches to induce or repress protein-protein interactions. Among all histone modifications, lysine methylation is especially important for chromatin function due to its stability and direct contribution to heritable patterns of gene expression.[2] To understand how such modest structural modifications can control biomolecular recognition events, it is critical to understand the underlying noncovalent interactions involved.

---

[1] Khorasanizadeh, S. *CELL* **116,** 259-272.

[2] Martin, C.; Zhang, Y. *Nat Rev Mol Cell Biol* **2005**, *6,* 838-49.

Methylation of Lys induces a protein-protein interaction through the binding of methyl lysine (KMe_n, n = 1-3) in an aromatic cage. This interaction was first described for the binding of methylated Histone 3 (H3) tail to the HP1 chromodomain (Figure 4.1).[3],[4] HP1 and methylated H3 interact specifically whether lysine 9 is mono, di or trimethylated. However, the binding is most effective when methyllysine is trimethylated.[5] In addition, more recent findings have shown that phosphorylation of serine 10 prevents interaction of HP1 with methylated H3.[6] Therefore, a binary switch mechanism has been proposed for the recognition of methllysine containing peptides by chromodomains. Interestingly, binding of a methylated lysine in an aromatic cage is not exclusive to chromodomains. PHD fingers and Tudor domains also assemble three aromatic residues around methyllysine of the H3 tail.[7],[8]

Recognition of methylated lysine by an aromatic cage appears to be mediated by cation-π interactions between the methylated ammonium group and the side chains of three aromatic residues. The cation-π interaction is defined by the attractive interaction between a positively charged moiety (simple cations, ammonium groups, etc.) and the

---

[3] Jacobs, S. A.; Khorasanizadeh, S. *Science* **2002**, *295,* 2080-2083.

[4] Nielsen, P. R.; Nietlispach, D.; Mott, H. R.; Callaghan, J.; Bannister, A.; Kouzarides, T.; Murzin, A. G.; Murzina, N. V.; Laue, E. D. *Nature* **2002**, *416,* 103-7.

[5] Fischle, W.; Wang, Y. M.; Jacobs, S. A.; Kim, Y. C.; Allis, C. D.; Khorasanizadeh, S. *Genes & Development* **2003**, *17,* 1870-1881.

[6] Eissenberg, J. C.; Elgin, S. C. R. *Nature* **2005**, *438,* 1090-1091.

[7] Mellor, J. *Cell* **2006**, *126***,** 22-4.

[8] Sims, R. J., III; Reinberg, D. *Genes Dev* **2006**, *20,* 2779-86.

quadrupole moment of an aromatic ring.[9] The magnitude of the cation-π interaction in proteins is dependent on a number of factors, including the electronic density of the aromatic ring (Phe vs Trp, for example), the distribution of positive charge across the cationic moiety, and the degree of solvent exposure of the interaction, as well as the contribution of other forces, such as van der Waals interactions and the hydrophobic effect.[9] Numerous examples of functional cation-π interactions exist in structural biology, and they have been demonstrated to be important to protein structure and stability and the functioning of enzymes and ion-channels.[9]

Due to the potential importance of cation-π interactions in the recognition of the post-translationally modified amino acids KMe_n (n = 1-3) and the still growing body of theoretical and experimental knowledge concerning the various energetic components of the interaction, a number of questions remain that need to be addressed experimentally regarding the interplay between electrostatics, van der Waals interactions, and the hydrophobic effect.[10,11,12,13,14,15,16] Moreover, in the context of chromodomain, it is not

---

[9] Ma, J. C.; Dougherty, D. A. *Chemical Reviews* **1997**, *97,* 1303-1324.

[10] Eriksson, M. A. L.; Morgantini, P. Y.; Kollman, P. A. *J. Phys. Chem. B* **1999**, *103,* 4474-4480.

[11] Hunter, C. A.; Low, C. M. R.; Rotger, C.; Vinter, J. G.; Zonta, C. *Proc. Nat. Acad. Sci. USA* **2002**, *99***,** 4873-4876.

[12] Mo, Y. R.; Subramanian, G.; Gao, J. L.; Ferguson, D. M. *J. Am. Chem. Soc.* **2002**, *124*, 4832-4837.

[13] Ruan, C. H.; Rodgers, M. T. *J. Am. Chem. Soc.* **2004**, *126,* 14600-14610.

[14] Costanzo, F.; Della Valle, R. G.; Barone, V. *J. Phys. Chem. B* **2005**, *109,* 23016-23023.

[15] Reddy, A. S.; Sastry, G. N. *J. Phys. Chem. A* **2005**, *109***,** 8893-8903.

clear to what degree a charge-quadrupole interaction imbues specificity to a biologically significant ligand-receptor interaction or if the interaction is primarily due to hydrophobic and/or van der Waals interactions between the methyl groups and the aromatic pocket. To this end, we have synthesized the neutral analog of KMe3, tert-butyl norleucine (tBuNle; 2-amino-7,7-dimethyloctanoic acid), and investigated its interaction with Trp in a β-hairpin model system and then compared these results to in vitro binding assays with the HP1 chromodomain. This hairpin model system has been previously used to investigate the cation-π interaction between KMe3 and Trp.[17] In this model system, we find striking contrasts between the behaviour of the two sidechains with Trp that provide insight into the role of hydrophobicity and the importance of the charge-quadrupole component of the Trp-KMe3 interaction. Furthermore, in vitro binding studies of the neutral tBuNle analog of the H3 tail peptide demonstrate that the positive charge is *required* to give a selective, high affinity interaction between the histone tail and the HP1 chromodomain protein.

---

[16] Xu, Y. C.; Shen, J. H.; Zhu, W. L.; Luo, X. M.; Chen, K. X.; Jiang, H. L. *J. Phys. Chem. B* **2005**, *109*, 5945-5949.

[17] Hughes, R. M.; Waters, M. L. *J. Am. Chem. Soc.* **2005**, *127*, 6518 - 6519.

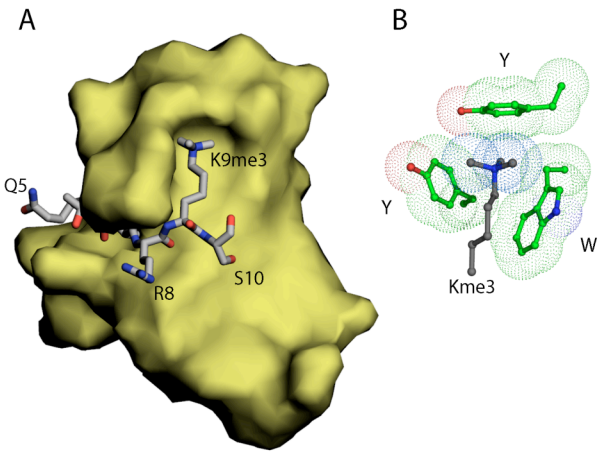

Figure 4.1. A) crystal structure of the HP1 chromodomain (yellow surface) in complex with lysine 9-trimethylated histone H3 tail residues 5 through 10 (grey stick). B) Aromatic cage (green) formed by two tryrosines and one tryptophan captures the methyllysine (grey).

ii. Results and Discussion.

In our previous study of peptides **WK** and **WKMe3** (Figure 4.2), we found that methylation of Lys enhanced its interaction with Trp significantly, but that the driving force became more hydrophobic in nature, and the enthalpic component, attributed to the charge-quadrupole interaction, decreased relative to unmodified Lys.[17] This leads to the question as to whether the positive charge is indeed necessary for interaction with an aromatic residue or an aromatic pocket in aqueous solution, or whether hydrophobic and van der Waals interactions alone will suffice. We chose to investigate the interaction of Trp with tBuNle because the size and shape of KMe3 and tBuNle are virtually identical (see Figure 4.3), as are the polarizabilities (11.3 vs 12.0 $Å^3$) (see Experimental Section), but the charge, and hence ability to participate in a cation-π interaction, differs significantly. Hence, if hydrophobicity and van der Waals interactions are the primary

driving force for interaction with Trp, the two sidechains should interact in the same manner with Trp, but not if the charge-quadrupole component is important.

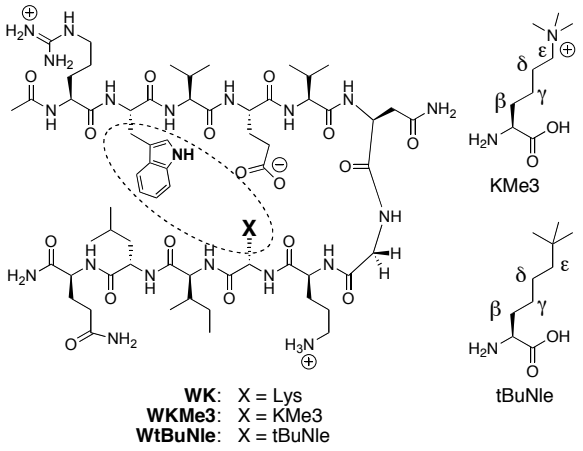

Figure 4.2. β-Hairpin peptide containing KMe3 or tBuNle. Peptides are referred to by the residues at positions 2 (Trp) and 9 (X) in the text.

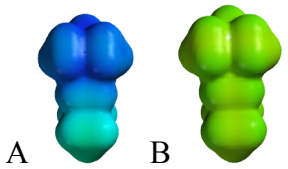

Figure 4.3. Electrostatic potential maps of the (a) KMe3 sidechain and (b) tBuNle sidechain. Electrostatic potential maps were generated with MacSpartan: HF/6-31g*; Isodensity value = 0.02; range = -75 (red, electron rich) to +125 kcal/mol (blue, electron poor).

The unnatural amino acid, tBuNle, was synthesized from pseudo-ephedrine glycinamide and 1-bromo-5,5-dimethylhexane[1, 2, 18] via the method of Myers, et al.[19] and incorporated into the peptide via standard solid phase peptide synthesis to give the

[18] Rybczynski, P. J.; Zeck, R. E.; Dudash, J., Jr.; Combs, D. W.; Burris, T. P.; Yang, M.; Osborne, M. C.; Chen, X.; Demarest, K. T. *J. Med. Chem.* **2004**, *47*, 196-209.

[19] Myers, A. G.; Schnider, P.; Kwon, S.; Kung, D. W. *J. Org. Chem.* **1999**, *64,* 3322-3327.

peptide **WtBuNle** (see Experimental Section). The sidechain-sidechain interaction, as well as its impact on hairpin stability, was investigated by NMR and compared to **WKMe3**. The interaction between residue 9 (X) and Trp can be characterized by the extent of upfield shifting of the X sidechain (Figure 4.4). Greater upfield shifting indicates closer proximity to the face of the Trp indole ring. We have previously shown that KMe3 exhibits enhanced interaction with Trp relative to the unmethylated Lys, particularly at the ε-CH_2 and the methyl positions (Figure 4.4a). Surprisingly, tBuNle exhibits little upfield shifting; the ε-CH_2 and methyl groups are less shifted even than unmodified Lys. This indicates that tBuNle has no preference for interaction with the face of Trp, despite its large hydrophobic surface area. This clearly demonstrates the importance of the electrostatic component of the cation-π interaction. Without polarization of the methyl groups, there is no specific interaction between the sidechain and the aromatic ring. This is similar to the preference observed for binding of a trimethylammonium group with Dougherty's cyclic aromatic host relative to a *tert*-butyl group in an early study of cation–π interactions in water.[20] Despite this lack of interaction between Trp and tBuNle, **WtBuNle** is as well folded as **WKMe3**, as determined from the similarity of the downfield shifting of the Hα protons of the two peptides relative to random coil values (Figure 4.4b). Quantification of the fraction folded indicates that **WtBuNle** is a very well folded hairpin (96±1% based on Gly splitting; 90±7% based on Hα chemical shifts), as is **WKMe3** (93±1% based on Gly splitting; 91±15% based on Hα

[20] Petti, M. A.; Shepodd, T. J.; Barrans, J. R. E.; Dougherty, D. A. *J. Am. Chem. Soc.* **1998**, *110,* 6825 - 6840.

chemical shifts).[21] This indicates that the tBuNle provides stability to the hairpin through means other than specific interaction with the face of the indole ring of Trp. This is likely due to non-specific hydrophobic interactions between tBuNle and other sites on the face of the β-hairpin.

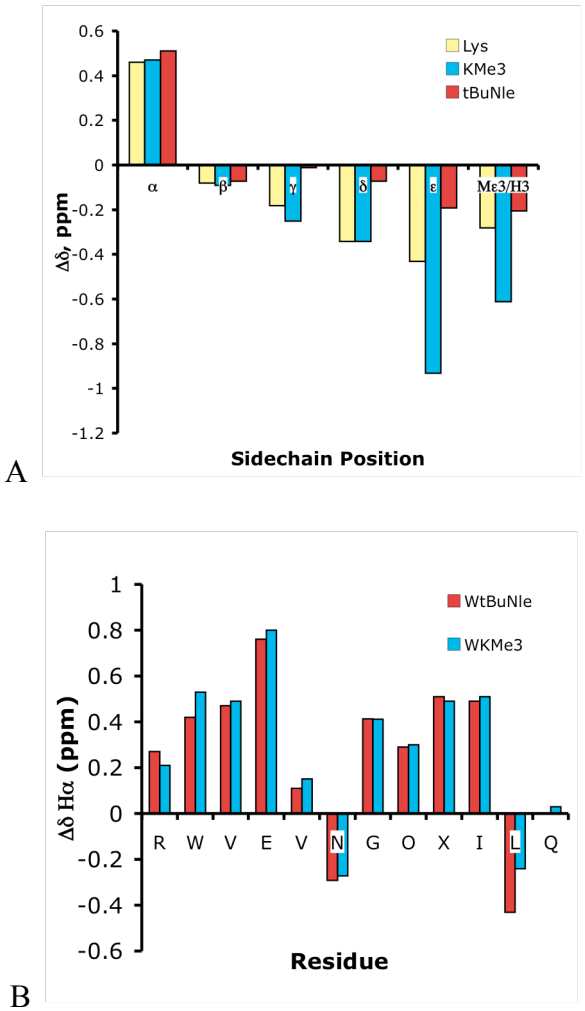

Figure 4.4. (A) tBuNle and KMe3 sidechain upfield shifts relative to random coil values. (B) Hα shifts relative to random coil values. Glycine shifts reflect the splitting.

[21] Maynard, A. J.; Sharman, G. J.; Searle, M. S. *J. Am. Chem. Soc.* **1998**, *120,* 1996-2007.

Double mutant cycles were performed in which the interacting residues at positions 2 and 9 were mutated to non-interacting residues Ser and Val to determine the magnitude of the isolated sidechain-sidechain interaction.[3-5,22] These experiments give a value of -1.0 (± 0.1) kcal/mol for the Trp-KMe3 interaction and a value of -0.6 (± 0.1) kcal/mol for the Trp-tBuNle interaction. This data demonstrates the larger magnitude of the cation-π interaction versus the alkyl-Trp interaction and provides an approximation of the magnitude of the simple hydrophobic interaction between the alkyl sidechain and the aromatic ring. This value can be compared to the interaction energy of –0.3 kcal/mol for Trp with Nle.[22]

Both **WKMe3** and **WtBuNle** exhibit high thermal stability, as determined by NMR (Figure 4.5). Fitting of the thermal denaturation data with a modified Van't Hoff equation[23],[24] reveals that **WKMe3** exhibits a favorable entropy of folding and a slightly unfavorable enthalpy of folding, indicative of multiple sites of favorable interaction with the Trp ring and a favorable hydrophobic component to folding (Table 4.1). By comparison, the **WtBuNle** shows an extremely favorable folding entropy and a significantly unfavorable enthalpy of folding, as well as a larger ΔC_p value. The considerable increase in folding entropy upon going from the trimethyl Lys to the tbutyl sidechain, and the corresponding decrease in enthalpic favorability, is consistent with a greater hydrophobic driving force for folding of **WtBuNle** as well as elimination of the favorable electrostatic interaction between Trp and KMe3. Comparison of the

[22] Tatko, C. D.; Waters, M. L. *J. Am. Chem. Soc.* **2004**, *126,* 2028-2034.

[23] Griffith-Jones, S. R.; Maynard, A. J.; Searle, M. S. *J. Mol. Biol.* **1999**, *292,* 1051-1069.

[24] Hughes, R. M.; Waters, M. L. *J. Am. Chem. Soc.* **2006**, *128,* 12735-42.

thermodynamic parameters for **WKMe3**, **WtBuNle**, and **WK** indicates that the attraction between KMe3 and Trp has a significant hydrophobic component, but the specificity of the interaction is not due to a simple hydrophobic effect, as is the case for **WtBuNle**.

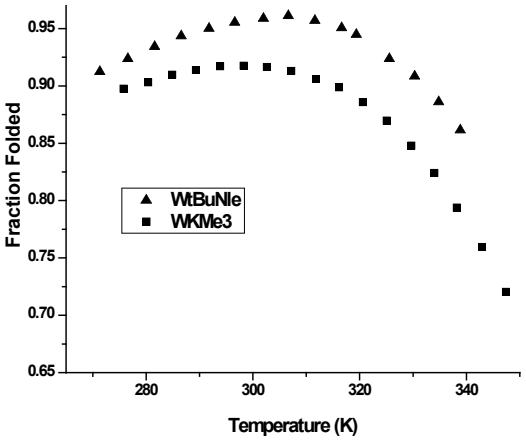

Figure 4.5. Thermal denaturation profiles of **WKMe3**, **and WtBuNle** peptides as determined by NMR. The fraction folded was determined from the Gly splitting. Error is ±0.5 K in temperature and ±1% in fraction folded. Conditions: 50 mM NaOAc-*d4* buffer, pD 4.0 (uncorrected).

Table 4.1. Thermodynamic Parameters[a] for **WKMe3 and WtBuNle** at 298 K[2]

Peptide	ΔH° (kcal/mol)	ΔS° (cal/mol K)	ΔC_p° (cal/mol K)
WK	-2.6 (0.1)	-6.2 (0.2)	-182 (27)
WKMe3L	-0.1 (0.1)	+4.5 (0.3)	-243 (36)
WtBuNle	+2.0 (0.4)	+12.9 (1.4)	-330 (50)

(a) Determined from the temperature dependence of the Gly chemical shift from 0 to 80 °C. Units are: ΔH°: kcal/mol; ΔS°: cal/mol K; ΔC_p°: cal/mol K. Errors (in parentheses) are determined from the fit. Error for ΔC_p° values estimated at 15%.

Although there is no specific interaction between tBuNle and Trp in our β-hairpin model system, it was not clear that the same effect would be observed in the binding of the Histone 3 peptide to the HP1 chromodomain: the aromatic pocket made up of a Trp, and two Tyr residues is designed to perfectly accommodate a group with the same size and shape as either a trimethylammonium or a tert-butyl group (Figure 4.1B). Given the hydrophobicity of the tBuNle sidehain and the similar polarizability of tBuNle and KMe3, as well as the exposure of the aromatic pocket to solvent on the surface of the protein, it seemed likely that a mutant Histone 3 peptide containing the tBuNle sidechain at position 9 would bind to chromodomain as strongly as the Histone peptide containing KMe3, despite the lack of a positive charge. Hence, we synthesized the modified H3 peptide (NH_2-ARTKQTAR**(tBuNle)**STGGKAY-COOH; **H3-tBuNle9**), and compared it to the native sequence containing KMe3 (NH_2-ARTKQTAR**(KMe3)**STGGKAY-COOH; **H3-K9Me3**) as a positive control, the partially methylated variants KMe2 (NH_2-ARTKQTAR**(KMe2)**STGGKAY-COOH; **H3-K9Me2**) and KMe (NH_2-ARTKQTAR**(KMe)**STGGKAY-COOH; **H3-K9Me**), as well as Lys (NH_2-ARTKQTAR**K**STGGKAY-COOH; **H3-K9**) as a negative control. Specific binding was found for the trimethylated peptide, with a K_d of 10 uM, with concomitantly weaker binding for **H3-K9Me2** and **H3-K9Me**, and virtually no binding for **H3-K9** (Figure 4.6). We then tested the binding of the neutral analog, **H3-tBuNle9,** and found it is nearly as poor as the unmethylated peptide **H3-K9** for binding to the HP1 chromodomain (Figure 4.6). This observation was surprising given the similarity in size and shape, as well as the greater hydrophobicity of the tert-butyl group relative to the trimethylammonium group of KMe3. Indeed, **H3-K9Me** and **H3-K9Me2** bind more strongly than does **H3-**

tBuNle9, despite the fact that they do not fill the binding pocket of HP1 chromodomain.[5] This clearly demonstrates the essential nature of the cation-π component to binding of the lysine-methylated H3 tail to chromodomains.

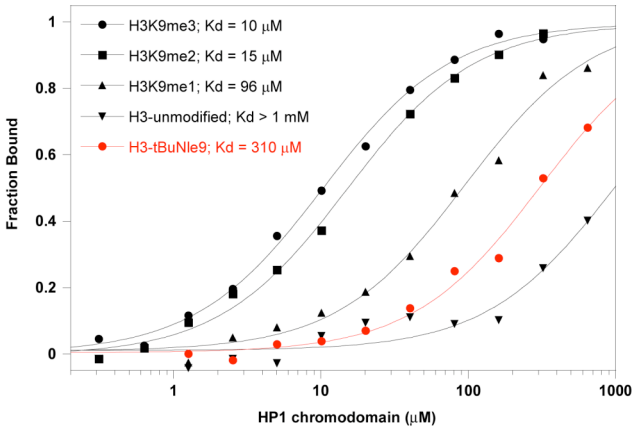

Figure 4.6. Binding of **H3-K9Me3**, **H3-K9Me2, H3-K9Me, H3-tBuNle9**, and **H3-K9** to the HP1 chromodomain as determined by fluorescence polarization assay. *Drosophila* HP1 chromodomain was purified and used in binding studies with fluoresceinated peptides as previously described.[5] Binding assays were performed at 15 degree celcius in phosphate buffer pH 7.5 and containing 25 mM NaCl and 1 mM DTT.

iii. Conclusions

In conclusion, this study provides substantial insight into why lysine methylation is successful in making critical interactions that are required for controlling gene expression. We have demonstrated the essential nature of the cation-π component to the interaction of the H3 peptide tail and the HP1 chromodomain. This data enhances our fundamental understanding of how the methylation of lysine functions cooperatively within the broad spectrum of post-translational modifications. For example, the cation-π component for docking of a chromodomain on a lysine-methylated histone tail is especially useful for controlling epigenetic signaling via a phosphorylation switch.

Recent studied have shown that phosphorylation of the residue adjacent to the methyllysine reduces the affinity of the chromodomain for the histone tail by 100-fold and effectively blocks recognition of the methyllysine signal.[25],[26] Therefore, the presence of a phosphate group immediately adjacent to the methyllysine dramatically reduces the stability of the cation-π bond between the methyllysine and the aromatic cage. Among well-known post-translational modifications that contribute to biomolecular signaling, lysine methylation of histone tails is a stable modification during the cell cycle which is inherited during cell division.[2] Although recent studies have identified bona fide nucleosome-specific lysine-demethylases, it appears these contribute to the resetting of a fraction of methyllysine signals by mechanisms that are poorly understood. Therefore, the reversible phosphorylation of the residue adjacent to the methyllysine is a novel biomolecular feature for on-off switching of the lysine methylation signal. Phosphorylation blocks the docking of proteins to methyllysines, thus chromatin can undergo maximal compaction in preparation of the metaphase chromosomes.[26],[27] Subsequent events that reverse the phosphorylation allow reestablishing functional chromatin boundaries by recruiting specific methyllysine-docking factors. This is consistent with a histone code that suggests distinct histone modifications act sequentially or in combination to bring about important events for eukaryotic gene regulation.[28]

---

[25] Fischle, W.; Tseng, B. S.; Dormann, H. L.; Ueberheide, B. M.; Garcia, B. A.; Shabanowitz, J.; Hunt, D. F.; Funabiki, H.; Allis, C. D. *Nature* **2005**, *438,* 1116-22.

[26] Flanagan, J. F.; Mi, L. Z.; Chruszcz, M.; Cymborowski, M.; Clines, K. L.; Kim, Y. C.; Minor, W.; Rastinejad, F.; Khorasanizadeh, S. *Nature* **2005**, *438,* 1181-1185.

[27] Hirota, T.; Lipp, J. J.; Toh, B. H.; Peters, J. M. *Nature* **2005**, *438*, 1176-1180.

[28] Strahl, B. D.; Allis, C. D. *Nature* **2000**, *403,* 41-45.

Additionally, these results recall prescient studies by Dougherty and co-workers, who showed binding discrimination between interaction of an aromatic host with a trimethyl ammonium group and a tert-butyl group in a small molecule model system in borate buffer.[20] Likewise, the data from our β-hairpin model system predicts the in vitro behaviour of the H3 peptide-chromodomain binding. Valuable mechanistic information is readily obtained from the model system which is not directly available from the protein-peptide interaction, giving a fuller understanding of the forces underlying the preference for KMe3 recognition and firmly establishing the importance of the charge-quadropole interaction to binding *and* specificity. Finally, this study provides insight into the subtle features of noncovalent interactions that contribute to biomolecular recognition, and indicates that the simple separation of interactions into polar and hydrophobic can be too simplistic to fully understand or control biomolecular recognition.

B. Trifluoro homonorleucine and an alkyl-π interaction.

i. Background and significance.

Halogenation is commonly carried out in the pharmaceutical industry in order to enhance the binding affinities and/or metabolic activities of various drug candidate molecules. Fluorination, chlorination, and bromination are commonly used to enhance the hydrophobicity of compounds, which is thought to increase their affinity for binding sites, without adding a great deal of steric bulk to the molecule.[29] However, there are a number of non-covalent interactions involving the halogens that may not be fully

---

[29] Bohm, H. J.; Banner, D.; Bendels, S.; Kansy, M.; Kuhn, B.; Muller, K.; Obst-Sander, U.; Stahl, M.; *Chembiochem* **2004,** 5, (5), 637-643.

appreciated by the pharmaceutical industry, leading to unanticipated interactions with halogenated drugs in protein binding sites. These interactions include fluorine—carbonyl interactions (orthogonal multipolar interactions) that are moderately favorable in solution that have been shown to exist in protein crystal structures and quantified using model systems.[30] Additionally, iodination of aromatic rings has been shown to enhance the magnitude of aromatic-aromatic interaction within a designed β-hairpin peptide via direct halogen-π interaction.[31] Within the context of our β-hairpin model system, we have investigated the effects of fluorination of an alkyl sidechain on its interaction with the aromatic amino acid tryptophan (Trp). Our results indicate that, in the proximity of aromatic residues, repulsive electronic effects due to a fluorine-π interaction can counterbalance increases in hydrophobicity due to fluorination, leading to lower interaction energies with Trp. These results indicate that while the fluorination of medicinal compounds may increase their hydrophobicity, the drug target site must be well defined in order to achieve the anticipated enhancement in binding affinity.

---

[30] (a) Schweizer, E.; Hoffmann-Roder, A.; Olsen, J. A.; Seiler, P.; Obst-Sander, U.; Wagner, B.; Kansy, M.; Banner, D. W.; Diederich, F. *Organic & Biomolecular Chemistry* **2006,** 4, (12), 2364-2375. (b) Hof, F.; Scofield, D. M.; Schweizer, W. B.; Diederich, F. *Angew. Chem. Int. Ed.* **2004,** 43, (38), 5056-5059. (c) Olsen, J.; Seiler, P.; Wagner, B.; Fischer, H.; Tschopp, T.; Obst-Sander, U.; Banner, D. W.; Kansy, M.; Muller, K.; Diederich, F. *Organic & Biomolecular Chemistry* **2004,** 2, (9), 1339-1352. (d) Olsen, J. A.; Banner, D. W.; Seiler, P.; Wagner, B.; Tschopp, T.; Obst-Sander, U.; Kansy, M.; Muller, K.; Diederich, F. *Chembiochem* **2004,** 5, (5), 666-675. (e) Olsen, J. A.; Banner, D. W.; Seiler, P.; Sander, U. O.; D'Arcy, A.; Stihle, M.; Muller, K.; Diederich, F. *Angew. Chem. Int. Ed.* **2003,** 42, (22), 2507-2511.

[31] Tatko, C. D.; Waters, M. L. *Organic Letters* **2004,** 6, (22), 3969-3972.

ii. Design and Synthesis.

The peptides investigated in this study (Figure 4.7) were designed, synthesized, and characterized using methods previously discussed in this chapter. The sidechain tert-Butyl Norleucine (tBuNle) should make a useful comparison to tFhNle due to its identical length and anticipated similarity in hydrophobicity. Calculated LogP values, or the partition coefficient between octanol and water, suggest that the hydrophobicities of the two sidechains are similar (Figure 4.8).

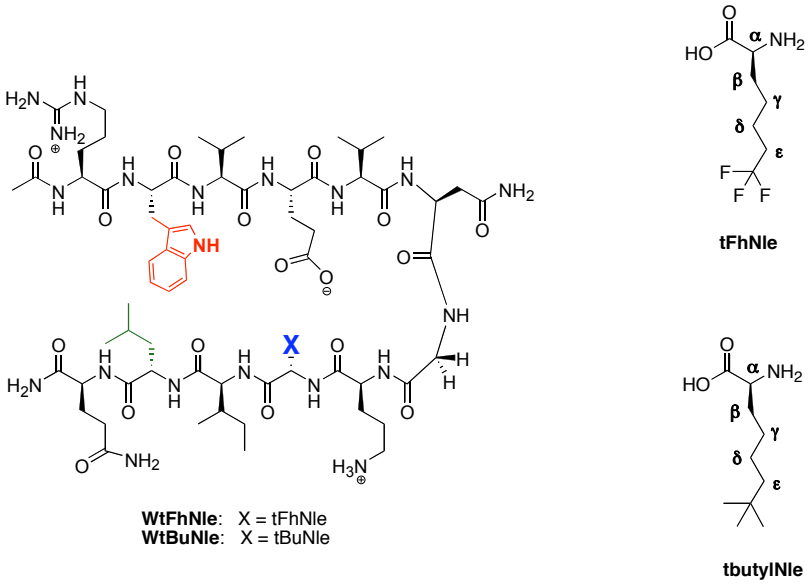

Figure 4.7. (a) β-hairpin peptide containing tFhNle or tBuNle. Peptides are referred to by the residues at positions 2 (Trp) and 9 (X) in the text.

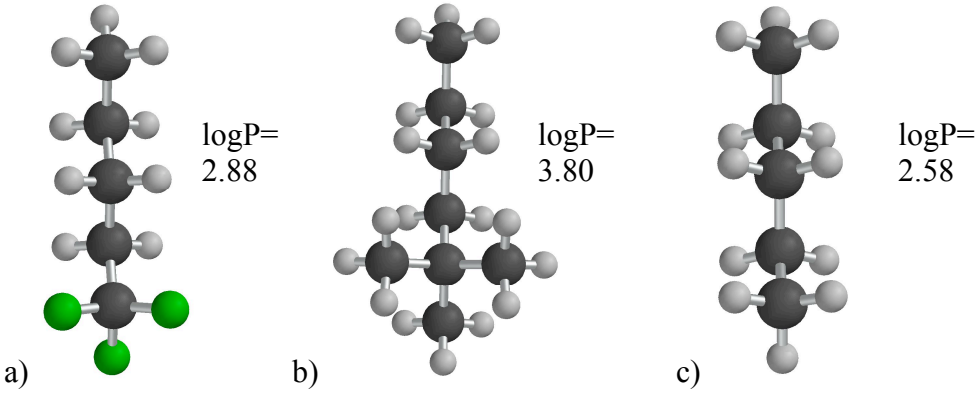

Figure 4.8. Calculated logP values for sidechains of a) tFhNle and b) tBuNle. c) Pentane is shown for comparison (MacSpartan 2004: HF/6-31g**; Ghose-Crippen method).

iii. Results and Discussion.

The peptides **WtFhNle** and **WtBuNle** are both well folded β-hairpins with similar stabilities, as demonstrated by H_α chemical shifts (Figure 4.8a). Fraction folded based on the Gly splitting gives a population of 92% for **WtFhNle** and 96% for **WtBuNle**. Presumably, based on the discussion of tBuNle undertaken earlier in this chapter, both hairpins are stabilized by significant non-specific, hydrophobic interactions, particularly in regard to their interactions with Trp. Comparison of the upfield shifts of the tFhNle and tBuNle sidechains, however, begins to paint more subtle picture of the interactions that are stabilizing the hydrophobic cluster of the β-hairpin (Figure 4.9). While the terminal portions of the tBuNle sidechain are most upfield shifted, indicating that they are interaction more with the face of the Trp ring than the rest of the sidechain, the tFhNle ligand is most upfield shifted at the δ position, and even slightly downfield shifted, relative to random coil, at the ε postion. This is a significant effect given the identical length and similarly patterned functionality of the two ligands. The proposed difference in the two interactions is due to the electron density around the electronegative fluorines

at the termini of the tFhNle sidechain. These fluorines do not interact favorably with the similarly electron-rich face of the Trp ring. In contrast, the tBuNle ligand can interact with the face of the ring via van der Waals interactions, particularly at its bulky termini, where hydrophobic and van der Waals forces combine make it the most favorable site of interaction with the ring. Data taken from double mutant cycles supports this idea, giving interaction energies of -0.42 kcal/mol for the tFhNle-Trp interaction and -0.58 kcal/mol for the tBuNle-Trp interaction. This is consistent with the upfield shifting profiles, which indicate more contact (on average) for the tBuNle sidechain with the Trp ring.

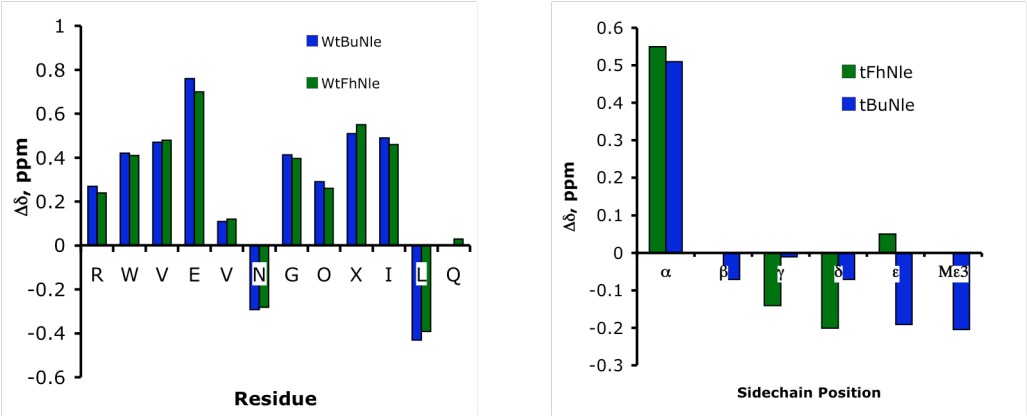

Figure 4.9. (a) H_α chemical shifts for **WtBuNle** and **WtFhNle**. (b) Upfield shifts of tBuNle and tFhNle sidechains.

Another valuable comparison is to work discussed earlier in this thesis (Chapter 3), concerning the interaction of a variety of acylated Lys residues with Trp. The interaction of trifluoroacetylated lysine (FAc) with Trp gives a very similar upfield shifting profile to that of tFhNle, in that fluorination moves the bulk of the upfield shifting away from the amide NH, supporting the general notion of the repulsive effect of fluorination in proximity to aromatic rings (Figure 4.10).

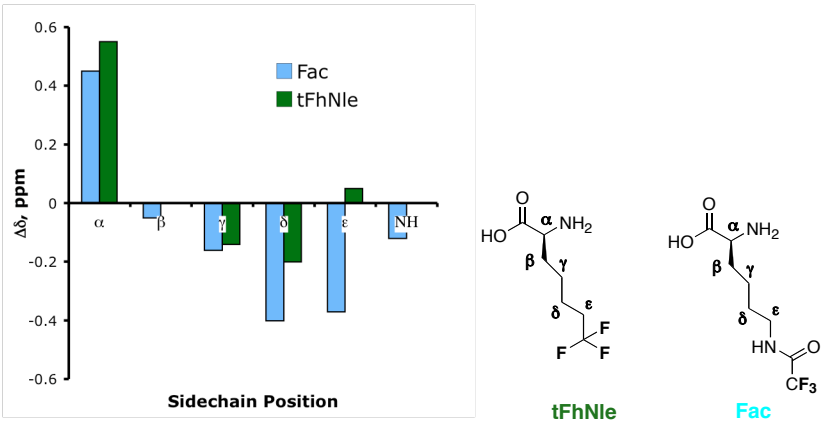

Figure 4.10. (a) Upfield shifts of sidechains tBuNle and tFhNle. (b) Diagram of amino acid sidechains tFhNle and Fac.

Thermodynamic analysis of **WtBuNle** and **WtFhNle** by NMR indicates that both have a significant entropic driving force for folding (Figure 4.11; Table 4.2). This is expected, given the generally non-specific, hydrophobic nature of both interactions. However, the entropic component of folding for **WtbutylNle** is much greater than that of **WtFhNle**, as is the heat capacity, indicative of a stronger hydrophobic clustering in the peptide.

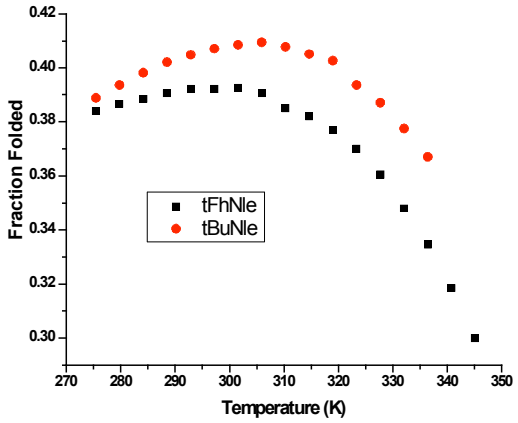

Figure 4.11. Thermal denaturation profiles of **WtFhNle**, **and WtBuNle** peptides by NMR. The fraction folded was determined from the Gly splitting. Error is ±0.5 K in temperature and ±1% in fraction folded. Conditions: 50 mM NaOAc-*d4* buffer, pD 4.0 (uncorrected).

Table 4.2. Thermodynamic Parameters[a] for **WtFhNle and WtbutylNle** at 298 K[10]

Peptide	ΔH° (kcal/mol)	ΔS° (cal/mol K)	ΔC_p° (cal/mol K)
WtFhNle	-0.8 (0.1)	+2.1 (0.5)	-246 (37)
WtBuNle	+2.0 (0.4)	+12.9 (1.4)	-334 (50)

[a] Determined from the temperature dependence of the Gly chemical shift from 0 to 80 °C. Units are: ΔH°: kcal/mol; ΔS°: cal/mol K; ΔC_p°: cal/mol K. Errors (in parentheses) are determined from the fit. Error for ΔC_p° values estimated at 15%.

iv. Conclusion

In conclusion, the comparison of the interactions of two hydrophobic amino acid sidechains with Trp indicates that the two have surprisingly different modes of interaction with the aromatic ring. While both sidechains create highly stable β-hairpin peptides, there are distinct differences in sidechain upfield shifting profiles and folding thermodynamics that show the effects of "hydrophobic" fluorines are more complex than generally anticipated. Specifically, a fluorinated group can control interaction geometry

through repulsive interactions with electron rich groups such as aromatic rings. Thus, the role of fluorination is more complex than simply increasing hydrophobicity. This finding has implications for drug design and molecular recognition in general, as this data indicates that fluorination could be used to orient ligands within binding pockets via either attractive (multipolar & hydrophobic) or repulsive (F-π) interactions.

C. Experimental Section

i. Small molecule synthesis

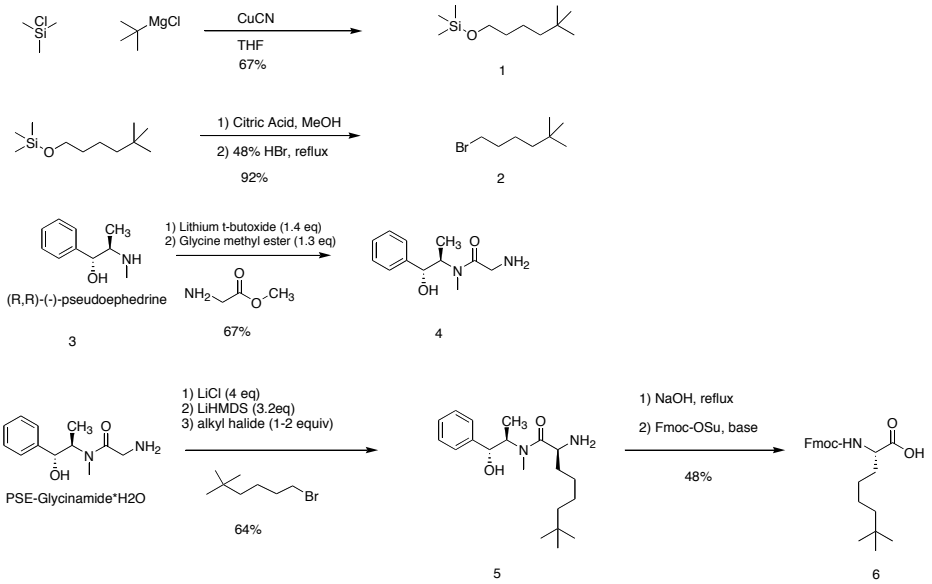

Scheme 4.1. Synthesis of Fmoc-L-tButylNle-OH

Synthesis of 1,1-dimethyl hexane trimethylsilyl ether 1 (Scheme 4.1).[32] 0.030 g CuCN was added to a dry 3-neck flask fitted with a reflux condenser under argon. 25 mL of 1M t-butyl MgCl in THF was added via syringe, followed by the slow addition (dropwise; 12 minutes) of trimethyl chlorosilane (3.10 mL). Reaction was refluxed for 2 hours. After cooling to room temperature, 5 mL of water was carefully added to the reaction, and the resulting mixture was filtered through a Buchner funnel. The resulting filtrate was dried with sodium sulfate and the solvent was removed in vacuo. The resulting oil was chromatographed on silica gel (1:1 Hexanes:EtOAc), giving 3.37 g of a light yellow oil (16.7 mmol; 67% yield). ESI-MS: calculated = 202.18; actual = 202.2 NMR (600

[32] Shirahata, A. Tet. Lett. **1989**, *30*, 6393 – 6394.

MHz,CDCl3): 3.575 (t, 2H), 1.482 (q, 2H), 1.263 (m, 2H), 1.142 (m, 2H), 0.824 (s, 9H), 0.013 (s, 9H).

Synthesis of 1-bromo, 5,5-dimethyl hexane 2 (Scheme 4.1).[33] Product **1** was dissolved in methanolic citric acid (1g citric acid in 20 mL methanol) and allowed to stir for 30 minutes at room temperature. The solvent was removed in vacuo and the resulting oil was taken up into EtOAc and washed with water (2 X 25 mL). The organic layer was then dried with sodium sulfate and the solvent removed in vacuo. The resulting oil was then taken up in 25 mL 48% HBr and allowed to reflux for 3 hours. The resulting solution was cooled to room temperature and extracted with 1:1 CH_2Cl_2:Et_2O (2 X 25 mL). The organic layer was combined and washed with $NaHCO_3$ (2 X 25 mL) and brine (1 X 25 mL), dried with sodium sulfate, and the solvent removed in vacuo. Resulting oil was purifined via silica gel flash chromatography (4:1 EtOAc:Hexanes), giving 2.98 g of a slightly yellow oil (15.4 mmol, 92% yield). APCI-MS: calculated = 192.1; actual = 192.2 NMR (400 MHz,CDCl3): 3.565 (t, 2H), 1.974 (m, 2H), 1.337 (m, 2H), 1.024 (s, 9H).

Synthesis of (R,R)-(-)-pseudoephedrine glycinamide hydrate 3 (Scheme 4.1). A 250 mL round bottom flask is charged with (R,R)-(-)pseudoephedrine (10 g; 60.5 mmol) and glycine methyl ester (9.88g; 78.7 mmol) in 50 mL THF, followed by 15 minutes of stirring at room temperature under argon. Lithium tert-butoxide powder (6.78g; 84.7 mmol) was added in one portion. The reaction was then stirred for 2 hours, followed by the addition of water (75 mL), and the resulting mixture was concentrated in vacuo. The resulting oil is taken up in hot THF (50 mL) and water (2 mL) was added to

[33] Rybczynski, P. J., et al. J. Med Chem. **2004**, *47*, 196 – 209.

the hot solution. Crystallization occurred upon cooling to room temperature. Allowed solution to sit at -20 deg C overnight. Crystals collected by filtration and dried after washing with diethyl ether. After leaving under vacuum overnight, the white crystalline powder weighed 9.66 g (40.4 mmol; 67% yield). ESI-MS: calculated = 239; actual = 239.1 Spectroscopic data matched published data. NMR (400 MHz,CDCl3): 7.27-7.38 (m, 5H), 4.50-4.60 (m, 1.5H), 3.81 (m, 0.5H), 3.681 (d, 0.5H), 3.388 (d, 1H), 3.313 (d, 0.5H), 2.934 (s, 1.5H), 2.774 (s, 1.5H), 2.420 (s(br), 3H), 1.029 (d, 1.5H), 0.951 (d, 1.5H).

Alkylation of (R,R)-(-)-pseudoephedrine glycinamide hydrate 3 (Scheme 4.1). An oven dried 3-neck round bottom flask was charged with dry LiCl (0.606g; 14.4 mmol) and allowed to cool to room temperature under vacuum. The flask was then flushed with argon, and THF was added (20 mL). The resulting suspension was allowed to stir for 20 minutes at room temperature. Solid PSE glycinamide **3** (0.862 g; 3.6 mmol) was then added in one portion, and the solution immersed in an isopropanol bath maintained at 0 deg C with a Neslab Cryotrol cold finger and allowed to stir for 30 minutes. Next, LiHMDS is added via dry syringe dropwise (14 mL of a 1M solution in THF), followed by 20 minutes of stirring. Finally, product **2** (0.802 g; 4.2 mmol) is added slowly over 10 minutes via syringe to the enolate solution. The reaction mixture was then allowed to stir for 23 hours at 0 deg C. The reaction was quenched with the addition of 10 mL H_2O and acidified to near pH 0 with 6M HCl. The resulting acidic solution was extracted with ethyl acetate (3 X 50 mL), dried with sodium sulfate, and rotovapped to dryness. The resulting oil was then purified via silica gel flash chromatography via gradient elution (column washed with 100 mL CH2Cl2, followed by washes of 20:1 CH2Cl2:MeOH (400

mL), 10:1 CH2Cl2:MeOH (220 mL), and 5:1 CH2Cl2:MeOH (200 mL). (Yield: 0.770g, 2.3 mmol, 64% yield). NMR (600 MHz, CDCl3): 8.194, (br, 2H), 7.24-7.41 (m, 5H), 4.909 (s, 1H), 4.473 (d, 1H), 4.270 (t, 1H), 2.868 (s, 3H), 2.799 (br, 3H), 1.765 (m, 2H), 1.04-1.35 (m, 6H), 0.811 (s, 9H). ESI-MS: calculated = 334.26 actual = 334.3.

Synthesis of Fmoc-L-tbutylNle-OH 6 (Scheme 4.1). Product 5 was taken up in 4.6 mL of 1N NaOH and 20 mL of H2O. The resulting mixture was refluxed for 5.5 hours, allowed to cool to room temperature, and filtered through a Buchner funnel. The filtered solution was washed with ethyl acetate (1 X 25 mL), frozen, and lyophilized to dryness. The resulting oil was dissolved in 25 mL of H2O with stirring. 0.387 g of sodium bicarbonate was added, followed by 25 mL of dioxane. The resulting solution was cooled in an ice bath for 30 minutes. Fmoc-OSu (0.935 g; 2.8 mmol) was dissolved in 10 mL dioxane and added to the chilled solution dropwise via pipette. The reaction was stirred for 1 hour at ice temperature and 3 hours at room temperature. Reaction followed by TLC (10:1 CH2Cl2: MeOH). Water was then added (30 mL) and the resulting solution was extracted with 75 mL 1:1 EtOAc/Ether. The organic layer was separated and back extracted with 2% sodium bicarbonated (2 X 25 mL). The aqueous layers were combined and acidified to pH 1, followed by extraction with EtOAc (2 X 50 mL). The organic layer was dried with sodium sulfate and the solvent removed in vacuo, giving product **6** as a clear oil (0.454 g; 48% overall yield for two steps). NMR (600 MHz, CDCl3): 7.7465 (d, 2H), 7.582 (d, 2H), 7.383 (t, 2H), 7.297 (t, 2H), 5.2355 (d, 1H), 4.397 (m, 2H), 4.215 (t, 1H), 1.898 (m, 1H), 1.708 (m, 1H), 1.4 – 1.5 (m, 6H), 0.842 (s, 9H). ESI-MS: calculated = 409.23 actual = 409.3.

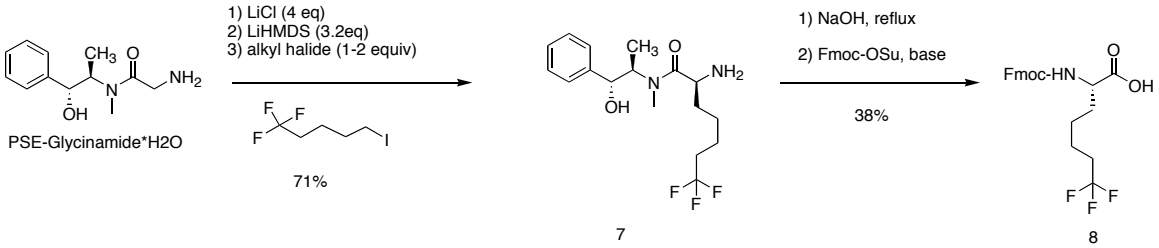

Scheme 4.2. Synthesis of Fmoc-L-tFhNle-OH

Synthesis of 7 (Scheme 4.2). Identical procedure followed as reported for the synthesis of compound 5. 5-Iodo-1,1,1-trifluoropentane (1.11 g; 4.41 mmol) obtained from Matrix Scientific, Inc. was used as the alkyl halide. (Yield: 1.036g, 2.99 mmol, 71% yield). NMR (300 MHz, CDCl3): 8.230 (br, 2H), 7.24-7.40 (m, 5H), 4.879 (m, 1H), 4.464 (d, 1H), 4.431 (d, 1H), 4.256 (t, 1H), 2.868 (s, 3H), 2.505 (br, 3H), 1.924 (m, 1H), 1.736 (m, 1H), 1.410 (m, 4H), 0.790 (m, 2H). ESI-MS: calculated = 346.187 actual = 346.2.

Synthesis of Fmoc-L-tFhNle-OH 8 (Scheme 4.2). Identical procedure followed as reported in synthesis of compound **6**, giving product **8** as a clear oil (0.454 g; 48% overall yield for two steps). NMR (300 MHz, CDCl3): 7.75 (d, 2H), 7.56 (d, 2H), 7.387 (t, 2H), 7.297 (t, 2H), 5.20 (d, 1H), 4.417 (m, 2H), 4.205 (t, 1H), 1.4 – 2.1 (m, 8H). ESI-MS: calculated = 421.15 actual = 421.2.

ii. Concentration Study.

The hairpin **WtBuNle** exhibits aggregation behaviour in the 1 mM and above concentration range. In order to determine the most suitable concentrations for NMR analysis, a concentration study was performed by CD (10 mM sodium phosphate buffer, pH 6.4, 298K). The peptide was found to be monomeric near and below approximately 0.5 mM concentration. As a result, the NMR studies of the WtbutylNle hairpin were carried out at concentrations of 0.5 mM or less. The thermal denaturation, for example, was executed at 0.316 mM.

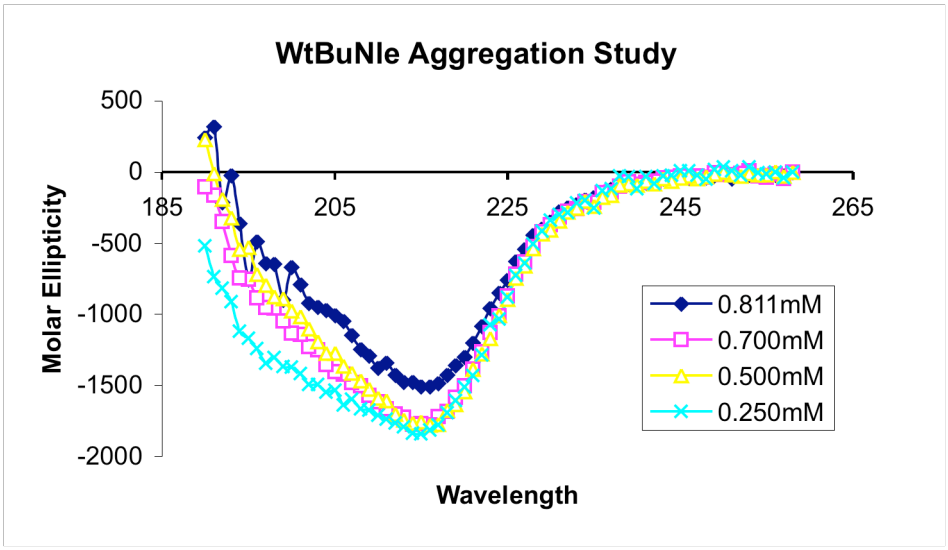

Figure 4.12. Concentration study by CD of the peptide **WtBuNle**.

iii. Quantification of Folding

To determine the chemical shifts of the fully folded state, 14-residue disulfide-linked analogs of peptides were synthesized with the sequence of Ac-CRWVEVNGOXILQC-NH2, where X = KMe3 or tbutylNle. The disulfide bond between Cys1 and Cys14 constrains the peptide to a β-hairpin. To determine the unfolded chemical shifts, 7-mers

were synthesized with sequences Ac-RWVEVNG-NH2 and Ac-NGOXILQ-NH2, where X = KMe3 or tbutylNle. The chemical shifts for residues in the strand and one turn residue were obtained from each 7-mer peptide. The fraction folded was determined from equation 1.

$$\text{Fraction Folded} = [\delta_{obs} - \delta_0]/[\delta_{100} - \delta_0] \qquad \text{(eqn 1)}$$

$$\Delta G = =-0.001987*298*\ln(ff/(1-ff)) \qquad \text{(eqn 2)}$$

iv. Characterization of Structure

Methods used to indicate the formation of β-hairpin structure include the analysis of Hα shifting relative to random coil, backbone amide shifts relative to random coil, and the identification of cross strand NOEs. The β-hairpin should have backbone hydrogen bonded amides between cross-strand residue pairs Arg-Gln, Val-Ile, and Val-Orn in all hairpin peptides. The presence of these hydrogen bonds is readily demonstrated by downfield shifting of the amide hydrogens in these positions relative to random coil. As seen below, both peptides exhibit significant downfield shifting at key positions along the strand. As expected for β-hairpins, the termini are frayed and show little or no amide shifting. The Asn amide shows significant downfield shifting as expected for a Type I' turn.

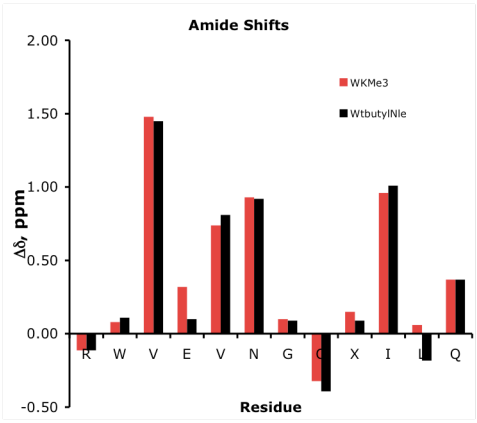

Figure 4.13. Backbone amide shifts of peptides **WKMe3** and **WtBuNle**.

Finally, the identification of numerous cross-strand NOEs in all hairpin peptides indicates that all peptides have β-hairpin structure.

Figure 4.14. WtBuNleCyc Cross-strand NOEs:

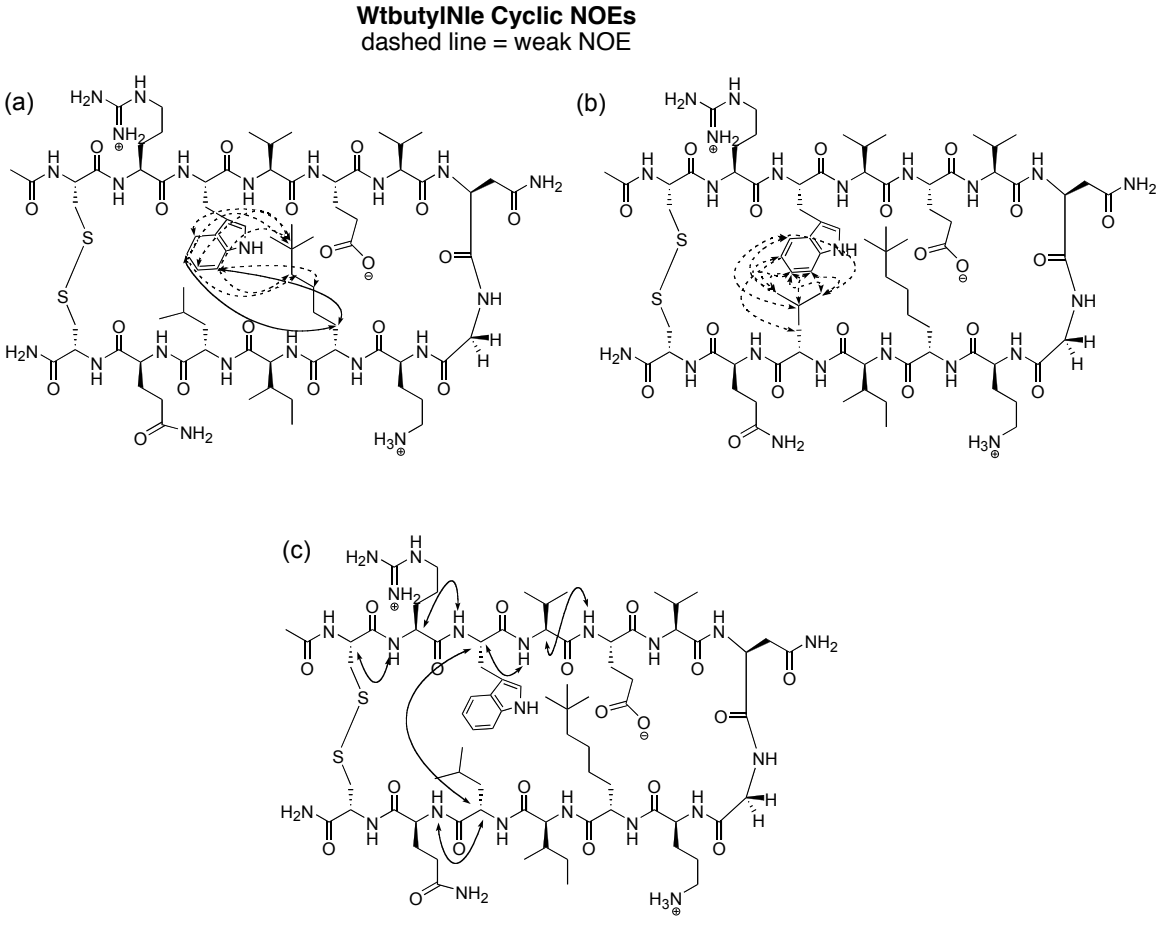

Table 4.3. NOEs observed at 298 K (S=Strong; M=Medium; W=Weak) for peptide **WtBuNleCyc** (Ac-RWVEVNGO(tBuNle)ILQ-NH_2):

Residue	Proton	Residue	Proton	Intensity
Trp 3	Ar 4	Leu 12	δ	W
Trp 3	Ar 4	Leu 12	γ	W
Trp 3	Ar 4	Tbutyl10	$(CH_3)_3$	W
Trp 3	Ar 7	Leu 12	δ	W
Trp 3	Ar 7	Tbutyl10	$(CH_3)_3$	W
Trp 3	Ar 7	Tbutyl10	δ	W
Trp 3	Ar 7	Tbutyl10	ε	W
Trp 3	Ar 7	Tbutyl10	β	M
Trp 3	Ar 6	Leu 12	δ	W
Trp 3	Ar 6	Leu 12	γ	W
Trp 3	Ar 6	Tbutyl10	$(CH_3)_3$	W
Trp 3	Ar 5	Ile 11	α	M
Trp 3	Ar 5	Tbutyl10	β	M
Trp 3	Ar 5	Tbutyl10	ε	W
Trp 3	Ar 5	Tbutyl10	$(CH_3)_3$	W
Trp 3	Ar 5	Leu 12	δ	W
Trp 3	Ar 5	Leu 12	β	W
Trp 3	α	Leu 12	α	S
Trp 3	NH	Arg 2	α	S
Arg 2	NH	Cys 1	α	S
Gln 13	NH	Leu 12	α	S
Val 6	NH	Glu 5	α	S
Val 4	NH	Trp 3	α	S

v. Thermodynamic Analysis

Peptides were analyzed assuming a two-state system. The equilibrium constant was determined from the fraction folded (f) by K = f/(1-f). The free energy was then calculated from $\Delta G° = - RT\ln K$. In order to determine the thermodynamic parameters, $\Delta H°$, $\Delta S°$, and $\Delta Cp°$, the temperature dependence of the Gly chemical shift difference was fit to the following equation:[34]

$$\text{Fraction Folded} = [\exp(x/RT)]/[1 + \exp(x/RT)], \text{ where}$$

$$x = T(\Delta S°_{298} + a \ln(T/298) + b (T - 298) - (c/2) (1/T^2 - 1/298^2)) - (\Delta H°_{298} + a (T - 298) + (b/2) (T^2 - 298^2) - c (1/T - 1/298))].$$

[34] Maynard, A.J. Sharman, G. J. and Searle, M. S. *J. Am. Chem. Soc.* **1998**, *120*, 1996-2007.

Temperature Dependence of the Fraction Folded from Glycine Chemical Shift Data for the peptides in this study:

Table 4.4. Thermal Denaturation data for **WtBuNle** and **WtFhNle**:

WtBuNle: **WtFhNle**:

Temp (K)	fraction folded	Temp (K)	fraction folded
271.33	0.921	275.45	0.893
276.60	0.932	279.81	0.899
281.63	0.943	284.16	0.903
286.61	0.953	288.52	0.908
291.80	0.959	292.87	0.912
296.63	0.964	297.23	0.912
302.00	0.968	301.58	0.913
306.64	0.970	305.94	0.908
311.62	0.966	310.29	0.895
316.66	0.960	314.64	0.888
319.38	0.954	319.00	0.877
325.60	0.932	323.35	0.860
330.33	0.917	327.71	0.838
		332.06	0.809
		336.42	0.778
		340.77	0.741
		345.13	0.698

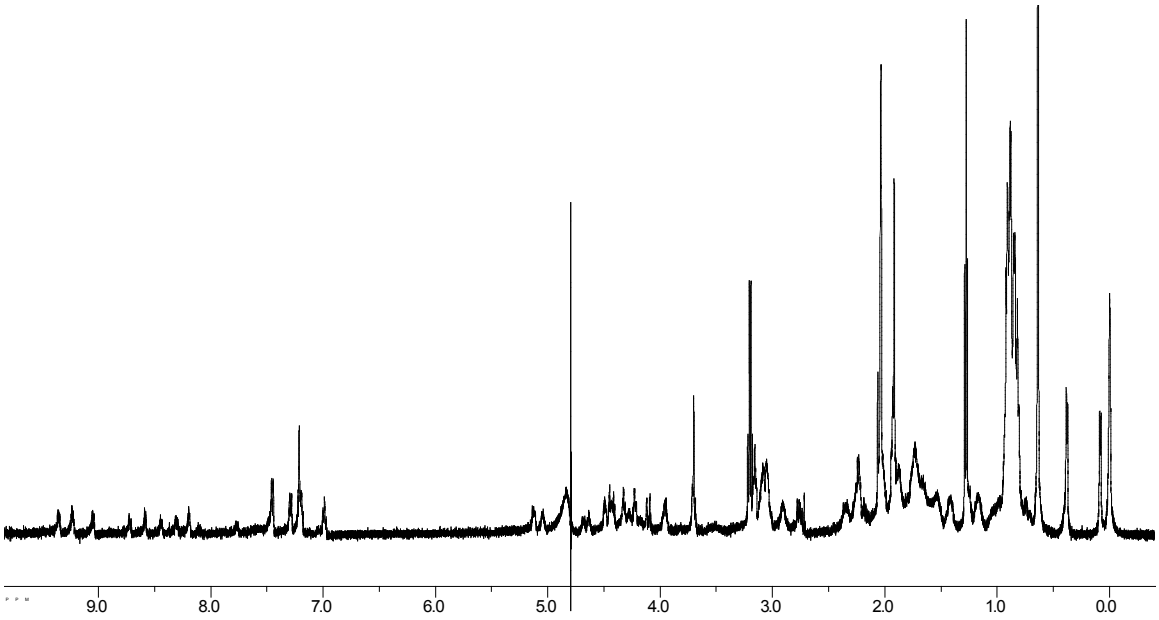

Figure 4.15. [1]HNMR of Peptide **WtBuNle**: Ac-Arg-Trp-Val-Glu-Val-Asn-Gly-Orn-tbutylNle-Ile-Leu-Gln-NH2

Table 4.5. Proton Chemical Shift Assignments for Peptide **WtBuNle**.

	α	β	γ	δ	ε	Amide	Amine
R	4.49	1.68	1.57	3.15		8.03	7.13,6.63
W	5.12	3.08	7.451,7.287	7.210,7.193	6.986	8.30	10.11
V	4.49	2.02	0.86			9.20	
E	5.05	2.00	2.20			8.30	
V	4.21	1.93	0.90			9.03	
N	4.41	3.04,2.73				9.52	
G	4.1055, 3.692					8.64	
O	4.67	1.77	1.77	3.04		7.72	7.64
tBuNle	4.78	1.68	1.20	1.02	0.91 **$(CH_3)_3$**=0.639	8.42	
I	4.63	1.85	1.42,1.17,0.87	0.87		9.31	
L	3.95	1.25	0.92	0.38,0.095		8.19	
Q	4.31	2.01	2.26			8.70	

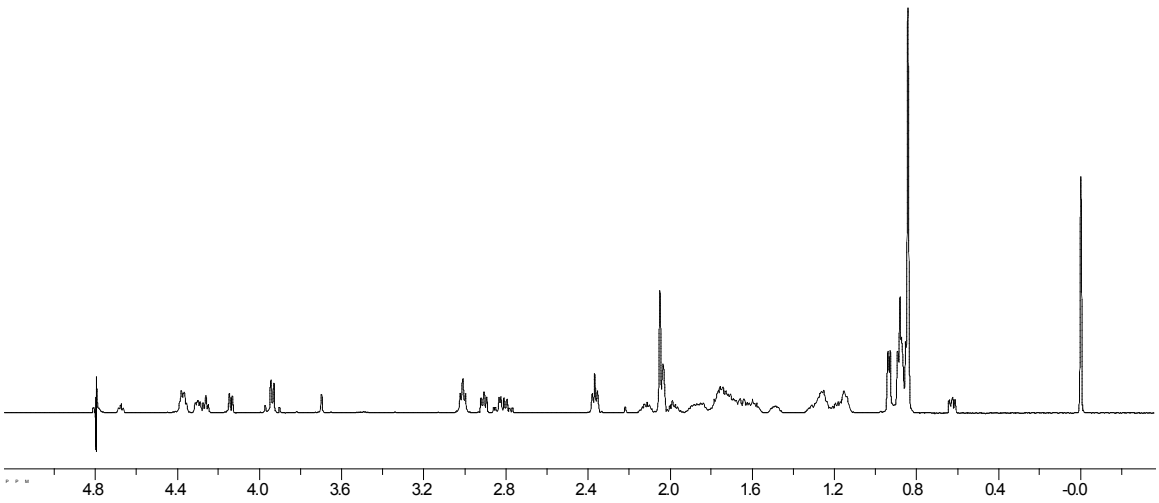

Figure 4.16. [1]HNMR of Peptide **tBuNle7**: Ac-Asn-Gly-Orn-tbutylNle-Ile-Leu-Gln-NH2

Table 4.6. Proton Chemical Shift Assignments for Peptide **tBuNle7**.

	α	β	γ	δ	ε	Amide	Amine
N	4.68	2.84					
G	3.94						
O	4.38	1.82	1.67	3.02			
tBuNle	4.27	1.75	1.26	1.15	1.15 **$(CH_3)_3$**=0.843		
I	4.14	1.79	1.39, 0.89	0.89			
L	4.38	-----	------	0.90			
Q	4.31	2.02	2.34				

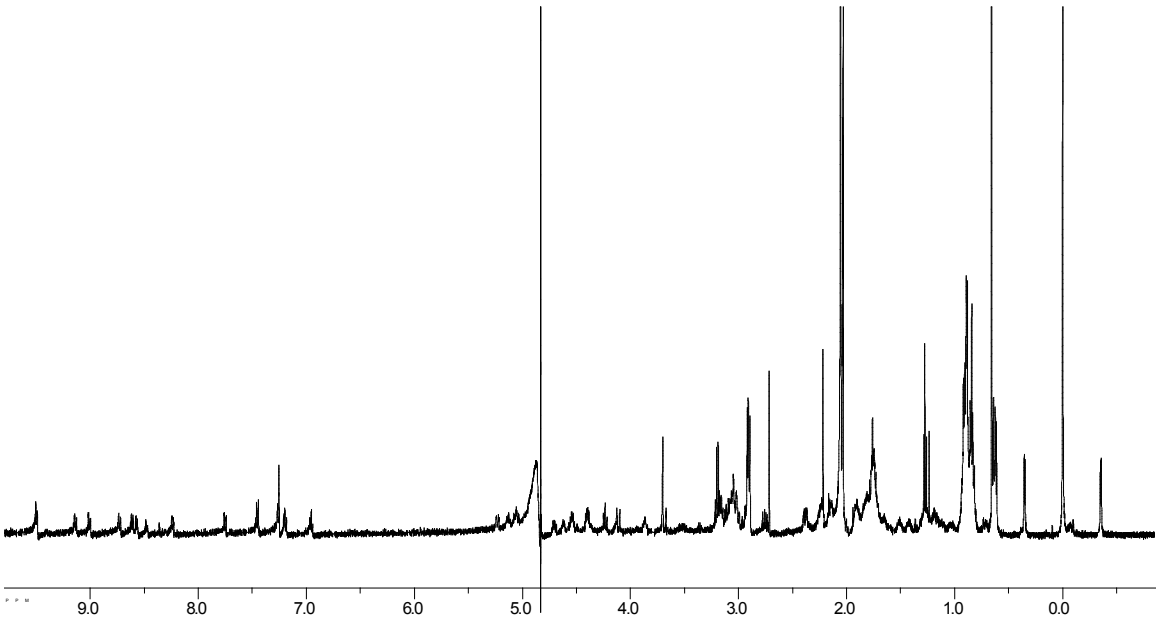

Figure 4.17. [1]HNMR of Peptide **WtbuNleCyc**: Ac-Cys-Arg-Trp-Val-Glu-Val-Asn-Gly-Orn-tbutylNle-Ile-Leu-Gln-Cys-NH2

Table 4.7. Proton Chemical Shift Assignments for Peptide **WtBuNleCyc.**

	α	β	γ	δ	ε	Amide
C	5.23	2.999,2.374				
R	4.615	1.80	1.51	3.16		8.725
W	5.13	3.06				8.56
V	4.53	2.02	0.874			9.49
E	5.07	1.99	2.186			8.60
V	4.233	1.912	0.897			9.13
N	4.397	3.085,2.74				
G	4.108,3.686					
O	4.702	1.78	1.78	3.046		7.75
tBuNle	4.92	1.717	1.241	0.928	0.928 **$(CH_3)_3$**=0.655	
I	4.702	-----	1.40,1.16,0.866	0.866		9.49
L	3.866	1.257	0.350	-.072, -0.361		8.233
Q	4.545	1.83	2.14			8.999
C	5.053	2.936				

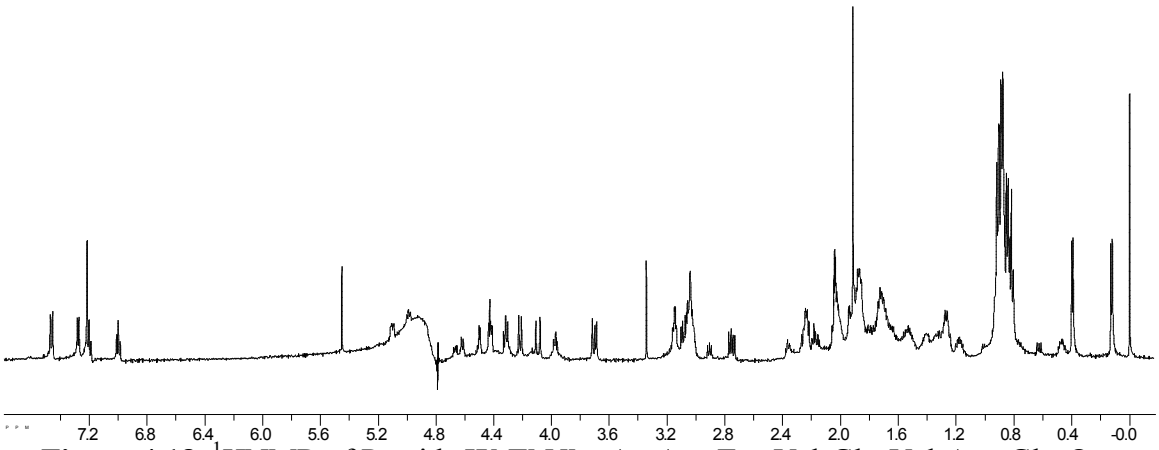

Figure 4.18. [1]HNMR of Peptide **WtFhNle**: Ac-Arg-Trp-Val-Glu-Val-Asn-Gly-Orn-TFhNle-Ile-Leu-Gln-NH2

Table 4.8. Proton Chemical Shift Assignments for Peptide **WtFhNle.**

	α	β	γ	δ	ε	Amide	Amine
R	4.42	1.66	1.53	3.14		8.05	7.12,6.67
W	5.11	3.07				8.33	10.15
V	4.22	1.92	0.90			9.02	
E	4.99	2.02,1.88	2.22			8.57	
V	4.50	2.03	0.87			9.14	
N	4.42	3.08,2.75				9.49	
G	4.096, 3.70					8.63	
O	4.66	1.83	1.75	3.04		7.78	7.64
TFhNle	4.84	1.69	1.30	1.30	1.87	8.48	
I	4.62	1.86	1.41,1.19, 0.88	0.88		9.28	
L	3.98	1.27	0.47	0.13,0.395		8.21	
Q	4.32	2.01,1.86	2.24			8.70	

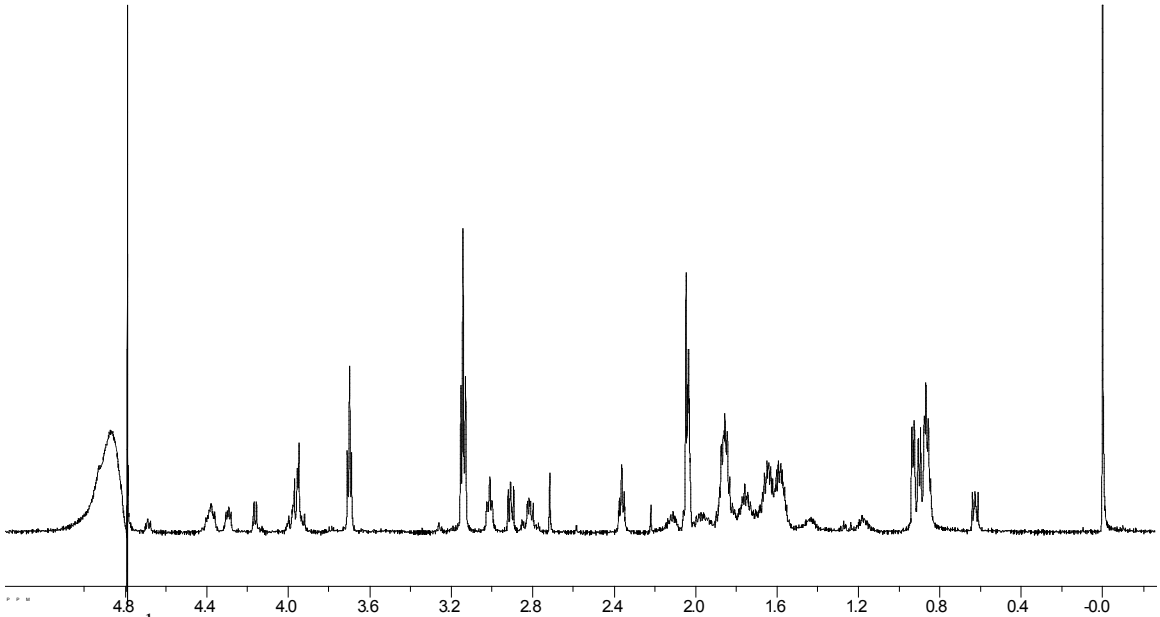

Figure 4.19. [1]HNMR of Peptide **tFhNle7**: Ac-Asn-Gly-Orn-TFhNle-Ile-Leu-Gln-NH2

Table 4.9. Proton Chemical Shift Assignments for Peptide **tFhNle7.**

	α	β	γ	δ	ε	Amide	Amine
N	4.69	2.80				8.43	
G	3.95					8.48	
O	4.40	1.88	1.74	3.01		8.25	7.63
TFhNle	4.29	1.70	1.56	1.43	1.81	8.24	
I	4.16	1.86	1.49,1.18, 0.89	0.89		8.28	
L	4.37	1.88	1.65	0.90		8.34	
Q	4.29	1.97,2.08	2.36			8.32	

Table 4.10. Proton Chemical Shift Assignments for Peptide **WTFhNlecyc**: Ac-Cys-Arg-Trp-Val-Glu-Val-Asn-Gly-Orn-TFhNle-Ile-Leu-Gln-Cys-NH2

	α	β	γ	δ	ε	Amide	Amine
C	5.05	2.96					
R	4.61	1.80	1.67,1.52	3.16		8.70	
W	5.12	3.04				8.58	
V	4.57	1.85	0.87			9.47	
E	5.02	2.03,1.88	2.17				
V	4.23	1.92	0.91			9.13	
N	4.41	3.05, 2.76					
G	4.109, 3.679						
O	4.70	1.80	1.80	3.05			
TFhNle	4.96	1.74	1.38	1.38	1.93		
I	4.70			0.89			9.48
L	3.88	1.26	0.36	-0.04, -0.35			8.24
Q	4.54	2.08,1.84	2.21				9.01
C	5.23	3.00,2.40					

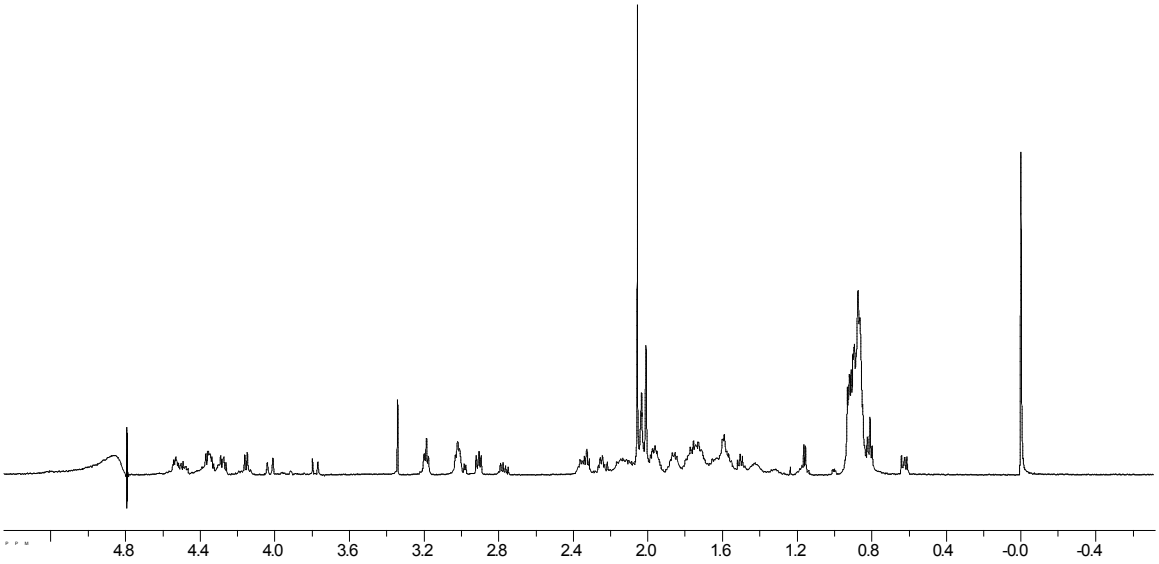

Figure 4.20. [1]HNMR of Peptide **VtFhNle**: Ac-Arg-Val-Val-Glu-Val-Asn-Gly-Orn-tFhNle-Ile-Leu-Gln-NH2

CHAPTER V

INVESTIGATION OF A CITRULLINE-π INTERACTION

A. Background and significance.

Citrullination of proteins (via the deiminiation of arginine) is a post-translational modification that is over-abundant in sufferers of rheumatoid arthritis (RA) (Figure 5.1).[1,2] This transformation is carried out by the enzyme protein arginine deiminase 4 (PAD4), whose activity appears to be under-regulated in the RA disease state. It is proposed that the increase in citrullinated proteins eventually results in the targeting of normal tissue by the immune system.[3] As a result, PAD4 is a target for drug discovery. Small molecule inhibitors of this enzyme could potentially slow the progression of RA or reduce the severity of its symptoms.

---

[1] Luo, Y.; Arita, K.; Bhatia, M.; Knuckley, B.; Lee, Y.; Stallcup, M. R.; Sato, M.; Thompson, P. R. *Biochem.* **2006**, ASAP.

[2] Thompson, P. R.; Fast, W. *ACS Chem. Biol.***2006**, *1*, 433-441.

[3] Utz, P. J.; Genovese, M. C.; Robinson, W. H. *Ann. Rheum. Dis.* **2004**, *63*, 330-332.

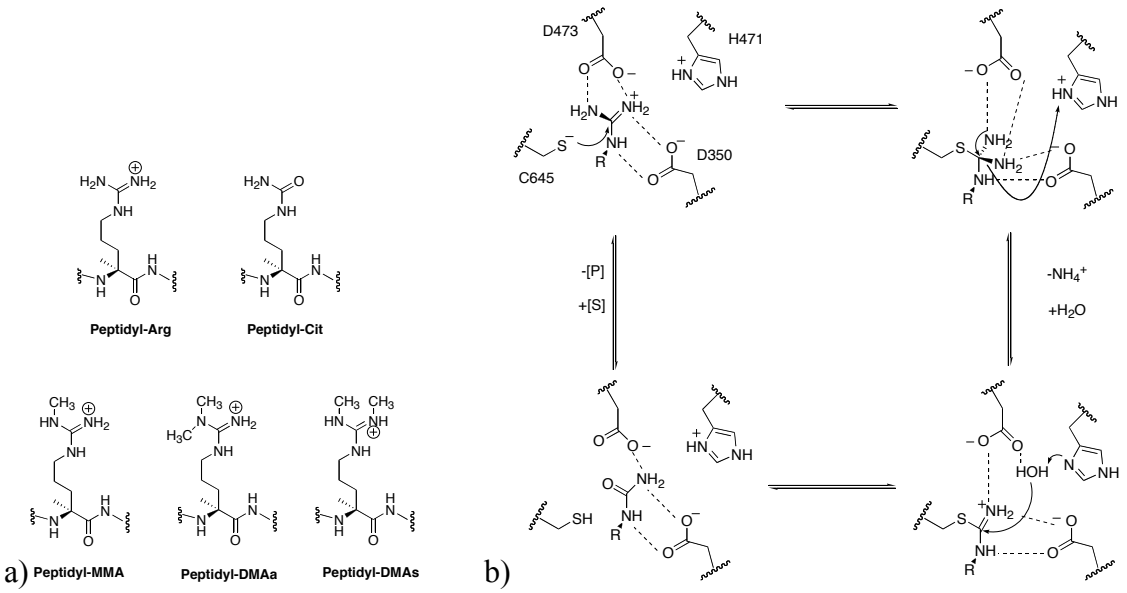

Figure 5.1 (adapted from reference 2) a) Cit, Arg, and methylated Arg sidechains. (b) Proposed mechanism for the deimination of Arg by PAD4.

Under normal physiological circumstances, PAD4 functions as a modifier of histone tails. The modification of arginine and methylated arginine to citrulline in histone tails is a novel and potentially critical portion of the histone code whose significance is still being determined.[4] For instance, it is known that the methylation of arginine in histone tails can lead to transcriptional activiation. While there is no known arginine demethylase, it is possible that citrullination might serve the same purpose, by turning off the methylated arginine signal.[2] Given our recent work in the area of methylated arginine and the cation-π interaction, a logical extension of this work is to examine the interaction between a citrulline residue and a π-system.[5] It is possible the loss of a cation-π

[4] Arita, K.; Shimizu, T.; Hashimoto, H.; Hidaka, Y.; Yamada, M.; Sato, M. *Proc. Nat. Acad. Sci.* **2006**, *103*, 5291-5296.

[5] Hughes, R. M.; Waters, M. L., *J. Am. Chem. Soc.* **2006**, *128*, 12735 – 12742.

interaction between arginine and a binding site lined with aromatic residues, such as the chromodomain, via citrullination may be a key factor in its influence on biological activity. The diminished affinity of citrulline for aromatic groups, in comparison to methylated arginines, would indicate that PAD4 is indeed functioning as a surrogate arginine demethylase.

B. Results and Discussion.

For the sake of comparison, we used the same twelve residue β-hairpin peptide used in our investigation of the Trp-Arg and Trp-DMA interactions discussed in Chapter 2 (Figure 5.2). Substitution of citrulline (Cit) into the same position used for Arg and DMA results in a hairpin that is slightly less well-folded than the peptide WR (80% versus 84%, based on the Gly splitting) (Figure 5.3). As the both peptides are similarly well-folded, they should provide an excellent framework for comparison of the Trp-Arg and Trp-Cit interactions. Furthermore, analysis of the sidechain upfield shifting profile is a key piece of data, since it indicates both proximity and orientation about the aromatic ring (Figure 5.4). One key difference between the Arg and Cit sidechains is the upfield shift of the terminal NH_2 group, indicating a change in geometry. The Arg sidechain is shifted upfield consistently at each position on the guanidinium group, while the Cit sidechain is shifted upfield significantly at the δ and internal NH positions, but not at the terminal NH_2. This is suggestive of a stacking interaction between Arg and Trp, and a non-stacking interaction between Cit and Trp. The precise orientation of this interaction is difficult to determine from our NMR data, but ab initio calculations give some insight into what might be occurring.

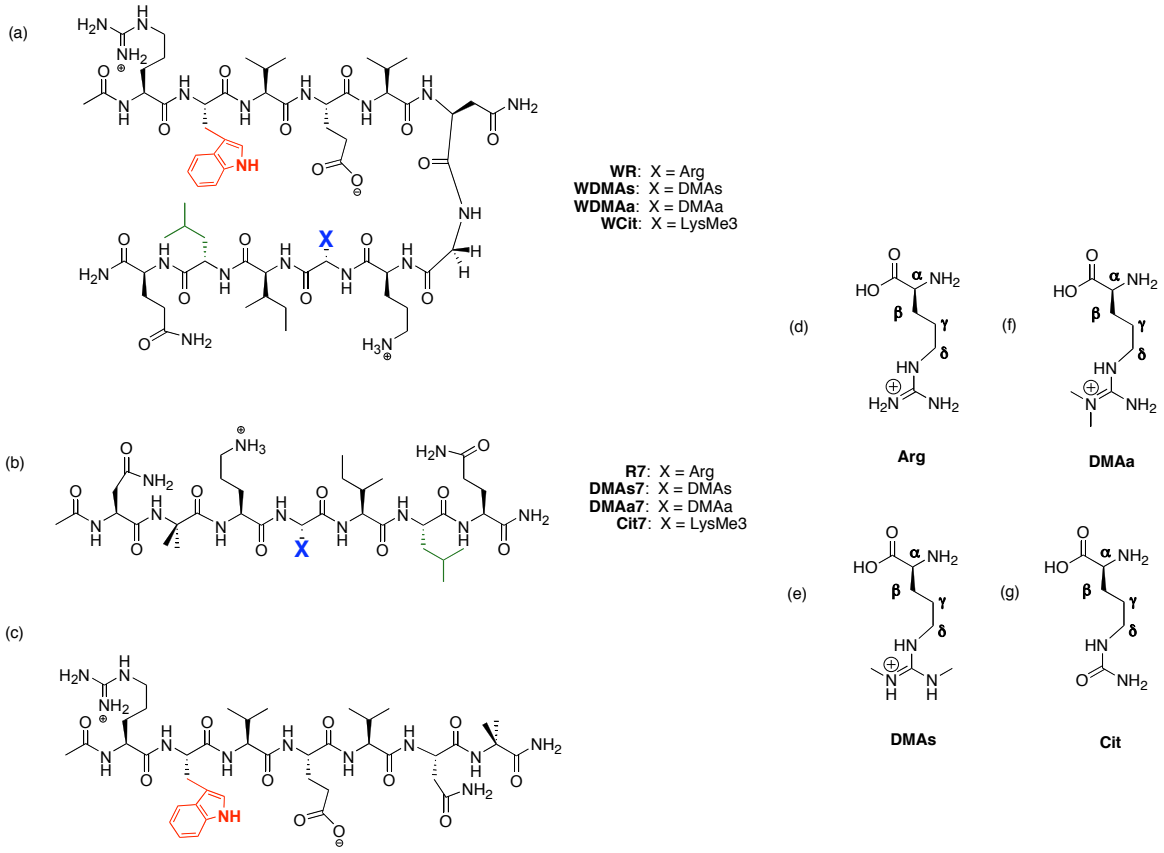

Figure 5.2. β-hairpin peptides used in this investigation.

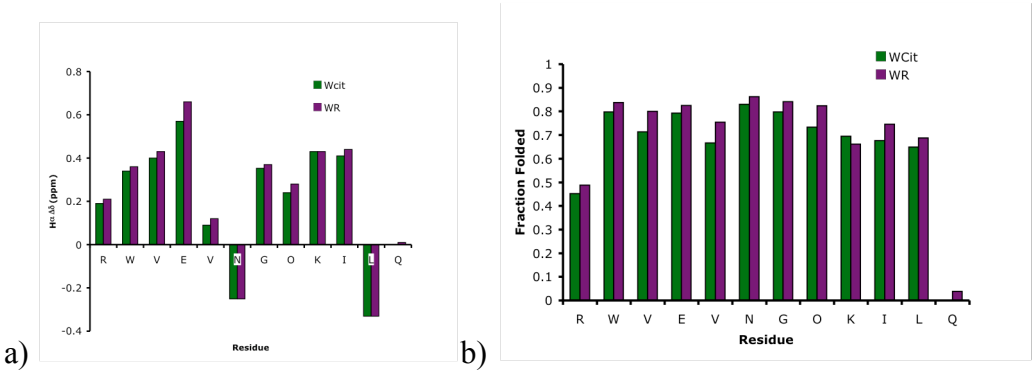

Figure 5.3. a) Hα shifts for **WCit** and **WR** peptides (Gly shifts based on the splitting). b) Fraction folded data for **WCit** and **WR** β-hairpin peptides.

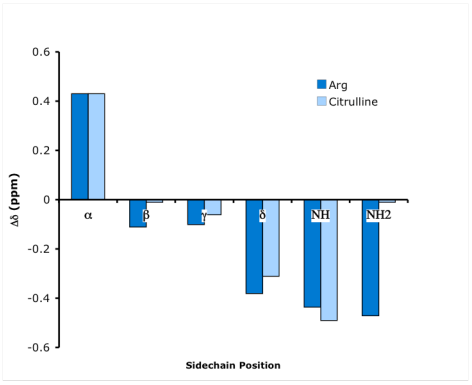

a)

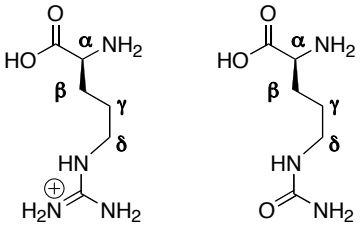

b) **Arg** **Cit**

Figure 5.4. a) Sidechain upfield shifts for Arg and Cit residues relative to random coil. b) Labeled Arg and Cit sidechains.

Starting from stacked conformations, geometry optimizations were undertaken for truncated Trp-Arg and Trp-Cit complexes in the gas phase and in water (implicit solvent; IEFPCM model).[6] The purpose of this experiment is two-fold: 1) to assist in the interpretation of our NMR data, and 2) to highlight the differences between preferred geometries in the gas phase and the aqueous phase. As seen in figure 5.5b and 5.5c, the Trp-Arg and Trp-Cit complexes do not remain stacked in the gas phase, instead preferring T-shaped (Trp-Arg) or V-shaped (Trp-Cit) orientations that maximize the electrostatic interactions (note the NH-O hydrogen bond between the indole NH and the citrulline carbonyl). In the presence of implicit solvent, however, the ligands are expected to balance the solvation effects with orientations that still enable favorable electrostatic contact with the Trp ring and hydrogen-bonding interactions with water. The results of our calculations are shown in figure 5.5d and 5.5e, and are consistent with the upfield shifting profiles seen in our NMR data in aqueous solution: the Arg remains stacked with Trp in order to maintain the cation-π interaction and hydrogen-bond with solvent, while the Cit is optimized to a conformation that

[6] Gaussian 03 (B04). Frisch, M. J., et al.

enables a polar-π interaction with the face of the indole ring while solvating the carbonyl and the terminal NH_2 group. Further calculation of the interaction energies between the complexes at the MP2/6-31g** level shows that the Arg-Trp stacked interaction (-2.95 kcal/mol) in implicit water is worth more than the Cit-Trp V-shaped interaction (-0.55 kcal/mol) (see Experimental section for details). Perhaps most importantly, the Cit-Trp stacking interaction in implicit water is repulsive (+2.88 kcal/mol), which suggests that the Cit-Trp orientation shown in 5.5c is a likely preferred orientation for the two sidechains within the folded β-hairpin.

a)

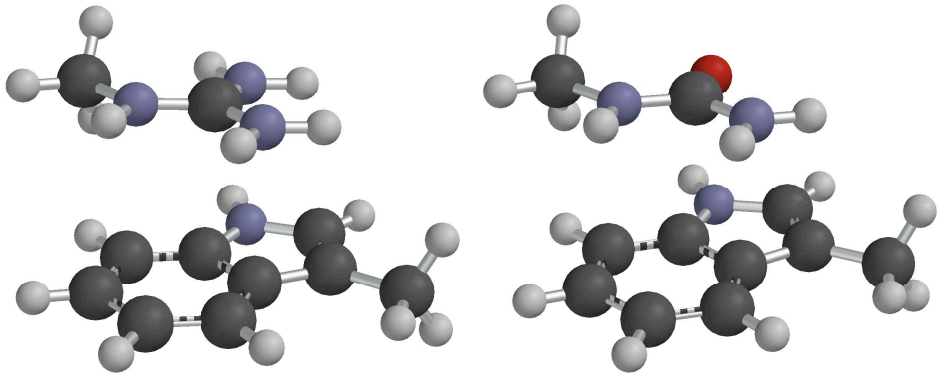

b)

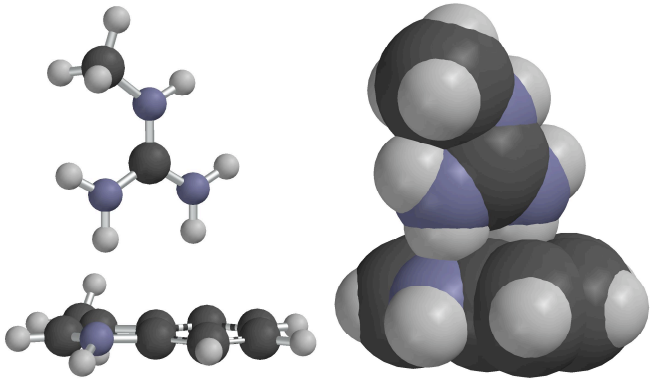

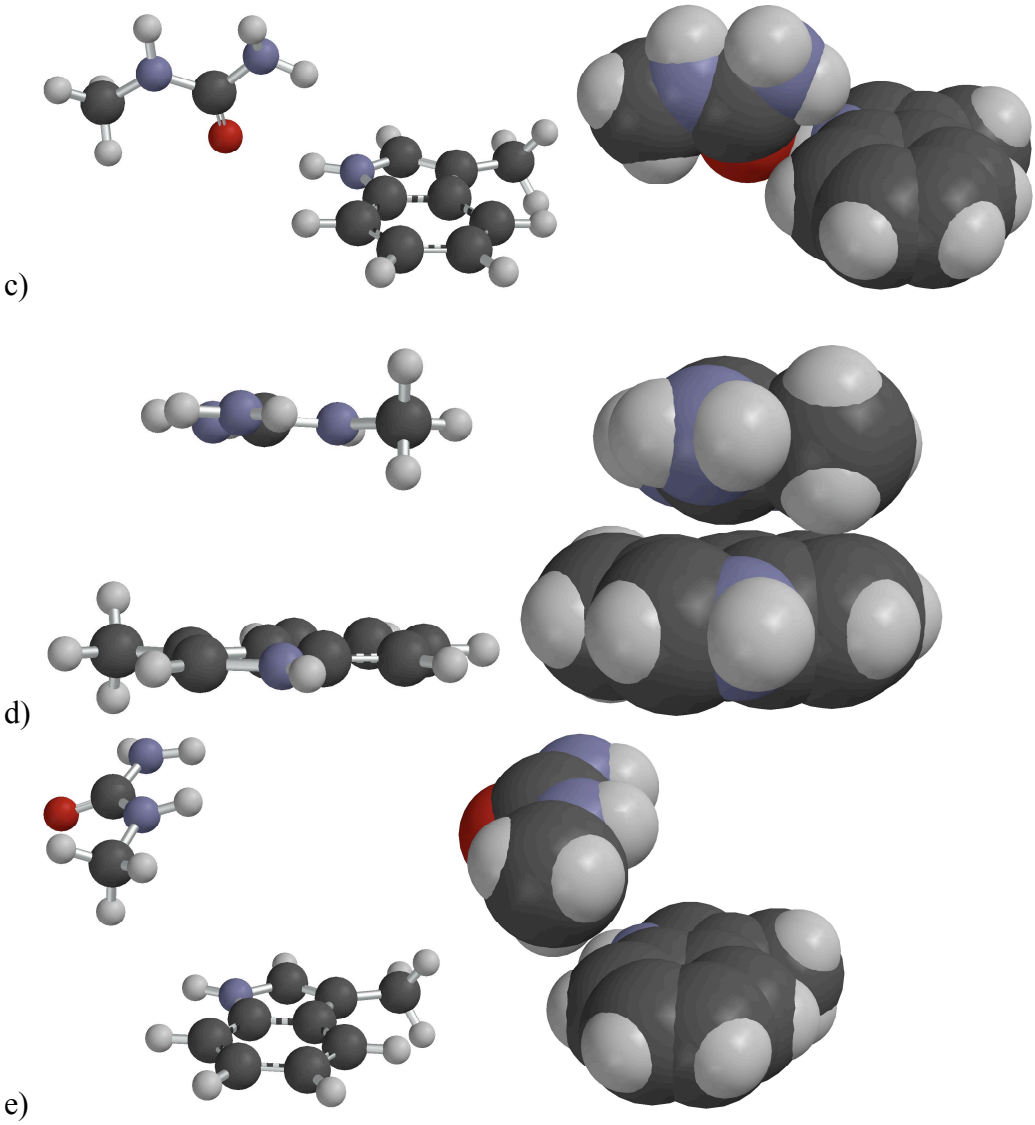

Figure 5.5. (a) Starting orientations for geometry optimizations of Trp-Arg and Trp-Cit complexes. (b) Results for gas phase optimization of Trp-Arg. (c) Results for gas phase opitimization of Trp-Cit. (d) Results for aqueous phase optimization of Trp-Arg. (e) Results for aqueous phase optimization of Trp-Cit. (Gaussian 03; HF/6-31g**; CPCM Implicit solvation model). Space filling models are shown to demonstrate proximity via Van der Waals contacts.

Comparison of the upfield shift profiles of Cit and methylated arginines DMAa and DMAs further demonstrates the difference between the interaction of the deiminated ligand with Trp (Figure 5.6). While the methyl groups of DMA are significantly upfield shifted, indicating stacking with the aromatic ring, the upfield shifting profile of Cit

shows more upfield shifting at the internal amide proton, indicating that it is likely not in a stacked orientation with the aromatic ring. Based on this data, it is clear that deimination of either DMAa or DMAs *in vivo* would eliminate the favorable stacking interaction with aromatic groups by substituting it with a lower affinity interaction (such as an amide-π interaction). To support this hypothesis, double mutant cycles were conducted in order to quantify the Trp-Cit interaction. This gave a value of -0.21 kcal/mol for the interaction. This is in contrast to a value of -0.5 kcal/mol for the Arg-Trp interaction and -1.0 kcal/mol for the DMA-Trp interactions (see Chapter 2). Based on this data, it is certainly possible that citrullination modulates transcription by weakening the interaction between histone tails and transcriptional cofactors such as chromodomains, which bind DMA via cation-π interactions.

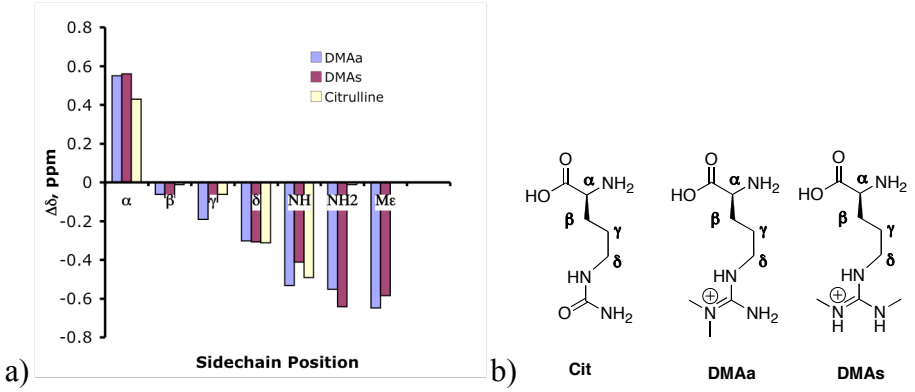

Figure 5.6. a) Comparison of upfield shifts for Cit, DMAa, and DMAs. b) Labeled Cit, DMAa, and DMAs sidechains.

Additionally, the thermodynamics of β-hairpin folding were investigated with VT-NMR (Figure 5.7; Table 5.1). Based on our thermal denturation data, it appears that, while there are small differences in the thermodynamics of folding between **WCit** and **WR**, that the values for entropy, enthalpy and heat capacity are within error. The primary differences occur when comparing the folding dynamics of **WCit** and the DMA-

containing peptides, where a more favorable entropy and heat capacity of folding are the primary differences upon going from Cit to the DMA ligands. These changes are consistent with the deimination of DMA resulting in a diminished interaction with Trp. Again, it might be gathered from this data that the deimination of methylated Arg to Cit in histone tails is a key signal for transcriptional deactivation via the decreased binding affinity of Cit with aromatic rings.

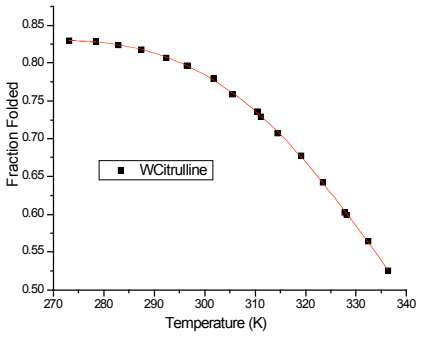

Figure 5.7 Thermal denaturation profile for peptide **WCit**.

Table 5.1. Thermodynamic Parameters[a] for Hairpin Folding at 298 K.

Peptide	ΔH°	ΔS°	$\Delta C_p°$
WCit	-3.6 (0.1)	-9.5 (0.2)	-176 (26)
WR	-3.7 (0.1)	-9.1 (0.2)	-193 (29)
WDMAs	-2.4 (0.2)	-2.6 (0.8)	-409 (61)
WDMAa	-2.3 (0.1)	-2.1 (0.4)	-355 (53)

(a) Determined from the temperature dependence of the Gly chemical shift from 0 to 80 °C. Units are: DH°: kcal/mol; DS°: cal/mol K; $DC_p°$: cal/mol K. Errors (in parentheses) are determined from the fit. Error for $DC_p°$ values from equation 9 estimated at 15%.

C. Conclusion.

The interaction between Cit and Trp has been compared to the interaction between Arg and Trp. These sidechains are related through the enzyme PAD4 and their proposed roles in the histone-mediated transcription of DNA. While subtle differences exist between the interaction of Arg and Cit with aromatic rings, it appears that the Cit-Trp interaction falls into the camp of polar-π interactions, such as those observed between acylated Lys and Trp, while the Arg-Trp interaction has definite cation-π character. It is apparent that both sidechains, in addition to undergoing favorable interactions with π-systems, can undergo numerous H-bonding interactions with other sidechains or with solvent molecules. This can be a complicating factor when analyzing their individual effects on the folding of our β-hairpin model system. Nonetheless, it is clear that the Trp-Arg interaction is slightly more favorable than the Trp-Cit interaction. Since the citrullination of methylated Args is also possible, the most important differences may be between the Trp-DMA and Trp-Cit interactions, since the Trp-DMA interactions are clearly more favorable. This lends credibility to the idea that PAD4 may function as a substitute arginine demethylase. Overall, analysis of the Trp-Cit interaction enables us to better place studies of the Arg-π interaction within the grand and complex context of the "histone code."

D. Experimental.

Table 5.2. Thermal denaturation data for peptide **WCit**.

Temperature (K)	Fraction Folded
273.12	0.829
278.51	0.828
282.95	0.823
287.51	0.818
292.41	0.806
296.51	0.796
301.83	0.779
305.51	0.759
310.47	0.736
311.16	0.729
314.51	0.707
319.15	0.677
323.51	0.642
327.74	0.602
328.18	0.599
332.51	0.564
336.42	0.525

Calculation of Interaction Energies.

The complexes shown in Figure 5.5 were optimized at the HF/6-31g** level in Gaussian 03 (B04). Interaction energies were determined via single point calculations at the MP2/6-31g** level (SCRF=IEFPCM; SOLVENT=WATER; SCF=TIGHT) using the equation below:

$$\Delta E_{MP2} = E_{A\text{-}B} - E_A - E_B$$

Where $E_{A\text{-}B}$ is the MP2 energy of the optimized complex, E_B is the MP2 energy of optimized monomer B, and E_A is the MP2 energy of optimized monomer A.

Table 5.3. Values used to calculate interaction energies for complexes in Figure 5.5.

	Warg_Stack	Wcit_Stack	Wcit_V
Complex	-646.36	-665.73	-665.73
Arg	-244.45		
Cit		-263.83	-263.83
Trp	-401.90	-401.90	-401.90
ΔE (hartrees)	-0.0047	0.0046	-0.0009
ΔE (kcal/mol)	-2.95	2.88	-0.56

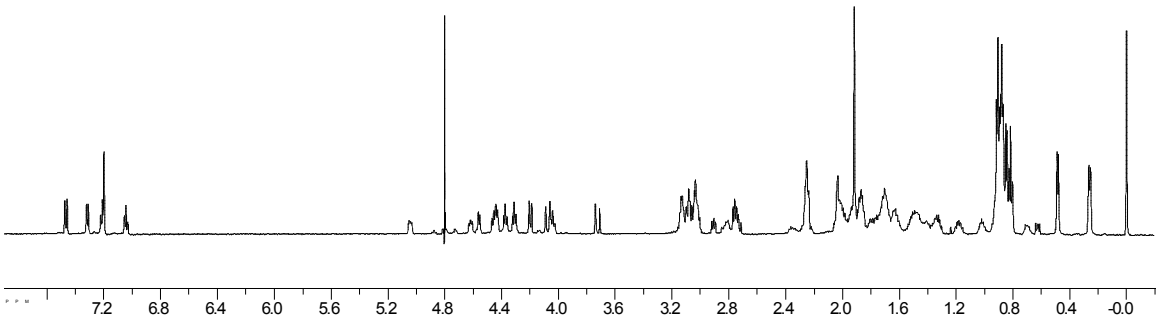

Figure 5.8. [1]HNMR of Peptide **WCit**: Ac-Arg-Trp-Val-Glu-Val-Asn-Gly-Orn-Cit-Ile-Leu-Gln-NH2

Table 5.4. Proton Chemical Shift Assignments of Peptide **WCit.**

	α	β	γ	δ	ε	Amide	Amine
R	4.37	1.62	1.54	3.13		8.05	6.65,7.12
W	5.04	3.10	7.311,7.466	7.043,7.209	7.199	8.32	10.12
V	4.42	1.98	0.85			8.95	
E	4.86	2.00	2.23			8.49	
V	4.19	1.97	0.90			8.88	
N	4.45	2.98,2.68				9.365	
G	4.076,3.7235					8.607	
O	4.61	1.80	1.77	3.01		7.83	7.65
Cit	4.75	1.61	1.51	2.79		8.482	5.80
I	4.54	1.88	1.30,0.87	0.87		9.07	
L	4.07	1.28	------	0.485,0.260		8.27	
Q	4.31	1.90	2.24			8.646	

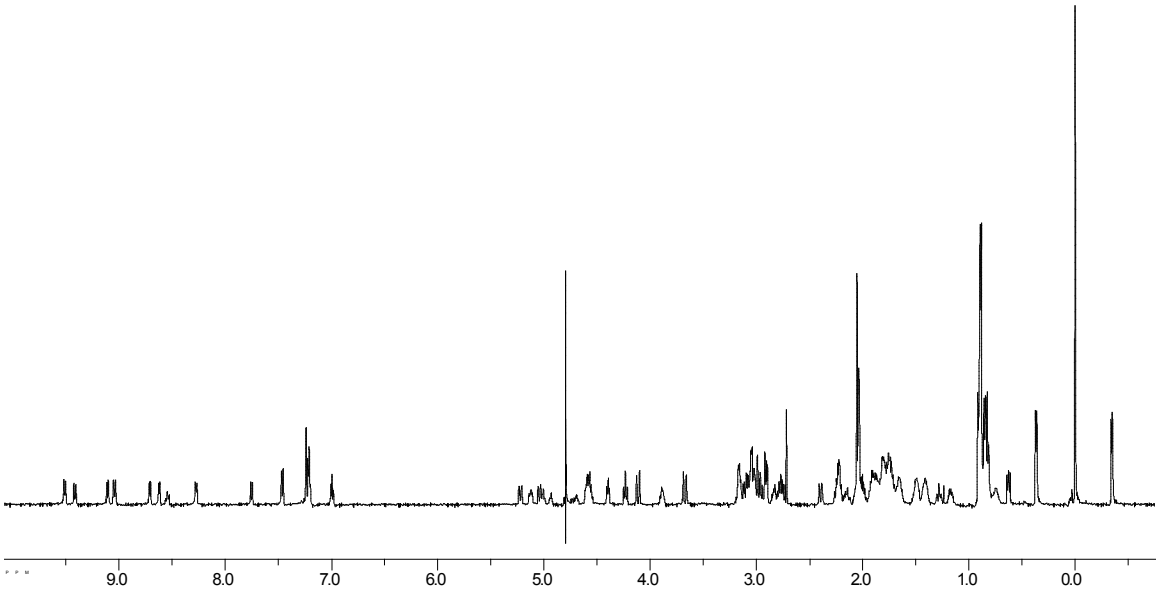

Figure 5.9. [1]HNMR of Peptide **WCitCyc**: Ac-Cys-Arg-Trp-Val-Glu-Val-Asn-Gly-Orn-Cit-Ile-Leu-Gln-Cys-NH2

Table 5.5. Proton Chemical Shift Assignments of Peptide **WCitCyc.**

	α	β	γ	δ	ε	Amide	Amine
C	5.048	3.00					
R	4.60	1.806	1.66,1.502	3.166		8.712	
W	5.126	3.033				8.618	
V	4.580	2.06	0.869			9.517	
E	5.009	1.947	2.228			8.54	
V	4.235	1.931	0.908			9.111	
N	4.399	3.12,2.759					
G	4.114,3.6725						
O	4.697	1.77	1.77	3.05		7.759	
Cit	4.939	1.689	1.470	2.814			
I	4.736	1.86	1.416,1.18,0.884	0.884		9.415	
L	3.8921	1.291	0.742,0.369	0.0406, -0.342		8.275	
Q	4.57	1.82	2.142			9.048	
C	5.23	2.96,2.39					

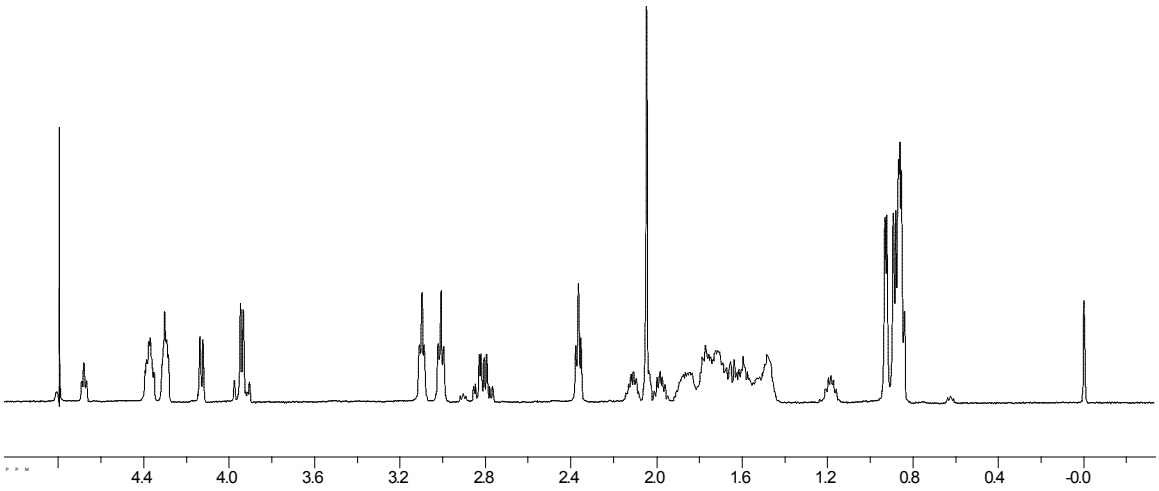

Figure 5.10. [1]HNMR of Peptide **Cit7mer**: Ac-Asn-Gly-Orn-Cit-Ile-Leu-Gln-NH2

Table 5.6. Proton Chemical Shift Assignments of Peptide **Cit7mer.**

	α	β	γ	δ	ε	Amide	Amine
N	4.68	2.84				8.428	
G	3.942					8.561	
O	4.37	1.76	1.76	3.01		8.138	7.64
Cit	4.32	1.62	1.57	3.10		8.29	6.29
I	4.13	1.83	1.37	0.91		8.248	
L	4.40	1.68	0.914	0.914		8.342	
Q	4.31	2.00	2.37			8.342	

CHAPTER VI

EXPERIMENTAL AND COMPUTATIONAL INVESTIGATION OF A β-HAIRPIN RECEPTOR FOR ATP

A. Background and significance.

Protein-nucleotide interactions have been studied for quite some time, as indicated by the presence of nearly 6,000 structures of protein-DNA complexes in the Protein Data Bank (http://www.pdb.org). A more recent challenge that has been undertaken by a number of researchers is the design of peptidic and peptidomimetic receptors for individual nucleotides (ATP, GTP, TTP, CTP), and single and double stranded DNA.[1] Particularly challenging is the development of receptors with both high affinity and selectivity between different nucleotides. This is an important goal that has potential applications in the study of DNA base-repair enzymes, assays for use in

[1] a) Cooper, W. J.; Waters, M. L. *Curr. Op. Chem. Biol.* **2005,** 9, (6), 627-631. b) Imanishi, M.; Yan, W.; Morisaki, T.; Sugiura, Y. *Biochem. Biophys. Res. Comm.* **2005,** 333, (1), 167-173. c) Hirata, A.; Ueno, M.; Aizawa, Y.; Ohkubo, K.; Morii, T.; Yoshikawa, S. *Bioorg. Med. Chem.* **2005,** 13, (9), 3107-3116. d) Butterfield, S. M.; Sweeney, M. M.; Waters, M. L. *J. Org. Chem.* **2005,** 70, (4), 1105-1114. e) Luedtke, N. W.; Liu, Q.; Tor, Y. *Biochemistry* **2003,** 42, (39), 11391-11403. f) Hastings, C. A.; Barton, J. K. *Biochemistry* **1999,** 38, (31), 10042-10051.g) Aizawa, Y.; Sugiura, Y.; Ueno, M.; Mori, Y.; Imoto, K.; Makino, K.; Morii, T. *Biochemistry* **1999,** 38, (13), 4008-4017. h) Aizawa, Y.; Sugiura, Y.; Morii, T. *Biochemistry* **1999,** 38, (5), 1626-1632. i) Okahata, Y.; Niikura, K.; Sugiura, Y.; Sawada, M.; Morii, T. *Biochemistry* **1998,** 37, (16), 5666-5672. j) Lescrinier, T.; Hendrix, C.; Kerremans, L.; Rozenski, J.; Link, A.; Samyn, P.; Van Aerschot, A.; Lescrinier, E.; Eritja, R.; Van Beeumen, J.; Herdewijn, P. *Chemistry-a European Journal* **1998,** 4, (3), 425-433. k) Nolte, A.; Klussmann, S.; Bald, R.; Erdmann, V. A.; Furste, J. P. *Nature Biotechnology* **1996,** 14, (9), 1116-1119. l) Cheng, X.; Kay, B. K.; Juliano, R. L. *Gene* **1996,** 171, (1), 1-8. m) Sardesai, N. Y.; Zimmermann, K.; Barton, J. K. *J. Am. Chem. Soc.* **1994,** 116, (17), 7502-7508.

chemical biology, and the development of peptide-based therapeutics for gene therapy. One exciting development in this field has been the development of a β-hairpin receptor for various nucleotides (ATP, GTP, TTP, CTP) and single stranded DNA.[2] This water-soluble, monomeric β-hairpin has been shown to bind ssDNA with an affinity rivaling that of proteins (Figure 6.1).

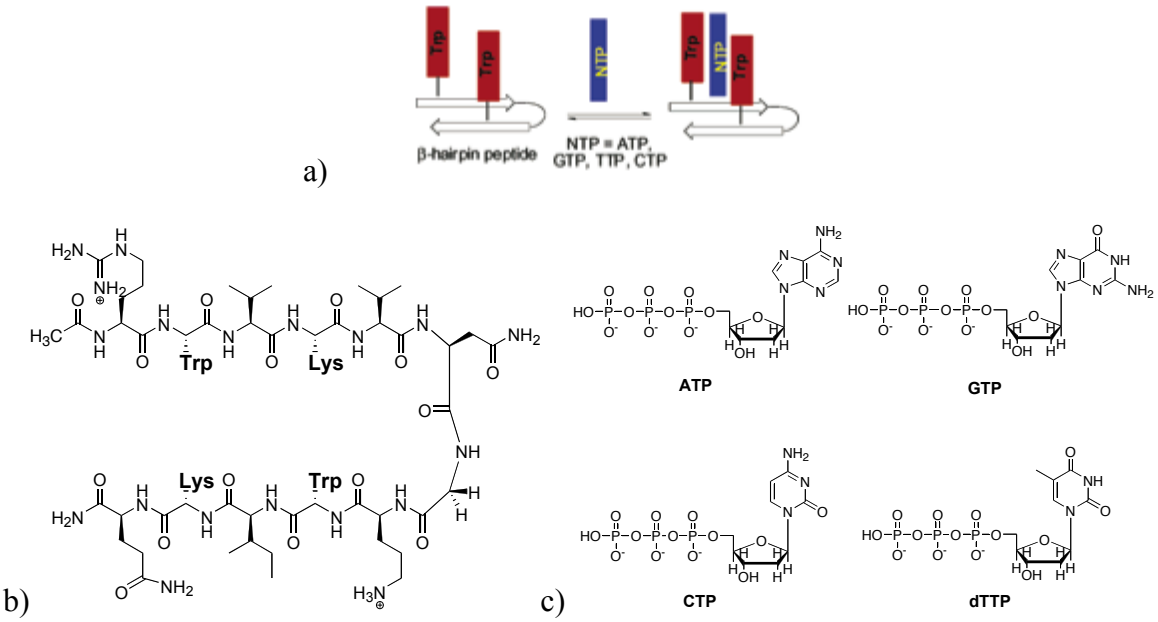

Figure 6.1 (a) Schematic of β-hairpin nucleotide binding interaction. (b) Structure of WKWK, a receptor for ATP. (c) Structures of various nucleotides.

Efforts to make this receptor highly selective for ATP over various other nucleotides have been met with varying degrees of success,[2] perhaps due to a limited body of knowledge regarding the finer structural details of the β-hairpin receptor itself. In

[2] Butterfield, S. M.; Sweeney, M. M.; Waters, M. L., *Journal of Organic Chemistry* **2005,** 70, (4), 1105-1114.

this study, we set out to further characterize the hairpin structure through a series of computational and experimental efforts designed to give insight into the mechanism of ATP binding (based on computationally determined β-hairpin structure) and the potential for enhancing the selectivity of the receptor based on the acquired structural knowledge.

Earlier studies conducted by Butterfield and Waters showed the fundamental importance of the Trp and Lys residues to the binding of ATP. Mutation of the Trp residues to smaller aromatics significantly decreased the affinity of the receptor for ATP. Based on the degree of upfield shifting (observed by NMR) of the adenine ring in the presence of the β-hairpin, as well as the quenching of Trp fluorescence in the presence of ATP, it is inferred that π-π stacking interactions between the Trp ring and the adenine ring are important to the binding of ATP. Also important are electrostatic interactions between the negatively charged phosphate tail of ATP and the positively charged residues Lys residues on the β-hairpin. This was demonstrated by the mutation of Lys residues to neutral Thr, which decreased the binding affinity for ATP by a factor of 20, indicating that each Lys-phosphate interaction is worth about -1.5 kcal/mol per Lys.[2] Comparison of the ATP binding affinity to ADP and AMP gave similar results. Overall, this data corresponds well to what has been observed in data mining surveys of ATP-binding proteins: hydrogen bonding, π-π stacking, and cation-π interactions all contribute to ATP binding. One survey of 68 high-resolution crystal structures of ATP-binding proteins found, on average, 2.7 hydrogen bonds, 1.0 π-π stacking interactions, and 0.8 cation-π interactions per ATP-protein complex.[3]

[3] Mao, L.; Wang, Y.; Liu, Y.; Hu, X. *J. Mol. Biol.* **2004**, *336*, 787-807.

B. Results and Discussion.

Determination of WKWK NMR Structure. Initial efforts at predicting the structure of **WKWK** were based on an existing β-hairpin NMR structure of a trpzip peptide available from the PDB (PDB ID:1LE1). This structure was taken from the PDB, and its residues modified using Sybyl to match the sequence **WKWK**. The sequence was subsequently minimized and subjected to MD simulation in explicit water using the molecular dynamics (MD) program GROMACs.[4] MD simulations were carried out using this equilibrated structure in the presence of ATP and AMP. These studies indicated the potential importance of electrostatic contacts between other positively charged residues in the β-hairpin (Orn8 and Arg1, Fig 6.1b), in addition to the already characterized Lys residues. While simulations using this model structure were initially useful, it was important to have a structure determined from our NMR data for the sake of accuracy, and to insure that our initial assumptions regarding the structure of **WKWK** were correct.

Using the program CNS_Solve,[5] and all available NMR data (NOEs, ^{1}H chemical shifts, J^{3} coupling constants), the experimentally determined structure of **WKWK** matched well with our initial computationally determined structure (Figure 6.2a). We used this NMR structure for all future simulation work. Both our "hacked" structure and our NMR structure revealed that the orientation of the Trps in our ATP receptor were different than those in the trpzip peptide (Figure 6.2b). In fact, the Trps are

[4] Lindahl. E.; Hess, B.; van der Spoel, D. J. Mol. Mod. **2001**, *7*, 306-317.

[5] Brunger, A.T.; Adams, P.D.; Clore, G.M.; Delano, W.L.; Gros, P.; Grosse-Kunstleve, R.W.; Jiang, J.-S.; Kuszewski, J.; Nilges, N.; Pannu, N.S.; Read, R.J.; Rice, L.M.; Simondson, T.; Warren, G.L. *ACTA CRYST.* **1998**, *D54*, 905-921.

not unlike those of the aromatic groups found in β-sheets in WW domain proteins, which contain two highly conserved Trp residues (Fig. 6.2c). Initial assessment of this structure indicated that it presents a large recognition surface for the adenine moiety of ATP with a number of potential points for electrostatic contacts with the triphosphate tail (Lys, Orn, Arg).

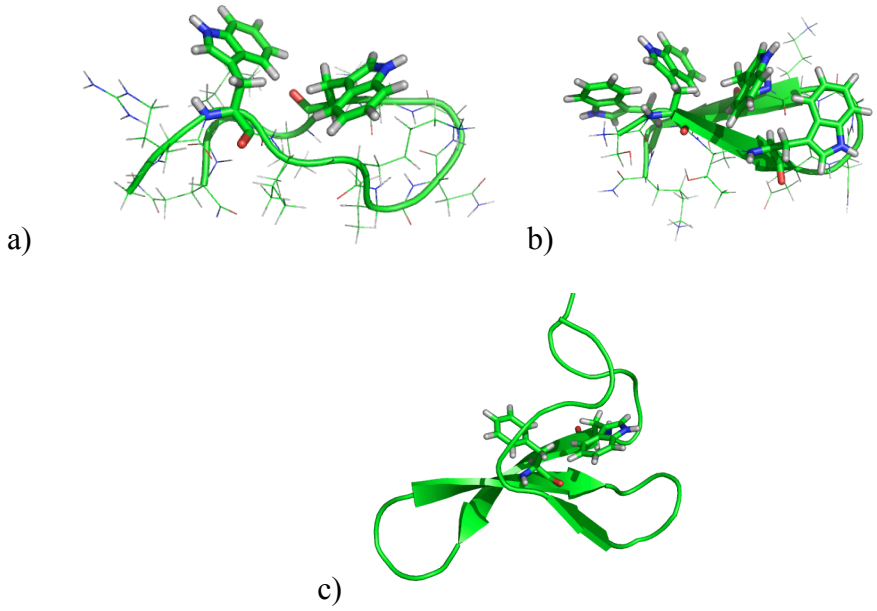

Figure 6.2. (a) Average NMR structure of **WKWK**. (b) NMR structure of trpzip peptide (1LE1). (c) Aromatic group orientation in WW domain (1K94).

WKWK Mutations. A series of mutations to WKWK were chosen based on the initial MD simulations and the experimentally determined structure of the β-hairpin. Manual docking of ATP with the hairpin in Sybyl (manual rotation and translation of ATP within the binding pocket of the NMR structure) shows a variety of potential orientations during which the ATP can simultaneously obtain π-π stacking interactions

with the Trp rings and maintain electrostatic contact with a positively charged residue (Figure 6.3a). Mutations were chosen to test the effect of neutralizing these residues to determine if indeed they were equally important to the binding of ATP, regardless of their location within the hairpin structure (Table 6.1; Figure 6.4).

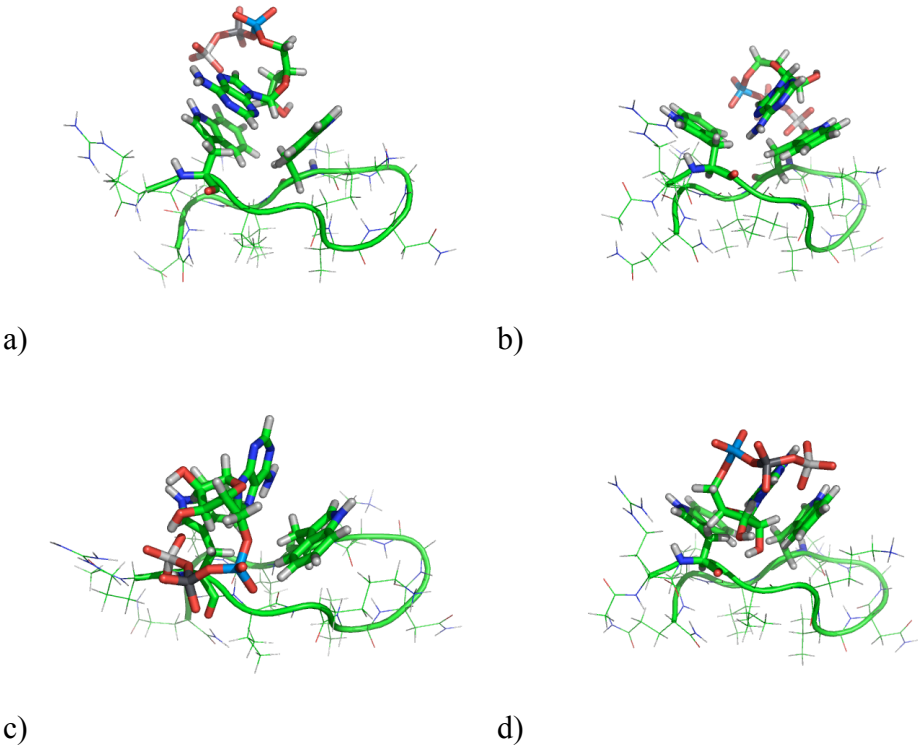

Figure 6.3 (a-d). Possible orientations of ATP in **WKWK** binding pocket.

Table 6.1. Selected mutations for peptide **WKWK**.

Name	Sequence	Position of Mutation
WKWK	Ac-**R**-W-V-**K**-V-N-G-**O**-W-I-**K**-Q-NH_2	-----
O8Q	Ac-R-W-V-K-V-N-G-**Q**-W-I-K-Q-NH_2	**8**
O8T	Ac-R-W-V-K-V-N-G-**T**-W-I-K-Q-NH_2	**8**
O8Dab	Ac-R-W-V-K-V-N-G-**Dab**-W-I-K-Q-NH_2	**8**
O8K	Ac-R-W-V-K-V-N-G-**K**-W-I-K-Q-NH_2	**8**
R1Cit	Ac-**Cit**-W-V-K-V-N-G-O-W-I-K-Q-NH_2	**1**
K4Q	Ac-R-W-V-**Q**-V-N-G-O-W-I-K-Q-NH_2	**4**
K11Q	Ac-R-W-V-K-V-N-G-O-W-I-**Q**-Q-NH_2	**4**

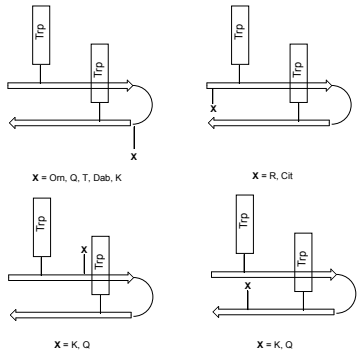

Figure 6.4. Positions of mutant sites in **WKWK** hairpin.

Each selected mutation requires some degree of explanation. The Orn residue at position 8 in the turn of the β-hairpin is not on the binding face of the receptor (Fig. 6.4). Therefore, it was not initially thought to be important to binding. However, initial manual docking studies and MD simulations suggested otherwise. For this reason, Orn was mutated to the neutral residue Gln, and was tested for potential distance dependence of the interaction via the residues Lys (one methylene longer) and Dab (one methylene shorter). For the sake of consistency, the mutation **O8T** was studied, since Thr was used original mutation selected for the Lys residues in the initial studies.[2] To investigate the electrostatic contribution of Arg to binding, Citrulline was selected as the most logical mutation for Arg, since they are structurally similar, enabling Cit to be a neutral replacement for Arg (See Chapter 5). Furthermore, the mutants **K4Q** and **K11Q** were chosen for comparison to the original mutants of Butterfield and Waters **K4T** and **K11T**, since more recent studies suggested that Thr might be a poor choice for as mutation for Lys because of its lower β-sheet propensity.[6]

[6] (a) Cochran, A.G.; Tong, R. T.; Starovasnik, M. A.; Park, E. J.; McDowell, R. S.; Theaker, J. E.; Skelton, N. J. *J. Am. Chem. Soc.* **2001**, *123*, 625 – 632. (b) Russell, S. J.; Blandl, T.; Skelton, N.; Cochran, A. G. *J. Am. Chem. Soc.* **2003**, *125*, 388 – 395.

Binding studies for WKWK and mutants. Binding studies were conducted for **WKWK** and the mutant hairpins with both AMP and ATP. The binding of AMP was measured by NMR due to the weaker AMP binding constants, which required higher concentrations of receptor and nucleotide. The binding of ATP was measured by the change in fluorescence of the Trp residues, which allowed for the use of lower concentrations of both receptor and nucleotide. Binding of AMP to the mutant hairpins indicated, not surprisingly, that the binding affinity of the receptor was diminished for the neutralized mutants **R1Cit** and **O8Q**. Interestingly, the mutation of Orn to Lys or Dab also diminished binding to AMP relative to the parent sequence **WKWK**. This effect may be due to conformational effects due to replacing Orn in the turn of the hairpin, and will be addressed later in this chapter.

Table 6.2. Binding affinities for AMP (determined by NMR titration)

Peptide	K_d (M^{-1})	ΔΔG (kcal/mol)
WKWK*	6.90 ± 0.1	(-2.95)
O8Dab	12.8 ± 0.1	+0.37
O8K	11.9 ± 0.1	+0.33
O8Q	15.6 ± 0.2	+0.49
R1Cit	18.2 ± 0.1	+0.58

**matches S.B. value*

ATP binding studies with the **WKWK** mutants show similar trends in the data, although binding of the triphosphate shows clearer differences between closely related

mutant sequences. Some trends from the AMP binding studies remain the same (**O8Dab** and **O8K** bind ATP more poorly than **WKWK**), while others show intriguing differences. While the **O8Q** mutant decreases binding affinity for ATP by 0.73 kcal/mol, the **R1Cit** mutant only decreases binding by 0.27 kcal/mol. One might expect this ATP-hairpin interaction to be subject to the polyelectrolyte effect, in which change in the charge state of the receptor will decrease binding affinity by approximately the same amount.[7] However, it appears that structure, rather than the charge state of the receptor alone, is playing a key role in determining the important electrostatic contacts between the peptide and ATP. As a result, the unstructured N-terminus of the hairpin (R1) plays less of a role in binding than do charged residues in the structured regions of the hairpin (K4, O8, K11). This is supported by our NMR data, which shows little hairpin structure at the terminal residues (discussed in next section). Additionally, our set of Thr mutants (**O8T**, **K4T**, **K11T**) display lower binding affinities than their corresponding Gln mutants (**O8Q**, **K4Q**, **K11Q**). Again, this may be related to structure changes of the receptor due to the lower β-sheet propensity of Thr. These differences in binding affinities are of some significance. The Lys to Gln mutants predict an average value of 0.94 kcal/mol for each Lys-ATP interaction, while the Lys to Thr mutants predict an average value of 1.43 kcal/mol for each Lys-ATP interaction. Butterfield and Waters estimated the contribution of the Trp-Adenine aromatic interaction to be 1.8 (± 0.2) kcal/mol based on salt studies with ATP and AMP. By comparison, assuming that the interaction energy is divided equally among the two Trp(s) in the receptor, a single Trp-Adenine interaction appears to

[7] Zhang, W.; Bond, J. P.; Anderson, C. F.; Lohman, T. M.; Record, M. T. *Proc. Nat. Acad. Sci. USA* **1996,** *93*, (6), 2511-2516.

be nearly equal in magnitude to a phosphate-Lys interaction (both are approximately 0.9 kcal/mol). This establishes a benchmark for the enhancement of nucleotide affinity. Since all the interactions are approximately equal, the path to selectivity may wind through the enhancement of one interaction over the other. Since the electrostatic interaction between the positively charged residues and the phosphate tail is largely non-specific, the most promising option for selectivity may be enhancement of the electrostatic complimentarity between Trp (likely via a non-natural surrogate) and aromatic functionality of the nucleotide.

Table 6.3. Binding affinities for ATP (determined by fluorescence titration)

Peptide	K_d (μM)	ΔΔG (kcal/mol)
WKWK*	303 ± 22	(-3.38)
O8Dab	387 ± 28	+0.14
O8K	384 ± 40	+0.14
O8Q	1047 ± 56	+0.73
O8T	1765 ± 103	+1.04
R1Cit	479 ± 75	+0.27
WQWK	1655 ± 140	+1.01
WKWQ	1294 ± 105	+0.86
WTWK†	3789 ± 344	+1.50
WKWT†	3014 ± 184	+1.36

*Differs from initial K_d determined for **WKWK** (170 uM). †K_d determined by S. B.

NMR characterization of WKWK mutants. One and two-dimensional NMR techniques were used to characterize the structure of the **WKWK** mutants. As seen below, the H_α shifts of the mutant hairpins compare well with those of the parent sequence **WKWK**, indicating that all mutant sequences still retain β-hairpin structure (Figure 6.5). However, some of the hairpins (**O8T**, for instance) show less H_α shifting than the native sequence indicating a lower β-hairpin population. Table 6.4 shows that the hairpins are all equally well folded based on the Gly splitting (within experimental error), with the exception of **O8T**, which is slightly less well folded (90%).

Figure 6.5. Hα shifts for **WKWK** and selected mutant peptides.

Table 6.4 Fraction folded (taken from Gly splitting)

Peptide	Fraction Folded
WKWK	0.96
O8K	0.96
O8Dab	0.94
O8Q	0.93
O8T	0.90
R2Cit	0.95
K11Q	0.96
K4Q	0.94

Error in fraction folded is ± 1%.

It is clear that the presence of Thr in the β-hairpin is slightly more destabilizing to the hairpin than Gln as a substitution for a positively charged residue (Lys or Orn). It is proposed that these changes are due to subtle conformational differences in the β-hairpin, which may include a change in the Trp binding pocket relative to the parent peptide **WKWK**. We attempt to address these questions, among others, via the computational methods discussed in the subsequent section.

Molecular dynamics simulations of WKWK and selected mutants. Molecular dynamics simulations were carried out for the peptide **WKWK** in complex with ATP. Four different simulations, each with different orientations of ATP in the binding pocket of the receptor were undertaken in order to examine possible binding orientations of ATP. Additionally, simulations of **WKWK** mutants were undertaken in order to examine how various mutations might perturb the ATP binding interface of the parent sequence **WKWK**.

In our simulations of ATP in complex with **WKWK**, ATP was placed in the **WKWK** "binding pocket" in four different starting orientations, each orientation containing a different stacking orientation of the adenine ring with respect to the Trps (see Figure 6.3). This enables the adenine ring to interact with the Trps while the phosphate tail is free to seek out different favorable electrostatic contacts during the simulation. The simulations were carried out in explicit water at 300 K and 1 atm pressure (Amber 8-p148). Special parameters were used for the simulation of ATP that were developed specifically for use with the Amber force field.[8] The most stable binding orientation of ATP was evaluated by monitoring the average potential energy during the

[8] Meagher, K. L.; Redman, L. T.; Carlson, H. A. *J. Comput. Chem.* **2003**, *24*, 1016-1025.

simulation (Figure 6.6). Of the four peptide-ATP complexes, orientation 1 (satp1, Fig. 6.3a) was clearly the most stable, indicating that it is a likely orientation for ATP.

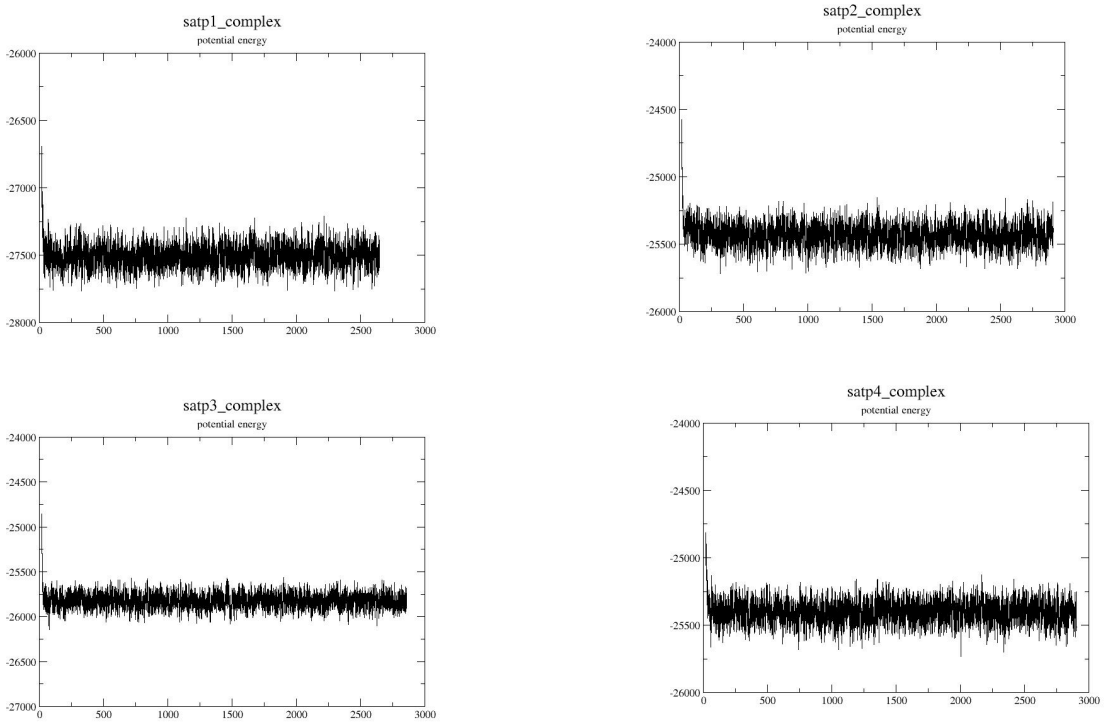

Figure 6.6. Plots of potential energy taken from the simulations of **WKWK** and ATP.

Table 6.5 Average potential energy from ATP-hairpin simulations.

Complex	Average Potential Energy (kcal/mol)
satp1	-27508.1
satp2	-25435.7
satp3	-25823.5
satp4	-25405.8

Snapshots taken from the trajectory for complex **satp1** reveal the critical contacts occurring between the peptide-ATP complex. Figure 6.7(a) shows the complex near the beginning of the simulation, while 6.7(b) and 6.7(c) are taken from near the middle and the end of the simulation.

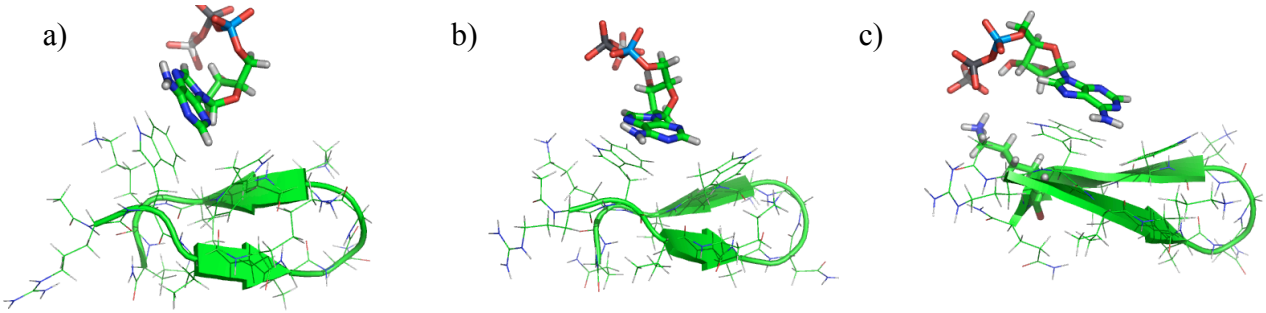

Figure 6.7. Snapshots taken from the simulation of ATP with **WKWK** (satp1). a) near beginning of simulation. b) near middle of simulation. c) near end of simulation.

By the end of the simulation, a well-defined H-bond occurs between K11 and the phosphate tail of ATP, while the adenosine ring is clearly interacting with the Trp rings. The ribose ring, which has been shown experimentally to interact with the Trp rings via NMR, is also in contact with the Trp rings as the simulation progresses. While it is important to acknowledge that the brevity of the simulations precludes complete exploration of the phase space of the binding interaction, the contacts observed here are consistent with our experimental data and may serve as a guide for design of future receptors. Furthermore, these simulations highlight the origin of our poor selectivity among various nucleotides: there is no narrow binding pocket, but rather a fairly shallow concave binding face established by the Trp rings that allows for numerous possible

stacking orientations while the phosphate tail is free to contact a number of positively charged residues located elsewhere in the hairpin.

Additional simulations of the mutant peptides **K4T** and **K4Q** were undertaken in order to analyze potential structural differences caused by the two mutations. These simulations were initiated by taking the average NMR structure of **WKWK** and mutating the appropriate Lys residue to either Thr or Gln using the program Sybyl. The mutant structures were then loaded into Amber 8, solvated with TIP3P explicit water, neutralized, and minimized. The resulting minimized structures were gradually heated from 0 to 300 K before being subjected to 2 ns of MD simulation using Amber ff99. The lowest energy structures were extracted from each simulation and are shown in Figure 6.8 below. While no differences in the structures are immediately obvious (other than the orientations of the two mutant sidechains), backbone superposition of the two structures shows that the orientation of the Trps are only slightly perturbed. While it is difficult to relate this directly to our binding data, this small perturbation of the binding pocket indicates that electrostatic differences between the interaction of the ATP phosphate tail with Gln and Thr are the most likely source for the observed differences in binding affinities.

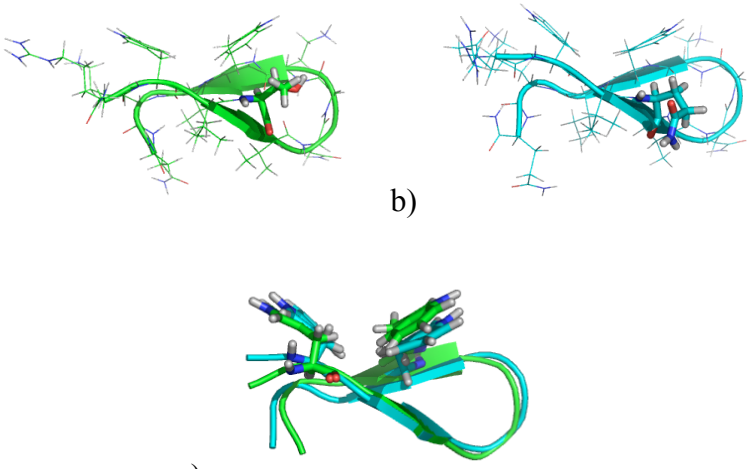

Figure 6.8. a) **K4T** low energy structure b) **K4Q** low energy structure c) superimposed **K4T** (green) and **K4Q** (blue).

C. Conclusions.

In this chapter we have investigated a number of critical contacts involved in the binding of ATP by a β-hairpin peptide. Various contributing factors, such as electrostatics and hairpin stabilities have been evaluated. Both experimental and computational efforts have converged to give a more detailed picture of the binding interactions involved in our receptor. Since nucleotide selectivity is our ultimate goal, this work suggests a number of potential avenues by which selectivity may be achieved. One such way is through the use of Trp analogues designed to better complement the electrostatic potential surface (for example, halogenated indole rings) of a particular nucleotide ring (adenine, guanine, etc.). Another method is to develop ways to restrict access to our "open-faced" binding pocked. This could occur through the addition of a third β-strand or an α-helix designed to orient residues above and around the Trp-

nucleotide interface. Clearly, more work is required in order to design selectivity into our receptor. However, this work provides a good starting point for such a discussion.

D. Experimental

i. Job plots and concentration studies of WKWK mutants. Job plots of **WKWK** constructed by Butterfield indicated that the hairpin binds to ATP with a 1:1 stoichiometry. We constructed our own Job plots to assure that our mutations to the parent peptide did not disturb this binding stoichiometry (Figure 6.9). A series of solutions were prepared in which the total peptide + ATP concentration was held constant at 3 mM, but mole fraction of the peptide was varied. Plots were constructed with NMR, with solutions made up in 10 mM d_3-acetate buffer, pH 5.0 (uncorrected). The concentration of the peptide-nucleotide complex is determined by the equation below, where Δ is the change in the peptide chemical shift relative to the free peptide, Δ_o is the change in chemical shift as determined by fitting of the NMR titration data to an equation [**2**], and $[R_o]$ is the total peptide concentration. A plot of [complex] versus mole fraction of peptide was constructed as shown below (equation [**1**]).

$$[\text{complex}] = (\Delta / \Delta_o) \text{ X } [R_o] \qquad [\mathbf{1}]$$

a)

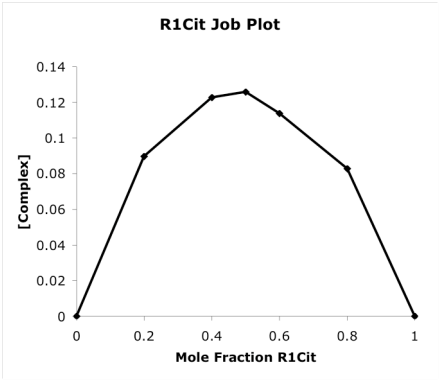

b)

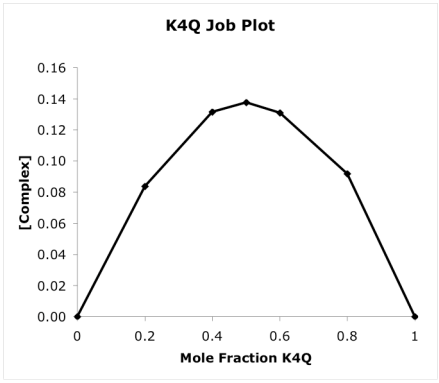

c)

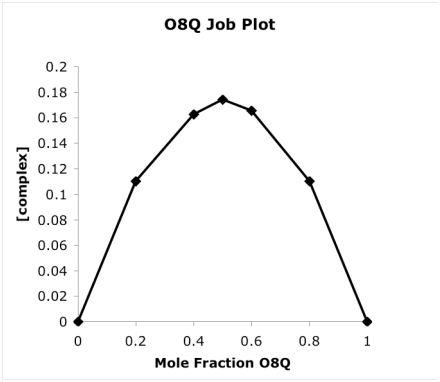

Figure 6.9. a) **R1Cit** Job Plot b) **K4Q** Job Plot c) **O8Q** Job Plot

ii. Concentration studies. Additionally, concentration studies of the peptides were conducted by CD, and indicate that the +3 charged mutant hairpins exhibit some aggregation at or above 500 μM in concentration. This could affect the results of our AMP titrations, which were conducted using receptor concentrations in the range of 1 – 2 mM. However, this is not a concern with our ATP concentrations, in which the receptor concentration was well below 100 μM for all of our studies.

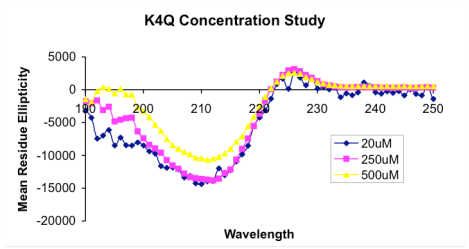

a)

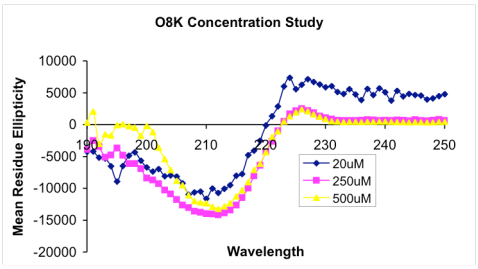

b)

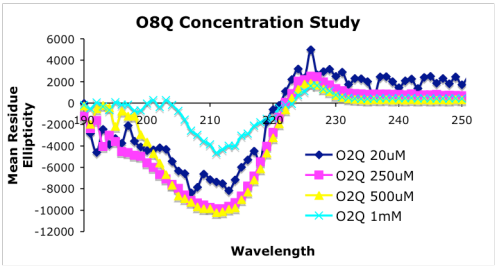

c)

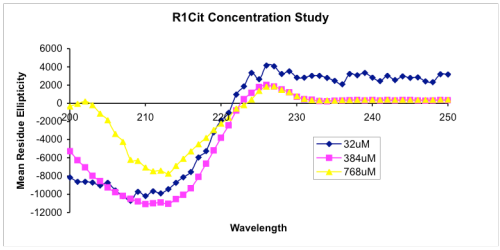

d)

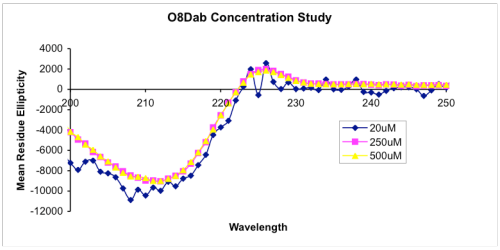

e)

Figure 6.10. Concentration studies of peptides a) K4Q b) O8K c) O8Q d) R1Cit e) O8Dab. (298K, 20 mM sodium phosphate buffer, pH 6.0).

iii. NMR Titrations. Peptides were dissolved in 10 mM d3-acetate buffer, pH 5.0 (uncorrected), using DSS as an internal standard. The concentration of peptide was held constant between 1-4 mM for titrations with AMP. AMP was added to the peptide solutions from a 0.6 M stock in D_2O in 1 – 6 μL increments. A 1D proton spectrum was then acquired, using 8 – 64 scans with water presaturation. Binding was measured by fitting the upfield shifting of the tryptophan H-5 protons to the following equation for 1:1 binding in Kaleidagraph, where δ_{obs} is the observed chemical shift of a tryptophan proton, δ_R is the chemical shift of the tryptophan proton in the absence of nucleotide, Δ_o is the maximum change in chemical shift at 100% complexation, $[R_o]$ is the concentration of the receptor, $[S_o]$ is the concentration of the nucleotide, and K is the binding constant:

$$\delta_{obs} = \delta_R + \Delta_o/2[R_o]\{[R_o] + [S_o] + 1/K - sqrt(([R_o] + [S_o] + 1/K)\ 2 - 4[R_o][S_o])\} \qquad [\mathbf{2}]$$

Table 6.6. NMR Titration Data for WKWK + AMP ([WKWK = 1.3 mM])

Trp H-5 Shift (ppm)	[AMP] mM
7.090	0
7.069	1.43
7.048	2.94
7.033	4.44
7.017	6.19
6.996	9.76
6.983	12.79
6.975	16.83
6.969	20.11
6.964	26.04
6.961	31.65

Table 6.7. NMR Titration Data for O8K + AMP ([O8K = 2.08 mM])

Trp H-5 Shift (ppm)	[AMP] mM
7.099	0
7.079	2.23
7.056	4.48
7.034	6.45
7.018	8.54
6.994	12.37
6.981	16.47
6.973	20.20
6.966	24.84
6.962	30.13
6.959	38.25

Table. 6.8. NMR Titration Data for O8Dab + AMP ([O8Dab = 1.54 mM])

Trp H-5 Shift (ppm)	[AMP] mM
7.089	0
7.070	2.445
7.047	4.65
7.026	6.40
7.005	8.10
6.982	11.54
6.970	15.17
6.963	18.76
6.956	24.58
6.949	30.01
6.947	36.33

Table 6.9. NMR Titration Data for O8Q + AMP ([O8Q = 1.52 mM])

Trp H-5 Shift (ppm)	[AMP] mM
7.087	0
7.068	1.57
7.048	3.07
7.039	4.78
7.024	5.995
7.004	11.28
6.990	15.39
6.982	19.26
6.974	21.65
6.968	28.94
6.965	33.59

Table 6.10. NMR Titration Data for R1Cit + AMP ([R1Cit] = 3.42 mM)

Trp H-5 Shift (ppm)	[AMP] mM
7.133	0
7.118	1.405
7.093	3.83
7.079	6.50
7.060	7.45
7.031	12.0
7.016	16.21
7.006	20.31
6.996	24.13
6.985	29.51
6.979	36.57
6.975	40.04

iv. Fluoresence Titrations. Peptide samples were prepared in 10 mM acetate buffer, pH 5.0. Peptide concentrations were determined in 6M GdnHCl, using the absorbance of Trp residues at 280 nm (e = 5690 M-1 cm -1). ATP stock solutions were prepared in 10 mM sodium acetate buffer, pH 5.0, and concentrations were determined by UV/Vis spectroscopy. Fluoresence scans were obtained at 25 C, using an excitation wavelength of 297 for Trp, and monitoring the emission at 348 nm. Fluoresence titrations were fit to the following equation for 1:1 binding in KaleidaGraph, where I is the observed fluorescence intensity, I_o is the initial fluorescence intensity of the peptide, I_∞ is the fluorescence intensity at binding saturation, [L] is the concentration of the added nucleotide, and K_d is the dissociation constant:

$$I - [I_o + I_\infty([L]/K_d]/[1 + ([L]/K_d)] \qquad [\mathbf{3}]$$

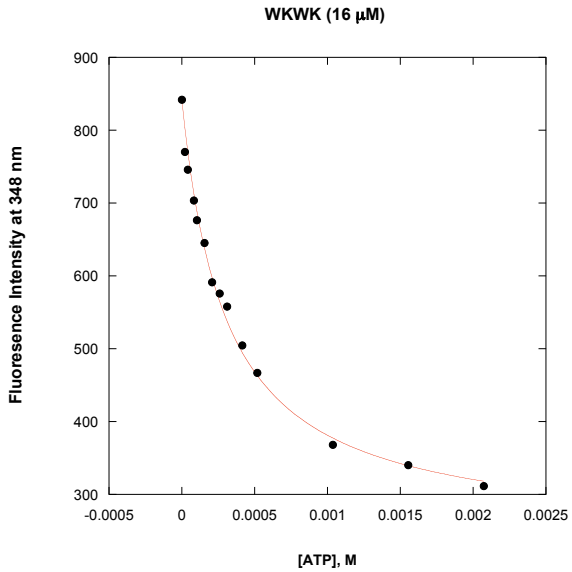

Figure 6.11. Fluorescence titration of **WKWK** with ATP.

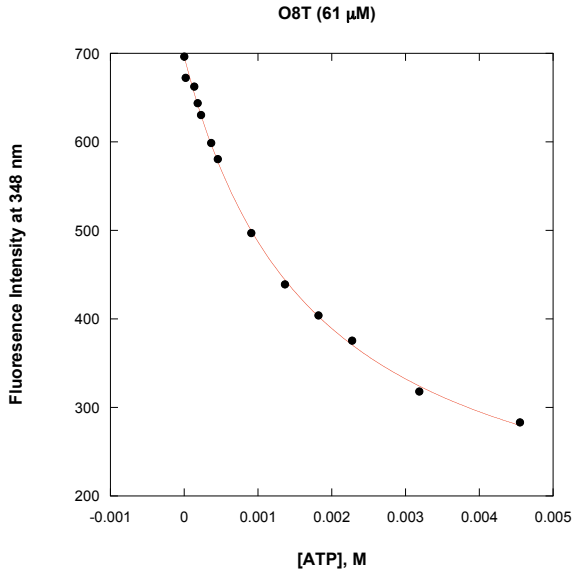

Figure 6.12. Fluorescence titration of **O8T** with ATP.

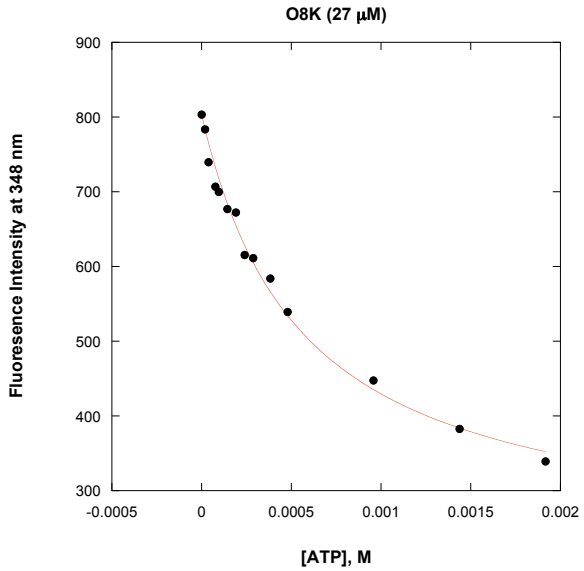

Figure 6.13. Fluorescence titration of **O8K** with ATP.

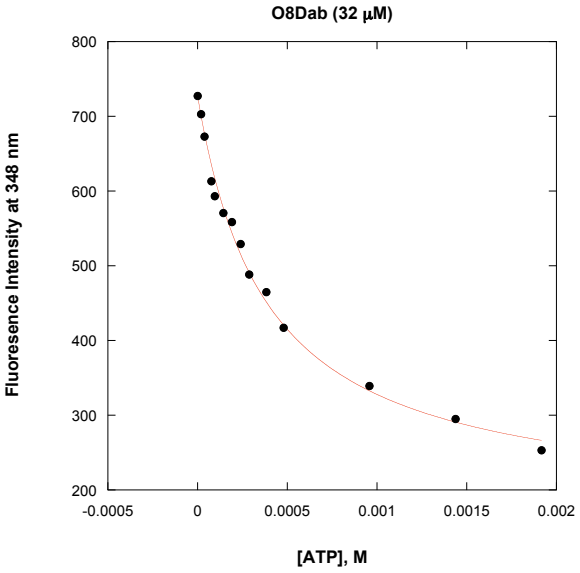

Figure 6.14. Fluorescence titration of **O8Dab** with ATP.

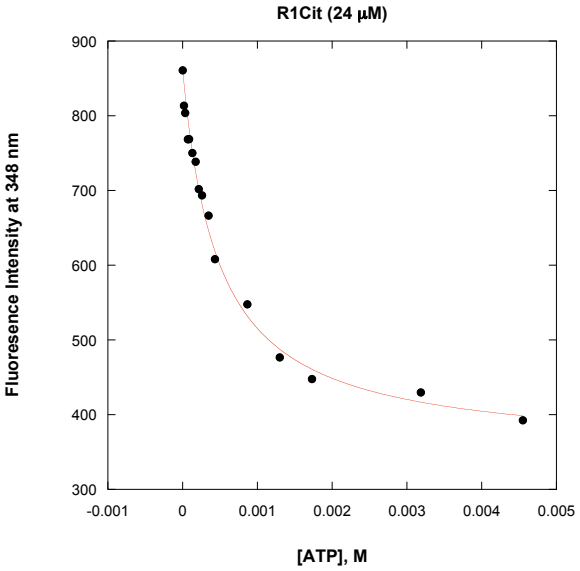

Figure 6.15. Fluorescence titration of **R1Cit** with ATP.

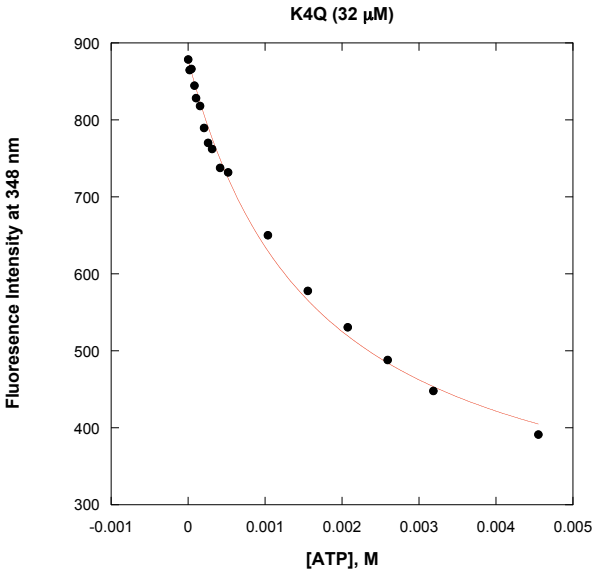

Figure 6.16. Fluorescence titration of **K4Q** with ATP.

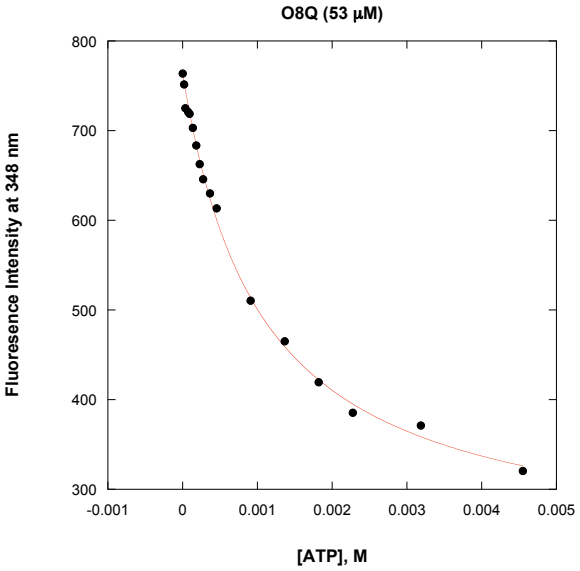

Figure 6.17. Fluorescence titration of **O8Q** with ATP.

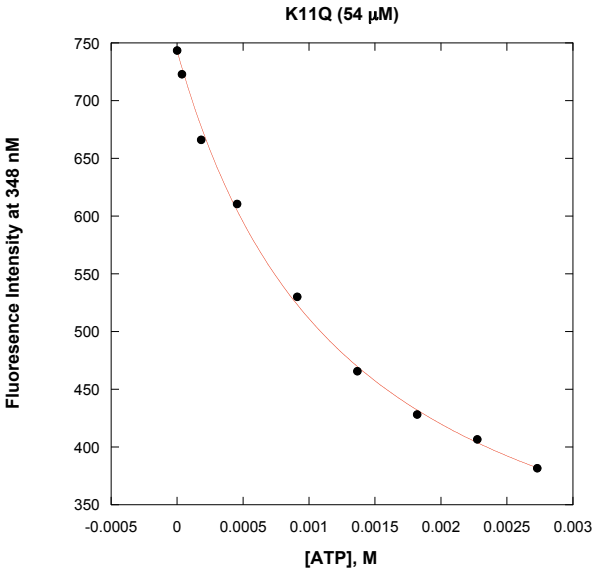

Figure 6.18. Fluorescence titration of **K11Q** with ATP.

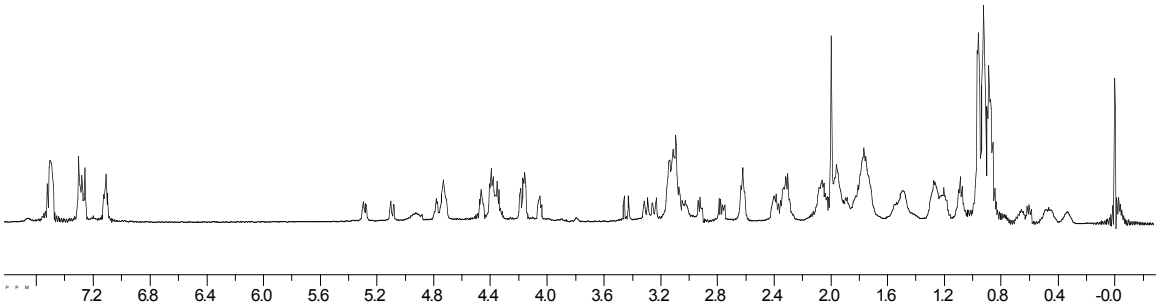

Figure 6.19. [1]HNMR of Peptide **R1Cit**: Ac-Cit-Trp-Val-Lys-Val-Asn-Gly-Orn-Trp-Ile-Lys-Gln-NH2

Table 6.11 Proton Chemical Shift Assignments for Peptide **R1Cit**.

	α	β	γ	δ	ε	Amide	Amine
Cit	4.47	1.76	1.53	3.14			
W	5.29	3.08,3.31					
V	4.18	1.89	0.91				
K	4.39	1.17,0.00	0.50	2.77			
V	4.73	2.05	0.94				
N	4.39	3.12,2.77					
G	4.18,3.45						
O	4.73	1.91	1.79	3.10			
W	5.10	3.12					
I	4.78	1.97	0.97				
K	4.06	1.27	0.39	0.67	2.63		
Q	4.35	1.99	2.32				

Table 6.12. Proton Chemical Shift Assignments for Peptide **R1Cit7**: Ac-Cit-Trp-Val-Lys-Val-Asn-Gly-NH2

	α	β	γ	δ	ε	Amide	Amine
Cit	4.26	1.71	1.39	2.97			
W	4.73	3.28					
V	3.98	1.95	0.85				
K	4.13	1.57	1.33	1.33	3.01		
V	4.09	2.07	0.94				
N	4.69	2.78					
G	3.90						

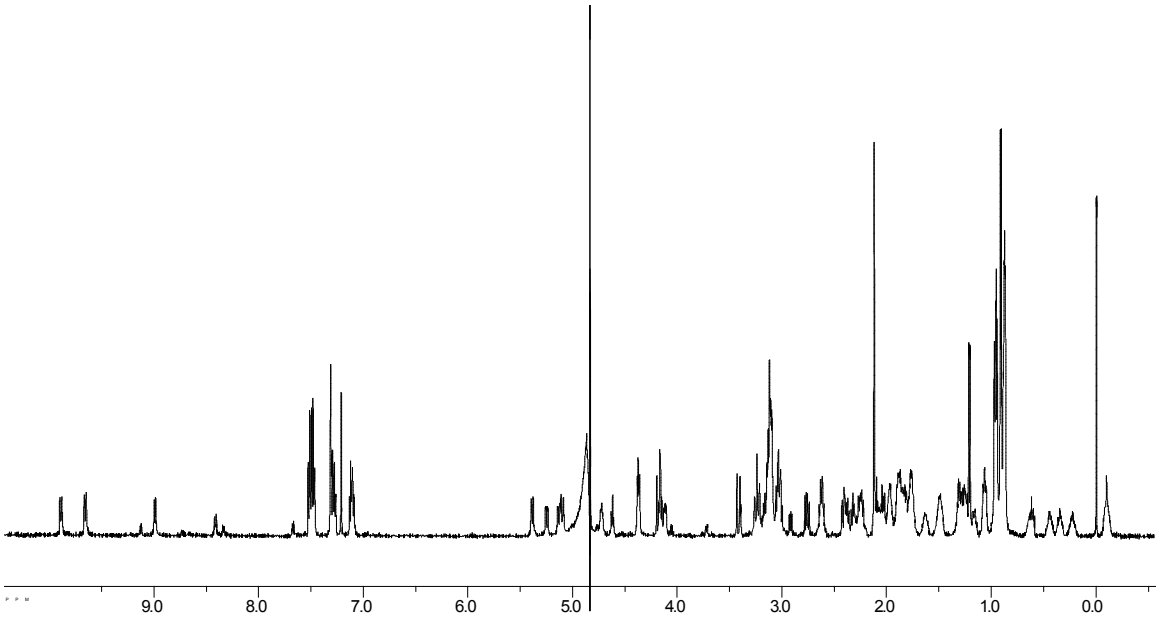

Figure 6.20. [1]HNMR of Peptide **R1CitCyc**: Ac-Cys-Cit-Trp-Val-Lys-Val-Asn-Gly-Orn-Trp-Ile-Lys-Gln-Cys-NH2

Table 6.13. Proton Chemical Shift Assignments for Peptide **R1CitCyc.**

	α	β	γ	δ	ε	Amide	Amine
C	5.11	3.11					
Cit	4.73	n.d.	n.d.	3.13			
W	5.39	3.24,3.04					
V	4.18	1.88	0.90				
K	4.38	1.13,-0.1	0.45	2.36			
V	4.79	2.03	0.93				
N	4.38	3.11,2.77					
G	4.19,3.42						
O	4.73	n.d.	n.d.	2.94			
W	5.11	3.11					
I	4.84	1.97	0.96				
K	4.12	1.27	0.29	0.64	2.63		
Q	4.63	1.91	2.24				
C	5.25	3.04,2.42					

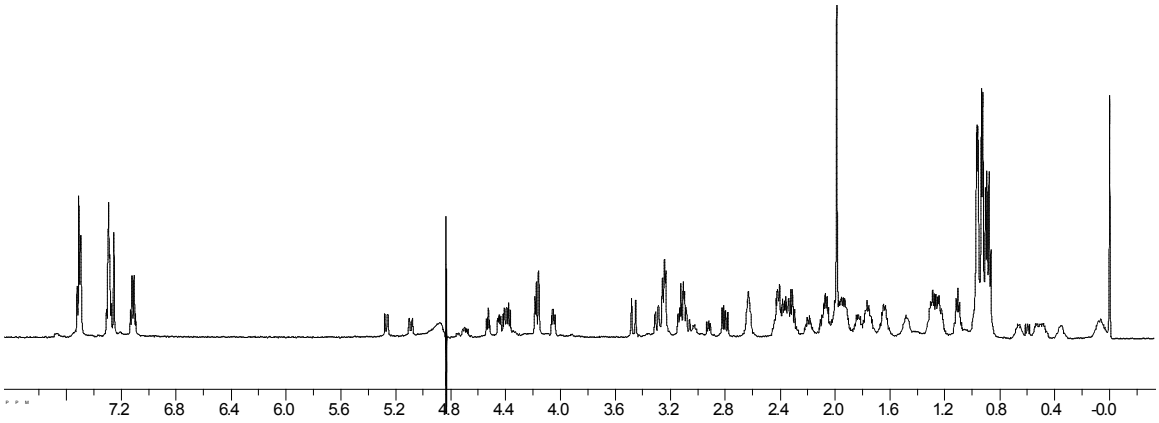

Figure 6.21. [1]HNMR of Peptide **O2Q**: Ac-Arg-Trp-Val-Lys-Val-Asn-Gly-Gln-Trp-Ile-Lys-Gln-NH2

Table 6.14. Proton Chemical Shift Assignments for Peptide **O2Q.**

	α	β	γ	δ	ε	Amide	Amine
R	4.55	1.81	1.67	3.26			
W	5.29	3.10,3.31					
V	4.19	1.94	0.93				
K	4.47	1.25,0.07	0.55	1.23	2.40		
V	4.74	2.08	0.96				
N	4.43	3.12,2.83					
G	4.20,3.49						
Q	4.72	2.24,2.03	2.43				
W	5.11	3.22,3.12					
I	4.78	1.98	1.51,1.29, 0.99	0.99			
K	4.07	1.31,0.36	0.48	0.68	2.65		
Q	4.40	2.10,1.97	2.34				

Table 6.15. Proton Chemical Shift Assignments for Peptide **O2Q7**: Ac-Asn-Gly-Gln-Trp-Ile-Lys-Gln-NH2

	α	β	γ	δ	ε	Amide	Amine
N	4.66	2.76					
G	3.84						
Q	4.23	1.86	2.12				
W	4.70	3.31,3.23					
I	4.02	1.71	0.80	0.80			
K	4.17	1.70	1.39	1.70	2.95		
Q	4.27	1.99	2.35				

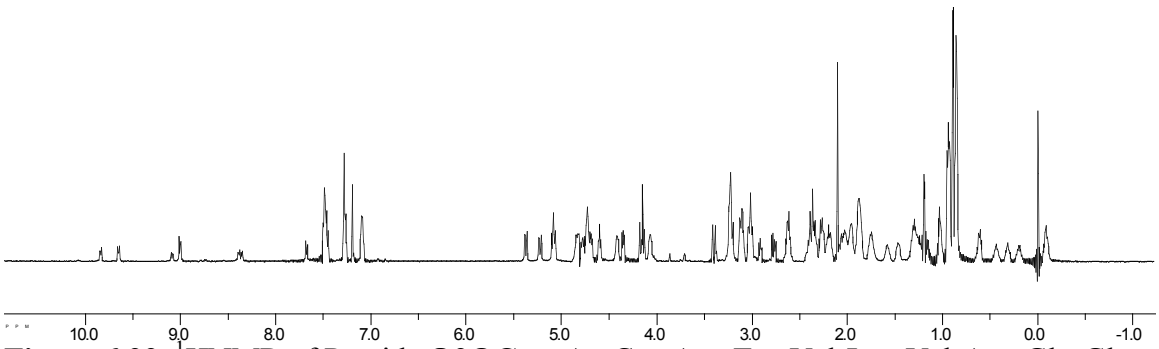

Figure 6.22. ^{1}HNMR of Peptide **O2QCyc**: Ac-Cys-Arg-Trp-Val-Lys-Val-Asn-Gly-Gln-Trp-Ile-Lys-Gln-Cys-NH2

Table 6.16. Proton Chemical Shift Assignments for Peptide **O2Qcyc.**

	α	β	γ	δ	ε	Amide	Amine
C	5.10	3.08					
R	4.75	1.90	1.76	3.25			
W	5.38	3.25,3.04					
V	4.17	1.88	0.89				
K	4.43	1.14, -0.07	0.45	2.32			
V	4.75	2.06	0.94				
N	4.36	3.12,2.79					
G	4.17,3.41						
Q	4.71	1.97	2.40				
W	5.10	3.08					
I	4.84	1.97	0.95	0.95			
K	4.09	1.28	0.25	0.64	2.63		
Q	4.61	1.89	2.23				
C	5.24	3.02,2.38					

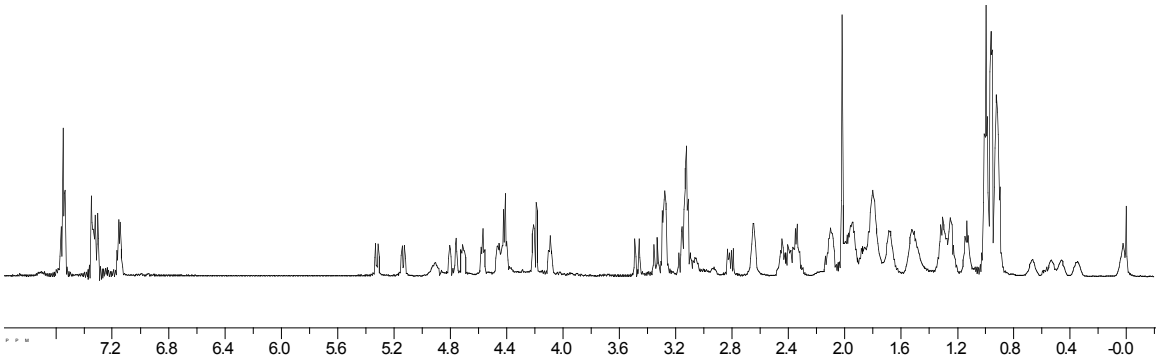

Figure 6.23. [1]HNMR of Peptide **O2K**: Ac-Arg-Trp-Val-Lys-Val-Asn-Gly-Lys-Trp-Ile-Lys-Gln-NH2

Table 6.17. Proton Chemical Shift Assignments for Peptide **O2K.**

	α	β	γ	δ	ε	Amide	Amine
R	4.53	1.75	1.75	3.25		8.16	7.23
W	5.29	3.32,3.08				8.62	10.15
V	4.16	1.90	0.90			9.00	
K	4.43	1.17,0.00	0.50	n.d.	2.39	8.37	
V	4.73	2.06	0.95			9.54	
N	4.39	3.12,2.78				9.50	
G	4.17,3.44					8.55	
K	4.68	1.78	n.d.	1.48	3.09	7.70	
W	5.10	3.13				8.69	10.15
I	4.78	1.96	1.25,0.97	0.97		9.71	
K	4.06	1.26	0.38	0.63	2.62	8.36	
Q	4.38	1.95	2.32			8.73	

Table 6.18. Proton Chemical Shift Assignments for Peptide **O2K7**: Ac-Asn-Gly-Lys-Trp-Ile-Lys-Gln-NH2

	α	β	γ	δ	ε	Amide	Amine
N	4.66	2.77					
G	3.85						
K	4.23	1.61	n.d.	1.22	2.88		
W	4,71	3.26					
I	4.06	1.73	1.07,0.83	0.83			
K	4.15	1.71	n.d.	1.40	2.97		
Q	4.28	1.99	2.36				

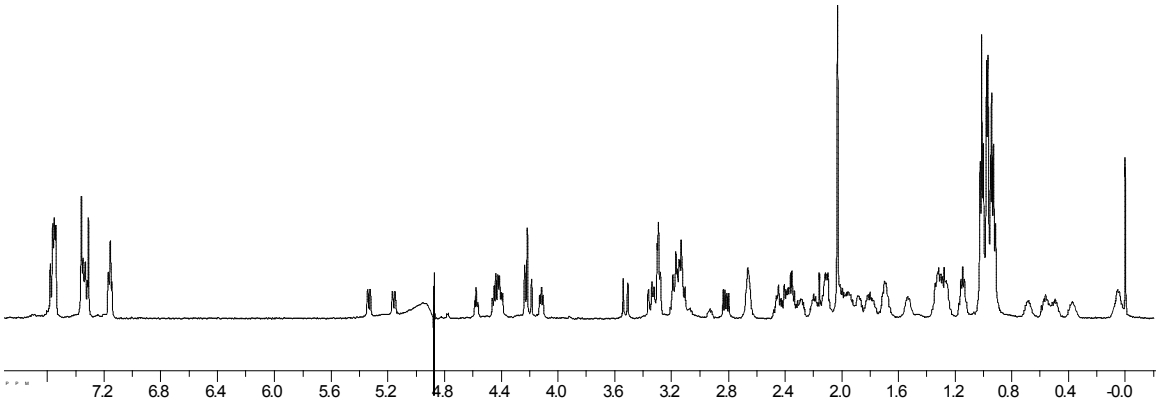

Figure 6.24. [1]HNMR of Peptide **O2Dab**: Ac-Arg-Trp-Val-Lys-Val-Asn-Gly-Dab-Trp-Ile-Lys-Gln-NH2

Table 6.19. Proton Chemical Shift Assignments for Peptide **O2Dab.**

	α	β	γ	δ	ε	Amide	Amine
R	4.53	1.78	1.65	3.25		8.16	
W	5.29	3.31,3.08				8.62	10.15
V	4.17	1.90	0.92			8.83	
K	4.37	1.23,0.00	0.51	1.12	2.36	8.43	
V	4.73	2.07	0.94			9.53	
N	4.40	3.10,2.77					
G	4.15,3.48					8.63	
Dab	4.84	2.15	3.11			7.75	
W	5.11	3.27,3.13				8.88	
I	4.79	1.97	1.49,1.26,0.98	0.98		9.75	
K	4.07	1.26,0.33	0.45	0.65	2.62	8.36	
Q	4.38	2.07,1.94	2.31			8.74	

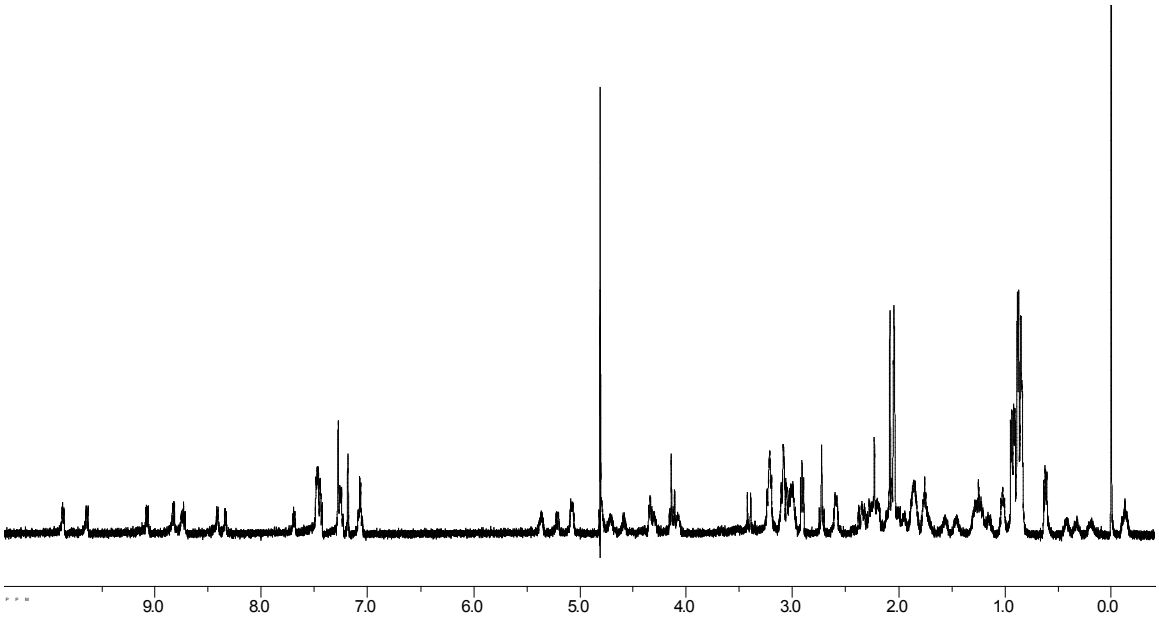

Figure 6.25. [1]HNMR of Peptide **O2DabCyc**: Ac-Cys-Arg-Trp-Val-Lys-Val-Asn-Gly-Dab-Trp-Ile-Lys-Gln-Cys-NH2

Table 6.20. Proton Chemical Shift Assignments for Peptide **O2DabCyc.**

	α	β	γ	δ	ε	Amide	Amine
C	5.078	3.055					
R	4.718	1.867	1.578	3.22		8.726	
W	5.367	3.016				8.742	
V	4.729	1.995	0.901			9.635	
K	4.31	1.133	0.43	-0.125	2.289	8.414	
V	4.148	1.859	0.867			8.828	
N	4.344	3.03,2.75					
G	4.125,3.409						
Dab	4.88	2.172	3.06			7.71	
W	5.07	3.055					
I	4.776	1.956	1.237,0.924	0.924		9.86	
K	4.086	1.234	0.617	0.274	2.586	8.336	
Q	4.59	1.88	2.21			9.078	
C	5.219	2.91,2.398					

Table 6.21. Proton Chemical Shift Assignments for Peptide **O2Dab7**: Ac-Asn-Gly-Dab-Trp-Ile-Lys-Gln-NH2

	α	β	γ	δ	ε	Amide	Amine
N	4.66	2.77					
G	3.84						
Dab	4.40	1.99	2.94				
W	4.70	3.25					
I	4.06	1.72	1.36,1.07,0.83	0.83			
K	4.14	1.71	n.d.	1.39	2.97		
Q	4.28	1.99	2.36				

Table 6.22. Proton Chemical Shift Assignments for Peptide **K11Q**: Ac-Arg-Trp-Val-Lys-Val-Asn-Gly-Orn-Trp-Ile-Gln-Gln-NH2

	α	β	γ	δ	ε	Amide	Amine
R	4.45	1.78	1.68	3.23			
W	5.25	3.30,3.08					
V	4.72	2.02	0.93				
K	4.39	1.16, -0.02	0.48	n.d.	2.36		
V	4.17	1.88	0.90				
N		3.08,2.77					
G	4.18,3.45					8.55	
O	4.72	1.78	1.78	3.10			
W	5.10	3.23,3.13					
I		1.96	1.44,1.25,0.97	0.97			
Q	4.20	0.99,0.85	1.49,1.25				
Q	4.35	1.91	2.30				

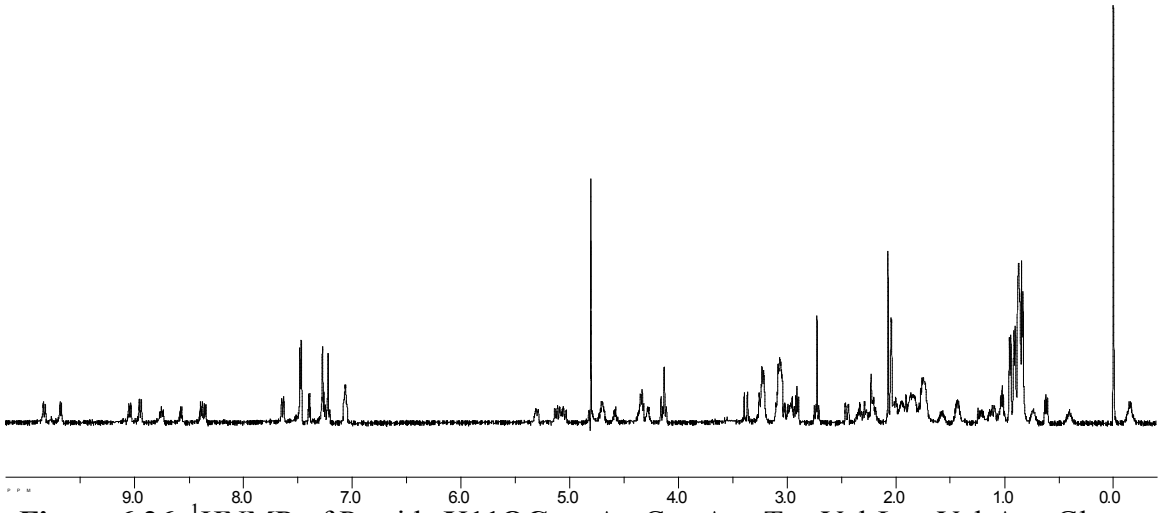

Figure 6.26. [1]HNMR of Peptide **K11QCyc**: Ac-Cys-Arg-Trp-Val-Lys-Val-Asn-Gly-Orn-Trp-Ile-Gln-Gln-Cys-NH2

Table 6.23. Proton Chemical Shift Assignments of Peptide **K11QCyc**.

	α	β	γ	δ	ε	Amide	Amine
C	5.014	2.92					
R	4.655	------	------	3.186		8.553	
W	5.279	3.05					
V	4.702	2.014	0.858			9.655	
K	4.33	1.069, -0.173	0.428	n.d.	2.257	8.31	
V	4.116	1.88	0.827			8.936	
N	4.31	2.82,2.70					
G	4.1455,3.815						
O	4.709	1.78	1.78	3.038		7.616	
W	5.061	3.10					
I	4.796	1.999	0.928	0.928		9.80	
Q	4.264	0.866	1.38			8.35	
Q	4.546	1.93	2.12			9.006	
C	5.10	2.87,2.28					

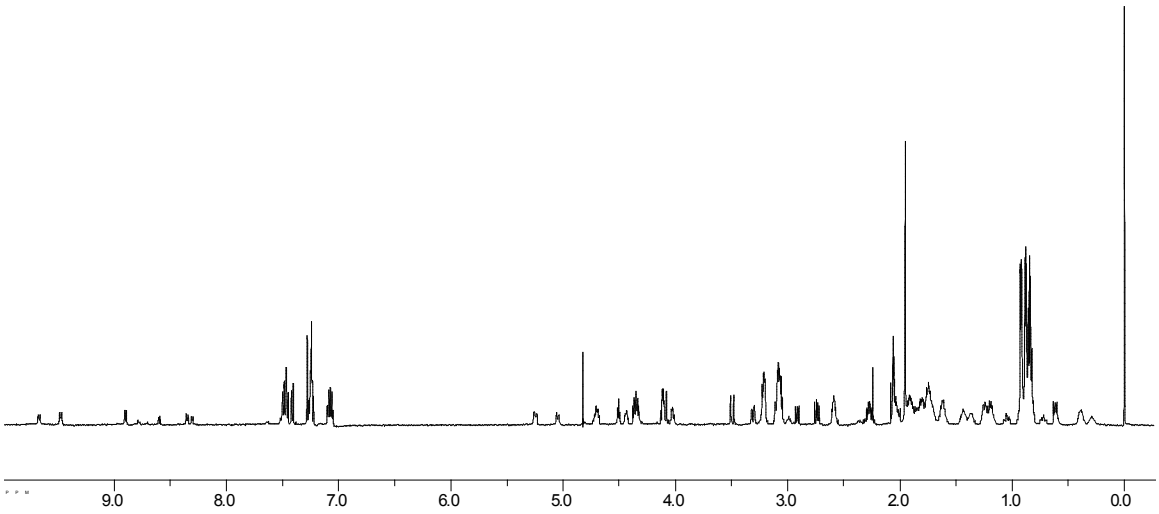

Figure 6.27. [1]HNMR of Peptide **K4Q**: Ac-Arg-Trp-Val-Gln-Val-Asn-Gly-Orn-Trp-Ile-Lys-Gln-NH2

Table 6.24. Proton Chemical Shift Assignments of Peptide **K4Q**.

	α	β	γ	δ	ε	Amide	Amine
R	4.508	1.766	1.633	3.219			
W	5.25	3.30,3.09				8.60	
V	4.688	2.039	0.899				
Q	4.438	0.727,0.383	1.368,1.055			8.352	
V	4.125	1.859	0.867			8.89	
N	4.367	3.06,2.78					
G	4.093,3.493						
O	4.696	1.78	1.78	3.07			
W	5.055	3.10				8.789	
I	4.719	1.899	1.45,1.20,0.92	0.92		9.656	
K	4.036	1.243	0.359	0.618	2.59	8.31	
Q	4.344	1.922	2.27				

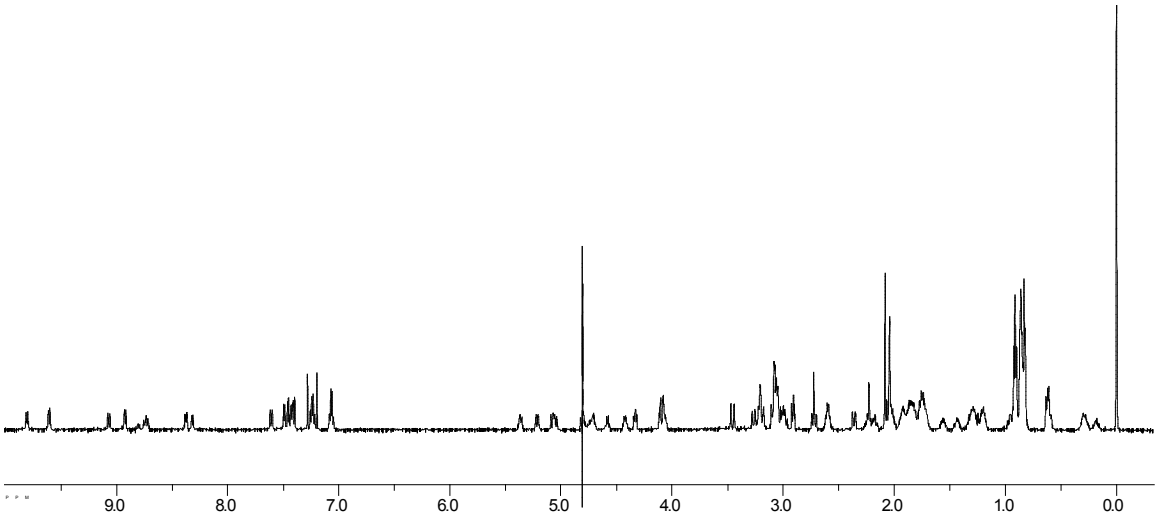

Figure 6.28. [1]HNMR of Peptide **WQWKCyc**: Ac-Cys-Arg-Trp-Val-Gln-Val-Asn-Gly-Orn-Trp-Ile-Lys-Gln-Cys-NH2

Table 6.25. Proton Chemical Shift Assignments for Peptide **K4QCyc.**

	α	β	γ	δ	ε	Amide	Amine
C	5.068	3.13,3.06					
R	4.147	0.865	-----	2.73			
W	5.358	3.123					
V	4.764	2.092	0.874			9.60	
Q	4.413	0.342	1.678			8.374	
V	4.116	1.749	0.842			8.905	
N	4.326	3.06,2.76					
G	4.095,3.456						
O	4.74	1.81	1.81	3.06			
W	5.068	3.13,3.06					
I	4.741	1.952	0.905	0.905		9.811	
K	4.077	1.248	0.483	------	2.66	8.30	
Q	4.59	1.95	2.19			9.069	
C	5.217	2.97,2.27					

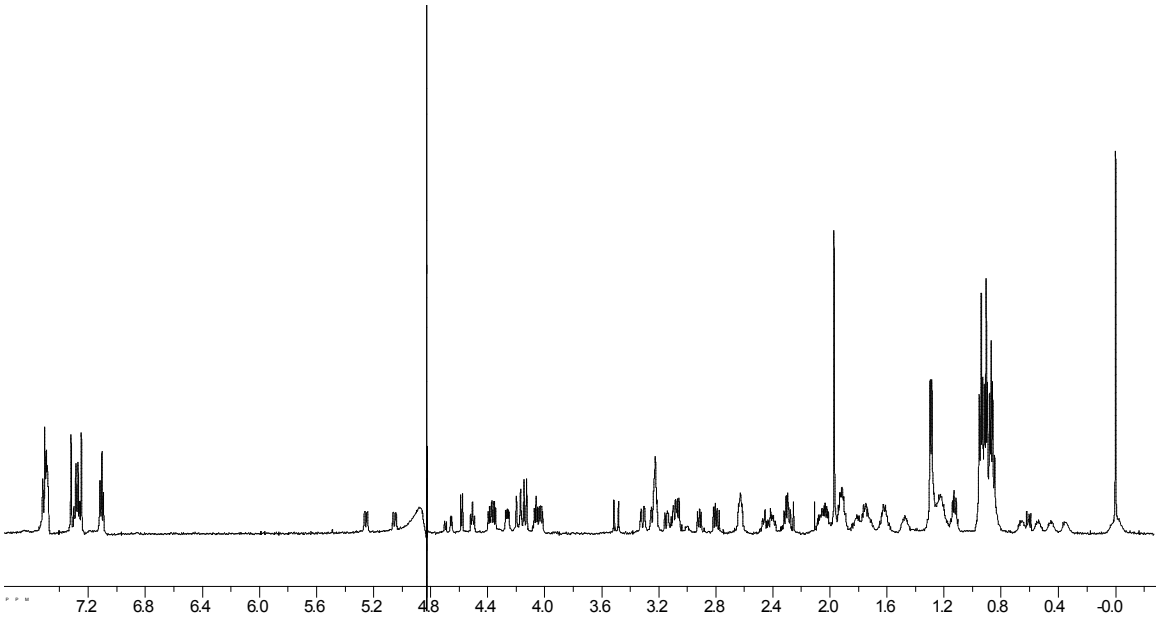

Figure 6.29. [1]HNMR of Peptide **O8T**: Ac-Arg-Trp-Val-Lys-Val-Asn-Gly-Thr-Trp-Ile-Lys-Gln-NH2

Table 6.26. Proton Chemical Shift Assignments for Peptide **O8T.**

	α	β	γ	δ	ε	Amide	Amine
R	4.48	1.72	1.63	3.21			
W	5.23	3.06					
V	4.64	2.00	0.90			9.43	
K	4.247	-0.01	0.521	1.16	2.41	8.35	
V	4.122	1.88	0.872			8.80	
N	4.36	3.08.2.79					
G	4.153,3.471						
T	4.57	4.04	1.27				
W	5.04	3.12					
I	4.68	1.90	1.45,1.21, 0.92	0.92			
K	4.013	1.25	0.40	0.67	2.60	8.33	
Q	4.33	1.98	2.28				

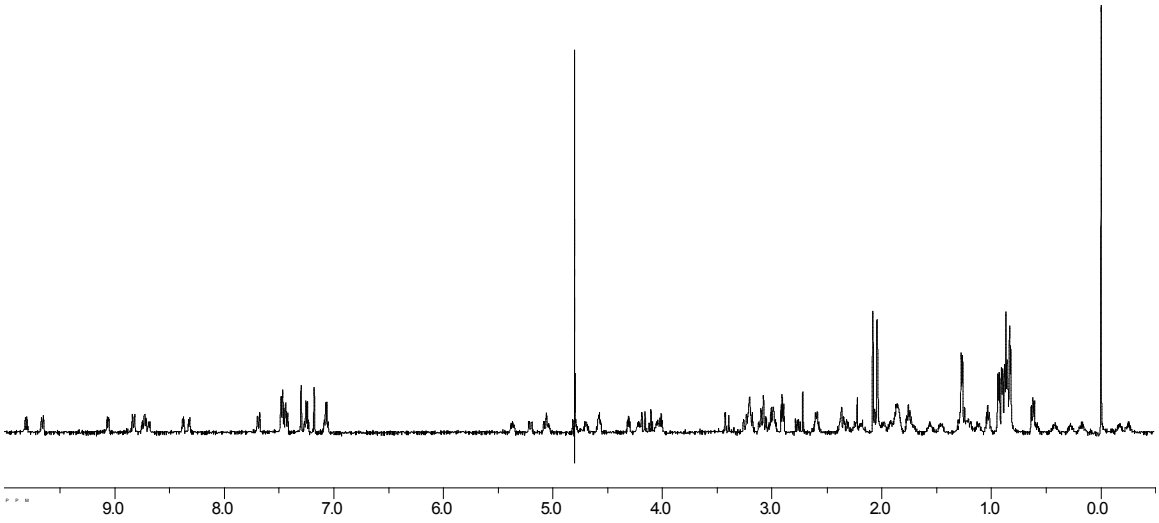

Figure 6.30. [1]HNMR of Peptide **O8TCyc**: Ac-Cys-Arg-Trp-Val-Lys-Val-Asn-Gly-Thr-Trp-Ile-Lys-Gln-Cys-NH2

Table 6.27. Proton Chemical Shift Assignments for Peptide **O8TCyc.**

	α	β	γ	δ	ε	Amide	Amine
C	4.89	2.83					
R	4.523	1.66	1.66	3.016		8.539	
W	5.187	2.852				8.547	
V	4.508	1.836	0.703			9.469	
K	4.04	0.914	-0.383	0.227	2.156	8.19	
V	3.93	1.64	0.66			8.64	
N	4.125	3.234,3.992					
G	3.992,3.234						
T	4.39	3.87	1.09			7.51	
W	4.867	2.98				8.492	
I	4.55	1.74	1.20,0.74	0.74		9.625	
K	3.867	1.039	0.039	0.453	2.391	8.133	
Q	4.391	1.83	2.01			8.875	
C	5.023	2.82,2.18					

Table 6.28. Proton Chemical Shift Assignments for Peptide **K7**: Ac-Asn-Gly-Orn-Trp-Ile-Lys-Gln-NH2

	α	β	γ	δ	ε	Amide	Amine
N	4.657	2.79					
G	3.845						
O	4.275	1.71	1.65	2.954			
W	4.697	3.275					
I	4.048	1.603	0.853	0.853			
K	4.165	1.74	1.55	-----	2.95		
Q	4.275	1.82	2.30				

CHAPTER VII

CATION-π INTERACTIONS IN A SMALL MOLECULE MODEL SYSTEM

A. Background and significance.

The cation-π interaction is known to be an important interaction in protein stability, molecular recognition, and enzymatic catalysis.[1] In recent years, this interaction has been increasingly utilized in the field of organic chemistry by catalytic and asymmetric induction systems.[2] However, it has been suggested that in certain supramolecular systems studied in organic solution, the interaction between a charged π-system and an aromatic ring has less influence on conformational stability than other competing non-covalent interactions, including CH—O and NH—O interactions.[3] In this study, we use

---

[1] (a) Ma. J. C.; Dougherty, D. A. *Chem. Rev.* **1997**, 97, 1303-1324. (b) Castellano, R. K. Diederich, F.; Meyer, E. A. *Angew. Chem. Int. Ed.* **2003**, 42, 1210-1250. (c) Gallivan, J. P.; Dougherty, D. A. *Proc. Natl. Acad. Sci. U.S.A.* **1999**, 96, 9459-9464. (d) Zacharias, N.; Dougherty, D.A. *Trends Pharmacol. Sci.* **2002**, 23, 281-287. (e) Munoz-Caro, C.; Nino, A. *Biophys. Chem.* **2002**, 96, 1-14. (f) Quiocho, F. A.; Hu, G.; Gershon, P.D.; *Curr. Opin. Struct. Biol.* **2000**, 10, 78-86. (g) Yamamoto-Katayama, S.; Ariyoshi, M.; Ishihara, K.; Hirano, T.; Jingami, H.; Morikawa, K. *J. Mol. Biol.* **2002**, 316, 711-723. (h) Lee, S.; Lin, X.; McMurray, J.; Sun, G. *Biochemistry* **2002**, 41, 12107-12114. (i) Eichman, B. F.; O'Rourke, E. J.; Radicella, J. P.; Ellenberger, T. *Embo. J.* **2003**, 22, 4898-4909.

[2] (a) Yamada, S.; Morita, C. *J. Am. Chem. Soc.* **2002**, *124*, 8184-8185. (b) Acharya, P.; Plashkevych, O.; Morita, C.; Yamada, S.; Chattopadhyaya, S. *J. Org. Chem.* **2003**, *68*, 1529-1538.

[3] (a) Raymo, F.; Bartberger, M.; Houk, K.; Stoddart, F. *J. Am. Chem. Soc.* **2001**, *123*, 9264-9267. (b) Houk, K.; Menzer, S.; Newton, S.; Raymo, F.; Stoddart, F.; Williams, D.

designed model systems to investigate the orientation effects of a cation-π interaction versus competing CH— and NH—O interactions in organic solution. We find that in organic solution, within the context of our model systems, the cation-π interaction predominates over other possible non-covalent interactions. This effect is complex and due to favorable energies for the cation-π interaction in chloroform biased towards the stacked orientation by energetic and entropic effects, including the presence of an unexpected oxygen-arene interaction within the designed system.

B. Design

Model systems 1 and 2 (Figure 7.1) are based on a previously reported system designed to examine offset stacked aromatic interactions.[4] The orientation dependence of model system 1 on the cation-π interaction has been previously investigated in aqueous solution.[4b] Model system 2 was designed as a control for monitoring the influence of the methoxy group present in model system 1 on the stacking interaction in organic solvents. Comparison of the preference for stacking interactions between the two sets of molecules should indicate what role, if any, that the methoxy group is playing in the dominant conformations of model system 1 molecules in different solvents.

J. Am. Chem. Soc. **1999**, *121*, 1479-1487. (c) Raymo, F.; Houk, K.; Stoddart, F. J. Org. Chem. **1998**, *63*, 6523-6528.

[4] (a) Rashkin, M. J.; Waters, M. L. *J. Am. Chem. Soc*. **2002**, *124*, 1860-1861. (b) Rashkin, M. J.; Hughes, R. M.; Calloway, N. T.; Waters, M. L. *J. Am. Chem. Soc*. **2004**, *126*, 13320-13325. (c) Martin, C. B.; Mulla, H. R.; Willis, P. G.; Cammers-Goodwin, R. *J. Org. Chem*. **1999**, *64*, 7802-7806.

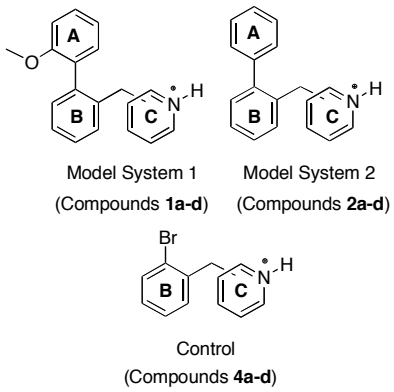

Figure 7.1. Designed model systems 1 and 2

In our initial investigation in water, it was shown that the stacking interaction is highly favored over potential interactions between polarized hydrogens on the pyridinium ring and the methoxy group.[4b] However, in a different solvent environment, the stacking interaction (cation-π) might not be more favorable than other possible non-covalent interactions, which could result in a solvent-induced conformational switch in our model system. For example, NH—O and CH—O hydrogen bonds are predicted to be more favorable in organic solvent than in water.[5] This is readily demonstrated by Hunter's simplified electrostatic model, in which electrostatic interactions are treated as pair-wise hydrogen bonds, and their free energies of interaction in a wide variety of solvents calculated from AM1 electrostatic potentials.[6] However, predicting the magnitude of CH—O and NH—O interactions relative to a competing cation-π interaction is a challenging problem that requires high-level computational treatment.[7] Accordingly,

---

[5] Houk, K. N.; Menzer, S.; Newton, S. P.; Raymo, F. M.; Stoddart, J. F.; Williams, D. J. *J. Am. Chem. Soc.* **1999,** *121*, (7), 1479-1487.

[6] Hunter, C. A. *Angew. Chem. Int. Ed.* **2004**, *43*, 5310-5324.

[7] Gallivan, J. P.; Dougherty, D. A. *J. Am. Chem. Soc.* **2000**, *122*, 870-874.

high-level (MP2/6-31g**) ab initio calculations have been performed to predict the relative magnitudes of cation-π and CH-- and NH—O interactions in chloroform.

C. Results and Discussion

Synthesis. The synthesis of model system 1 (compounds **1a – 1d)** has been described previously.[4b] The synthesis of model system 2 (compounds **2a – 2d)** is shown in Scheme 7.1. Compound **2a** was synthesized starting with the reduction of 2-bromobenzaldehyde with sodium cyanoborohydride to compound **3**. Compound **3** was brominated with phosphorous tribromide, followed by reaction with pyridine. Suzuki coupling of the cationic species **4a** with phenyl boronic acid gave compound **2a**. Compounds **2b – 2d** were synthesized starting with the reaction of 2-bromobenzaldehyde with the appropriate pyridyl Grignard reagent.[8] The resulting compounds were acylated with acetic anhydride, followed by deoxygenation with samarium iodide.[9] Suzuki coupling with phenyl boronic acid, followed by protonation with HBF_4, yielded compounds **2b – 2d**.

---

[8] Trecourt, F.; Breton, G.; Bonnet, V.; Mongin, f.; Marsais, F.; Queguiner, G. *Tet. Lett.* **1999**, *40*, 4339-4342.

[9] Kato, Y.; Mase, T. *Tet. Lett.* **1999**, *40*, 8823-8826.

Scheme 7.1. Synthesis of model system 2 compounds **2a – 2d**.

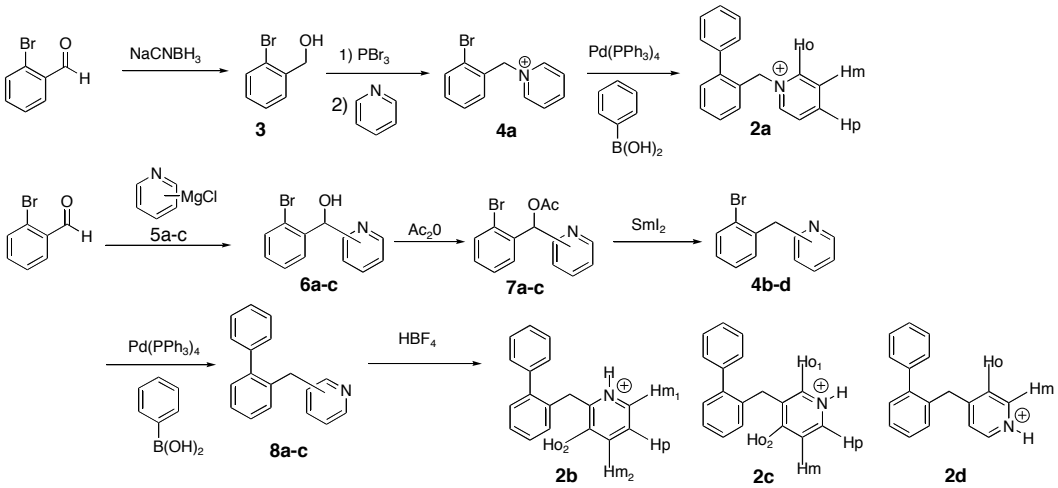

Investigation of Conformational Preferences. We investigated the tendency of the pyridinium ring C to stack with the anisole ring A in both model systems (Figures 7.1 and 7.2) in chloroform. The magnitude of the stacking interaction is described qualitatively by the upfield shifting of the pyridine ring protons relative to control compounds **4a - d**. As seen in our earlier studies in water,[4b] the magnitude of the upfield shifting varies according to the position of the cation, with the ipso compound exhibiting the most upfield shifting due to its proximity to the A ring (Figure 7.3).

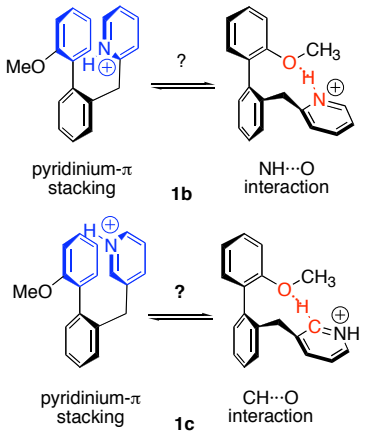

Figure 7.2. Possible interaction geometries of model system 1.

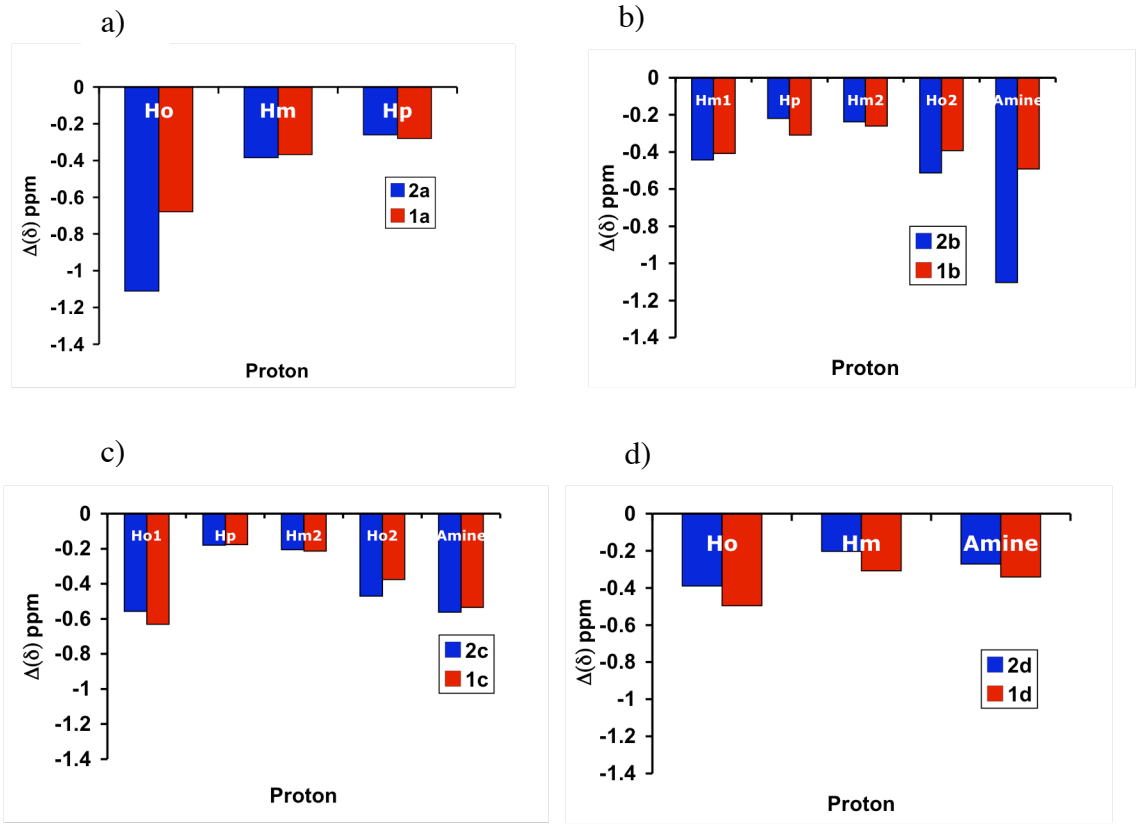

Figure 7.3. Upfield shifting of the pyridinium rings in chloroform of (a) compounds **1a** and **2a**; (b) compounds **1b** and **2b**; (c) compounds **1c** and **2c**; (d) compounds **1d** and **2d**. Compounds and pyridinium protons are labeled as shown in **Scheme 7.1**.

As shown in Figures 7.3c and 7.3d, both the meta and para-substituted compounds from model systems 1 and 2 show similar magnitudes of upfield shifting at all pyridinium ring protons, with differences between systems 1 and 2 of ≤ 0.1 ppm. Since compounds **2c** and **2d** do not contain a methoxy group, this indicates that the stacking interaction in **1c** and **1d** occurs with little interference from C-H---O or N-H---O interactions in chloroform. This is not surprising for the para-substituted compound **1d**, in which the NH is not able to access a hydrogen bond with the oxygen on the A ring. However, some interaction between the methoxy group and the pyridinium ring might be

anticipated for compound **1c**, in particular a C-H—O interaction (see examples in Figure 7.2).

Analysis of the ipso and ortho-substituted compounds **1a** and **1b** is slightly more ambiguous (Fig. 7.3a and 7.3b). While both sets of compounds exhibit similar magnitudes of upfield shifting at most positions, the amine of **1b** is signficantly less upfield shifted than the amine of **2b**, suggesting the presence of a potential NH—O bond in **1b**. Additionally, in the case of the ipso-substituted compounds **1a** and **2a**, the ortho protons are significantly less upfield shifted in **1a** than in **2a**, suggesting the possible presence of a CH—O interaction in compound **1a**.

Comparison of Model System 1 in D_2O and Chloroform. Comparison of the pyridinium ring upfield shifts of model system 1 in chloroform and D_2O reveals similar magnitudes of $\Delta\delta$ for both solvents (Figure 7.4a-d). The similarity of the patterns in upfield shifting of the pyridinium ring suggests similar conformations of molecules **1a-d** in both chloroform and D_2O. This points towards the absence of significant competing NH—O and CH—O interactions in chloroform.

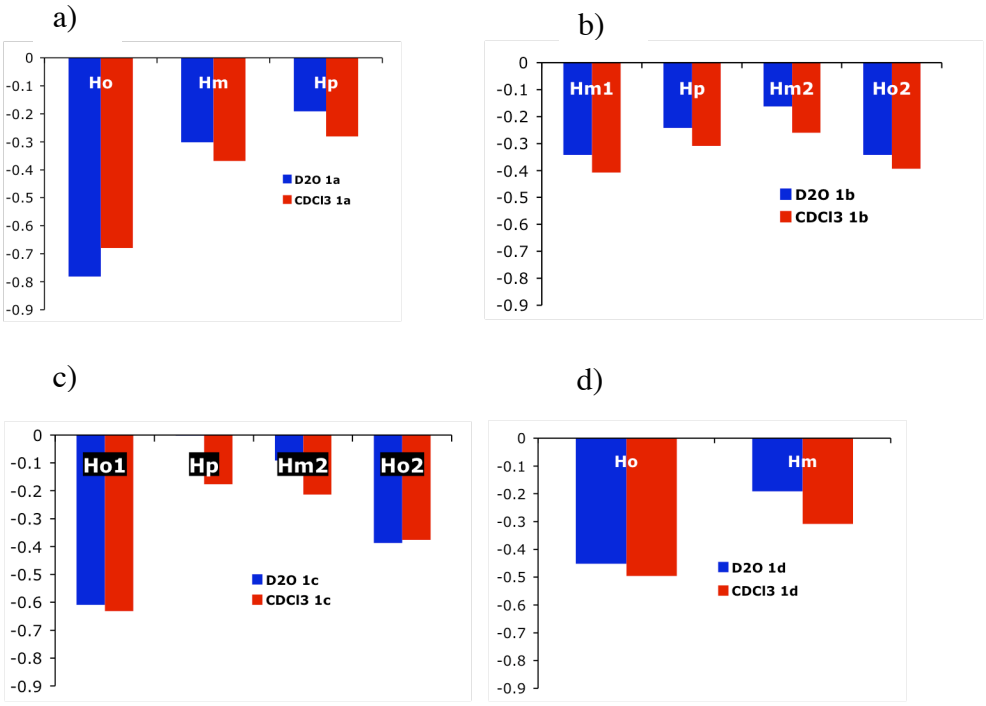

Figure 7.4. Upfield shifting of the pyridinium rings of (a) compound **1a** in D_2O and $CDCl_3$; (b) compound **1b**; (c) compound **1c**; (d) compound **1d**.

Upfield Shifts of Ring A in Chloroform and D_2O. Upfield shifting of the upper biaryl ring A is more sensitive to solvent effects than the pyridinium ring C. While the pattern of upfield shifting is similar among **1a-d** in chloroform and D_2O, the magnitude of the shift is consistently higher in $CDCl_3$ (Figure 7.5a-d), indicating possible conformational differences between the two environments. However, since the pattern of interaction remains much the same between chloroform and D_2O, it is likely that the preferred conformations of the molecules are similar in both solvents but that the populations of the stacked conformations differ.

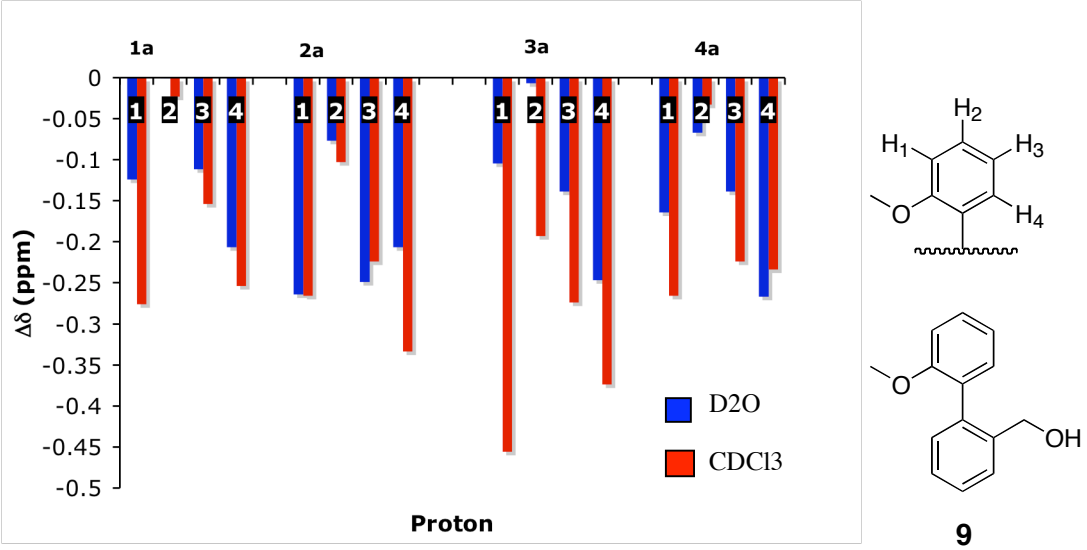

Figure 7.5. Upfield shifting of the upper biaryl ring of (a) compound **1a** in D_2O and $CDCl_3$; (b) compound **1b**; (c) compound **1c**; (d) compound **1d**. Δδ measured relative to control compound **9**.

Crystal Structure of Ipso Compound. Crystals of the ipso compound **1a** were obtained by slow evaporation from $CDCl_3$. The resulting crystal structure indicated that, instead of the stacking orientation proposed for **1a-d** in D_2O (Fig. 7.2), the preferred orientation in the solid state orients the methoxy group over the pyridinium ring with aromatic rings A and C in an offset stacked conformation (Figure 7.6). This raises the proposition that the same conformation may be well populated in organic solvent. This is because, in addition to the cation-π interaction, the lone pairs of oxygen are able to donate into the electron-deficient π-system. This would not be the case in D_2O, where solvation of the methoxy group would be favored over π-donation. This effect, known as an oxygen-arene interaction, has been demonstrated and quantified in a series of elegant studies by Reich and co-workers.[10] They find that, in some cases, the interaction is worth ~0.5 kcal/mol.

[10] Gung, B. W.; Xue, X. W.; Reich, H. J. *J. Org. Chem.* **2005**, 70, 7232 – 7237.

As a result, additive effects between this interaction and the cation-π interaction must be present in our system, and are likely influencing the orientations of the stacked conformers in $CDCl_3$.

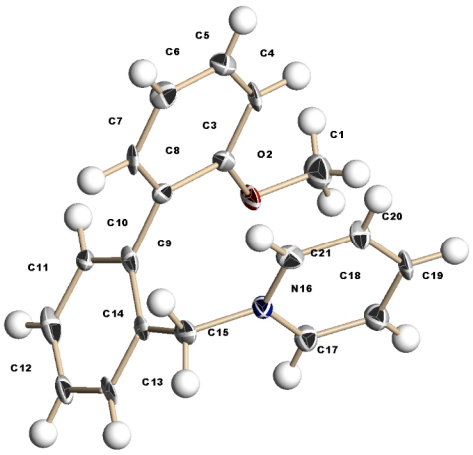

Figure 7.6. Crystal structure of compound **1a**.

Molecular Modeling. To determine whether the preference for the stacking interaction observed in compounds **1a-d** arises from a stronger driving force for interaction or from differences in conformational strain, and to demonstrate energetic differences between the different stacked orientations, we performed a computational study of compounds based on model system 1. The goal of this study is to quantitate energy differences between the cation-π and conformationally feasible NH—O or CH—O interactions in chloroform in the absence of a tether (Figure 7.7). Following literature methodology[11] the interaction energies between anisole and 2, 3, 4, and N-methyl pyridine were calculated

[11] Biot, C.; Buisine, E.; Rooman, M. *J. Am. Chem. Soc.* **2003**, *125*, 13988-13994.

in the gas phase and in chloroform at the MP2/6-31g** level (see Experimental).[12] Starting conformations for the geometry optimizations were based on optimized structures of compounds **1a-d** and optimized in the absence of spatial or geometric constraints (Figure 7.8) in order to achieve optimal interaction energies for the cation-pi, NH-O, and CH-O interactions in question. Counterions were omitted from these calculations due to the ambiguity of their placement in the starting complexes. Although some anions have shown considerable damping of cation-π interactions binding in organic solvents due binding with the cation,[13] it is less likely that a diffuse positive charge, such as that on a pyridinium ring, is as sensitive to the presence of the anion as a ligand more closely resembling a point charge.

The results of our calculations show that the cation-π interaction is predicted to be energetically competitive with NH—O and CH—O interactions in chloroform and, in the case of N-methyl pyridinium, is stronger than the competing CH—O interaction (Table 7.1). Furthermore, it appears that the stacking orientations that place the methoxy group in the immediate vicinity of the pyridinium ring enhance the stacking interaction through oxy-arene effects (Table 7.1, Poses 2 and 3). Based upon these results, it appears that in model systems 1 and 2, the presence of a molecular tether between the A and C rings adds an unfavorable entropic component to forming the proposed hydrogen bonding

---

[12] For other computational studies of pyridine complexes, see (a) Yamada, S.; Misono, T.; Tsuzuki, S. *J. Am. Chem. Soc.* **2004**, *126*, 9862-9872. (b) Mignon, P.; Loverix, S.; De Proft, F.; Geerlings, P. *J. Phys. Chem. A* **2004**, *108*, 6038-6044.

[13] (a) Bartoli, S.; Roelens, S. *J. Am. Chem. Soc.* **2002**, *124*, 8307-8315. (b) Anderson, M. A.; Ogbay, B.; Arimoto, R.; Sha, W.; Kisselev, O. G.; Cistola, D. P.; Marshall, G. R. *J. Am. Chem. Soc.* **2006**, *128*, 7531-7541.

interactions, requiring the formation of 9 or 10-membered hydrogen bonded macrocycles. Thus, the stacking interaction predominates even in the presence of enthalpically favored NH and CH—O hydrogen bonds, and can be further enhanced via an unanticipated oxygen-arene interaction.

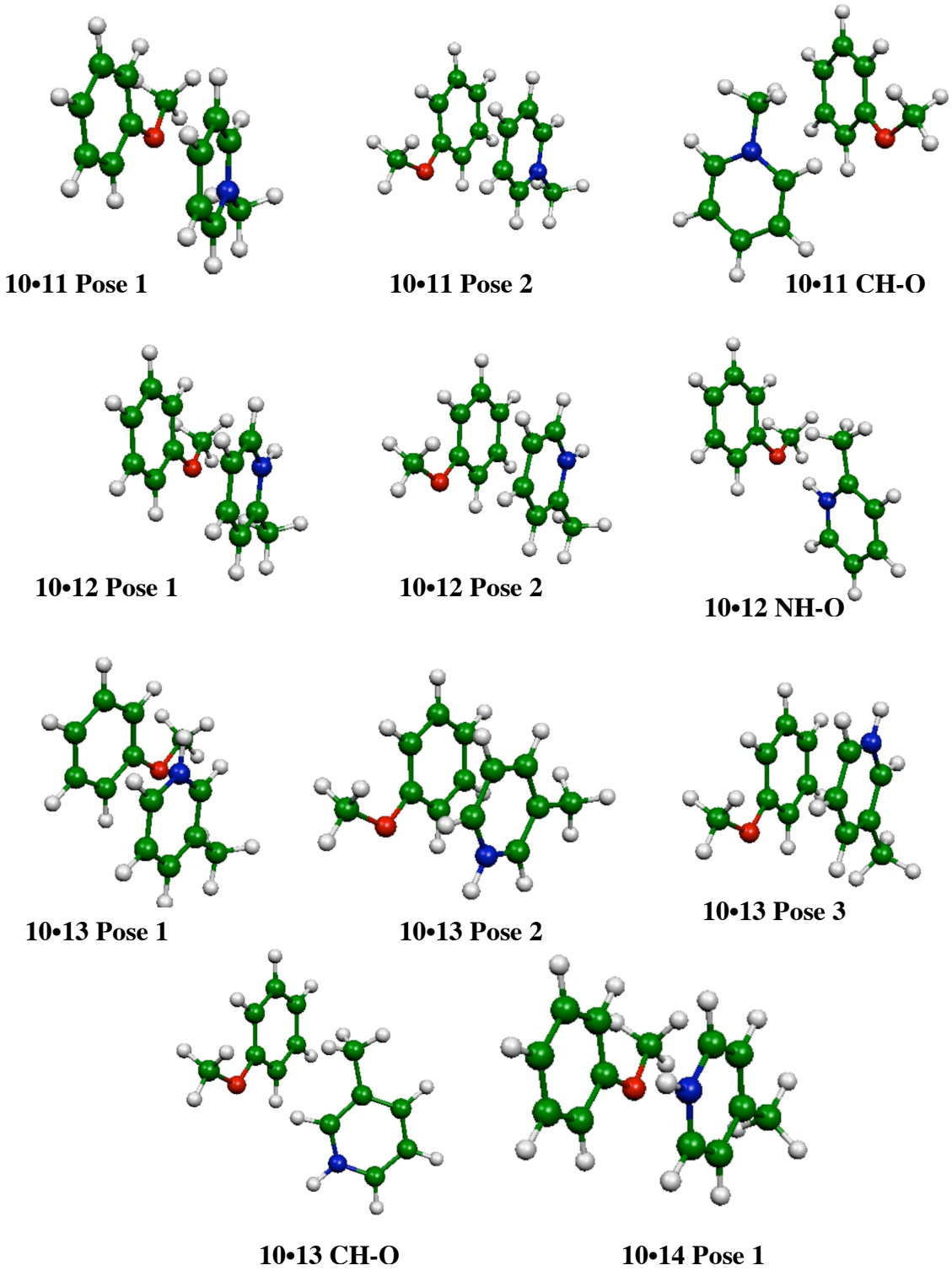

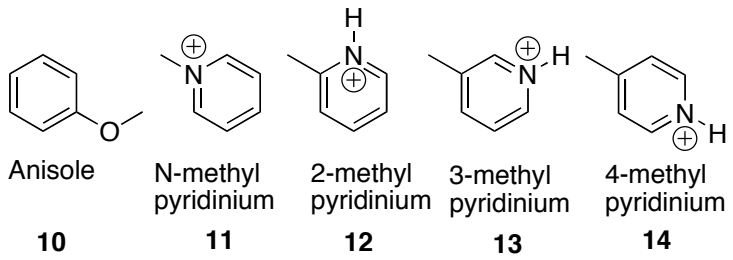

Figure 7.7. Small molecules used to calculate ΔE of interaction in chloroform and various optimized complexes.

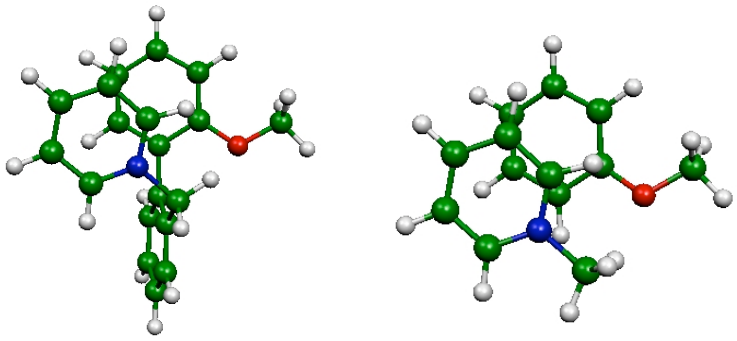

Figure 7.8. (a) Example gas-phase optimized structure of **1a**. (b) Starting conformation of anisole/N-methyl pyridinium (**10•11**) stacked complex based on structure of **1a**.

Table 7.1. Calculated magnitudes of π-stacking versus NH or CH–O interactions between model compounds in chloroform.[a]

Complex	ΔE (cation-π) Pose 1	ΔE (cation-π) Pose 2	ΔE (cation-π) Pose 3	ΔE (NH – O)	ΔE (CH – O)
10•11	-8.6	-8.6	---	---	-7.3
10•12	-6.9	-8.1	---	-7.8	---
10•13	-5.6	-8.2	-8.0	---	-6.6
10•14	-8.0	---	---	---	---

(a) Structures optimized in Gaussian 03 at MP2/6-31g** level. All values reported in kcal/mol. Chloroform modeled implicitly with IEFPCM solvation model. As a result, calculations are uncorrected for BSSE. See experimental section for full computational details, structures, and accompanying gas-phase calculations.

Titration of 4-ethylpyridine. Finally, we evaluated the chemical shifts of protonated 4-ethylpyridine in the presence of anisole (Figure 7.9). While only small changes in chemical shifts were observed (on the order of 0.01 ppm), the NH—O interaction appears to be slightly favored in the 1:1 complex, as expected, based on the magnitude of

downfield shifting of the amine proton. Upon increased anisole concentration, the competing interactions (indicated by upfield shifting of the pyridine protons versus downfield shifting of the NH) demonstrate similar chemical shifts. This is in agreement with our calculations, which suggest modest energetic differences between the cation-π and competing non-covalent interactions.

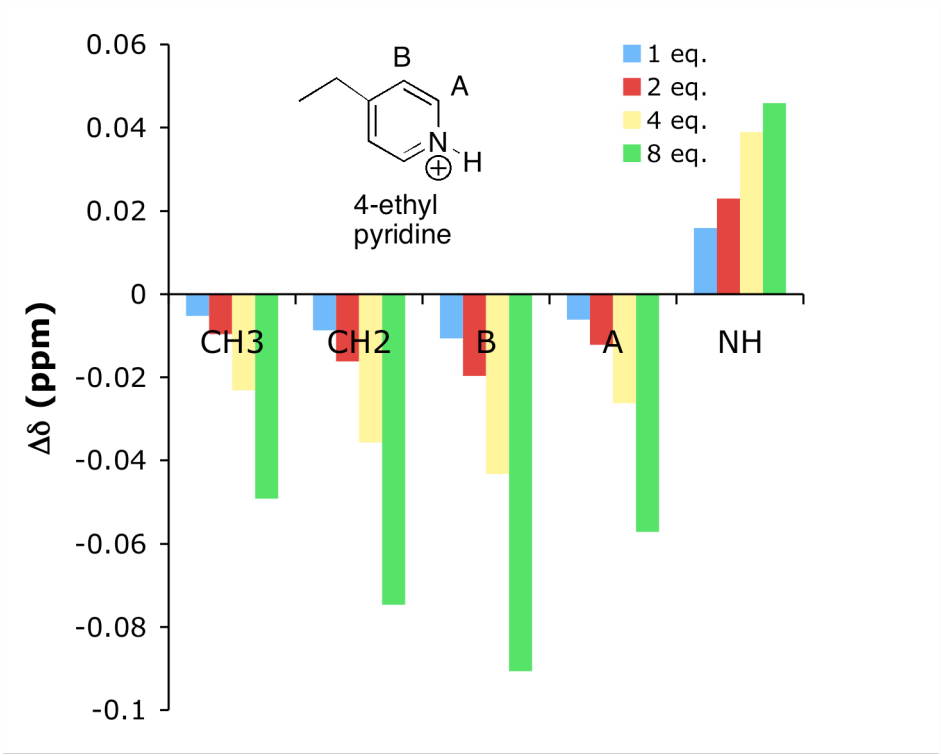

Figure 7.9. Changes in chemical shifts of 4-ethylpyridine in the presence of n equivalents of anisole (n = 1-8).

D. Conclusions.

In summary, a series of compounds has been designed to investigate the magnitude of a cation-π interaction versus NH—or CH—O interactions in organic solution. While NH—and CH—O interactions may play a small role in the conformational stabilities of these compounds, the cation-π interaction dominates the

energetic landscape, even in organic solution. X-ray crystallography suggests that the preferred orientation of stacking may differ between water and chloroform. Theoretical calculations at the MP2/6-31g** level have helped quantify the relative magnitudes of these competing interactions and demonstrates the enhancement of the stacking interaction by the oxygen-arene effect. The cation-π interaction between a positively charged π-system and an aromatic ring, long known the be important in aqueous molecular recognition, is becoming a more popular element of designed catalytic and asymmetric induction systems due to its surprising strength and ability to control substrate orientation in organic solution. We anticipate that these studies will further elucidate its role in the conformational preferences of designed supramolecular systems.

E. Experimental Section.

i. General. All reagents and solvents were purchased from commercial sources and used without additional purification unless otherwise noted. Tetrahydrofuran and methylene chloride were dried via a column of neutral alumina under nitrogen prior to use.

ii. Synthesis.

2-Bromobenzyl alcohol, 3. A round-bottom flask was charged with argon, THF, and 2-bromobenzaldehyde (1.58 g, 8.56 mmol at room temperature. To the flask, $NaCNBH_3$ (538 mg, 8.56 mmol) was added and allowed to stir for one hour. The reaction mixture was quenched with 1N HCl (10 mL) and diluted with diethyl ether. The organic layer was subsequently washed with 20 mL of water followed by 20 mL of brine. The organic layer was dried over magnesium sulfate and concentrated *in vacuo*. The resulting white solid was taken on to the synthesis of **4** without further purification.

2-Bromobenzyl-N-pyridine, 4. A round-bottom flask was charged with argon, $CHCl_3$ (25 mL), and **3** (8.56 mmol). Phosphorous tribromide (271 μL, 2.85 mmol) was added and the reaction mixture was allowed to stir for 1.5 hours. The reaction was quenched with water (10 mL). The reaction was washed with 25 mL portions of sodium bicarbonate, water, and brine, respectively. Finally, the organic layer was dried over magnesium sulfate and concentrated *in vacuo*. The resulting yellow oil was then taken up in 2 mL of pyridine and allowed to stand overnight. The resulting white crystalline product was purified with successive washes of diethyl ether (1.27 g, 60% yield). ^1H

NMR (500 MHz, CDCl3) δ 9.42 (d, 2H, J = 6.5 Hz), 8.54 (dd, 1H, J_1 = 7.5 Hz, J_2 = 7.5 Hz), 8.20 (d, 1H, J = 5 Hz), 8.11 (dd, 2H, J_1 = 6.5 Hz, J_2 = 6.5 Hz), 7.62 (d, 1H, J = 8 Hz), 7.47 (t, 1H, J_1 = 7.5 Hz, J_2 = 8 Hz), 7.34 (t, 1H, J_1 = 8 Hz, J_2 = 7.5 Hz), 6.41 (s, 2H); ^{13}C NMR (100 MHz, CDCl3) δ 146, 145, 134, 134, 132, 132, 129, 128, 125, 64; LR-MS (FAB): calculated = 248; actual = 247.8.

1-(biphenyl-2-ylmethyl)-pyridinium bromide, 1a. A round-bottom flask was charged with argon, dioxane (25 mL), compound **4** (215 mg, 0.87 mmol), compound **2** (88 mg, 0.72 mmol), and 1 mL of H_2O at room temperature. To the flask, $Pd(PPh_3)_4$ (4 mol %) and Na_2CO_3 (1.4 equiv., 97 mg) were added along with a reflux condenser. The reaction was allowed to reflux for 2 hours. The reaction mixture was concentrated *in vacuo* and triturated with ether. The resulting solution was partitioned with water and EtOAc, and the aqueous layer washed with EtOAc (1X). The aqueous layer was subsequently frozen, lyophilized, and purified with reverse-phase HPLC (water/acetonitrile gradient) to yield 50 mg of a clear oil (28% yield). ^{1}H NMR (500 MHz, $CDCl_3$) δ 8.31 (d, 2H, J = 6 Hz), 8.28 (t, 1H, J = 7.5 Hz), 7.73 (dd, 2H, J_1 = 7 Hz, J_2 = 7.5 Hz), 7.68 (d, 1H, J = 7 Hz), 7.49 (m, 2H), 7.37 (m, 3H), 7.30 (d, 1H, J = 7.5 Hz), 7.07 (m, 2H), 5.91 (s, 2H); ^{13}C NMR (100 MHz, $CDCl_3$) δ 145, 144, 143, 139, 131, 131, 131, 130, 129, 129, 128, 128, 128, 63; LR-MS (FAB): calculated = 246; actual = 245.99.

(2-bromophenyl)-pyridin-2-yl-methanol, 6a. A dry round bottom flask charged with argon and a stirbar was filled with isopropylmagnesium chloride (2 M in THF, 5.2 mL, 10.4 mmol) followed by the dropwise addition of 2-bromopyridine (1 mL, 10.4 mmol) while stirring at room temperature. After one hour 2-bromobenzaldehyde (1.34 mL, 11.5 mmol) was added and stirred for another two hours while monitored by TLC (1:1

Hexanes/EtOAc). The reaction was quenched with 10 mL 1N HCl. The aqueous layer was washed with ether and then neutralized with 1N NaOH resulting in a cloudy solution. The suspension was then extracted into ether. The resulting organic layer was then washed with water and brine followed by drying over magnesium sulfate and concentrated *in vacuo*, recovering 1.45 g of an off-white colored powder (52% yield). Product carried on to next step without further purification. ^{1}H NMR (400 MHz, $CDCl_3$) δ 8.56 (d, 1H, J = 5 Hz), 7.61 (t, 1H, J = 7 Hz), 7.56 (d, 1H J_1 = 7 Hz), 7.33 (d, 1H, J = 8 Hz) 7.23 (m, 2H), 7.11 (t, 1H, J = 8 Hz), 6.73 (d, 1H, J = 2 Hz), 5.48 (d. 1H, J = 2 Hz); LR-MS (ESI): calculated = 264.1; actual = 264.0.

(2-Bromophenyl)-pyridin-3-yl-methanol, 6b. See synthesis of **6a**. (69%yield). ^{1}H NMR (300 MHz, $CDCl_3$) δ 8.66 (s, 1H), 8.50 (d, 1H, J = 5 Hz), 7.70 (dt, 1H, J_1 = 7 Hz, J_2 = 2 Hz), 7.61 (dd, 1H, J_1 = 7 Hz, J_2 = 2 Hz), 7.56 (d, 1H, J = 7 Hz), 7.38 (t, 1H, J = 2 Hz), 7.26 (m, 1H), 7.19 (t, 1H, J_1 = 7 Hz, J_2 = 2 Hz), 6.35 (s, 1H); LR-MS (ESI): calculated = 264.1; actual = 264.0.

(2-Bromophenyl)-pyridin-4-yl-methanol, 6c. In a separatory funnel, 4-bromopyridine hydrochloride (2.5 g, 12.8 mmol) was deprotonated with 20 mL of 2M K_2CO_3 and extracted into 20mL of dichloromethane. The organic layer was dried over $MgSO_4$ and evaporated. The resulting oil was taken up into 20 mL of THF in a round-bottom flask and placed under an atmosphere of nitrogen. While stirred at room temperature isopropylmagnesium chloride (2M in THF, 6.4 mL, 12.8 mmol) was added dropwise and stirred for 1 hour. After one hour, 2-bromobenzaldehyde (1.58 mL, 12.8mmol) was added and stirred for another two hours while monitored by TLC (1:1 hexanes/ethyl acetate). The reaction was quenched with 10 mL 1N HCl. The aqueous layer is washed

with ether then neutralized with 1N NaOH resulting in a cloudy solution. The suspension was then extracted into ether. The resulting organic layer was then washed with water and brine followed by drying over magnesium sulfate and concentrated *in vacuo*, giving 1.05 g of an off-white colored powder (31% yield). Product carried on to next step without further purification. ^{1}H NMR (300 MHz, $CDCl_3$) δ 8.54 (d, 2H, J = 6 Hz), 7.57 (d, 1H, J_1 = 8 Hz, J_2 = 2 Hz), 7.46 (d, 1H, J_1 = 7 Hz, J_2 = 2 Hz), 7.35 (m 3H), 7.18 (t, 1H, J_1 = 7 Hz, J_2 = 2 Hz), 6.24 (s, 1H).

Acetic acid (2-bromo-phenyl)-pyridin-2-yl-methyl ester, 7a. A round-bottom flask charged with anhydrous methylene chloride, compound **6a** (394 mg, 1.49 mmol), acetic anhydride (167 μL, 181 mg, 1.78 mmol), pyridine (143 μL, 140 mg, 1.78 mmol), and DMAP (36 mg, 0.298 mmol) and stirred overnight at room temperature. The reaction mixture was quenched with water and adjusted to neutral pH. The water was extracted with methylene chloride and the organic layer was dried over magnesium sulfate and concentrated *in vacuo*. The product was purified by column chromatography with 1:1 hexanes : ethyl acetate as the mobile phase resulting in 122 mg of a yellow oil (52% yield). ^{1}H NMR (300 MHz, $CDCl_3$) δ 8.63 (d, 1H, J = 5 Hz), 7.69 (dd, 1H, J_1 = 8 Hz, J_2 = 2 Hz), 7.57 (dd, 1H, J_1 = 2 Hz, J_2 = 2 Hz), 7.49 (dd, 1H, J_1 = 8 Hz, J_2 = 2 Hz), 7.43 (d, 1H, J = 3 Hz), 7.33 (t, 1H, J = 7 Hz), 7.21 (m, 3H), 2.20 (s, 3H). LR-MS (CI): calculated = 305.0; actual = 306.0.

Acetic acid (2-bromo-phenyl)-pyridin-3-yl-methyl ester, 7b. See synthesis of **7a**. (84% yield). ^{1}H NMR (300 MHz, $CDCl_3$) δ 8.66 (s, 1H), 8.70 (d, 1H, J = 5 Hz), 7.70 (dd, 1H, J_1 = 8 Hz, J_2 = 2Hz), 7.57 (d, 1H, J = 8 Hz), 7.52 (d, 1H, J = 8 Hz), 7.43 (t, 1H, J = 7

Hz), 7.29 (m, 1H), 7.20 (m, 2H), 2.17 (s, 3H); LR-MS (ESI): calculated = 305.0; actual = 305.0.

Acetic acid (2-bromo-phenyl)-pyridin-4-yl-methyl ester, 7c. See synthesis of **7a.** (84% yield). ^{1}H NMR (300 MHz, $CDCl_3$) δ 8.73 (d, 2H, J = 6 Hz), 7.74 (d, 1H, J_1 = 8 Hz, J_2 = 1 Hz), 7.50 (m, 2H), 7.42 (d, 1H, J = 6 Hz), 7.35 (m, 1H), 7.31 (s, 2H), 5.44 (s, 3H).

2-Bromobenzyl-2-pyridine, 8a. In a round bottom flask charged with Ar and a stirbar was added **4a** (167mg, 0.55mmol) and t-BuOH (61mg, 0.8mmol, 78μL) in 5mL of THF. This was followed by the addition with SmI_2 (1.6mmol, 16.4mL, 0.1M in THF) dropwise over approximately 10 minutes. The mixture was stirred for 2 hours while monitored by TLC (10:1 hexanes/ethyl acetate). The reaction was quenched with water and extracted with ether followed by washes with water and brine. The organic layer was dried over magnesium sulfate and concentrated *in vacuo*. The resulting oil was purified by column chromatography (10:1 hexanes : ethyl acetate) to give 56 mg of product (46% yield). ^{1}H NMR (500 MHz, $CDCl_3$, protonated with HBF_4) δ 14.04, (broad singlet, 1H), 8.85 (d, 1H J = 6 Hz), 8.35 (dd, 1H, J_1 = 8 Hz, J_2 = 8 Hz), 7.89 (dd, 1H, J_1 = 6.8 Hz, J_2 = 6.8 Hz) 7.63 (d, 1H, J = 8 Hz), 7.58 (d, 1H, J = 8 Hz), 7.52 (d, 1H, J = 8 Hz), 7.41 (dd, 1H, J_1 = 7.5 Hz, J_2 = 7.5 Hz), 7.28 (dd, 1H, J_1 = 8.5 Hz, J_2 = 6.5 Hz), 4.64 (s, 2H); ^{13}C NMR (100 MHz, $CDCl_3$) δ 156, 147, 142, 134, 133, 133, 131, 129, 127, 125, 125, 40; LR-MS (ESI): calculated = 248; actual = 247.83.

2-Bromobenzyl-3-pyridine, 8b. See synthesis of **8a.** ^{1}H NMR (500 MHz, $CDCl_3$, protonated with HBF_4) δ 14.09, (broad singlet, 1H), 8.76 (s, 1H), 8.72 (s, 1H) 8.26 (d, 1H, J = 8 Hz), 7.91 (t, 1H, J_1 = 6.5 Hz, J_2 = 7.5 Hz), 7.61 (d, 1H, J = 8 Hz), 7.37 (d, 2H, J = 4 Hz), 7.23 (dd, 1H, J = 8.25), 4.35 (s, 2H); ^{13}C NMR (100 MHz, $CDCl_3$) δ 147, 142,

141, 140, 136, 134, 132, 130, 129, 127, 125, 39; LR-MS (ESI): calculated = 248; actual = 247.83.

2-Bromobenzyl-4-pyridine, 8c. See synthesis of **8a**. ^{1}H NMR (500 MHz, $CDCl_3$, protonated with HBF_4) δ 13.69 (broad triplet, 1H), 8.73 (s, 2H), 7.73 (d, 2H, J = 6 Hz) 7.64 (d, 1H, J = 8 Hz), 7.39 (dd, 1H, J_1 = 7.5 Hz, J_2 = 7.5 Hz), 7.33 (d, 1H, J = 6.75 Hz), 7.26 (dd, 1H, J_1 = 8.5 Hz, J_2 = 7.5 Hz) 4.41 (s, 2H); ^{13}C NMR (100 MHz, $CDCl_3$) δ 162, 142, 135, 134, 132, 130, 129, 127, 125, 42; LR-MS (ESI): calculated = 248; actual = 247.83.

2-(biphenyl-2-ylmethyl)-pyridine, 1b. A round-bottom flask was filled with argon, 20mL benzene, compound **8a** (92 mg, 0.37 mmol), and compound **2** (54 mg, 0.45 mmol) at room temperature. To the flask $Pd(PPh_3)_4$ (23mg, 0.02mmol) and 2 mL of 2M K_2CO_3 were added. The reaction was allowed to stir overnight under reflux. Upon cooling, 5 mL of 30% H_2O_2 was added and stirred for 30 minutes. The reaction mixture was extracted into ether and washed with 20 mL of water followed by 20 mL of brine. The organic layer was dried over magnesium sulfate and concentrated *in vacuo*. The resulting oil was purified by column chromatography (10:1 hexanes : ethyl acetate) to give a yellow oil. ^{1}H NMR (500 MHz, $CDCl_3$, protonated with HBF_4) δ 12.86, (broad singlet, 1H), 8.405 (s, 1H), 8.12 (t, 1H, J = 8 Hz), 7.67 (t, 1H, J = 6.5 Hz), 7.40 (s, 1H), 7.37 (m, 2H), 7.30 (dd, 2H, J_1 = 7 Hz, J_2 = 6 Hz), 7.25 (m, 2H), 7.12 (d, 1H, J = 8 Hz), 7.07 (d, 2H, J = 7 Hz), 4.43 (s, 2H); ^{13}C NMR (100 MHz, $CDCl_3$) δ 156, 146, 143, 141, 140, 132, 131, 131, 129, 129, 129, 129, 128, 127, 125, 38; LR-MS (ESI): calculated = 246; actual = 246.05.

3-(biphenyl-2-ylmethyl)-pyridine, 1c. See synthesis of **1b**. ^{1}H NMR (500 MHz, $CDCl_3$, protonated with HBF_4) δ 13.53 (broad singlet, 1H), 8.58 (d, 1H, J = 4 Hz), 8.16 (s, 1H), 7.79 (d, 1H, J = 8 Hz), 7.71 (dd, 1H, J_1 = 6 Hz, J_2 = 7.5 Hz), 7.34 (m, 6H), 7.25 (m, 1H), 7.09 (d, 2H, J = 6.5 Hz), 4.17 (s, 2H); ^{13}C NMR (100 MHz, $CDCl_3$) δ 147, 143, 141, 141, 140, 135, 131, 131, 129, 129, 129, 128, 128, 128, 127, 37; LR-MS (ESI): calculated = 246; actual = 246.05.

4-(biphenyl-2-ylmethyl)-pyridine, 1d. See synthesis of **1b**. ^{1}H NMR (500 MHz, $CDCl_3$, protonated with HBF_4) δ 13.42 (broad singlet, 1H), 8.53 (s, 2H), 7.38 (d, 1H, J = 4 Hz), 7.37 (d, 1H, J = 4 Hz), 7.34 (m, 5H), 7.29 (m, 2H), 7.08 (d, 2H, J = 7.5 Hz), 4.22 (s, 2H); ^{13}C NMR (100 MHz, $CDCl_3$) δ 164, 143, 141, 141, 134, 131, 131, 129, 129, 129, 128, 128, 127, 40; LR-MS (ESI): calculated = 246; actual = 245.87.

iii. ^{1}HNMR Spectra of Model Systems and Reference Compounds

Figure 7.10. ^{1}HNMR of 2-Bromobenzyl-N-pyridine, 4.

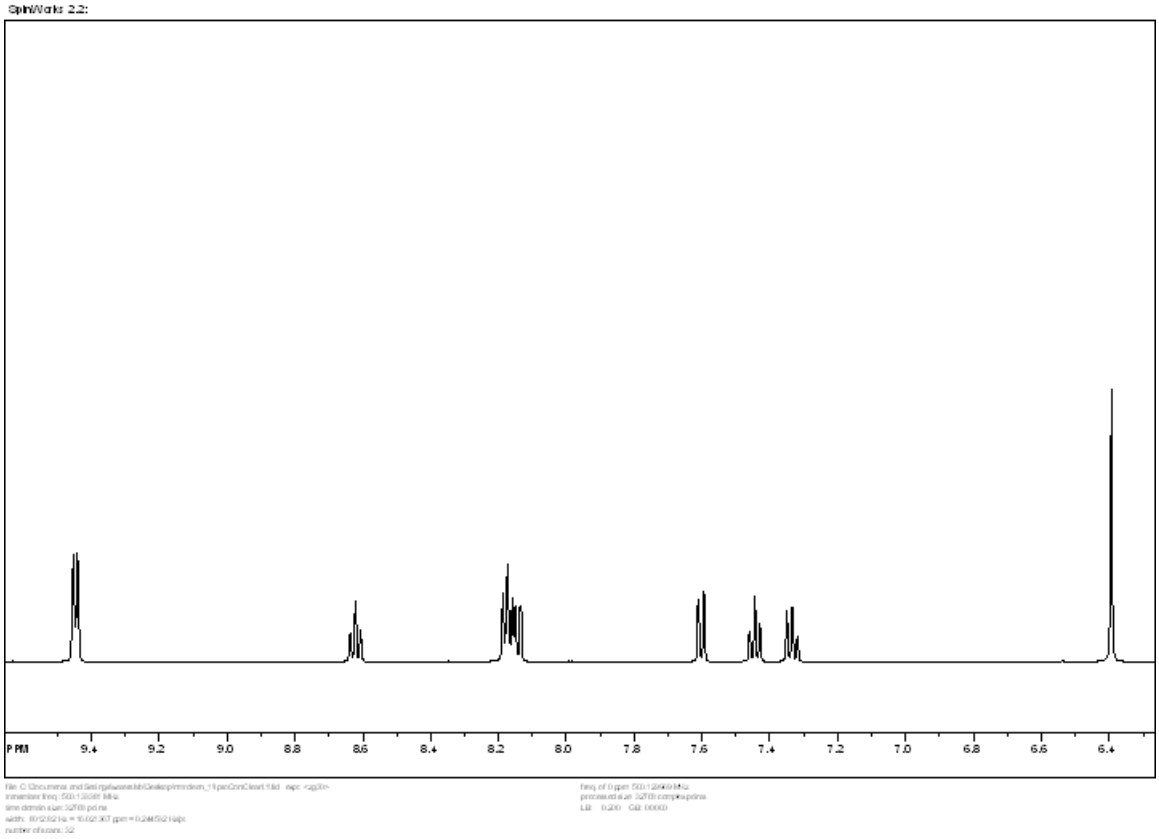

Figure 7.11. ^{1}HNMR of 2-Bromobenzyl-2-pyridine, 8a.

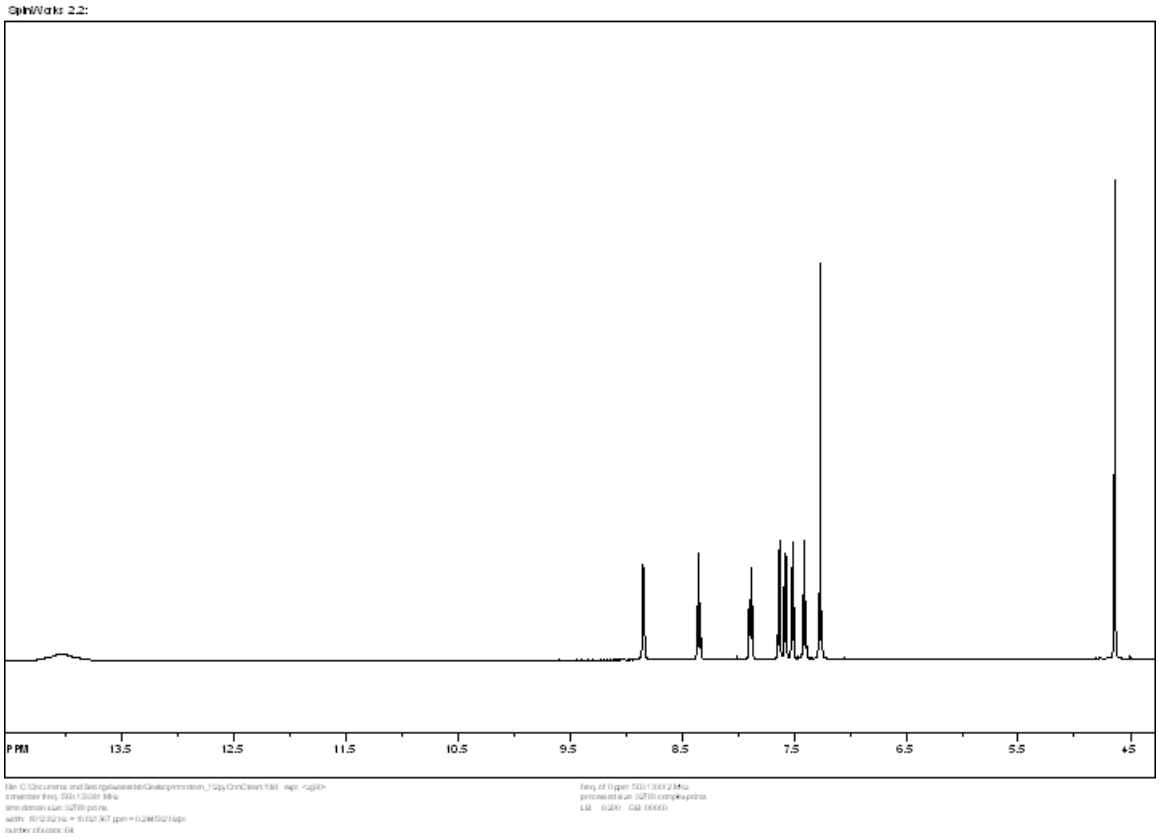

Figure 7.12. ^{1}HNMR of 2-Bromobenzyl-3-pyridine, 8b.

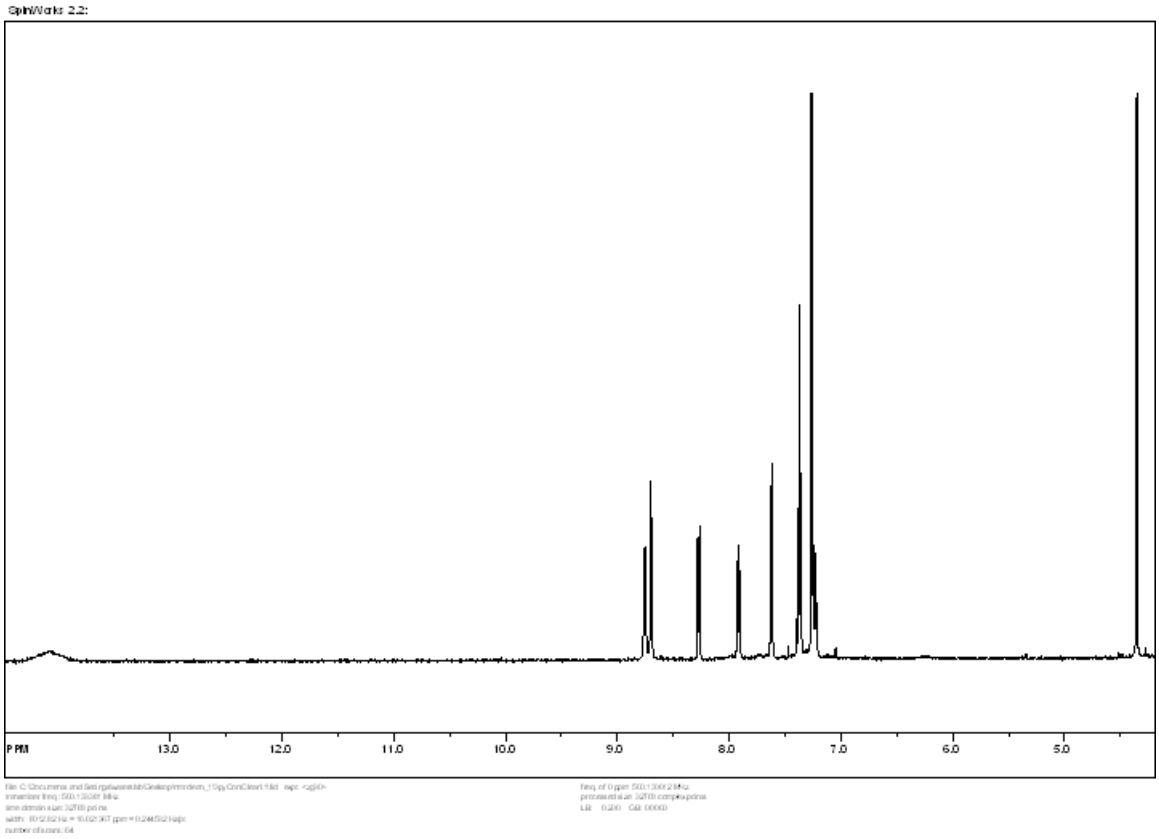

Figure 7.13. ^{1}HNMR of 2-Bromobenzyl-4-pyridine, 8c.

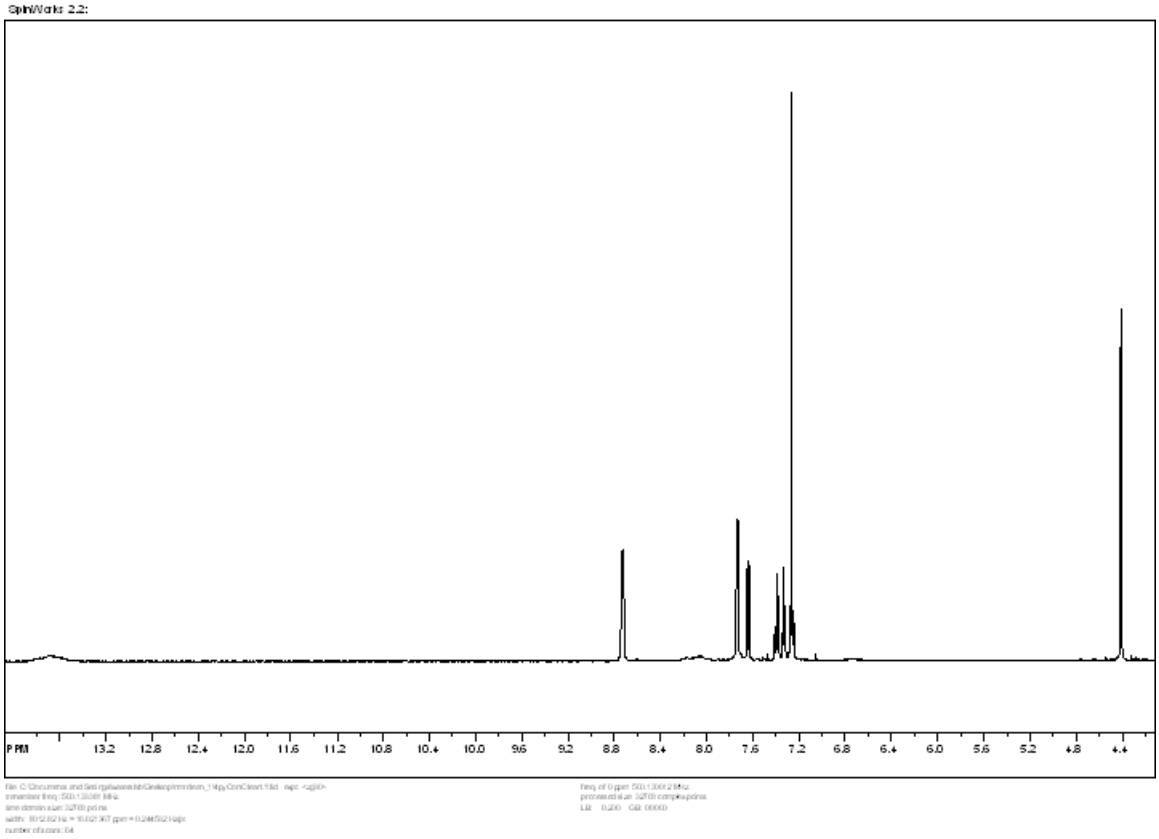

Figure 7.14. ^{1}HNMR of 1-(biphenyl-2-ylmethyl)-pyridinium bromide, 1a.

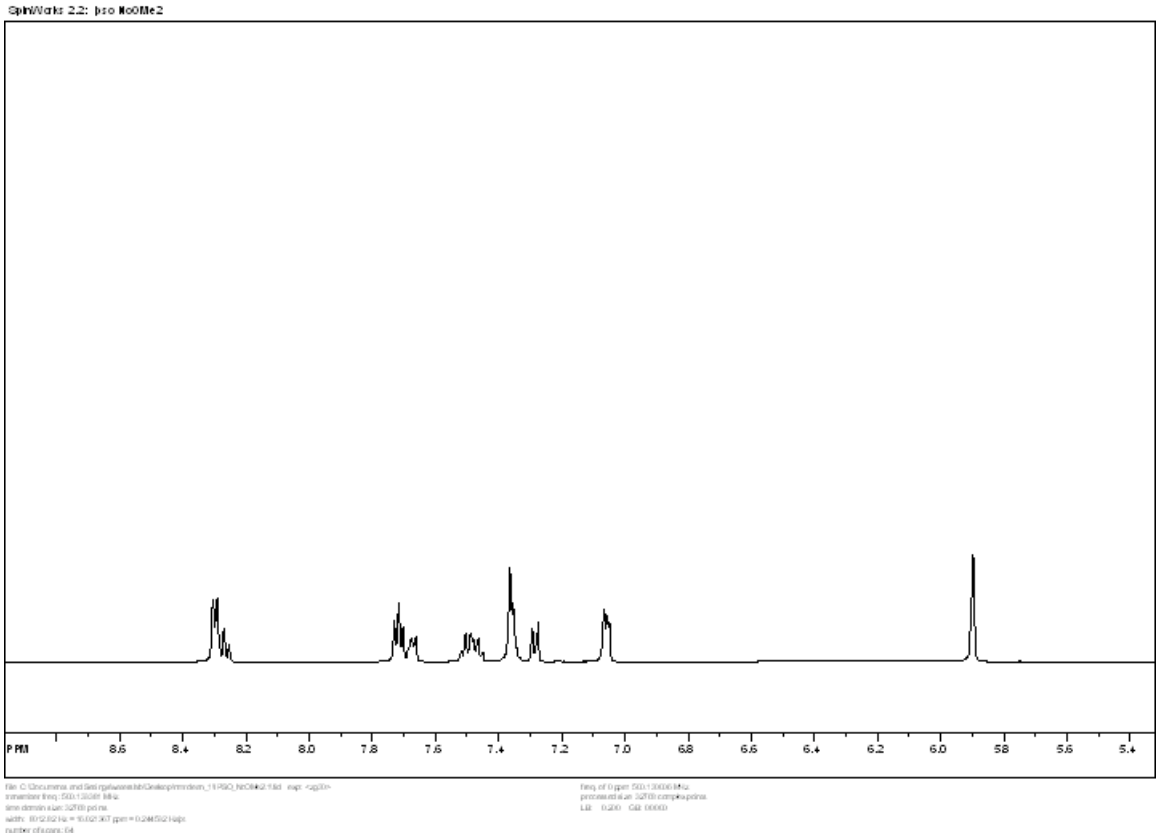

Figure 7.15. ^{1}HNMR of 2-(biphenyl-2-ylmethyl)-pyridine, 1b.

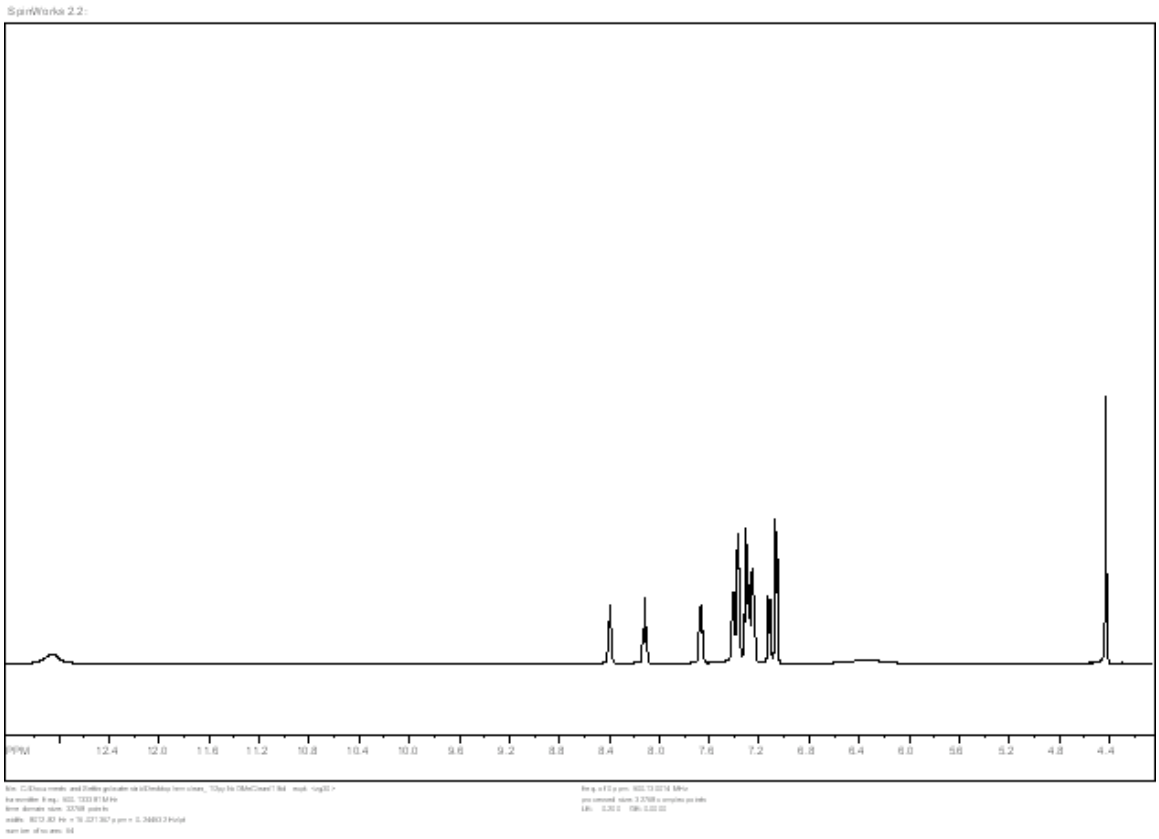

Figure 7.16. ^{1}HNMR of 3-(biphenyl-2-ylmethyl)-pyridine, 1c.

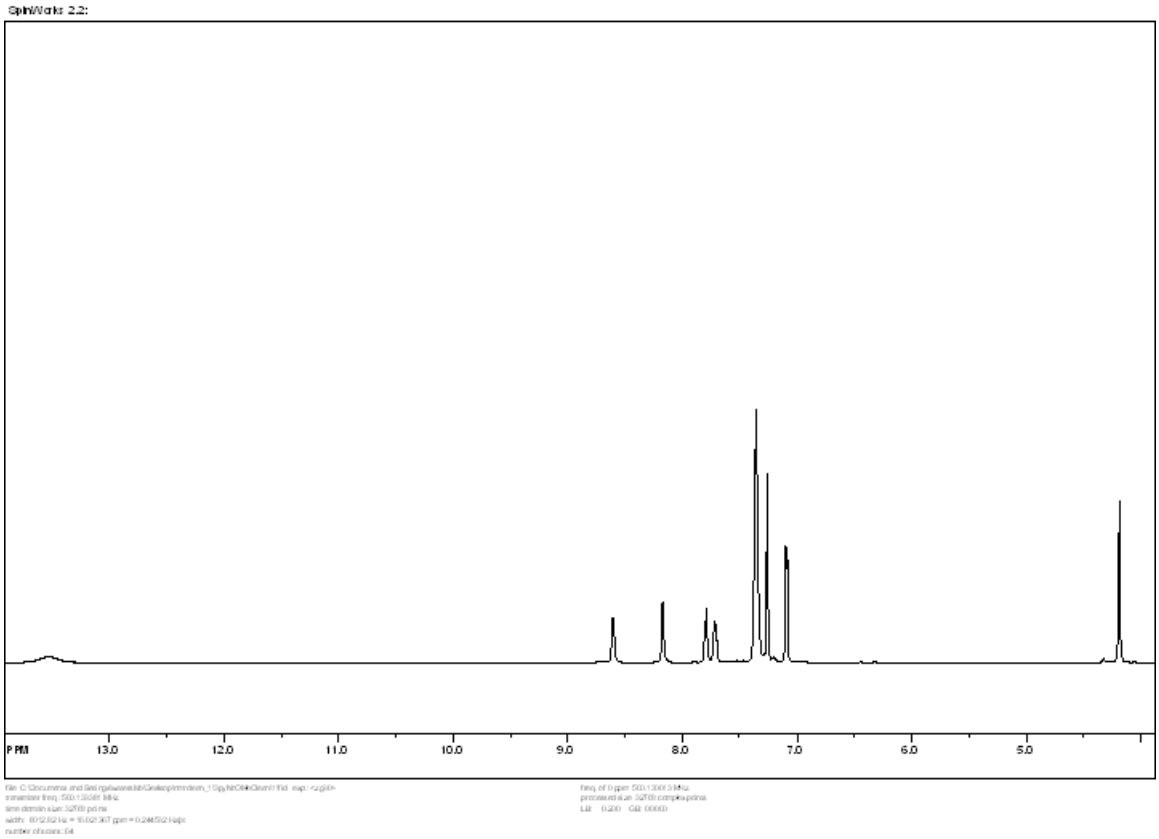

Figure 7.17. ^{1}HNMR of 4-(biphenyl-2-ylmethyl)-pyridine, 1d.

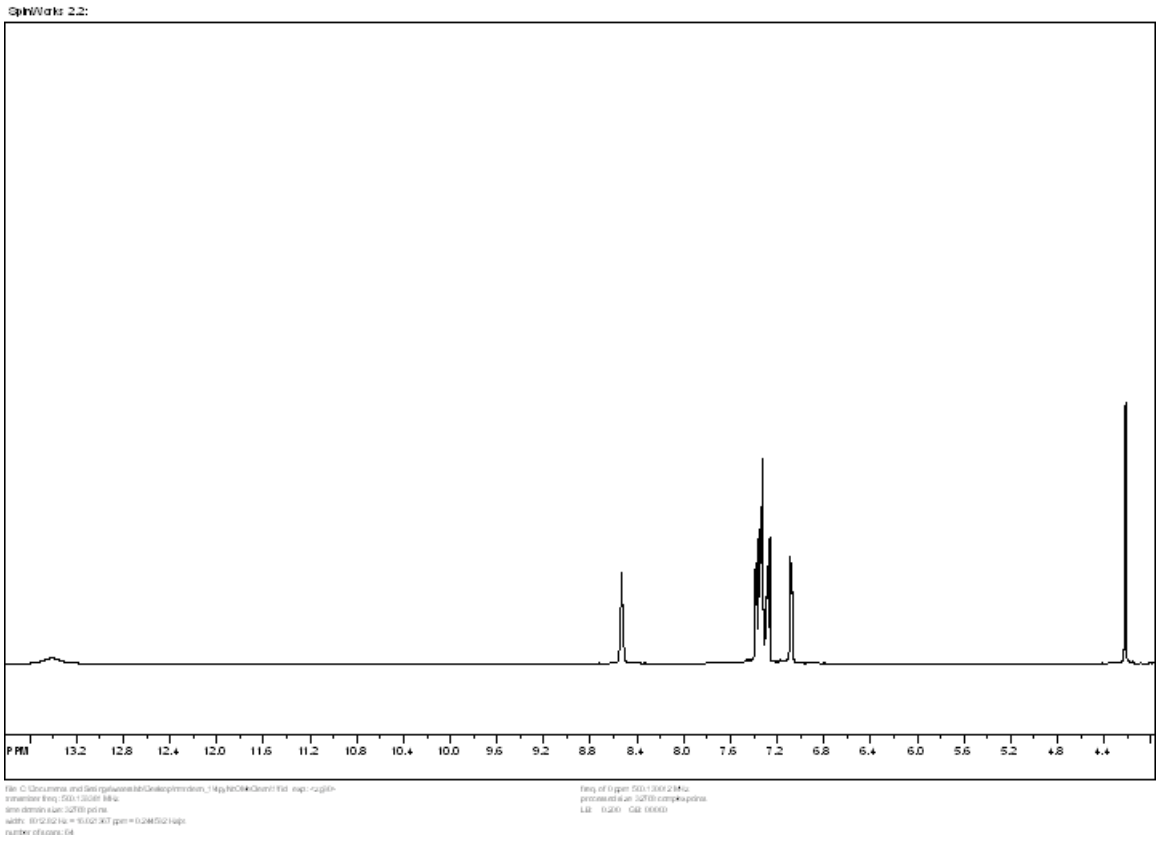

iv. Molecular Modeling. Gas phase and implicit solvent calculations (IEF-PCM=Chloroform) were performed using Gaussian 03 (B 04).[14] Low energy structures were determined by optimizations of anisole and Ipso-, 2-, 3-, or 4-methylpyridine alone and in complex at the MP2/6-31g** level. Starting orientations for the optimizations were chosen based on model structures of experimental compounds 1a-d. Structures were optimized separately for gas phase and solution phase calculations (i.e., solvated energies were not measured with single-point calculations in implicit solvent on gas phase optimized structures). Following methodology of Rooman, et al,[15] interaction energies were measured by the following equation:

$$\Delta E_{MP2} = E_{A\text{-}B} - E_A - E_B$$

Where $E_{A\text{-}B}$ is the MP2 energy of the optimized complex, E_B is the MP2 energy of optimized monomer B, and E_A is the MP2 energy of optimized monomer A. While gas phase calculations were corrected for basis-set superposition error (BSSE), BSSE corrections are unavailable for implicit solvent calculations, resulting in overestimations

---

[14] Gaussian 03, Revision B.04, Frisch, M. J.; Trucks, G. W.; Schlegel, H. B.; Scuseria, G. E.; Robb, M. A.; Cheeseman, J. R.; Montgomery, Jr., J. A.; Vreven, T.; Kudin, K. N.; Burant, J. C.; Millam, J. M.; Iyengar, S. S.; Tomasi, J.; Barone, V.; Mennucci, B.; Cossi, M.; Scalmani, G.; Rega, N.; Petersson, G. A.; Nakatsuji, H.; Hada, M.; Ehara, M.; Toyota, K.; Fukuda, R.; Hasegawa, J.; Ishida, M.; Nakajima, T.; Honda, Y.; Kitao, O.; Nakai, H.; Klene, M.; Li, X.; Knox, J. E.; Hratchian, H. P.; Cross, J. B.; Bakken, V.; Adamo, C.; Jaramillo, J.; Gomperts, R.; Stratmann, R. E.; Yazyev, O.; Austin, A. J.; Cammi, R.; Pomelli, C.; Ochterski, J. W.; Ayala, P. Y.; Morokuma, K.; Voth, G. A.; Salvador, P.; Dannenberg, J. J.; Zakrzewski, V. G.; Dapprich, S.; Daniels, A. D.; Strain, M. C.; Farkas, O.; Malick, D. K.; Rabuck, A. D.; Raghavachari, K.; Foresman, J. B.; Ortiz, J. V.; Cui, Q.; Baboul, A. G.; Clifford, S.; Cioslowski, J.; Stefanov, B. B.; Liu, G.; Liashenko, A.; Piskorz, P.; Komaromi, I.; Martin, R. L.; Fox, D. J.; Keith, T.; Al-Laham, M. A.; Peng, C. Y.; Nanayakkara, A.; Challacombe, M.; Gill, P. M. W.; Johnson, B.; Chen, W.; Wong, M. W.; Gonzalez, C.; and Pople, J. A.; Gaussian, Inc., Wallingford CT, 2004.

[15] Biot, C.; Buisine, E.; Rooman, M. *J. Am. Chem. Soc.* **2003**, 125, 13988.

of the energies of complexation. However, the relative magnitudes of interaction should still be the same, allowing a qualitative analysis of interaction preferences.

Table 7.2. Gas Phase interaction energies for anisole/methyl pyridine complexes.

	IpsoStkGas	IpsoCHOGas
ΔE (MP2) kcal/mol	-15.39	-14.93
BSSE Corrected (kcal/mol)	-10.59	-11.18
	2pyStkGas	2pyNHOGas
ΔE (MP2) kcal/mol	-20.47	-20.32
BSSE Corrected (kcal/mol)	-9.78	-16.58
	3pyStkGas	3pyCHOGas
ΔE (MP2) kcal/mol	-19.34	-14.1
BSSE Corrected (kcal/mol)	-9.09	-10.5
	4pyStkGas	
ΔE (MP2) kcal/mol	-15.1	
BSSE Corrected (kcal/mol)	-10.08	

In the gas phase, there were two cases in which structures starting from stacked conformations optimized to other conformations (3pyStkGas and 2pyStkGas). This is consistent with literature precedent for the preferred orientations of aromatic rings in the gas phase.[16] Additionally, optimized complexes displaying NH and CH--O interactions differed significantly from their starting geometries, reflecting orientation preferences not achievable with the tethered model systems.

[16] Hunter, C.A.; Lawson, K.R.; Perkins, J.; Urch, C.J. *J. Chem. Soc., Perkin Trans. 2*, **2001**, 651-669.

Scheme 7.2. Optimized Gas Phase complexes (see Table 7.2 above).

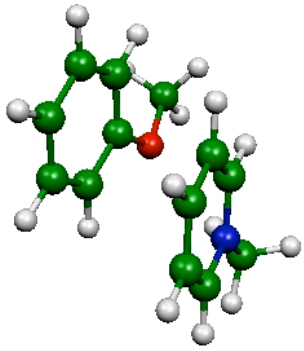

IpsoStkGas

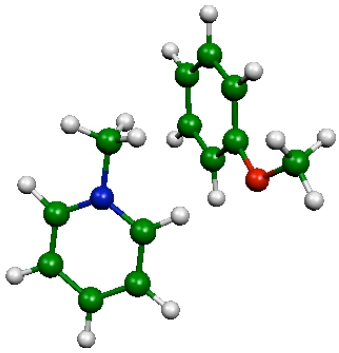

IpsoCHOGas

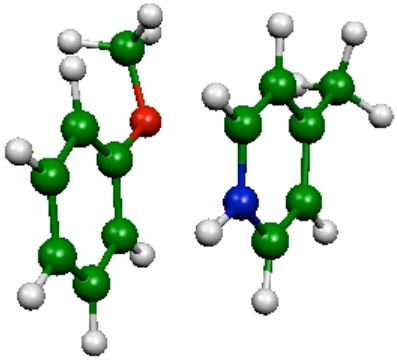

4pyStkGas

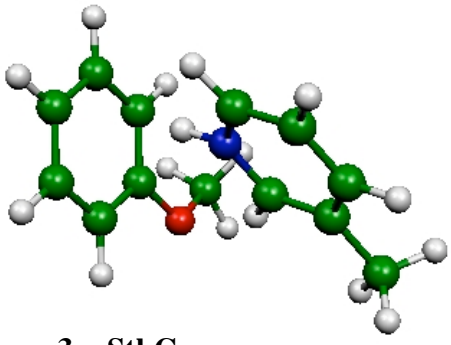

3pyStkGas

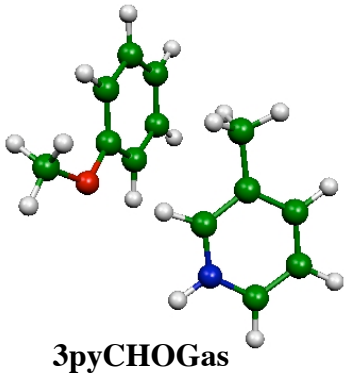

3pyCHOGas

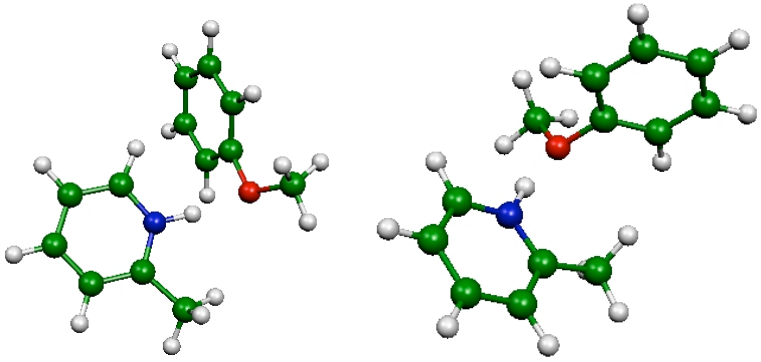

2pyStkGas **2pyNHOGas**

v. 4-ethylpyridine/anisole titration. 500 uL of 4-ethylpyridine (TCI America) was added to 500 uL of distilled, deionized water. HBF_4 was added dropwise until the solution reached pH 1 (Congo Red). The resulting solution was frozen and lyophilized for 72 hours. Dry $CDCl_3$ (2 mL) was added to the resulting oil, resulting in a two-phase mixture of $CDCl_3$ and 4-ethylpyridine. The $CDCl_3$ layer was separated out and determined by integration against TMS to be approximately 55 mM in protonated 4-ethylpyridine. A solution of anisole was dried with $MgSO_4$, and added to the 4-ethyl pyridine sample in increments of 1-2 equivalents. Changes in chemical shifts were measured relative to those of protonated 4-ethylpyridine alone in chloroform. ^{1}H NMR (600 MHz, CDCl3) δ 13.28 (dd, broad, 1H), 8.76 (dd, 2H, J_1 = 5.4 Hz, J_2 = 5.4 Hz), 7.83 (d, 2H, J = 6 Hz), 2.96 (q, 2H), 1.36 (t, 3H).

vi. X-ray Crystallographic Data (Dr. Peter S. White, UNC)

Table 7.3. Crystal data and structure refinement for c05378.

Identification code	c05378	
Empirical formula	C19 H18 Br N O	
Formula weight	356.25	
Temperature	100(2) K	
Wavelength	1.54178 Å	
Crystal system	Monoclinic	
Space group	$P2_1/c$	
Unit cell dimensions	a = 14.253(2) Å	α= 90°.
	b = 8.2825(14) Å	β= 107.277(9)°.
	c = 14.4981(17) Å	γ = 90°.
Volume	1634.3(4) $Å^3$	
Z	4	
Density (calculated)	1.448 Mg/m^3	
Absorption coefficient	3.426 mm^{-1}	
F(000)	728	
Crystal size	0.13 x 0.06 x 0.03 mm^3	
Theta range for data collection	3.25 to 60.00°.	
Index ranges	-15<=h<=15, -5<=k<=8, -15<=l<=15	
Reflections collected	5369	
Independent reflections	2082 [R(int) = 0.0773]	
Completeness to theta = 60.00°	85.8 %	
Absorption correction	None	
Refinement method	Full-matrix least-squares on F^2	
Data / restraints / parameters	2082 / 0 / 200	
Goodness-of-fit on F^2	1.082	
Final R indices [I>2sigma(I)]	R1 = 0.0684, wR2 = 0.1580	

R indices (all data)	R1 = 0.0975, wR2 = 0.1751
Largest diff. peak and hole	1.032 and -1.026 e.Å^{-3}

Table 7.4. Atomic coordinates (x 10^4) and equivalent isotropic displacement parameters ($Å^2$x 10^3) for c05378. U(eq) is defined as one third of the trace of the orthogonalized U^{ij} tensor.

	x	y	z	U(eq)
Br(1)	9461(1)	1311(1)	7826(1)	24(1)
C(1)	4183(8)	108(12)	5990(7)	38(3)
O(2)	3891(5)	1782(7)	5908(4)	25(1)
C(3)	3666(6)	2471(11)	6678(6)	21(2)
C(4)	3775(7)	1690(11)	7576(6)	25(2)
C(5)	3523(7)	2499(11)	8309(6)	25(2)
C(6)	3136(7)	4044(11)	8167(6)	27(2)
C(7)	3022(7)	4818(11)	7268(6)	24(2)
C(8)	3275(6)	4059(11)	6519(6)	19(2)
C(9)	3129(7)	4893(10)	5591(6)	20(2)
C(10)	3914(7)	5589(11)	5340(6)	20(2)
C(11)	3745(8)	6480(12)	4464(7)	32(2)
C(12)	2821(7)	6582(11)	3836(6)	26(2)
C(13)	2025(7)	5881(10)	4072(6)	22(2)
C(14)	2158(6)	5048(10)	4922(6)	19(2)
C(15)	1268(7)	4415(11)	5154(6)	24(2)
N(16)	1282(6)	2630(9)	5334(5)	21(2)
C(17)	1394(6)	1601(11)	4656(6)	22(2)
C(18)	1397(7)	-26(11)	4792(6)	26(2)
C(19)	1248(6)	-653(11)	5623(6)	23(2)
C(20)	1102(7)	431(11)	6320(6)	24(2)
C(21)	1110(7)	2046(11)	6148(6)	23(2)

Table 7.5. Bond lengths [Å] and angles [°] for c05378.

C(1)-O(2)	1.442(12)
O(2)-C(3)	1.374(10)
C(3)-C(8)	1.420(13)
C(3)-C(4)	1.420(12)
C(4)-C(5)	1.391(13)
C(5)-C(6)	1.385(14)
C(6)-C(7)	1.419(13)
C(7)-C(8)	1.391(13)
C(8)-C(9)	1.471(12)
C(9)-C(10)	1.400(13)
C(9)-C(14)	1.440(12)
C(10)-C(11)	1.426(13)
C(11)-C(12)	1.363(13)
C(12)-C(13)	1.405(13)
C(13)-C(14)	1.376(12)
C(14)-C(15)	1.500(13)
C(15)-N(16)	1.501(12)
N(16)-C(17)	1.346(11)
N(16)-C(21)	1.363(11)
C(17)-C(18)	1.361(13)
C(18)-C(19)	1.385(13)
C(19)-C(20)	1.414(13)
C(20)-C(21)	1.361(13)
C(3)-O(2)-C(1)	117.6(7)
O(2)-C(3)-C(8)	115.3(7)
O(2)-C(3)-C(4)	124.5(8)
C(8)-C(3)-C(4)	120.1(8)
C(5)-C(4)-C(3)	119.9(8)

C(6)-C(5)-C(4)	120.9(8)
C(5)-C(6)-C(7)	119.1(8)
C(8)-C(7)-C(6)	121.9(9)
C(7)-C(8)-C(3)	118.2(8)
C(7)-C(8)-C(9)	120.1(8)
C(3)-C(8)-C(9)	121.7(8)
C(10)-C(9)-C(14)	118.0(8)
C(10)-C(9)-C(8)	121.7(8)
C(14)-C(9)-C(8)	120.3(8)
C(9)-C(10)-C(11)	120.6(8)
C(12)-C(11)-C(10)	120.1(9)
C(11)-C(12)-C(13)	120.1(8)
C(14)-C(13)-C(12)	121.3(9)
C(13)-C(14)-C(9)	119.8(8)
C(13)-C(14)-C(15)	118.3(8)
C(9)-C(14)-C(15)	121.7(7)
C(14)-C(15)-N(16)	114.5(7)
C(17)-N(16)-C(21)	119.9(8)
C(17)-N(16)-C(15)	119.7(7)
C(21)-N(16)-C(15)	120.3(7)
N(16)-C(17)-C(18)	121.1(8)
C(17)-C(18)-C(19)	120.2(8)
C(18)-C(19)-C(20)	118.5(9)
C(21)-C(20)-C(19)	118.8(8)
C(20)-C(21)-N(16)	121.4(8)

Table 7.6. Anisotropic displacement parameters ($Å^2$x 10^3)for c05378. The anisotropic displacement factor exponent takes the form: $-2\pi^2[h^2a^{*2}U^{11} + ... + 2 h k a^* b^* U^{12}]$

	U^{11}	U^{22}	U^{33}	U^{23}	U^{13}	U^{12}
Br(1)	33(1)	20(1)	20(1)	2(1)	9(1)	2(1)
C(1)	50(7)	24(7)	40(6)	-2(4)	15(5)	6(5)
O(2)	46(4)	10(4)	19(3)	-1(2)	9(3)	6(3)
C(3)	19(5)	17(6)	21(5)	1(3)	-1(4)	3(4)
C(4)	39(6)	5(6)	31(5)	2(3)	9(4)	2(4)
C(5)	30(6)	25(6)	19(5)	4(4)	4(4)	2(4)
C(6)	42(6)	25(6)	17(5)	-8(4)	14(4)	1(4)
C(7)	34(6)	4(5)	32(6)	-4(3)	9(4)	-1(4)
C(8)	18(5)	18(6)	19(4)	1(3)	-1(4)	-5(4)
C(9)	33(6)	8(5)	24(5)	-1(3)	16(4)	3(4)
C(10)	29(5)	12(5)	16(4)	-1(3)	2(4)	-2(4)
C(11)	50(7)	15(6)	42(6)	1(4)	30(5)	-2(5)
C(12)	44(6)	12(6)	26(5)	3(3)	14(5)	-5(4)
C(13)	36(6)	4(5)	28(5)	3(3)	11(4)	7(4)
C(14)	26(5)	5(5)	24(5)	0(3)	4(4)	5(4)
C(15)	32(6)	13(5)	24(5)	-2(4)	4(4)	8(4)
N(16)	32(5)	16(5)	15(4)	0(3)	7(3)	-3(3)
C(17)	29(5)	19(6)	21(4)	-2(4)	11(4)	0(4)
C(18)	34(6)	21(6)	23(5)	-1(4)	9(4)	2(4)
C(19)	27(5)	6(5)	35(5)	2(3)	10(4)	2(4)
C(20)	26(5)	19(6)	29(5)	4(4)	13(4)	-6(4)
C(21)	29(6)	27(6)	16(4)	-1(4)	11(4)	4(4)

Table 7.7. Hydrogen coordinates (x 10^4) and isotropic displacement parameters ($Å^2$x 10^3) for c05378.

	x	y	z	U(eq)
H(1A)	4779	-23	6536	57
H(1B)	4314	-237	5394	57
H(1C)	3654	-552	6097	57
H(4)	4020	617	7675	30
H(5)	3619	1984	8916	30
H(6)	2949	4578	8666	32
H(7)	2766	5885	7174	28
H(10)	4565	5467	5756	24
H(11)	4277	7002	4318	39
H(12)	2716	7129	3238	32
H(13)	1382	5985	3636	27
H(15A)	679	4677	4610	29
H(15B)	1205	4982	5733	29
H(17)	1473	2017	4073	27
H(18)	1503	-732	4316	31
H(19)	1244	-1787	5721	27
H(20)	999	40	6899	28
H(21)	994	2781	6605	28

Table 7.8. Torsion angles [°] for c05378.

C(1)-O(2)-C(3)-C(8)	-173.0(8)
C(1)-O(2)-C(3)-C(4)	5.2(12)
O(2)-C(3)-C(4)-C(5)	-179.9(8)
C(8)-C(3)-C(4)-C(5)	-1.7(13)
C(3)-C(4)-C(5)-C(6)	2.1(14)
C(4)-C(5)-C(6)-C(7)	-1.7(14)
C(5)-C(6)-C(7)-C(8)	1.0(14)
C(6)-C(7)-C(8)-C(3)	-0.6(13)
C(6)-C(7)-C(8)-C(9)	178.9(8)
O(2)-C(3)-C(8)-C(7)	179.3(8)
C(4)-C(3)-C(8)-C(7)	1.0(12)
O(2)-C(3)-C(8)-C(9)	-0.2(12)
C(4)-C(3)-C(8)-C(9)	-178.6(8)
C(7)-C(8)-C(9)-C(10)	103.0(10)
C(3)-C(8)-C(9)-C(10)	-77.4(11)
C(7)-C(8)-C(9)-C(14)	-75.5(11)
C(3)-C(8)-C(9)-C(14)	104.1(10)
C(14)-C(9)-C(10)-C(11)	2.5(13)
C(8)-C(9)-C(10)-C(11)	-176.0(8)
C(9)-C(10)-C(11)-C(12)	-3.8(14)
C(10)-C(11)-C(12)-C(13)	3.3(14)
C(11)-C(12)-C(13)-C(14)	-1.6(14)
C(12)-C(13)-C(14)-C(9)	0.4(13)
C(12)-C(13)-C(14)-C(15)	176.5(8)
C(10)-C(9)-C(14)-C(13)	-0.9(12)
C(8)-C(9)-C(14)-C(13)	177.6(8)
C(10)-C(9)-C(14)-C(15)	-176.8(8)
C(8)-C(9)-C(14)-C(15)	1.7(12)

C(13)-C(14)-C(15)-N(16)	123.7(9)
C(9)-C(14)-C(15)-N(16)	-60.3(10)
C(14)-C(15)-N(16)-C(17)	-56.3(11)
C(14)-C(15)-N(16)-C(21)	128.5(8)
C(21)-N(16)-C(17)-C(18)	-3.9(13)
C(15)-N(16)-C(17)-C(18)	-179.2(8)
N(16)-C(17)-C(18)-C(19)	2.4(14)
C(17)-C(18)-C(19)-C(20)	-0.5(13)
C(18)-C(19)-C(20)-C(21)	0.2(13)
C(19)-C(20)-C(21)-N(16)	-1.8(14)
C(17)-N(16)-C(21)-C(20)	3.6(13)
C(15)-N(16)-C(21)-C(20)	178.8(8)

REFERENCES

Acharya, P.; Plashkevych, O.; Morita, C.; Yamada, S.; Chattopadhyaya, S., *J. Org. Chem.* **2003,** 68, 1529 - 1538.

Atkins, P. W., *Physical Chemistry*. 6th Edition ed.; Oxford University Press: Oxford, U.K., 1998.

Bedford, M. T.; Richard, S., *Molecular Cell* **2005,** 18, 263 - 272.

Benoiton, L., *Can. J. Chem.* **1964,** 42, 2043 - 2047.

Biot, C.; Buisine, E.; Rooman, M., *J. Am. Chem. Soc.* **2003,** 125, 13988 - 13994.

Bisson, A. P.; Lynch, V. M.; Monahan, M. C.; Anslyn, E. V., *Angew. Chem. Int. Ed.* **1997,** 36, 2340 - 2342.

Blanco, F. J.; Serrano, L., *Eur. J. Biochem.* **1995,** 230, 634 - 649.

Broccheiri, L.; Karlin, S., *Proc. Natl. Acad. Sci. USA* **1994,** 91, 9297 - 9301.

Brunger, A. T.; Adams, P. D.; Clore, G. M.; Delano, W. L.; Gros, P.; Grosse-Kunstleve, R. W.; Jiang, J.-S.; Kuszewski, J.; Nilges, N.; Pannu, N. S.; Read, R. J.; Rice, L. M.; Simondson, T.; Warren, G. L., *ACTA CRYST.* **1998,** D54, 905 - 921.

Burley, S. K.; Petsko, G. A., *FEBS Letters* **1986,** 203, 139 - 143.

Burley, S. K.; Petsko, G. A., *Adv. Prot. Chem.* **1988,** 39, 125 - 189.

Caron, C.; Boyault, C.; Khochbin, S., *BioEssays* **2005,** 27, 408 - 415.

Case, D. A.; Darden, T. A.; T. E. Cheatham, I.; Simmerling, C. L.; Wang, J.; Duke, R. E.; Luo, R.; Merz, K. M.; Wang, B.; Pearlman, D. A.; Crowley, M.; Brozell, S.; Tsui, V.; Gohlke, H.; Mongan, J.; Hornak, V.; Cui, G.; Beroza, P.; Schafmeister, C.; Caldwell, J. W.; Ross, W. S.; Kollman, P. A. *AMBER 8*, University of California, San Francisco: 2004.

Castellano, R. K.; Diederich, F.; Meyer, E. A., *Angew. Chem. Int. Ed.* **2003,** 42, 1210 - 1250.

Ciani, B.; Jordan, M.; Searle, M. S., *J. Am. Chem. Soc.* **2003,** 125, 9038 - 9047.

Cochran, A. G.; Skelton, N. J.; Starovasnik, M. A., *Proc. Natl. Acad. Sci. USA* **2001,** 98, 5578 - 5583.

Cochran, A. G.; Tong, R. T.; Starovasnik, M. A.; Park, E. J.; McDowell, R. S.; Theaker, J. E.; Skelton, N. J., *J. Am. Chem. Soc.* **2001,** 123, 625 - 632.

Cosgrove, M. S.; Boeke, J. D.; Wolberger, C., *Nat. Struct. Mol. Biol.* **2004,** 11, 1037 - 1043.

Cote, J.; Richard, S., *J. Biol. Chem.* **2005,** 280, 28476 - 28483.

Crowley, R. B.; Golovin, A., *Proteins: Structure, Function, and Bioinformatics* **2005,** 59, 231 - 239.

Cumpstey, I.; Sundin, A.; Leffler, H.; Nilsson, U. J., *Angew. Chem. Int. Ed.* **2005,** 44, 5110 - 5112.

de Vos, A. M.; Ultsch, M.; Kossiakoff, A. A., *Science* **1992,** 255, 306 - 312.

Dhalluin, C.; Carlson, J. E.; Zeng, L.; He, C.; Aggarwal, A.; Zhou, M., *Nature* **1999,** 399, 491 - 496.

Duan, G.; Smith, V. H.; Weaver, D. F., *Chem. Phys. Lett.* **1999,** 310, 323 - 332.

Duan, G.; Smith, V. H.; Weaver, D. F., *J. Phys. Chem. A* **2000,** 104, 4521 - 4532.

Duan, G.; Smith, V. H.; Weaver, D. F., *Int. J. Quant. Chem.* **2000** 80, 44 - 60.

Dyer, R. B.; Maness, S. J.; Franzen, S.; Fesinmeyer, R. M.; Olsen, K. A.; Andersen, N. H., *Biochemistry* **2005,** 44, 10406 - 10415.

Eichman, B. F.; O'Rourke, E. J.; Radicella, J. P.; Ellenberger, T., *EMBO J.* **2003,** 22, 4898 - 4909.

Fesinmeyer, R. M.; Hudson, F. M.; Andersen, N. H., *J. Am. Chem. Soc.* **2004,** 126, 7238 - 7234.

Fesinmeyer, R. M.; Hudson, F. M.; Olsen, K. A.; White, G. W. N.; Euser, A.; Andersen, N. H., Chemical shifts provide fold populations and register of beta hairpins and beta sheets. *Journal of Biomolecular Nmr* **2005,** 33, (4), 213-231.

Fischle, W.; Wang, Y. M.; Jacobs, S. A.; Kim, Y. C.; Allis, C. D.; Khorasanizadeh, S., *Genes and Development* **2003,** 17, 1870 - 1881.

Flanagan IV, J. F.; Mi, L.; Chruszcz, M.; Cymborowski, M.; Clines, K. L.; Kim, Y.; Minor, W.; Rastinejad, F.; Khorasanizadeh, S., *Nature* **2005,** 438, 1181 - 1185.

Flocco, M. M.; Mowbray, S. L., *J. Mol. Biol.* **1994,** 235, 709 - 717.

Foster, J. E.; Holmes, S. F.; Erie, D. A., *Cell* **2001,** 106, 243 - 252.

Gallivan, J. P.; Dougherty, D. A., *Proc. Natl. Acad. Sci. USA* **1999,** 96, 9459 - 9464.

Gallivan, J. P.; Dougherty, D. A., *J. Am. Chem. Soc.* **2000,** 122, 870 - 874.

Griffith-Jones, S. R.; Maynard, A. J.; Searle, M. S., *J. Mol. Biol.* **1999,** 292, 1051 - 1069.

Griffiths-Jones, S. R.; Maynard, A. J.; Searle, M. S., *J. Mol. Biol.* **1999,** 121, 11577 - 11578.

Griffiths-Jones, S. R.; Maynard, A. J.; Sharman, G. J.; Searle, M. S., *Chem. Commun.* **1998**, 789 - 790.

Honda, S.; Kobayashi, N.; Munekata, E., *J. Mol. Biol.* **2000,** 295, 269 - 278.

Hong, L.; Schroth, G. P.; Matthews, H.; Yau, P.; Bradbury, E. M., *J. Biol. Chem.* **1993,** 268, 305-314.

Houk, K.; Menzer, S.; Newton, S.; Raymo, F.; Stoddart, F.; Williams, D., *J. Am. Chem. Soc.* **1999,** 121, 1479 - 1487.

Hughes, R. M.; Waters, M. L., *J. Am. Chem. Soc.* **2005,** 127, 6518 - 6519.

Hughes, R. M.; Waters, M. L., *J. Am. Chem. Soc.* **2006**, 128, 41, 13586 – 13591.

Hughes, R. M.; Waters, M. L. *J. Am. Chem. Soc.* **2006**, 128, 39, 12735 – 12742.

Hughes, R. M.; Waters, M. L. *Curr. Op. Struct. Biol*. **2006**, 16, 514 – 524.

Hunter, C. A., *Angew. Chem. Int. Ed.* **2004,** 43, 5310 - 5324.

Hutchinson, E. G.; Sessions, R. B.; Thornton, J. M.; Woolfson, D. N., *Prot. Sci.* **1998,** 7, 2287 - 2300.

Jacobs, S.; Harp, J.; Khorasanizadeh, S., *Biophysical J.* **2003,** 84, 503A.

Jacobs, S. A.; Khorasanizadeh, S., *Science* **2002,** 295, 2080 - 2083.

Jacobs, S. A.; Taverna, S. A.; Zhang, Y.; Briggs, S. D.; Li, J.; Eissenberg, J. C.; Allis, C. D.; Khorasanizadeh, S., *EMBO J.* **2001,** 20, 5232-5241.

Kaiser, E.; Colescott, R. L.; Bossinger, C. D.; Cook, P. I., *Analytical Biochemistry* **1970,** 34, 595 - 598.

Karlin, S.; Zuker, M.; Brocchieri, L., *J. Mol. Biol.* **1994,** 239, 227 - 248.

Kawahara, S.; Tsuzuki, S.; Uchimaru, T., *J. Phys. Chem. A* **2004,** 108, 6744.

Kearney, P. C.; Mizoue, L. S.; Kumpf, R. A.; Forman, J. E.; McCurdy, A. E.; Dougherty, D. A., *J. Am. Chem. Soc.* **1993,** 115, 9907 - 9919.

Khorasanizadeh, S., *Biophysical J.* **2003,** 84, 485A.

Kortemme, T.; Ramirez-Alvarado, M.; Serrano, L., *Science* **1998,** 281, 253 - 256.

Kretsinger, J. T.; Schneider, J. P., *J. Am. Chem. Soc.* **2003,** 125, 7907 - 7913.

Kumaki, Y.; Nitta, K.; Hikichi, K.; Matsumoto, T.; Matsushima, N. J., *Biochemistry* **2004,** 136, 29 - 37.

Lachner, M.; Jenuwein, T., *Current Opinion in Cellular Biology* **2002,** 14, 286 - 298.

Lamar, J.; Hu, J.; Bueno, A. B.; Yang, H.-C.; Guo, D.; Copp, J. D.; McGee, J.; Gitter, B.; Timm, D.; May, P.; McCarthy, J.; Chen, S.-H., *Bioorganic and Medicinal Chemistry Letters* **2004,** 14, 239 - 243.

Lee, D. Y.; Teyssier, C.; Strahl, B. D.; Stallcup, M. R., *Endocrine Reviews* **2005,** 26, 147 - 170.

Lee, S.; Lin, X.; McMurray, J.; Sun, G., *Biochemistry* **2002,** 41, 12107 - 12114.

Li, H.; Ilin, S.; Wang, W.; Duncan, E. M.; Wysocka, J.; Allis, C. D.; Patel, D. J., *Nature* **2006,** 442, 91 - 95.

Lindroth, A. M.; Shultis, D.; Jasencakova, Z.; Fuchs, J.; Johnson, L.; Schubert, D.; Patnaik, D.; Pradhan, S.; Goodrich, J.; Schubert, I.; Jenuwein, T.; Khorasanizadeh, S.; Jacobsen, S. E., *EMBO J.* **2004,** 23, 4286 - 4296.

Loladze, V. V.; Ermolenko, D. N.; Makhatadze, G. I., *Protein Science* **2001,** 10, 1343 - 1352.

Luque, L. E.; Grape, K. P.; Junker, M., *Biochemistry* **2002,** 41, 13663 - 13671.

Ma, J. C.; Dougherty, D. A., *Chem. Rev.* **1997,** 97, 1303 - 1324.

Mahalakshmi, R.; Raghothama, S.; Balaram, P., *J. Am. Chem. Soc.* **2006,** 128, 1125 - 1138.

Martin, C. B.; Mulla, H. R.; Willis, P. G.; Cammers-Goodwin, R., *J. Org. Chem.* **1999,** 64, 7802 - 7806.

Masumoto, H.; Hawke, D.; Kobayashi, R.; Verreault, A., *Nature* **2005,** 436, 294.

Maynard, A. J.; Sharman, G. J.; Searle, M. S., *J. Am. Chem. Soc.* **1998,** 120, 1996 - 2007.

McBride, A. E.; Silver, P. A., *Cell* **2001**, (106), 5 - 8.

McCurdy, A. E.; Jimenez, L.; Stauffer, D. A.; Dougherty, D. A., *J. Am. Chem. Soc.* **1992,** 114, 10314 - 10321.

Mecozzi, S.; West, A. P.; Dougherty, D. A. *Proceedings of the National Academy of Sciences of the United States of America* **1996,** 93, (20), 10566-10571.

Merkel, J. S.; Regan, L., *Folding & Design* **1998,** 3, 449 - 455.

Meyer, E. A.; Castellano, R. K.; Diederich, F., *Angew. Chem. Int. Ed.* **2003,** 42, 1211.

Mignon, P.; Loverix, S.; De Proft, F.; Geerlings, P., *J. Phys. Chem. A* **2004,** 108, 6038 - 6044.

Miller, S. C.; Scanlan, T. S., *J. Am. Chem. Soc.* **1997,** 119, 2301 - 2302.

Mitchell, J. B. O.; Nandi, C. L.; McDonald, I. K.; Thornton, J. M., *J. Mol. Biol.* **1994,** 239, 315 - 331.

Mitchell, J. B. O.; Nandi, C. L.; McDonald, I. K.; Thornton, J. M.; Price, S. L., *J. Mol. Biol.* **1994,** 239, 315 - 331.

Moore, D. S., In *The Basic Principles of Statistics*, W. H. Freeman and Co.: New York, N. Y., 1995; pp 630 - 633.

Munoz-Caro, C.; Nino, A., *Biophys. Chem.* **2002,** 96, 1 - 14.

Myers, A. G.; Schnider, P.; Kwon, S.; Kung, D. W., *J. Org. Chem.* **1999,** 64, 3322-3327.

Ngola, S. M.; Kearney, P. C.; Mecozzi, S.; Russell, K.; Dougherty, D. A., *J. Am. Chem. Soc.* **1999,** 121, 1192 - 1201.

Nishihara, M.; Perret, F.; Takeuchi, T.; Futaki, S.; Lazar, A. N.; Coleman, A. W.; Sakai, N.; Matile, S., *Org. Biomol. Chem.* **2005,** 3, 1659 - 1669.

OriginLab *Origin*, 7.5; OriginLab Corporation, One Roundhouse Plaza, Northampton, MA 01060, U.S.A.

Owen, D. J.; Ornaghi, P.; Yang, J. C.; Lowe, N.; Evans, P. R.; Ballario, P.; Neuhaus, D.; Filetici, P.; Travers, A. A., *EMBO J.* **2000,** 19, (6141 - 6149).

Pace, C. N., *Methods in Enzymology* **1986,** 131, 266 - 280.

Pellequer, J.; Zhao, B.; Kao, H.; Bell, C. W.; Li, K.; Li, Q. X.; Karu, A. E.; Roberts, V. A., *J. Mol. Biol.* **2000,** 302, 691 - 699.

Perutz, M. F., *Phil. Trans. Phys. Sci. Eng.* **1993,** 345, 105 - 112.

Perutz, M. F.; Fermi, G.; Abraham, D. J.; Poyart, C.; Bursaux, E., *J. Am. Chem. Soc.* **1986,** 108, 1064 - 1078.

Petti, M. A.; Shepodd, T. J.; Barrans, J. R. E.; Dougherty, D. A., *J. Am. Chem. Soc.* **1988,** 110, 6825 - 6840.

Prabhu, N. V.; Sharp, K. A., *Annual Rev. Phys. Chem.* **2005,** 56, 521 - 548.

Quiocho, F. A.; Hu, G.; Gershon, P. D., *Current Opinion in Structural Biology* **2000,** 10, 78 - 86.

Rashkin, M. J.; Hughes, R. M.; Calloway, N. T.; Waters, M. L., *J. Am. Chem. Soc.* **2004,** 126, 13320 - 13325.

Rashkin, M. J.; Waters, M. L., *J. Am. Chem. Soc.* **2002,** 124, 1860 - 1861.

Raymo, F.; Bartberger, M.; Houk, K.; Stoddart, F., *J. Am. Chem. Soc.* **2001,** 123, 9264 - 9267.

Raymo, F.; Houk, K.; Stoddart, F., *J. Org. Chem.* **1998,** 63, 6523 - 6528.

Rensing, S.; Arendt, M.; Springer, A.; Grawe, T.; Schrader, T., *J. Org. Chem.* **2001,** 66, 5814 - 5821.

Russell, S. J.; Blandl, T.; Skelton, N. J.; Cochran, A. G., *J. Am. Chem. Soc.* **2003,** 125, 388 - 395.

Rybczynski, P. J.; Zeck, R. E.; Dudash, J., Jr. ; Combs, D. W.; Burris, T. P.; Yang, M.; Osborne, M. C.; Chen, X.; Demarest, K. T., *J. Med. Chem.* **2004,** 47, 196-209.

Scharer, K.; Morgenthaler, M.; Paulini, R.; Obst-Sander, U.; Banner, D. W.; Schlatter, D.; Benz, J.; Stihle, M.; Diederich, F., *Angew. Chem. Int. Ed.* **2005,** 44, 2 - 6.

Searle, M. S.; Griffiths-Jones, S. R.; Skinner-Smith, H. J., *J. Am. Chem. Soc.* **1999,** 121, 11615 - 11620.

Sengupta, A.; Mahalakshmi, R.; Shamala, N.; Balaram, P., *J. Pept. Res.* **2005,** 65, 113 - 129.

Sharman, G. J.; Searle, M. S., *J. Am. Chem. Soc.* **1998,** 120, 5291 - 5300.

Shi, X.; Hong, T.; Walter, K. L.; Ewalt, M.; Michishita, E.; Hung, T.; Carney, D.; Peña, P.; Lan, F.; Kaadige, M. R.; Lacoste, N.; Cayrou, C.; Davrazou, F.; Saha, A.; Cairns, B. R.; Ayer, D. E.; Kutateladze, T. G.; Shi, Y.; Côté, J.; Chua, K. F.; Gozani, O., *Nature* **2006,** 442, 96 - 99.

Shi, Z. S.; Olson, C. A.; Kallenbach, N. R., *J. Am. Chem. Soc.* **2002,** 124, 3284 - 3291.

Shirahata, A., *Tet. Lett.* **1989,** 30, 6393-6394.

Shoemaker, D. P., Garland, C. W., and Nibler, J. W. Experiments in Physical Chemistry, 4th Ed.; McGraw Hill; 1981, 727-730. , In *Experiments in Physical Chemistry*, 4th Edition ed.; McGraw HIll: 1981; pp 727 - 730.

Simonsson, M.; Heldin, C.; Ericsson, J.; Gronroos, E., *J. Biol. Chem.* **2005,** 280, 21797 - 21803.

Singh, J.; Thornton, J. M., *J. Mol. Biol.* **1990,** 211, 595 - 615.

Smith, A. W.; Chung, H. S.; Ganim, Z.; Tokmakoff, A., *J. Phys. Chem. B* **2005,** 109, 17025 - 17027.

Snowden, T. S.; Bisson, A. P.; Anslyn, E. V., *J. Am. Chem. Soc.* **1999,** 121, 6324 - 6325.

St. Charles, R.; Padmanabhan, K.; Arni, R. V.; Padmanabhan, K. P.; Tulinsky, A., *Protein Science* **2000,** 9, 265 - 272.

Stauffer, M.; Dougherty, D. A., *Tetrahedron Letters* **1988,** 29, 6039.

Stauffer, M.; Dougherty, D. A., *Science* **1990,** 250, 1558.

Steiner, T.; Koellner, G., *J. Mol. Biol.* **2001,** 305, 535 - 557.

Tatko, C. D.; Waters, M. L., *Prot. Sci.* **2003,** 12, 2443 - 2452.

Tatko, C. D.; Waters, M. L., *J. Am. Chem. Soc.* **2004,** 126, 2028 - 2034.

Thompson, S. E.; Smithrud, D. B., *J. Am. Chem. Soc.* **2002,** 124, 442 - 449.

Toth, G.; Kover, K. E.; Murphy, R. F.; Lovas, S., *J. Phys. Chem. B* **2004,** 108, 9287.

Toth, G.; Murphy, R. F.; Lovas, S., *Prot. Eng.* **2001,** 14, 543 - 547.

Toth, G.; Watts, C. R.; Murphy, R. F.; Lovas, S., *Prot. Struct. Func. Gen.* **2001,** 43, 373 - 381.

Tsuzuki, S.; Honda, K.; Uchimaru, T.; Mmikami, M.; Tanabe, K., *J. Am. Chem. Soc.* **2000,** 122, 11450 - 11458.

van der Spoel, D.; van Buuren, A. R.; Tieleman, P.; Berendsen, H. J. C., *J. Biomolecular NMR* **1996,** 8, 229 - 238.

Wei, Y.; Horng, J.; Vendel, A. C.; Raleigh, D. P.; Lumb, K. J., *Biochemistry* **2003,** 42, 7044 - 7049.

Wintjens, R.; Lievin, J.; Rooman, M.; Buisine, E., *J. Mol. Biol.* **2000,** 302, 395 - 410.

Woods, A. S., *J. Proteome Res.* **2004,** 3, 478 - 484.

Wüthrich, K., *NMR of Proteins and Nucleic Acids*. John Wiley and Sons, Inc.: 1986.

Wysocka, J.; Swigut, T.; Xiao, H.; Milne, T. A.; Kwon, S. Y.; Landry, J.; Kauer, M.; Tackett, A. J.; Chait, B. T.; Badenhorst, P.; Wu, C.; Allis, C. D., *Nature* **2006,** 442, 86 - 90.

Yamada, S.; Misono, T.; Tsuzuki, S., *J. Am. Chem. Soc.* **2004,** 126, 9862 - 9872.

Yamada, S.; Morita, C., *J. Am. Chem. Soc.* **2002,** 124, 8184 - 8185.

Yamamoto-Katayama, S.; Ariyoshi, M.; Ishihara, K.; Hirano, T.; Jingami, H.; Morikawa, K., *J. Mol. Biol.* **2002,** 316, 711 - 723.

Zacharias, N.; Dougherty, D. A., *Trends Pharmacol. Sci.* **2002,** 23, 281 - 287.

Zeng, L.; Zhou, M. M., *FEBS Letters* **2002,** 513, (124 - 128).